DISSERTATIONES CHIMICAE UNIVERSITATIS TARTUENSIS
7

ADSORPTION OF ORGANIC COMPOUNDS ON ANTIMONY, BISMUTH AND CADMIUM ELECTRODES

ALAR JÄNES

TARTU 1998

DISSERTATIONES CHIMICAE UNIVERSITATIS TARTUENSIS

7

DISSERTATIONES CHIMICAE UNIVERSITATIS TARTUENSIS
7

ADSORPTION OF ORGANIC COMPOUNDS ON ANTIMONY, BISMUTH AND CADMIUM ELECTRODES

ALAR JÄNES

TARTU UNIVERSITY
PRESS

Department of Chemistry, University of Tartu, Estonia

Dissertation is accepted for the commencement of the Degree of Doctor of Philosophy in Chemistry on February 10th, 1998 by the Doctoral Committee of Department of Chemistry, University of Tartu.

Opponents: D.Sc. Chemistry, Prof. O. A. Petrii, Moscow
D.Sc. Chemistry, Prof. Em. V. Past, Tartu

Commencement: April 3rd, 1998 at 15.00 o'clock in room 204 of the Main Building of University of Tartu, Ülikooli 18, EE2400, Tartu, Estonia

Publication of this dissertation is granted by University of Tartu

Tartu Ülikooli Kirjastuse trükikoda
Tiigi 78, EE2400 Tartu
Tellimus nr. 80.

CONTENTS

LIST OF ORIGINAL PUBLICATIONS

The thesis consists of the review and the eleven articles listed below. They are referred in the text by Roman numerals I–XI. The review summarizes and supplements the articles.

I. E. Lust, A. Jänes, Structure of the Electrical Double Layer and Adsorption of Cyclohexanol on the Faces of an Antimonium Single Crystal, Russian J. of Electrochemistry, 30 No. 3 (1994) 321–328.

II. A. A.-J. Jänes, E. J. Lust, Adsorption of Cyclohexanon on the Single Crystal Bismuth and Antimony Electrodes, Russian J. of Electrochemistry, 31 No. 6 (1995) 648–651 (in Russian).

III. E. J. Lust, K. K. Lust, A. A.-J. Jänes, Influence of the Crystallographic Structure of the Electrode Surface on the Structure of the Electrical Double Layer and Adsorption of Organic Molecules. Russian J. of Electrochemistry, 31, No. 8 (1995) 876–890 (in Russian).

IV. A. A.-J. Jänes and E. J. Lust, Adsorption of Cyclohexancarboxylic Acid on Faces of the Bismuth and Antimony Single Crystals, Russian J. of Electrochemistry, 32, No. 8 (1996) 1020–1022 (in Russian).

V. E. Lust, A. Jänes, K. Lust and P. Miidla, Adsorption of Isomers of Butanol on Bismuth Single Crystal Plane Electrodes, J. Electroanalyt. Chem., 413 (1996) 175–185.

VI. E. Lust, A. Jänes, K. Lust and M. Väärtnõu, Electric Double Layer Structure and Adsorption of Cyclohexanol on Single Crystal Cadmium, Antimony and Bismuth Electrodes, Electrochimica Acta, 42, No. 5, (1997) 771–783.

VII. E. Lust, A. Jänes, P. Miidla and K. Lust, Adsorption of Pyridine on the (111), (001) and $(01\bar{1})$ Faces of Bismuth, J. Electroanalyt. Chem., 425 (1997) 25–37.

VIII. E. Lust, A. Jänes, K. Lust, V Sammelselg and P. Miidla, Influence of Surface Pretreatment of Bismuth and Cadmium Electrodes to the Electric Double Layer and Adsorption Characteristics of Organic Compounds, Electrochimica Acta, Vol. 42, No. 19 (1997) 2861–2879.

IX. E. Lust, A. Jänes, K. Lust and R. Pullerits, Adsorption of Organic Compounds and Hydrophilicity of Bismuth, Cadmium and Antimony Electrodes, J. Electroanalyt. Chem., 431 (1997) 183–201.

X. E. Lust, A. Jänes, K. Lust and P. Miidla, Adsorption of Propanol on Bismuth Single Crystal Plane Electrodes, J. Electroanalyt. Chem., 436 (1997) 141–153.

XI. E. Lust, A. Jänes, K. Lust and P. Miidla, Adsorption of Normal Hexanol on Bismuth Single Crystal Plane Electrodes, J. Electroanalyt. Chem., (accepted JEC 07041).

1. INTRODUCTION

Discussion on the reasons for the interphase characteristics to dependence on the chemical nature and energy state of the electrode surface originated in the pioneering works of Borisova, Ershler and Frumkin [1, 2], where it was found that the double layer characteristics to a significantly degree depend on the electrode surface pretreatment. In 1967, A. N. Frumkin put forth an idea that double layer and adsorption parameters calculated on the basis of experimental data for solid electrodes with polycrystalline (PC) surface structure are of an apparent nature; he also stressed the necessity of conducting the highly accurate electrochemical measurements on individual faces of monocrystalline electrodes [3]. In 1972, the quantitative analysis of the electric double layer, adsorption of ions and organic molecules and the electrochemical kinetics of various reactions on different solid metals have been studied in the Laboratory of Electrochemistry and Department of Inorganic Chemistry reorganized to the Institute of Physical Chemistry of the University of Tartu at 1991 [4]. It should by noted that the principal double layer characteristics of the (111) face of monocrystalline Bi have been experimentally studied by M. Pärnoja, N. B. Grigoryev, and U. Palm under the supervision of A. N. Frumkin at The Institute of Electrochemistry of the Russian Academy of Sciences [5]. Systematic investigations on monocrystalline faces of Sb and Cd have been started in 1987 [6, 7].

In order to determine the true adsorption characteristics in the systems under study, elucidate crystallographic effects and produce modeling PC surfaces with specified parameters, large-scale investigations were performed at the Institute of Physical Chemistry aimed at studying the adsorption on various faces of single crystals of Bi, Sb and Cd in aqueous solutions. These problems are considered in this work [I–XI].

2. LITERATURE OVERVIEW

Adsorption of organic compounds at the metal | electrolyte solution interface is attracting considerable attention of everyone concerning with theoretical and applied electrochemistry. Indeed, unless the adsorption effects are taken into account it is impossible to understand the mechanism of most of the processes occurring at the mercury electrode and therefore to interpret the results of polarographic determinations.

Adsorption of organic compounds is widely used for regulating the processes of metal electrodeposition. It determines the behavior of organic compounds at positive electrodes of fuel cells and therefore their suitability as electrochemical fuel. The action of corrosion inhibitors is based on adsorption effects and they must also be taken into consideration in searches for new routes of organic electrochemical synthesis. Adsorption effects are also met in the general electrochemical industry. Investigations of adsorption phenomena at electrode | solution interfaces are of theoretical interest, extending our knowledges about the structure of the electric double layer.

2.1. Methods for Determination of the Adsorption Parameters

As shown in [8], if the rate of the adsorption of organic compounds is limited by diffusion, the equilibrium values of differential capacity at $\nu = 0$ can usually be found of a sufficient degree of accuracy by the extrapolation of the $C_{add}(\omega^{1/2})$– curve $(\omega = 2\pi\nu)$ to $\omega^{1/2} = 0$. According to the method [9, 10], the equilibrium values of differential capacity can be calculated by eqn. (1)

$$C_{add}(\omega = 0) = C_{add}^2(\omega)R_p^2(\omega)\omega^2 + 1/\left\{\left[C_{add}(\omega)R_p(\omega)\omega - 1\right]R_p(\omega)\omega\right\}, \qquad (1)$$

where $C_{add}(\omega)$ and $R_p(\omega)$ are the values of differential capacity and solution resistance at ω = const.

The components of the adsorption impedance have been calculated from the impedance data of the cell used for the measurements (series circuit), i.e. $C_S(\omega)$ and $R_S(\omega)$, following the procedure described in [8–11]. By extrapolating the $R_S(\omega)$-values to $\omega \to \infty$ the solution resistance $R_S(\omega)=R_{sol}$ has been determined. Since the amount of organic compounds added is small and does not affect the solution resistance, one can assume R_{sol} to be equal to the ohmic component R_S, of impedance in the pure base electrolyte solution. Then the series equivalents $R_S(\omega) - R_{sol}$ and $C_S(\omega)$ of impedance were converted into the parallel equivalents $C_P + C_{true}$ and R_P via the relations given in [8–11].

The charge density-potential $\sigma_0(E)$-curve for base electrolyte solution has been obtained by the integration of the $C(E)$-curve, starting from the potential of zero charge $E_{\sigma=0}$. The values of $E_{\sigma=0}$ for different singe crystal planes have been obtained from the position of the diffuse layer minimum on an independently measured differential capacity curves for a dilute solutions of the base electrolyte. The charge density-potential curves for solutions with different additions of adsorbate have been obtained by back integration of the $C(E)$-curves, starting from $E = -1.8$ V/SCE and assigning the value of $\sigma(E = -1.8\ \text{V})$ equal to $\sigma_0(E = -1.8\ \text{V})$, because there is no adsorption at $E = -1.8$ V/SCE. The shape of $\sigma(E)$-curves is typical of the behaviour observed for the adsorption of neutral organic molecules at ideally polarizable electrodes.

The values of the initial and final potentials for the potential step experiments were chosen with the help of the $C(E)$- and $j(E)$-curves. The initial potential E_i has been varied from –0.50 to –1.80 V/SCE. The final potential E_f was equal to –1.60 V/SCE for $c_{org} \leq 0.01$ M and –1.80 V/SCE for $c_{org} > 0.01$ M.

The chronoamperometric curves were integrated digitally to obtain the charge transients. The chronocoulometric curves display an initial fast–rising section, corresponding to the charging of the edl followed by a quasi–plateau in which the charge varies slowly and linearly with time. The slope of this segment is small (due to a very slight hydrogen evolution reaction). These linear segments of the transients have been extrapolated to zero time to obtain the relative charge densities $\Delta\sigma$. In this way, the faradaic contribution from hydrogen evolution was minimized. The relative charge densities $\Delta\sigma$ have been determined from these step measurements:

$$\Delta\sigma(E) = \sigma(E_i) - \sigma(E_f). \tag{2}$$

In eqn. (2) $\sigma(E_i)$ and $\sigma(E_f)$ are the charge densities at the metal side of the interface at potentials E_i and E_f, respectively. Knowing the value of $E_{\sigma=0}$, determined by impedance measurements in the dilute solutions of base electrolyte [12], the absolute charge densities have been calculated for each value of E by using the formula

$$\sigma(E) = \Delta\sigma(E) - \Delta\sigma(E_{\sigma=0}) \tag{3}$$

Capacitance curves have been twice back–integrated to obtain a surface tension $(\gamma–\gamma_0)$ decrease as a function of the electrode potential and adsorbate concentration [13]. The second integration was performed from the same negative charge at first, assigning the value of zero to the surface tension at the pzc in the base solution.

The pressure of the film of adsorbate π can be determined as

$$\pi(E) = \gamma_{c=0} - \gamma_c = \int_{E_0}^{E} \sigma_c \, dE - \int_{E_0}^{E} \sigma_{c=0} \, dE \tag{4}$$

where subscripts c and $c = 0$ indicate the presence and absence of adsorbate in the bulk of the electrolyte, respectively, and γ is surface tension.

The film pressure data have been used to calculate the relative Gibbs surface excess (Γ). First the film pressure is plotted against log c_{org} at E = const. The curves display a long linear section, its slope giving the limiting value of Γ_{max}

$$\Gamma = \frac{1}{RT}\left(\frac{\partial \pi}{\partial \ln c}\right)_{E,T,p} \tag{5}$$

As in the rising part of the curves, the slope changes dramatically, therefore, the related Gibbs excesses for the intermediate coverages have been determined from the electrode charge densities using the well-known formula

$$\Gamma = \frac{\sigma_\Gamma - \sigma_{\Gamma=0}}{\sigma_{\Gamma_{max}} - \sigma_{\Gamma=0}} \Gamma_{max} . \tag{6}$$

The values of $(\sigma_{\Gamma_{max}} - \sigma_{\Gamma=0})$ have been obtained by the extrapolation of the linear sections of the $\sigma(E)$- curves.

Differential capacity C_1 at the maximum coverage has been obtained by extrapolating $1/C$ vs. $1/c_{org}$ plots to $(1/c_{org}) \rightarrow 0$. The data taken at the potential of maximum adsorption E_{max} lie satisfactorily on a straight line. This is a proof that capacitance in the region of maximum adsorption is negligibly affected by problems of reversibility.

Since the surface pressure data are to some degree not quantitatively reliable, the surface coverage at $E = E_{max}$ has been first estimated from eqn. (7) based on Frumkin's two parallel condensers model [8, 11, 13–15]

$$\theta = (C_0 - C_\theta)/(C_0 - C_1), \tag{7}$$

where C_0 and C_1 are the capacitances at $\theta = 0$ and $\theta = 1$, respectively. The next step is the test of the Frumkin isotherm ($\log[\theta/(1-\theta)c]$ vs. θ plot) to derive the adsorption parameters. The standard Gibbs energy of adsorption ΔG^0_{ads} at E_{max} has been obtained by eqn. (8)

$$\Delta G^0_{ads} = -RT \ln(55.5\, B_m). \tag{8}$$

The adsorption isotherms at various E = const. and σ = const. have been calculated by the methods described in [8, 11, 16–19].

If the Frumkin–Damaskin model [8, 11] is accepted, further information on adsorption parameters can be obtained from an analysis of the adsorption–desorption peaks. The following analysis is not unquestionable per se. First, frequency effects are included; secondly, the validity of the formulae entails in particular a congruence of isotherms with respect to the potential and constants C_0 and C_1. However, the analysis is carried out in order to compare the adsorption of the same compound at the various planes of the same metal, using the same experimental variable. The values of C^{max} at E^{max} have been obtained by

using eqn. (1) and the value of C_0 has been obtained by extrapolation of $C_0(\omega^{1/2})$-dependence to $\omega \rightarrow 0$.

$$\mathrm{d}\left(C^{\max} - C_0\right) \Big/ \mathrm{d}\log c_{\mathrm{org}} = 2.3(C_0 - C_1)/(2 - a)\,. \tag{9}$$

Since C_0 and C_1 are known independently, a value of a at $E \approx E^{\max}$ can be obtained from eqn. (9).
The intercept is given by

$$\text{intercept} = \text{slope}\ (\log B_{\mathrm{m}} + a/2.3) + \left(C_0 + C_1\right)/2\,, \tag{10}$$

By using the values of a obtained from eqn. (9), and a value of $\log B_{\mathrm{m}}$, the adsorption equilibrium constant at $E_{\max}$, can be obtained from eqn. (10).

According to Frumkin's model, $(E^{\max} - E_{\max})^2$ should be linearly related to $\log c$ with a slope given by

$$\mathrm{d}(E^{\max} - E_{\max})^2 / \mathrm{d}\log c = 4.6RT\Gamma_{\max}/(C_0 - C_1)\,. \tag{11}$$

Since C_0 and C_1 are known, $\Gamma_{\max}$ can be estimated from eqn. (11). According to the data of the systematic analysis compounds adsorption on Bi, Sb and Cd single crystal plane electrodes it has been found that at the first approximation the Frumkin—Damaskin adsorption theory [8, 11] is valid.

2.2. Adsorption of Organic Compounds on Mercury, Gold and Silver Electrodes

The electrosorption behaviour of the same organic compounds on different metals and on different single crystal planes of the same metal under all the rest identical conditions can help to establish a scale of metal–water and water–water interactions for these various electrode materials. To this end the organic compounds must satisfy the requirement being weekly physisorbed on the metal surface. Whereas monofunctional aliphatic compounds (alcohols, amines, ethers, esters, ketones and carboxylic acids) are usually convenient candidates for this purpose, pyridine and more generally organic compounds with conjugated double bonds or sulphide groups are not suitable for this purpose, since they thend to form weak chemical bonds with the metal: this explains why the latter compounds often exhibit trends opposite to those shown by simple aliphatic compounds [20].

The adsorption of various aliphatic compounds on mercury, gold and silver electrodes has been investigated by several research groups. Differential capacity measurements have been used by Damaskin *et al.* [8] and Moncelli *et al.* [21] to investigate the adsorption of aliphatic alcohols at mercury drop electrode. Differential capacity measurements have been used by Damaskin and coworkers [22–28] to investigate the adsorption of esters, ketones, amines,

pyridine and carboxylic acids at mercury drop electrode. Beltowska-Brzezinska and co-workers [29–31] used the tensametric method to characterize the adsorption of a number of primary and secondary alcohols on polycrystalline gold electrode. Tucceri and Posades [32] investigated the adsorption of n-pentanol on thin gold film electrodes using capacitance and conductance measurements. Differential capacity measurements have been used by Dutkiewicz *et al.* [33, 34] to investigate the adsorption of carboxylic acids at gold single crystal electrodes. Chronocoulometry has been employed by Lipkowski *et al.* [35] to study diethyl ether adsorption and by Richer and Lipkowski [36–38] to study tert-pentanol adsorption at gold surfaces with low single crystal index. Petit *et al.* [39] and Hamelin and Valette [40–42] investigated pyridine adsorption of polycrystalline Au and the low index single crystal surfaces of gold, respectively, using differential capacity method.

Vitanov and co-workers determined the adsorption isotherms of n-hexanol [43], iso-butanol [44] and n-pentanol [45] on Ag(111) and Ag(100) at the potential of maximum adsorption from differential capacity measurements using the extrathermodynamic approach based on the two parallel capacitors model. Systematic studies of pyridine adsorption at silver single crystal electrodes have been carried out by Hamelin *et al.* [46–48].

2.3. Influence of the Crystallographic Structure and Roughness of the Electrode Surface on the Adsorption of Organic Molecules

It is commonly accepted that the electrochemical properties of a solid metal surface significantly depend not only on the chemical composition but also on the crystallographic structure of the surface of a metal studied. The discovery of the splitting effect of the adsorption–desorption maxima for organic compounds [49, 50] played an important role in developing the theory of electric double layer (EDL) and adsorption for the solid PC surface. On the basis of these data, A. N. Frumkin, V. V. Batrakov and B. B. Damaskin with co-workers [50, 51] developed the theoretical background for the quantitative description of experimental results on EDL and the adsorption of organic molecules at PC electrodes. In essence, the physical meaning of modern theories on the PC structure of solid electrode surface involves its modeling description as a combination of different monocrystalline faces [51–53]. As a first approximation, these models may be classified into two groups [51]. The first group treats the PCE surface as consisting only of relatively large monocrystalline regions with linear parameter $y^* \gg 10$ nm (y^* is so-called characteristic length), which corresponds to macropolycrystallinity. Within these regions, both the compact and

the diffuse layers at different homogeneous areas can be viewed as independent ones, and accordingly

$$C_{PC}^{app} = \sum_i f_i X_i C_{Hi} C_{Di} / (C_{Hi} + C_{Di}) \tag{12}$$

where C_{PC}^{app} refer to unit area of the apparent surface of the electrode, X_i is the share of face i on the surface, f_i is roughness factor, C_{Hi} and C_{Di} are the inner layer and diffuse layer capacities for the plane i, respectively. This is the so-called model of independent diffuse layers (IDL) [51–53]. In terms of the second model, the PC surface comprises only from the small crystallites (y* < 10 nm) whose size is comparable to parameters of EDL [54, 55]. In the case of such electrodes, compact layers in different monocrystalline areas are considered independent, whereas the diffuse layer is common for the entire surface of PCE and depends on the charge $\bar{\sigma}_{PC} = R\sum_i X_i \sigma_i$ averaged over the PC electrode surface and

$$C_{PC}^{app} = \frac{C_D(\bar{\sigma}) R \sum_i X_i C_{Hi}}{C_D(\bar{\sigma}) + R \sum X_i C_{Hi}} \tag{13}$$

This model is called the model of common diffuse layer (CDL) [54]. The influence of the base boundaries between the individual monocrystalline regions at PC electrode surface on the EDL capacity has been theoretically discussed in Ref. [51].

A new approach to the electric double layer capacity properties on rough electrodes was given in the papers of Daikhin, Kornyshev and Urbakh [56–58]. It was shown that the competition between the Debye length and the characteristic sizes of roughness will modify the Gouy–Chapman result for the diffuse layer capacitance. Obviously, the limiting value of the capacitance at short Debye lengths (κ^{-1}) should follow the Gouy–Chapman result, but with replaced by $S_{real} = R \cdot S_{geom}$. Thus, the diffuse layer simply follows every bump or dip of the electrode, which surface looks flat at the Debye scales. In the limit of long Debye lengths (dilute solutions) the roughness can not be manifested in the capacitance which would obey the native Gouy–Chapman expression and the analogy with macroscopic capacitance can be used [56–58]. Thus, when the distance between plates is much greater than any scales of micro-roughness of the plates, the latter can not affect the capacitance. These two statements are based on the simple geometrical arguments, i.e. on the interplay between the scales of roughness and the Debye "yardstick". As shown by Daikhin, Kornyshev and Urbakh [56–58] the crossover between these two limits can be simulated by the equation

$$C = \tilde{R}(\kappa) C_{G\text{-}C} \tag{14}$$

where the roughness function, $\tilde{R}(\kappa)$, varies between $\tilde{R}(0) = 1$ and $\tilde{R}(\infty) = R > 1$; κ is the Gouy length, i.e. the inverse Debye length.

It was demonstrated [56–58] that the Parsons–Zobel plot is not the most convenient tool for the characterization of surface roughness and the more informative would be the plot of $\tilde{R}(\kappa)$ versus κ. According to [56–58] the roughness function can be expressed as

$$\tilde{R}(\kappa) \approx \left[\frac{1}{C_{exp}} - \frac{1}{C_i}\right]^{-1} \cdot \frac{1}{C_{G\text{-}C}} \tag{15}$$

where C_i is evaluated from the measurements at high electrolyte concentration according to Valette–Hamelin approach [53]. In the case of weak non-fractal surface roughness the two universal limiting approximations are valid: (14) at high electrolyte concentrations, when the Debye length κ^{-1} is shorter than the smallest characteristic length of surface inhomogeneity l_{min} (i.e. $\kappa^{-1} << l_{min}$), the roughness function can be expressed as

$$\tilde{R}(\kappa) \approx R\left\{1 - \frac{1}{2R}\frac{\langle H^2 \rangle}{\kappa^2}\right\} \tag{16}$$

where $\langle H^2 \rangle$ is the mean square curvature of surface.

Equation (16) shows that the roughness function $\tilde{R}(\kappa)$ approaches the geometrical roughness factor R at small Debye length κ^{-1} (large concentrations). With the increase of κ^{-1} (the decrease of concentration) it decreases with respect to R, and the correction is proportional to the square of the Debye length, i.e. it is inversely proportional to the charge carriers concentration.

In the range of large Debye lengths (low electrolyte concentrations) the roughness function can be expressed as

$$\tilde{R}(\kappa) \approx 1 + \frac{\kappa h^2}{L} - \kappa^2 h^2 \tag{17}$$

where h is the height of the characteristic size of roughness in the z-direction (h denotes the root mean square departure of the surface from flatness); L is the length which is in the order of the maximal correlation length l_{max} (l_{max} is a measure of the average distance between consecutive peaks and valleys on the rough surface). As expected, at very low electrolyte concentrations ($\kappa^{-1} \to \infty$; $\kappa^{-1} >> l_{max}$) the roughness of surface is not detectable in the capacitance and the first correction to the flat surface result is linear in κ [56–58].

3. RESULTS AND DISCUSSION

The adsorption parameters of various organic compounds were established. It was found that at the first approximation the adsorption process of various aliphatic compounds at the Sb, Bi and Cd electrodes can be described by the Frumkin–Damaskin adsorption theory [8]. The systematic trends of dependence of attractive constant, limiting surface concentration and the shift of zero charge potential, due to the displacement of surface monolayer of H_2O by adsorbate molecules, on the chemical nature of metal and organic compound structure were established and discussed.

3.1. Comparative Behaviour of Adsorption of Cyclohexanol, Cyclohexanone and Cyclohexancarboxylic Acid on Antimony and Bismuth Single Crystal Plane Electrodes

Adsorption of cyclohexanol (CH) [I, III, VI], cyclohexanone (CHN) [II] and cyclohexancarboxylic acid (CHCA) [IV] was studied by measuring the impedance in aqueous solution of surface-inactive electrolyte. The adsorption parameters were calculated by the Frumkin–Damaskin adsorption theory [8, 59]. The values of adsorption parameters indicate that the structure of the adsorption layer significantly depends both on the electrode surface and on the geometrical structure of the adsorbate molecules. The data in [IV] show the attraction constant a to grow upon going from Sb to Bi and from Cd to Zn [I–IV, 60, 61]. Higher values of C' and lower values of Γ_m and A for the $(\bar{1}0\bar{1})$, $(2\bar{1}\bar{1})$ and $(01\bar{1})$ faces and a decrease of E_N in the series of faces $(111)>(001)>(01\bar{1})>(2\bar{1}\bar{1})>(\bar{1}0\bar{1})$ points to a more pronounced horizontal component in the distribution of molecules on the abovelisted faces as compared with the (111) face. The value E_N is also dependent on the structure of the hydrocarbon radical and the functional group of organic compounds. The value E_N grows in the sequence CHCA< CH< CHN [I–IV], i.e. with growing effective dipole moment of the adsorbate.

In order to evaluate the role of the functional group in the adsorption bonding between an adsorbate molecule and the surface, included in [IV] the differences between the adsorption energy for the face studied (x) and the less active (111) face, $[(\Delta G^0_{ads})_{(x)} - (-\Delta G^0_{ads})_{(111)}]$. It follows from [IV] that the difference $[(\Delta G^0_{ads})_{(x)}]$ increases with growing adsorption activity of the adsorbate. Such a result suggests that, although adsorption of organic molecules is primarily governed by the squeezing out effect, the chemical interaction of the adsorbate with

the surface also plays some role. This conclusion is confirmed by the data in [IV] which shows that the difference between the potential of zero charge $E_{\sigma=0}$ and the cathodic maximum of the adsorbate adsorption E_{max} at c_{ads}=const decreases in the sequence of electrodes as follows: Sb($2\bar{1}\bar{1}$) < Sb($01\bar{1}$) < Sb(111) < Sb(001) < Bi($2\bar{1}\bar{1}$) < Bi($01\bar{1}$) < Bi(111) < Bi(001) < Cd(0001) < Cd($10\bar{1}0$) < Cd($21\bar{1}0$) < Zn(0001) < Zn($10\bar{1}0$) < Zn($21\bar{1}0$). According to modeling concepts mentioned in [62] this sequence corresponds to a decrease in hydrophilicity of the electrodes upon going from Zn($21\bar{1}0$) to Sb($2\bar{1}\bar{1}$). Anomalous position of the ($E^{max} - E_{\sigma=0}$) vs. log c dependences for the (111) faces of Sb and Bi is principally due to very strong structure of the adsorption layer, which breaks down at higher negative potentials.

Our analysis has shown that regularities of the adsorption of organic molecules to a considerable degree depend on the chemical nature and crystallographic structure of the electrode surface as well as on the nature and molecular structure of the solvent molecules and the adsorbate. Mutual effect of the electrode material on the surface state of molecules of the adsorbate and the solvent as well as the effect of the adsorbate and the solvent on the state of the electron gas in the near-surface layer do actually exist, and to disregard these interactions is unjustified. On the one hand, the existence of the effects that are characteristic of a polycrystalline surface is due to the anisotropy in double layer parameters of energy homogeneous regions of the polycrystalline surface. On the other hand, these effects are brought about by specific features in the structure of the polycrystalline surface (the size of homogeneous regions, their vicinal or nonsingular nature, anisotropy of energetistic characteristics).

3.2. Adsorption of Propanol, Normal Hexanol and Isomers of Butanol on Bismuth Single Crystal Plane Electrodes

The adsorption behaviour of *n*-propanol [X], *n*-butanol, *sec*-butanol, *iso*-butanol, *tert*-butanol [V] and *n*-hexanol [XI] at singular Bi(111), Bi(001) and Bi($01\bar{1}$) has been studied by cyclic voltammetry, impedance and chronocoulometry methods. The presented results indicate that the adsorption parameters of *n*-PA, *n*-HA and isomers of butanol depends on the crystallographic structure of Bi planes.

The comparison of the Gibbs energies of adsorption for various organic compounds shows that the adsorption activity of organic compounds at the Bi | solution interface increases in order *n*-PA < *n*-BA < CH < CHE < CHCA < BAC < PY as the adsorption of organic compound at the air | solution interface rises, except PY. The anomalous position of PY is mainly caused by the weak chemosorption of this compound at Bi planes [VII], as well as on Ag and Au

planes [20, 40–42, 46–48]. It was found that the difference between the adsorption activities of various Bi planes increases in the sequence of adsorbates *n*-PA < *n*-BA < CHE < CHCA < CH < BAC < *n*-HA if the adsorption activity of organic compound at the air | solution interface, as well as at the Bi | solution interface rises. This is mainly caused by the result that with the decreasing of the molar volume of adsorbate the changes in the adsorbed layer structure, caused by the adsorption of one molecule, decreases in comparison with the adsorption of more large surfactants. Comparison of the adsorption data of various aliphatic organic compounds shows that the value of ΔG_A^0 increases in the order of electrodes Zn($2\bar{1}\bar{1}0$) < Zn($10\bar{1}0$) < Zn(0001) < Ag(110) < Ga < Ag(100) < Ag(111) < Cd($11\bar{2}0$) < Cd($10\bar{1}0$) < Cd(0001) < Bi(111) < Bi(001) < Hg < Bi($2\bar{1}\bar{1}$) < Bi($01\bar{1}$) < Sb(111) < Sb(001) < Sb($2\bar{1}\bar{1}$) as the hydrophilicity of electrode surface decreases [8, 20, 46, 63].

The positive values of the lateral interaction constant a for *n*-PA, *n*-HA and isomers of butanol means that the surfactant–surfactant and water–water interactions are much more attractive than the surfactant–water interaction. At the potentials of the adsorption–desorption maxima, the molecular interaction parameter a^m decreases in the sequence of planes (001) ≥ (111) > ($01\bar{1}$) as the superficial density of planes increases and the limiting Gibbs adsorption decreases. The dependence of the attractive interaction constant a on E is approximately parabolic and the value of a increases in the sequence of electrodes Bi < Hg < Zn.

The value of a increases in the order of adsorbates *n*-PA < *tert*-BA < *n*-BA ≤ *sec*-BA ≤ *iso*-BA < *n*-HA < BAC [71] < CH as the molar volume of the adsorbate molecule increases, except *n*-HA. The lower value of a for *n*-HA molecules than that for CH and BAC probably indicates that the hydrocarbon tail of this compound in the adsorption layer is not linear or *n*-HA molecules will have the more tilted orientation. If we assume at the first approximation that the water–water and the organic compound–water interactions are independent of the aliphatic compound studied then the attraction between the adsorbed aliphatic alcohol molecules rises in the presented order of adsorbates.

The limiting Gibbs adsorption Γ_{max} increases in the order of electrodes Bi($01\bar{1}$) < Bi(111) < Bi(001) as the superficial density of planes decreases. The projected area S_{max} decreases and Γ_{max} increases in the order *n*-HA < *n*-BA ≤ CH < *n*-PA. The decrease of Γ_{max} and of the limiting potential shift E_N values and the increase of S_{max} as the number of carbon atoms in the aliphatic alcohol molecule increases, can be explained by an increasingly tilted orientation of *n*-HA molecules compared with *n*-PA at the single crystal Bi(001) and Bi(111) planes, as well as at Hg [VII, 8, 63] electrodes. Very low values of Γ_{max} and the E_N values for *n*-PA and *n*-HA at Bi($01\bar{1}$) plane will indicate that the *n*-PA and *n*-HA molecules probably have a practically flat orientation on the most active Bi plane investigated.

3.3. Adsorption of Pyridine on the (111), (001) and ($01\bar{1}$) Faces of Bismuth

The experimental investigations [VII] indicate that the shape of the differential capacity curves is very sensitive to the crystallographic structure of electrode surface studied. As in the case of cyclohexanol [III, 60, 61, 64, 65] and butanol isomers [V] studied the height of adsorption — desorption maxima increase in order of planes Bi($01\bar{1}$) < Bi(111) < Bi(001) as the superficial density of surface atoms decreases. The values of attractive coefficient a obtained from the height or width of these adsorption — desorption maxima are in a good agreement with one another and the values of a increase in the sequence of planes Bi($01\bar{1}$) < Bi(111) < Bi(001), i.e. with the decrease of the interfacial density of atoms.

As for Hg electrode [66], the maximum adsorption of pyridine (PY) on Bi single crystal planes takes place at the noticeably negatively charged electrode surface ($-\sigma \approx 9 \div 11$ μC cm^{-2}). The potential of maximum adsorption E_{max} shifts towards the more and more negative values of E if c_{PY} increases. The same tendency is valid for Hg electrodes [66]. If the PY adsorption at Ag or Au electrodes takes place, the E_{max} with increasing c_{PY} shifts towards the more positive values of E [20, 46–48, 67, 68]. The opposite sign of E_{max} for these two groups of metals suggest that the PY molecules assume opposite orientations at the noble metal (Au, Ag) and Hg-like (Hg, Bi) metal surfaces. The established values of the shift of zero charge potential E_N, due to the displacement of surface water monolayer by PY molecules are positive for Hg and Bi electrodes, indicating that the pyridine molecules are oriented with the aromatic hydrocarbon ring towards the electrode surface. The same orientation of benzene and toluene molecules is valid at polycrystalline bismuth [69] and Hg [66] electrodes. The limiting capacity C_1 decreases and the maximum surface coverage Γ_{max} increases in the sequence of metals Bi ≤ Hg < Ag < Au [20, 46–48, 66–68, 70] if the adsorption activity of electrode increases. The higher value of Γ_{max} for Bi(111), in comparison with the values of Γ_{max} for Bi(001)and Bi($01\bar{1}$) planes, indicates that at this plane the PY molecules have more pronounced vertical orientation than at the Bi(001) and Bi($01\bar{1}$) planes. The values of Γ_{max} for Bi(111), Bi(001) and Bi($01\bar{1}$) are an intermediate between the values expected for the flat ($\Gamma_{max} = 4.5 \cdot 10^{-10}$ mol cm^{-2}) and for the vertical ($\Gamma_{max} = 6.5 \cdot 10^{-10}$ mol cm^{-2}) orientation of PY [VII], and therefore it may be assumed that PY molecules have a tilted orientation at the surface of Bi single crystal planes.

The orientation of the adsorbate at the metal|solution interface is a result of competition between interactions of the functional group with the metal and the solution phase. The adsorption activity of aliphatic compounds increases in the sequence of metals Au < Ag < Bi ≤ Hg, as the hydrophilicity of electrodes decreases. Therefore, as the absolute value of free energy of adsorption of PY

on Au planes is noticeable higher (15–20 kJ mol^{-1}) than for Bi, Hg and Ag we can conclude that there is a weak chemical interaction of PY molecules with the surface atoms of Au [20, 67, 68]. The absolute value of free energy of adsorption of PY on Ag is somewhat lower (3–5 kJ mol^{-1}) than for Bi and Hg electrodes, which is caused mainly by the higher hydrophilicity of Ag electrodes. The absolute values of free energy of PY adsorption on Bi [69, 70] and Hg [66] are comparable and, accordingly, the differences between the metal–adsorbate interaction are not large and the adsorption activity of PY increases, when the hydrophilicity of electrodes decreases in sequence Bi(111) > Hg > Bi(001) > Bi(01$\bar{1}$). The adsorption activity of PY on bismuth planes increases (except Bi(111)) if the superficial density of atoms increases. Just as in the case of cyclohexanol [III, 60, 61], butyl acetate [71], butanol isomers [V] and n-hexanol [XI] adsorption, the basal plane Bi(111), where the surface atoms are chemically saturated, has the lowest adsorption activity of PY, and the most active one is the singular Bi(01$\bar{1}$) plane, where unsaturated covalent bonds are distributed uniformly over the whole surface. The decreasing of a and Γ_{max} values with the decreasing of the negative charge density of metal shows that the orientation of PY molecules becomes less vertical and therefore the nitrogen atoms are moving towards the electrode surface, if σ increases. In the case of positively charged Bi electrodes the weak chemical interaction ($-\Delta G^0_{Me\text{-}PY} \approx 2 \div 3$ kJ mol^{-1}) is possible, but it is very weak in comparison with the PY–Au interaction ($-\Delta G^0_{Me\text{-}PY}$ = 15–20 kJ mol^{-1}).

3.4. Influence of the Surface Pretreatment of Bismuth, Antimony and Cadmium Electrodes to the Adsorption Characteristics of Organic Compounds

The systematic investigations [VIII] at variously prepared (electrochemically polished (EP) single crystal Sb, Bi and Cd planes, cleaved (C) at the temperature of liquid nitrogen, Bi(111), Sb(111) and Cd(0001), electrochemically etched (ECE) at high anodic currents Bi single crystal electrodes, chemically etched (CE) Bi, Sb and Cd electrodes, mechanically polished (MP) with Al_2O_3 and therefore electrochemically polished or chemically etched electrodes, wedge-shape two plane model polycrystalline electrodes (WME) with known crystallographic heterogeneity, solid drop (DE) Bi and Sb electrodes with remelted (R) and without additional remelting (WR) of surface) electrodes show that the electric double layer and adsorption characteristics systematically depend on the geometrical structure of the electrode surface (roughness) and energetic inhomogeneity of electrode surface. It was found that the value of differential capacity at the potential of diffuse minimum increases (c_{el} = const)

if the surface roughness increases in the order of electrodes $(Bi_{DE})^R$ < EP single crystal < cut single crystal < ECE single crystal < DE^{WR} < CE single crystal < MP single crystal < MP and CE PC. The deviation from linearity of Parsons–Zobel plots, as well as the values of Parsons–Zobel factor f_{P-Z} increase in the same order. The values of the inner layer capacity, as well as the values of fitting coefficient increase in the same order of electrodes. In the case of ECE, CE and MP electrodes it is impossible to establish the "correct" values of the fitting coefficient f_{P-Z}, at which the $C_H(\sigma)$-curves will have smooth shape. The computer simulation of the electric double layer and adsorption data of many electrodes shows that in the case of $(Bi_{DE})^R$, EP single crystal planes, ECE single crystal planes and CE single crystal planes, the independent diffuse layer (IDL) model is valid. The linear parameter of homogeneous surface regions which prevail at the surface of EP, ECE and $(Bi^{DE})^R$ electrodes y*>> 10 nm. Probably, the surface of MP CE polycrystalline electrodes and $(Bi^{DE})^{WR}$ consists mainly of many very small crystallites, which y*≤ 10 nm, and therefore for these electrodes the common diffuse layer (CDL) model would be valid.

The so-called "Debye length dependent roughness function" has been calculated, and using the non-linear regression analysis the various surface roughness models (sinusoidal corrugation, random Gaussian roughness, periodical system on linear defects, rectangular grating proposed in [56–58]) have been simulated.

As found in the case of EP single crystal, the surface roughness is very small (R ≈ 1.03–1.06) and it is impossible to choose the "true" surface roughness model. According to the result of AFM studies, the surface of cut at the room temperature of self made $Bi(111)^C$ consists from monoatomic or somewhat higher steps (0.25÷0.55 nm) (root mean square roughness h = 0.29 nm) and from small terraces with the medium lateral characteristic length (linear parameter) y^* > 10 nm. The theoretical simulation of so prepared $Bi(111)^C$ and $Sb(111)^C$ surfaces shows that these surfaces might be an interesting object of the experimental studies with the aim to select out the "best" (more probable) theoretical roughness model. In some experiments the edl properties of electrochemically etched (ECE) Bi, Sb ($KI + HCl + H_2O$, $i_{etc} > 1.5$ A cm^{-2}) and Cd ($H_3PO_4 + H_2O$, $i_{etc} > 0.5$ A cm^{-2}) have been studied. Electron microscopic and AFM images demonstrate the surface pittings with linear parameter $y^* \geq 0.8$ μm on the surface of $Bi(111)^{ECE}$. The medium depth of these surface pittings varies from 2.5 to 250 nm depending on the time of electrochemical etching (30 sec. or 3 min.). In the region (bottom) of the surface pitting the steps with height from 0.3 nm to 10 nm have been found. The same situation was valid for $Sb(111)^{ECE}$ electrode. The surface of electrochemically etched $Bi(001)^{ECE}$ has a more complicated structure than $Bi(111)^{ECE}$ and on the $Bi(001)^{ECE}$ surface the pyramids have been found. The surface of chemically etched ($HNO_3 + NH_4NO_3 + H_2O$) $Bi(111)^{CE}$, as well as $Bi(001)^{CE}$, $Sb(111)^{CE}$ and $Cd(0001)^{CE}$ electrodes has a more rough structure in comparison with the

electrochemically etched, cut or electrochemically polished single crystal plane electrodes. The experimental AFM studies and theoretical simulations of MP and MP CE electrodes show that the model of random Gaussian roughness or the periodic system of linear defects [56] would be valid. But it must be noted that the future experimental investigations of differently prepared PC electrodes in converted electrolyte solutions and theoretical simulations of experimental results using various roughness models are inevitable.

3.5. Adsorption of Organic Compounds and Hydrophilicity of Bismuth, Cadmium and Antimony Electrodes

The systematic analysis of the influence of the chemical nature of electrode metal as well of hydrocarbon chain structure and functional group nature to the adsorption characteristics of organic compounds at various electrodes has been carried out in [IX]. The ingredients of the standard Gibbs energy of adsorption, such as Gibbs energy of adsorption at the air|solution interface; the increase of Gibbs energy of adsorption at metal|electrolyte interface caused by the addition of surface inactive electrolyte to the solution; the metal–organic compound interaction energy and the metal–water interaction energy have been calculated. It was found that the values of $\Delta(\Delta G_A^0) = \Delta G_A^0 - \Delta G_{sol}^0$ (where ΔG_A^0 was obtained by using the generalized Frumkin isotherm and corresponding to the standard state the unit mole fraction of the organic species in the bulk of solution and monolayer coverage $\theta_A = 1$ of ideal noninteracting adsorbate) very weakly depend on the chemical nature of adsorbate: on the chemical properties of the functional group and on the structure of adsorbed layer. This effect was explained by the weak dependence of $\Delta(\Delta G_A^0)$ on the value of $\Gamma_{A,max}$. The systematic analysis shows that the interaction energy of functional groups >C=O, –COOH, and –COOR with Bi, Cd, Sb, Hg and other "Hg-like" metals is very weak and is practically independent of the length of the hydrocarbon chain (except HCOOH and CH_3COOH). It was found that the standard Gibbs energy of adsorption of neutral organic compound which interacts weakly with metals can also be used as a measure of their hydrophilicity. In the case of higher aliphatic alcohols adsorption the more pronounced interaction of –OH group with surface atoms is possible [16, 19]. But this interaction is very weak in comparison with the interaction established in the case of aromatic compounds studied [63, 67, 72, 73].

The hydrophilicity of electrodes increases in the sequence of metals PC–Sb ≤ PC–Bi ≤ Hg ≤ In(Ga) ≤ PC–Sn < PC–Pb ≤ Ag(111) < Ga ≤ PC–Cd ≤ Zn(0001). However, the dependence of $\Delta G_{Me\text{-}H_2O}^0$ on the chemical nature of metal is very weak, and only for the chemically more different electrodes (for

example PC–Sb and Zn(0001)) the difference in $\Delta G^0_{\text{Me-H}_2\text{O}}$ values is noticeably higher than the summary error of obtaining the $\Delta(\Delta G^0_A)$ values. Approximately the same order of hydrophilicity of metal has been established in [I–XI, 6–8, 16, 17, 19, 20, 74–76]. According to the data of cyclohexanole adsorption the hydrophilicity of "mercury like" and single crystal plane electrodes increases in order $Sb(01\bar{1}) < Sb(001) < Sb(111) < Bi(01\bar{1}) < Bi(2\bar{1}\bar{1}) < Bi(001) < Bi(111) < Pb(111) < Pb(100) \leq Pb(110) < Sn(110) < Cd(0001) < Cd(10\bar{1}0) < Cd(11\bar{2}0) < Zn(0001) < Zn(10\bar{1}0) < Zn(11\bar{2}0)$ i.e. with the decrease of the reticular density of planes, except all Pb planes, Bi(111) and Sb(111). The anomalous position of Bi(111) and Sb(111) is mainly caused by the different electronic structure of this plane [I–XI, 6, 7, 77]. According to the data of aliphatic alcohol adsorption the hydrophilicity of single crystal planes increases in order $Bi(01\bar{1}) < Bi(001) < Bi(111) < Ag(111) < Ag(100) < Ag(110) < Zn(0001) < Zn(10\bar{1}0) < Zn(11\bar{2}0)$.

The hydrophilicity of electrodes has been tested using the work function values W_e into UHV as well as the electrochemical work function values W_e^*, obtained according to Trasatti's conception [17, 62, 74, 75, 78]. The established relative values of so-called interfacial parameter ΔX ($\Delta X = (\delta\chi_s + \delta\chi_M)_{Hg} - (\delta\chi_s + \delta\chi_M)_M$) increase in the order of electrodes $Hg \leq Sb < Bi < In(Ga) < Sn < Pb < Ga < Cd < Zn$. Using the established ΔX values and $\Delta(\Delta G^0_A)$ values for various aliphatic compounds for different metals the $\Delta(\Delta G^0_A)$, ΔX-dependences have been constructed. At the first approximation these dependences can be considered linear and $\Delta(\Delta G^0_A)$ decreases when the value of ΔX rises. But the slope of $\Delta(\Delta G^0_A)$,ΔX-plots decreases if the adsorption activity of organic compound at the air|solution interface decreases and for n-propanol the difference between $\Delta(\Delta G^0_A)$ values for chemically very different metals (for example, Sb and Zn(0001)) is only somewhat higher than the total error of obtaining the $\Delta(\Delta G^0_A)$ values. This result is in a very good agreement with the data obtained from $\Delta(\Delta G^0_A)$, ΔG^0_{air}-dependences.

As in the literature there are no work function data for single crystal electrodes, prepared from "mercury-like" metals with low melting point, the electrochemical work function values W_e^* and corresponding ΔX^* values have been obtained according to Trasatti's conception [17, 62, 74, 75, 78]. As found the value of ΔX^* increases in the order $Sb(2\bar{1}\bar{1}) < Sb(001) < Sb(111) < Bi(01\bar{1}) < Bi(2\bar{1}\bar{1}) < Bi(001) < Bi(111) < Sn(001) < Pb(112) \leq Pb(110) \leq Pb(100) < Pb(111) < Cd(0001) < Cd(10\bar{1}0) < Cd(11\bar{2}0) < Ag(111) < Ag(100) < Ag(110) < Zn(0001) < Zn(10\bar{1}0) < Zn(11\bar{2}0)$ as the interfacial density of planes decreases, except single crystal Pb planes, Bi(111) and Sb(111) [IX].

Using the obtained ΔX^* values and the data of cyclohexanole adsorption at different single crystal electrodes the $\Delta(\Delta G_A^0)$, ΔX^*-dependence has been constructed. As found, at the first approximation the adsorption behavior of cyclohexanole at Sb, Bi, Pb, Cd and Zn single crystal plane electrodes can be described by a common linear $\Delta(\Delta G_A^0)$, ΔX^*-dependence and accordingly the hydrophilicity of single crystal plane electrodes increases in the order Sb($2\bar{1}\bar{1}$) < Sb(001) < Sb(111) < Bi($01\bar{1}$) < Bi($2\bar{1}\bar{1}$) < Bi(001) < Bi(111) < Pb(111) ≤ Pb(100) ≤ Pb(110)< Cd(0001) < Cd($10\bar{1}0$) < Cd($11\bar{2}0$) < Zn(0001) < Zn($10\bar{1}0$) < Zn($11\bar{2}0$). Thus, the two different approximations used in this work give practically the same order of the hydrophilicity of electrodes.

It must be noted that the further extensive theoretical and experimental investigations at the metal|UHV, metal|solution and air|solution interfaces are inevitable to obtain the correct quantitative $\Delta G^0_{Me\text{-}H_2O}$ values for single crystal Sb, Pb, Sn, Cd, Ag and Zn electrodes.

3.6. Conclusions

1. Comparison of the Gibbs energies of adsorption for various organic compounds shows that the adsorption activity of organic compounds at the Bi|solution interface increases in order *n*-PA < *n*-BA < CH < CHE < CHCA < BAC as the adsorption of organic compound at the air|solution interface rises.
2. The value of attractive interaction constant a increases in the order of adsorbates *n*-PA < *tert*-BA < *n*-BA ≤ *sec*-BA ≤ *iso*-BA < *n*-HA < BAC [71] < CH as the molar volume of the adsorbate molecule increases, except *n*-HA and CH. The lower value of a for *n*-HA molecules than that for CH and BAC probably indicates that the hydrocarbon tail of this compound in the adsorption layer is not linear or *n*-HA molecules will have the more tilted orientation.
3. At the potentials of the adsorption–desorption maxima, the molecular interaction parameter a^m decreases in the sequence of planes (001) ≥ (111) > ($01\bar{1}$) as the superficial density of planes increases and the limiting Gibbs adsorption decreases. The dependence of the attractive interaction constant a on E is approximately parabolic and the value of a increases in the sequence of electrodes Bi < Hg < Zn.
4. The limiting Gibbs adsorption Γ_{max} increases in the order of electrodes Bi($01\bar{1}$) < Bi(111) < Bi(001) as the superficial density of planes decreases.

The projected area S_{max} decreases and Γ_{max} increases in the order *n*-HA < *n*-BA ≤ CH < *n*-PA.

5. The systematic analysis shows that the interaction energy of functional groups >C=O, –COOH, and –COOR with Bi, Cd, Sb, Hg and other "Hg-like" metals is very weak and is practically independent of the length of the hydrocarbon chain (except HCOOH and CH_3COOH). It was found that the standard Gibbs energy of adsorption of neutral organic compound which interacts weakly with metals can also be used as a measure of their hydrophilicity. In the case of higher aliphatic alcohols adsorption the more pronounced interaction of –OH group with surface atoms is possible [16, 19]. But this interaction is very weak in comparison with the interaction established in the case of aromatic compounds studied [63, 67, 72, 73].
6. According to the data of cyclohexanole adsorption the hydrophilicity of "mercury like" and single crystal plane electrodes increases in order Sb(01$\bar{1}$) < Sb(001) < Sb(111) < Bi(01$\bar{1}$) < Bi(2$\bar{1}\bar{1}$) < Bi(001) < Bi(111) < Pb(111) < Pb(100) ≤ Pb(110) < Sn(110) < Cd(0001) < Cd(10$\bar{1}$0) < Cd(11$\bar{2}$0) < Zn(0001) < Zn(10$\bar{1}$0) < Zn(11$\bar{2}$0) i.e. with the decrease of the reticular density of planes, except all Pb planes, Bi(111) and Sb(111). The anomalous position of Bi(111) and Sb(111) is mainly caused by the different electronic structure of this plane.
7. The hydrophilicity of electrodes increases in the sequence of metals PC–Sb ≤ PC–Bi ≤ Hg ≤ In(Ga) ≤ PC–Sn < PC–Pb ≤ Ag(111) < Ga ≤ PC–Cd ≤ Zn(0001).
8. It was found that the value of differential capacity at the potential of diffuse minimum increases (c_{el} = const) if the surface roughness increases in the order of electrodes $(Bi_{DE})^R$ < EP single crystal < cut single crystal < ECE single crystal < DE^{WR} < CE single crystal < MP single crystal < MP and CE PC. The deviation from linearity of Parsons–Zobel plots, as well as the values of Parsons–Zobel factor f_{P-Z} increase in the same order. The values of the inner layer capacity, as well as the values of fitting coefficient increase in the same order of electrodes.

REFERENCES

1. T. I. Borisova B. V. Ershler and A. N. Frumkin, *Zh. Fiz. Khim.*, **22**, 925 (1948).
2. T. I. Borisova and B. V. Ershler, *Zh. Fiz. Khim.*, **24**, 337 (1950).
3. A. Frumkin, *J. Res. Inst. Hokkaido*, **15**, 61 (1967).
4. U. Palm, *Trans. Tartu State Univ.*, **757**, 3 (1986).
5. A. N. Frumkin, M. P. Pärnoja, N. B. Grigoryev and U. V. Palm, *Elektrokhim.*, **10**, 1130 (1974).
6. A. Jänes, E. Lust and R. Pullerits, *Proc. IX Symp. On Double Layer and Adsorption at Solid Electrodes*, Tartu: Tartu Univ. 53 (1991).
7. E. Lust and J. Ehrlich, Proc. IX Symp. On Double Layer and Adsorption at Solid Electrodes, Tartu: Tartu Univ. 112 (1991).
8. B. B. Damaskin, O. A. Petrii and V. V. Batrakov, Adsorption of Organic Compounds on Electrodes, Plenum Press, New York, 1971.
9. E. J. Lust and U. V. Palm, *Sov. Electrochem.*, **24**, 227 (1988).
10. R. P. Armstrong, W. P. Race and H. R. Thirsk, *J. Electroanal. Chem.*, **16** 517 (1968).
11. A. Frumkin, Potentsialy Nulevoga Zaryada, Nauka, Moskva, 1979 p. 206.
12. A. Frumkin, *Z. Physic*, **116**, 466 (1925).
13. A. Frumkin, *Z. Physic*, **35**, 792 (1926).
14. A. Frumkin, *Naturwiss*, **7**, 235 (1928).
15. E. J. Lust and U. V. Palm, *Elektrokhim.*, **21**, 1186 (1985).
16. L. M. Doubova, S. Valcher and S. Trasatti, *J. Electroanal. Chem.*, **376**, 73 (1994).
17. S. Trasatti, *Electrochim. Acta*, **37**, 2137 (1992).
18. G. Pezzatini, R. Moncelli, M. Innocenti and R. Guidelli, *J. Electroanal. Chem.*, **295**, 275 (1990).
19. M. L. Foresti, M. Innocenti and R. Guidelli, *J. Electroanal. Chem.*, **376**, 85 (1994).
20. J. Lipkowski and L. Stolberg, in J. Lipkowski and P. N. Ross (Eds.), Adsorption of Molecules at Metal Electrodes, VCH, New York, p. 171.
21. M. R. Moncelli, M. L. Foresti and R. Guidelli, *J. Electroanal. Chem.*, **295** 225 (1990).
22. A. N. Frumkin, .B. B. Damaskin and Yu. M. Gerovitch, Dokl. Akad. Nauk SSSR **158** (1964) 706.
23. O. A. Gusakova, B. B. Damaskin, N. V. Fedorovich and S. D. Pirozkov, *Elektrokhim.*, **8**, 1409 (1972).
24. A. V. Chizov, S. D. Pirozkov, B. B. Damaskin, in: A. N. Frumkin, B. B. Damaskin (Eds.), Adsorption and Electrical Double Layer in Electrochemistry, Nauka, Moscow, 1972, p. 59.
25. B. B. Damaskin, E. V. Stenina, V. A. Yusupova, and N. V. Fedorovich, *Elektrokhim.*, **10**, 1112 (1974).
26. O. A. Gusakova, B. B. Damaskin and N. V. Fedorovich, *Elektrokhim.*, **9**, 1134 (1973).
27. A. V. Vosekalnš, Ph.D. Thesis, University of Moscow, 1975.
28. L. D. Kliukina, B. B. Damaskin, Proc. Akad. Nauk SSSR, Ser. Khim. (1963) 1022.
29. M. Beltowska-Brzezinska, E. Dutkiewicz, P. Skoluda, *J. Electroanal. Chem.*, **181**, 235 (1984).

30. R. Holze, M. Beltowska-Brzezinska, *Electrochim. Acta*, **30**, 937 (1985).
31. R. Holze, M. Beltowska-Brzezinska, *J. Electroanal. Chem.*, **201**, 387 (1986).
32. R. I. Tucceri, D. Posadas, *Electrochim. Acta*, **32**, 27 (1987).
33. E. Dutkiewicz, P. Skoluda, A. Hamelin, *J. Electroanal. Chem.*, **248**, 209 (1988).
34. E. Dutkiewicz, P. Skoluda, A. Hamelin, *J. Electroanal. Chem.*, **240**, 291 (1988).
35. J. Lipkowski, C.N. Van Houng, C. Hinnen, R. Parsons, J. Chevalet, *J. Electroanal. Chem.*, **143**, 375 (1983).
36. J. Richter, J. Lipkowski, *Langmuir*, **2**, 630 (1988).
37. J. Richter, J. Lipkowski, *J. Electroanal. Chem.*, **251**, 217 (1988).
38. A. Iannelli, J. Richter, L. Stolberg, J. Lipkowski, *J. Plating Surf. Finish.*, **77**, 47 (1990).
39. M. Petit, C. N. Van Houng, T. Clavilier, *C. R. Acad. Sci. Ser. C.*, **266**, 300 (1968).
40. A. Hamelin, *J. Electroanal. Chem.*, **144**, 365 (1983).
41. A. Hamelin, G. Valette, *C. R. Acad. Sci. Ser. C.*, **267**, 127 (1968).
42. A. Hamelin, G. Valette, *C. R. Acad. Sci. Ser. C.*, **267**, 211 (1968).
43. T. Vitanov, A. Popov, *Elektrokhim.*,**10**, 1373 (1974).
44. T. Vitanov, A. Popov, *Elektrokhim.*,**12**, 319 (1976).
45. A. Popov, O. Velev and T. Vitanov, *J. Electroanal. Chem.*, **256** 405 (1988).
46. A. Hamelin, S. Morin, J. Richter, J. Lipkowski, *J. Electroanal. Chem.*, **272**, 241 (1989).
47. A. Hamelin, S. Morin, J. Richter, J. Lipkowski, *J. Electroanal. Chem.*, **285**, 249 (1990).
48. A. Hamelin, S. Morin, J. Richter, J. Lipkowski, *J. Electroanal. Chem.*, **304**, 195 (1991).
49. M. Salve, A. Alumaa and U. Palm, *Trans. Tartu State Univ.*, **289**, 54 (1971).
50. A. N. Frumkin, V. V. Batrakov and A. I. Sidnin, *J. Electroanal. Chem.*, **39**, 225 (1972).
51. V. V. Batrakov and B. B. Damaskin, *J. Electroanal. Chem.*, **65**, 361 (1975).
52. G. Valette and A. Hamelin, *J. Electroanal. Chem.*, **45**, 301 (1973).
53. U. V. Palm, M. P. Pärnoja and N. B. Grigoryev, *Elektrokhim.*, **13**, 1074 (1977).
54. I. A. Bagotskaya, B. B. Damaskin and M. D. Levi, *J. Electroanal. Chem.*, **115**, 189 (1980).
55. M. A. Vorotyntsev, *Elektrokhim.*, **17**, 197, 576, 1018 (1981).
56. L. I. Daikhin, A. A. Kornyshev, M. A. Urbakh, *Phys. Rev.* E **53**, 6192 (1996).
57. L. I. Daikhin, A. A. Kornyshev, M. A. Urbakh, *Proc. Of the Baltic Conf. On Interfacial Electrochemistry*, Tartu, p. 57 (1996).
58. L. I. Daikhin, A. A. Kornyshev, M. A. Urbakh, *Electrochim. Acta* **42**, 2853 (1997).
59. B. B. Damaskin, *Elektrokhim.*, **6**, 1135 (1970).
60. E. J. Lust and U. V. Palm, *Elektrokhim.*, **21**, 1381 (1985).
61. E. J. Lust and U. V. Palm, *Elektrokhim.*, **24**, 243 (1988).
62. A. Frumkin, B. Damaskin, N. Grigoryev and I. Bagotskaya, *Electrochim. Acta*, **19**, 69 (1974).
63. B. Damaskin, A. Frumkin and A. Chizov, *J. Electroanal. Chem.*, **28** 93 (1970).
64. E. J. Lust and U. V. Palm, *Sov. Electrochem.*, **22**, 378 (1986).
65. E. J. Lust and U. V. Palm, *Sov. Electrochem.*, **22**, 383 (1986).
66. D. Rolle and J.W. Schultze, *J. Electroanal. Chem.*, **229**, 141 (1987).
67. A. Iannelli, J. Merza and J. Lipkowski, *J. Electroanal. Chem.*, **376**, 49 (1994).

68. J. Lipkowski, L. Stolberg, P.–F. Yang, B. Pettinger, S. Mirwald, F. Henglein and D. M. Kolb, *Electrochim. Acta*, **39**, 1057 (1994).
69. A. P. Alumaa and U. V. Palm, *Elektrokhim.*, **8**, 471 (1972).
70. U. V. Palm, B. B. Damaskin, *Itogi Nauki i Tekh. Ser. Elektrokhim.*, **12**, 99 (1977).
71. E. J. Lust, J. J. Ehrlich and U. V. Palm, *Sov. Electrochem.*, **22**, 695 (1986).
72. B. B. Damaskin, and A. V. Chizov, *Elektrokhim.*, **6**, 1741 (1970).
73. U. V. Palm, B. B. Damaskin, *Itogi Nauki i Tekniki. Electrokhim.*, **12**, 99 (1977).
74. S. Trasatti, L. M. Doubova, *J. Chem. Faraday Trans.*, 91, 3311 (1995).
75. S. Trasatti, *J. Electroanal. Chem.*, **33**, 351 (1971).
76. I. A. Bagotskaya, Itogi Nauki i Tekh. Ser. Elektrokhim., **23**, 60 (1986).
77. B. B. Damaskin, *Elektrokhim.*, **1**, 63 (1965).
78. S. Trasatti, *Electrochim. Acta*, **37**, 2137 (1992).

ORGAANILISTE ÜHENDITE ADSORPTSIOON ANTIMON-, VISMUT- JA KAADMIUM-ELEKTROODIDEL

Kokkuvõte

Käesolevas töös uuriti elektrokeemilise impedantsi, kronokulonomeetria, elektronmikroskoopia ja AFM-meetodiga monokristalsete ning erisuguse pinnatöötlusega Bi-, Sb- ja Cd-elektroodide faasidevahelise pindkihi omadusi. Täheldati pinna eelneva töötluse mõju tahke faasi pinna karedusele ning energeetilisele ebaühtlusele.

Uuriti tsükloheksanooli (CH) [I, IV, VI], tsükloheksanooni (CHE) [II], tsükloheksaankarboksüülhappe (CHCA) [III], butanooli isomeeride (BA) [V], püridiini (PY) [VII], n-propanooli (n-PA) [X] ja n-heksanooli (n-HA) [XI] adsorptsiooni seaduspärasusi Sb ja Bi monokristalli eri tahkudel. Adsorptsiooni parameetrid arvutati Frumkini–Damaskini teooria alusel. Tulemustest järeldati, et adsorptsioonikihi ehitus sõltub oluliselt elektroodi pinnast ja adsorbaadi molekulide geomeetrilisest struktuurist. Erinevate orgaaniliste ühendite Gibbsi adsorptsioonienergiate võrdlemisel jõuti järeldusele, et orgaaniliste ühendite adsorptsiooniaktiivsus Bi|lahus-piirpinnal suureneb reas *n*-PA< *n*-BA< CH< CHE< CHCA< PY, samas reas kasvab ka adsorptsioon õhk|lahus-piirpinnal, v.a. püridiinil. PY anomaalne asend on tingitud peamiselt selle ühendi osalisest kemosorptsioonist Bi tahkudel. Leiti, et Bi tahkude adsorptsiooniliste aktiivsuste erinevus suureneb adsorbaatide reas *n*-PA< *n*-BA< CHE< CHCA< CH< *n*-HA. Alifaatsete ühendite võrdlusel leiti, et Gibbsi energia ΔG_A^0 suureneb järgnevas elektroodide reas: Zn($2\bar{1}\bar{1}0$) < Zn($10\bar{1}0$) < Zn(0001) < Ag(110) < Ga < Ag(100) < Ag(111) < Cd($11\bar{2}0$) < Cd($10\bar{1}0$) < Cd(0001) < Bi(111) < Bi(001) < Hg < Bi($2\bar{1}\bar{1}$) < Bi($01\bar{1}$) < Sb(111) < Sb(001) < Sb($2\bar{1}\bar{1}$), seega elektroodide pinna hüdrofiilsuse vähenedes. Leiti, et atraktsioonikoefitsent *a* suureneb adsorbaatide reas *n*-PA< *n*-BA< *n*-HA< CH, seega adsorbaadi molekuli moolruumala suurenedes, välja arvatud n-heksanoolil. Viimase madalamad *a* väärtused näitavad, et nende ühendite süsivesinikahel on adsorptsioonikihis mittelineaarne või osaliselt viltu orienteeritud. Kui esimeses lähenduses võeti, et interaktsioonid vesi–vesi ja orgaaniline ühend–vesi ei sõltu uuritud orgaanilistest ühenditest, siis leiti, et adsorbeerunud alifaatse alkoholi molekulide vaheline atraktsioon kasvab eespool kirjeldatud adsorbaatide reas.

Elektrokeemilise impedantsi, elektronmikroskoopia- ja AFM-meetodiga uuriti erisuguse pinnatöötlusega (elektrokeemiliselt ja keemiliselt poleeritud, vedela lämmastiku temperatuuril lõhestatud, elektrokeemiliselt ja keemiliselt söövitatud, mehhaaniliselt poleeritud ja seejärel keemiliselt söövitatud) Bi-, Sb- ja Cd-elektroodide faasidevahelise piirkihi omadusi [VIII]. Täheldati pinna eel-

neva töötluse mõju tahke faasi pinna karedusele ja energeetilisele ebaühtlusele ning viimase süstemaatilist mõju elektrilise kaksikkihi karakteristikutele, nagu diferentsiaalmahtuvus, difuusse kihi miinimumi potentsiaal, Parsonsi–Zobeli faktor, elektrilise kaksikkihi tiheda osa mahtuvus, pinna fraktaalsuse aste ning karedusfaktor. Vastavalt Daikhini–Kornysevi–Urbakhi mudelile arvutati erinevalt töödeldud elektroodide jaoks välja Debye ekraneerimispikkusest sõltuv karedusfunktsioon. Saadud andmete põhjal järeldati, et Debye ekraneerimispikkusest sõltuvat karedusfunktsiooni võib suhteliselt kontsentreeritud elektrolüüdilahuste korral ($0{,}03\text{M} < c_{NaF} < 0{,}1\text{M}$) lähendada Gaussi juhusliku pinnakareduse mudelile või lineaarsete defektide perioodilise süsteemi mudelile. Elektrokeemiliselt ja keemiliselt poleeritud monokristalsete Bi-, Sb- ja Cd-elektroodide karedus on väga väike, mistõttu osutus võimatuks eristada pinna karedust kirjeldavaid eri mudeleid ning seega kindlaks teha nende rakendatavus suhteliselt siledate pindade korral. Mitmesuguste teoreetiliste mudelite abil arvutati polükristalsete elektroodide pinnal prevaleerivate homogeensete alade ligikaudsed lineaarmõõtmed, mida võrreldi elektronmikroskoopia meetodil saadud tulemustega. Leiti, et AFM-meetodil määratud monokristalse ala keskmistatud pikkus on heas kooskõlas teoreetiliselt arvutatuga.

Käesolevas töös [IX] analüüsiti süstemaatiliselt elektroodi metalli, süsivesinikahela struktuuri ja funktsionaalse rühma mõju orgaaniliste ühendite adsorptsiooni seaduspärasustele. Analüüs näitas, et >C=O, –COOH ja –COOR interaktsioonienergia kõrge ülepingega metallide jaoks on väga nõrk ja praktiliselt sõltumatu süsivesinikahela pikkusest (v.a. HCOOH ja CH_3COOH).

Elektroodide hüdrofiilsuste võrdlemisel kasutati elektroni väljumistööde väärtusi vaakumis W_e. Leitud faasidevaheline parameeter ΔX, mis iseloomustab lahusti toimet metallile, suureneb elektroodide reas Hg ≤ Sb < Bi < In(Ga) < Sn < Pb < Ga < Cd < Zn. Et kirjanduses praktiliselt puuduvad elektroni väljumistöö väärtused monokristalsete elektroodide jaoks, siis leiti vastavalt Trasatti kontseptsioonile [17, 62, 74, 75, 78] elektrokeemilised väljumistöö väärtused We^* ja vastavad suurused ΔX^*. Leiti, et ΔX^* suureneb monokristalli tahu retikulaarse tiheduse vähenedes (v.a. Pb monokristalli tahud, Bi(111) ja Sb(111)) reas $Sb(2\bar{1}\bar{1}) < Sb(001) < Sb(111) < Bi(01\bar{1}) < Bi(2\bar{1}\bar{1}) < Bi(001) < Bi(111) < Sn(001) < Pb(112) \leq Pb(110) \leq Pb(100) < Pb(111) < Cd(0001) < Cd(10\bar{1}0) < Cd(11\bar{2}0) < Ag(111) < Ag(100) < Ag(110) < Zn(0001) < Zn(10\bar{1}0) < Zn(11\bar{2}0)$. Selgus, et kaks täiesti erinevat mudelit [IX] annavad praktiliselt sama elektroodide hüdrofiilsuse rea, mis näitab, et vee adsorptsioonienergia kasvab eeltoodud reas.

ACKNOWLEDGMENTS

The present study was performed at the Institute of Physical Chemistry of Tartu University.

I wish to express my greatest gratitude to my doctoral advisor Professor Enn Lust for continuous support and assistance throughout the years of our collaboration.

I am also very thankful to M. Sc. Karmen Lust for the help needed for the maintenance of computers.

I wish to thank all the staff of our institute for the very helpful and warm atmosphere.

The support received from Estonian Science Foundation, Open Estonia Foundation and Individual Science Foundation (G. Soros Foundation) are gratefully acknowledged.

PUBLICATIONS

I

Reprinted from the *Russian Journal of Electrochemistry* 30, No. 3,
E. Lust, A. Jänes, Structure of the Electrical Double Layer and
Adsorption of Cyclohexanol on the Faces
of an Antimonium Single Crystal, pages 321–328,

Russian Journal of Electrochemistry, Vol. 30, No. 3, 1994, pp. 321 - 328. Translated from Elektrokhimiya, Vol. 30, No. 3, 1994, pp. 357 - 365.

Structure of the Electrical Double Layer and Adsorption of Cyclohexanol on the Faces of an Antimonium Single Crystal

E. J. Lust and A. A.-J. Jänes

Tartu University, Ulikooli 18, Tartu, EE 2400 Estonia

Received July 20, 1993

Abstract – Impedance measurements were used to study the characteristics of the double-layer structure and the cyclohexanol adsorption on the faces of an antimonium single crystal and the polycrystalline surface of a solid-drop antimonium electrode. The values of zero-charge potential, compact-layer capacitance, and also cyclohexanol adsorption parameters were determined for faces $(01\bar{1})$, (111), (001), and $(2\bar{1}\,\bar{1})$ of an antimonium single crystal. It was found that the spread of zero-charge potentials and parameters of cyclohexanol adsorption on the faces of an antimonium single crystal is somewhat higher than the spread for corresponding bismuth single-crystal faces.

INTRODUCTION

In this work, we continued the studies started in [1 - 7] and, using the impedance method, studied the characteristics of the double-layer structure on the $(01\bar{1})$ and $(2\bar{1}\,\bar{1})$ faces of an antimonium single crystal in order to obtain a deeper understanding of the role of the electronic and crystallographic surface structures and reticular density of the faces of metal single crystals in electrochemical processes. We also studied the cyclohexanol (CH) adsorption on singular *F*-faces (001) and (111) and non-singular *K*-face $(2\bar{1}\,\bar{1})$ of a Sb single crystal, as well as a polycrystalline solid-drop antimonium electrode (DAE), the surface of which was additionally remelted (DAE-I) or remained unchanged (DAE-II). We chose antimonium electrodes and Sb single-crystal faces as the subject for our study because of the low symmetry of the Sb crystallographic structure (rhombohedral syngony) and the presence of two types of bonds, i.e., semiconductor intralayer (s^2p^3 valent state) and metallic interlayer bonds (with the participation of hybrid sp^3d^2 orbitals) between the atoms in the lattice, which leads to a sharp anisotropy both of volume and surface properties of individual crystallographic faces of Sb [8 - 10]. The presence of covalent semiconductor bonds between the atoms in the Sb and Bi lattices fixes the position of the surface atoms more rigidly than in the case of typical metals (for example, Au and Pb); therefore, the surface structure of Sb and Bi single-crystal faces proves to be more stable compared to Au single-crystal faces [11]. The high reproducibility of experimental data for the faces of Sb and Bi single crystals [4 - 6] is precisely due to their stable surface structure.

EXPERIMENTAL

Single-crystal and polycrystalline Sb electrodes were made using the method described in [1 - 7, 12 - 14]. All the reactants used were purified by the repeated rectification (water, cyclohexanol) or calcination (salts of high purity) at high temperatures [2]. A saturated calomel electrode (SCE) served as the reference electrode.

DOUBLE-LAYER STRUCTURE ON THE FACES OF AN ANTIMONIUM SINGLE CRYSTAL

As an illustration, Fig. 1 shows the dependences of the differential capacitance C on the electrode potential

Table 1. Double-layer characteristics for the faces of a Sb single crystal and a solid-drop antimonium electrode (DAE)

Electrode	$E_{q=0}^{\text{CAU}}$, V	$C_H^{q=0}$, μF/cm²	$C_H^{q\neq 0}$, μF/cm²	f_{P-Z}	$\frac{\partial E_{min}}{\partial \log c}$
$(01\bar{1})$	−0.380 ± 0.01	25.9 ± 0.9	15.8 ± 0.6	1.18 ± 0.05	30
$(2\bar{1}\,\bar{1})$	−0.330 ± 0.02	25.0 ± 1.0	15.4 ± 0.5	1.25 ± 0.07	50
(001) [6]	−0.360 ± 0.005	26.2 ± 0.5	16.4 ± 0.3	1.04 ± 0.02	20
(111) [6]	−0.450 ± 0.005	23.0 ± 0.4	15.2 ± 0.3	1.06 ± 0.02	10
DAE [13, 14]	−0.41 ± 0.01	25.6 ± 0.4	14.6 ± 0.3	1.03	

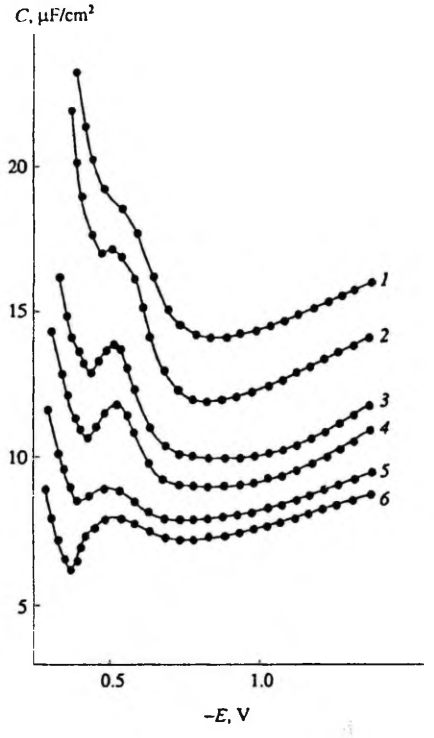

Fig. 1. C versus E-curves for face $(2\bar{1}\bar{1})$ of single crystal Sb at c_{NaF}; M: (*1*) 0.1; (*2*) 0.05; (*3*) 0.02; (*4*) 0.01; (*5*) 0.005; and (*6*) 0.002.

E for singular K-face $(2\bar{1}\bar{1})$ of a Sb single crystal in acidic (0.0005 M HCl) solutions of NaF. Similar to those on faces (001) and (111) [6, 7], the capacitance curves of faces $(01\bar{1})$ and $(2\bar{1}\bar{1})$ exhibit a well-pronounced minimum in the potential region from –0.30 to –0.60 V. The depth of this minimum decreases as the NaF concentration in the solution increases. However, in contrast to the singular F-face Sb(111) and Bi(111) and similar to faces (001), $(\bar{1}0\bar{1})$, $(01\bar{1})$, and $(2\bar{1}\bar{1})$ of a Bi single crystal [2 - 4], the potential of the diffuse minimum E_{min} for Sb(001), Sb$(01\bar{1})$, and Sb$(2\bar{1}\bar{1})$ shifts to negative values by 20, 30, and 60 mV, respectively, in the NaF concentration region c_{NaF} = 0.001 - 0.02 M. Since the dependence of E_{min} on c_{NaF} is mainly determined by the weak specific adsorption of F^- anions on these faces in the vicinity of $E_{q=0}$, Table 1 shows the $E^{extr}_{q=0}$ data obtained from the dependence of E_{min} on $(c)^{1/2}$ by extrapolating the found line to $(c)^{1/2} = 0$.

A comparison of the data of Table 1 with those of [2 - 4] shows that the scattering of $E_{q=0}$ values for the faces of an antimonium single crystal is somewhat higher than the scattering in the case of bismuth single-crystal faces and is caused by the increase in the electronic and crystallographic anisotropy when one goes from Bi to Sb.

It is evident from the data shown in Table 1 that, as in the case of bismuth single-crystal faces [2 - 4], the dependence of $E^{extr}_{q=0}$ on the recticular density for faces (001), $(01\bar{1})$, and $(2\bar{1}\bar{1})$ of a Sb single crystal is weak ($\Delta E^{extr}_{q=0} \leq 50$ mV) at the same electronic configuration. However, when comparing faces (001), $(2\bar{1}\bar{1})$, and $(01\bar{1})$ with the basal face (111), the difference $\Delta E^{extr}_{q=0}$ amounts to 70 - 120 mV. This is probably due to the different surface states of the mentioned faces, i.e., to the fact that the surface atoms of faces (001), $(01\bar{1})$, and $(2\bar{1}\bar{1})$ have unsaturated covalent bonds (s^2p^3-valent state), while all covalent bonds of the surface atoms of face (111) are chemically saturated, and these atoms tend to form bonds by means of hybrid sp^3d^2-orbitals [8 - 10].

On the basis of E_{min} values at different c_{NaF}, the $\partial E_{min}/\partial \log c$-dependences, which are practically linear, were plotted. As in the case of Bi single-crystal faces [2 - 4], the nonsingular face $(2\bar{1}\bar{1})$ of a Sb single crystal demonstrates the highest adsorption activity, which can be attributed to the stronger adsorption of F^- anions on a stepped surface than on a smooth surface. This result also agrees with the data of [1, 15], in which the authors found that the stepped surface of the face (110) of an Ag single crystal exhibits the highest adsorption activity with respect to F^- anions. However, according to the $\partial E_{min}/\partial \log c$ values in Table 1, the F^- adsorption on antimonium single-crystal faces is relatively weak, and the effect of the discreteness does not show up.

On the basis of experimental C values at various surface charges q = const, the so-called Parsons–Zobel dependences were plotted. For faces $(01\bar{1})$ and $(2\bar{1}\bar{1})$, the obtained dependences are linear in the concentration intervals $0.003 \leq c_{NaF} \leq 0.1$ M and $0.007 \leq c_{NaF} \leq 0.1$ M, respectively. The deviation of the C^{-1}, C_d^{-1}-dependences from linearity for faces $(2\bar{1}\bar{1})$ and $(01\bar{1})$, as well as the increase of the reciprocal of the slope f_{P-Z} for these faces compared with the data for faces (111) and (001) are caused by the substantially weaker specific adsorption of F^- anions on faces $(01\bar{1})$ and $(2\bar{1}\bar{1})$ and also by the crystallographic heterogeneity of face $(2\bar{1}\bar{1})$. In this case, it should be noted that the deviation of C^{-1}, C_d^{-1}-plots from linearity is also due to experimental errors [4, 16], but, in our opinion, the different behavior of various Sb faces is probably mainly due to their different surface characteristics.

As in the case of faces (001) and (111) of a Bi single crystal, for faces Sb(01$\bar{1}$) and Sb(2$\bar{1}\,\bar{1}$), a small decrease in the f_{P-Z} value is observed with the increase in the ac frequency ν and negative value of q. This result points to the fact that the increased f_{P-Z} values at $q = 0$ and $q > 0$ are caused by the weak specific adsorption of F^- anions on faces (01$\bar{1}$) and (2$\bar{1}\,\bar{1}$) of a Sb single crystal. Therefore, the adsorption activity of F^- anions increases in the sequence (111) < (001) < (01$\bar{1}$) < (2$\bar{1}\,\bar{1}$), i.e., [with the exception of face (111)] as the reticular density of the faces increases in the sequence (001) < (111) < (01$\bar{1}$) < (2$\bar{1}\,\bar{1}$).

From C versus E-curves, on the basis of the Gouy–Chapman–Stern–Grahame (GCSG) model [1, 16] and using the technique of [17], we calculated the dependences of the compact-layer capacitance C_H on the surface charge q for faces (01$\bar{1}$) and (2$\bar{1}\,\bar{1}$) of a Sb single crystal in the interval of c_{NaF} from 0.1 to 0.01 M. According to data of Fig. 2 and Table 1, just as in the case of Bi single-crystal faces [2 - 4], the tendency holds for the decrease of the compact-layer capacitance ($C_H^{q<0}$ at $q \ll 0$ and $C_H^{q=0}$ at $q = 0$) in the sequence (001) > (01$\bar{1}$) ≥ (2$\bar{1}\,\bar{1}$) > (111). Therefore, except for face (111), a rigorous rule [18] holds that is theoretically based on the model of rigid spheres and states that the more close-packed faces have the lowest capacitance of the metal–electrolyte contact. Bearing in mind that Sb is a semi-metal, the anomalous position of the C_H versus q-curve for face (111), as compared to faces (01$\bar{1}$) and (2$\bar{1}\,\bar{1}$) of a Sb single-crystal, is probably associated with different semiconductive properties of individual faces, i.e., with the fact that apart from the real capacitance of the compact layer, the C_H values also include the capacitance of the metal phase, which depends on the crystallographic orientation of the faces. The lower values of the compact-layer capacitance for the faces of a Sb single crystal compared to the corresponding value for Bi are, as in the case of polycrystalline electrodes [2 - 4, 6, 7, 14], due to the less pronounced hydrophily of the surface of Sb electrodes and to the more pronounced influence of the metal-phase capacitance in the case of Sb.

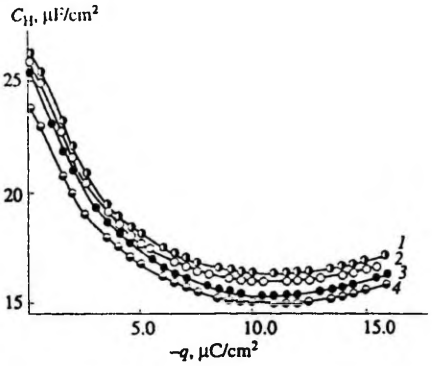

Fig. 2. C_H versus q-curves in 0.1 M NaF for faces of single crystal Sb: (*1*) (001); (*2*) (01$\bar{1}$); (*3*) (2$\bar{1}\,\bar{1}$); and (*4*) (111).

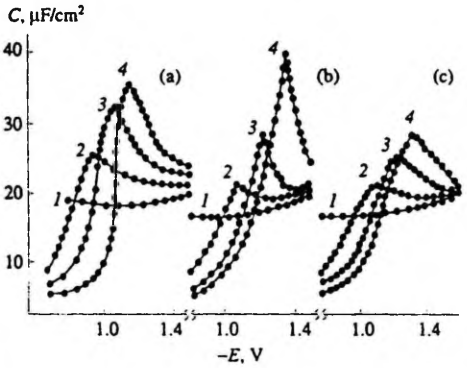

Fig. 3. C versus E-curves for faces: (a) Sb(001), (b) Sb(111), and (c) Sb(2$\bar{1}\,\bar{1}$) in (*1*) 0.1 M NaF and with additions of CH: (*2*) 0.02; (*3*) 0.05; and (*4*) 0.1 M.

CYCLOHEXANOL ADSORPTION ON THE FACES OF AN ANTIMONIUM SINGLE CRYSTAL

Figure 3 shows the dependences of the capacitance C on the potential E on faces Sb(001), Sb(111), and Sb(2$\bar{1}\,\bar{1}$) in the presence of CH in different concentrations in 0.1 M aqueous solutions of NaF. It is evident from Figs. 3a - 3c that C versus E-curves on Sb(001), Sb(111), and Sb(2$\bar{1}\,\bar{1}$) have the usual shape with sharp cathodic adsorption–desorption maxima at the potentials E^{max} and with the height increasing in the sequence (2$\bar{1}\,\bar{1}$) < (001) < (111). A similar tendency was also observed in the case of Bi single-crystal faces [19 - 21].

According to Fig. 3, an increase in the energy nonuniformity of the Sb-electrode surface leads to a decrease in the height of the adsorption–desorption peaks and an increase in their width in the sequence (111) < (001) < (2$\bar{1}\,\bar{1}$) and, therefore, to a decrease in the effective value of the attraction constant a, which is calculated from the width of the cathodic maxima of the CH adsorption in the sequence (111) > (001) > (2$\bar{1}\,\bar{1}$) for the faces of a Sb single crystal. The attraction constant at the potential of the maximum adsorption a_m decreases in the same sequence. Similar to the case of bismuth single-crystal faces, the dependence of a on E

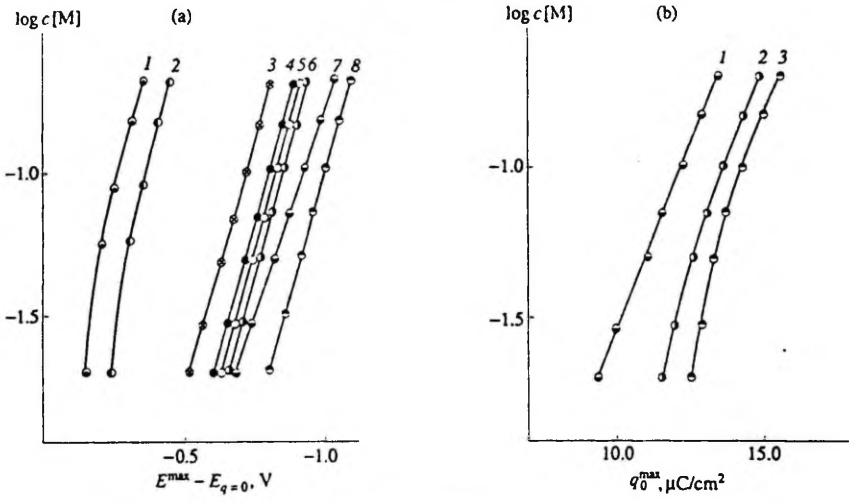

Fig. 4. The dependence of the adsorption-desorption peak potential on log *c* CH (a) for the electrodes: (*1*) Zn(11$\bar{2}$0); (*2*) Zn(0001); (*3*) Bi(001); (*4*) Bi(111); (*5*) Hg; (*6*) Sb(001); (*7*) Sb(111); and (*8*) Sb(2$\bar{1}\,\bar{1}$). The dependence of q_0^{max} on log *c* CH (b) for (*1*) Sb(111), (*2*) Sb(001), and (*3*) Sb(2$\bar{1}\,\bar{1}$).

during the CH adsorption on Sb(001), Sb(111), and Sb(2$\bar{1}\,\bar{1}$) has a parabolic shape, which, according to [22, 23], is due to a decrease in the area *S* per adsorbed molecule as the surface coverage increases. It should be noted that on the faces of a Sb single crystal, as on a Bi single crystal [19 - 21], the attraction constant increases in the sequence (2$\bar{1}\,\bar{1}$) < (001) < (111) as the hydrophilic properties increase in the same sequence. A similar relationship is observed at the adsorption of organic molecules on the faces of zinc [1, 24] and lead [25] single crystals, and also on metals that differ in their hydrophily (a_0 increases in the sequence Sb < Hg < Bi < Zn(0001) < Ga [2, 6 - 30]).

Figure 4a compares the dependences of the potentials of the adsorption–desorption peaks in the relative scale ($E^{max} - E_{q=0}$) on the logarithm of cyclohexanol concentration log*c* for Sb-crystal faces with the corresponding data for Bi-crystal faces [19 - 21], Zn [24], and Hg [26]. According to [28 - 30] and Fig. 4a, the surface hydrophilic properties decrease in the following sequence of electrodes Zn(11$\bar{2}$0) > Zn(0001) > Bi(001) > Bi(111) > Bi(2$\bar{1}\,\bar{1}$) > Hg > Sb(001) > Sb(111) > Sb (2$\bar{1}\,\bar{1}$).

Figure 4b shows the dependences of the surface charge in the supporting-electrolyte solution at the potentials of the adsorption–desorption peaks q_0^{max} on the logarithm of CH concentration for the faces of an Sb single crystal. It is evident from Fig. 4b that the observed tendency [28 - 30] for the independence of the charge of the cathodic desorption peak q_0^{max} from the nature of metal (its hydrophily) applies to the Sb crystal faces with a lesser degree of accuracy. In 0.1 M CH solutions on face (2$\bar{1}\,\bar{1}$), the cathodic peaks are situated at more negative charges than those of face (111), and face (001) occupies an intermediate position. This is indicative both of a strong interaction of CH molecules with face (2$\bar{1}\,\bar{1}$) and of a less pronounced hydrophily of face (2$\bar{1}\,\bar{1}$).

Using the *C* versus *E*-curves for Sb single-crystal faces and the technique of back integration, we obtained *q* versus *E*-curves in the presence of CH in the solution. According to [22, 23, 30], the fact that the *q* versus *E*-curves for the faces of a Sb single crystal intersect with the curve in the supporting-electrolyte solution at the same potential indicates that the *C* versus *E*-curves are in equilibrium and that the model of two parallel capacitors can be applied for describing the CH adsorption on Sb single-crystal faces.

From *C* versus *E*-curves, using the relationships that follow from the model of two parallel capacitors [22], we calculated the CH adsorption isotherms (Fig. 5) at the potential of the maximum adsorption $E = E_{max}$. The limiting electrode capacitance *C'* at the surface coverage θ = 1 was found by extrapolating the dependence of 1/*C* on 1/*c* at $E = E_{max}$ to 1/*c* = 0. The other parameters of the CH adsorption were found using the technique of

Frumkin–Damaskin [22] and are shown in Table 2, which uses the generally accepted symbols.

In Table 2, the values of the adsorption parameters point to a substantial difference in the adsorption behavior of CH on the studied faces of a Sb single crystal.

According to the values of B_m, $-\Delta G_A^m$ and $c_{\theta=0.5}$, the adsorption activity of CH increases in the sequence (111) < (001) < ($2\bar{1}\bar{1}$). A similar sequence was also found for the CH adsorption on Bi single-crystal faces [19 - 21]. A somewhat higher adsorption activity of face (001) than that of the face (111) can be attributed to the stronger adsorption bond between CH molecules and (001) surface atoms, each having one unsaturated covalent bond which increases the chemical activity of the surface [19 - 21]. Among the studied faces, the face ($2\bar{1}\bar{1}$) has the highest adsorption activity and is energetically nonsingular due to crystalographic factors [8, 9, 31]. There are a great number of steps on face ($2\bar{1}\bar{1}$) as well as three types of antimonium atoms having 0, 1, and 2 unsaturated covalent bonds from the three possible for each atom [8, 9, 31]. As in the case of Bi(111), all the atoms of the antimonium basal face (111) are chemically saturated, and the CH adsorption is mainly of a physical nature [19 - 21]. Moreover, the low adsorption activity of Sb(111), as compared with face Sb($2\bar{1}\bar{1}$), is associated with its highest hydrophily.

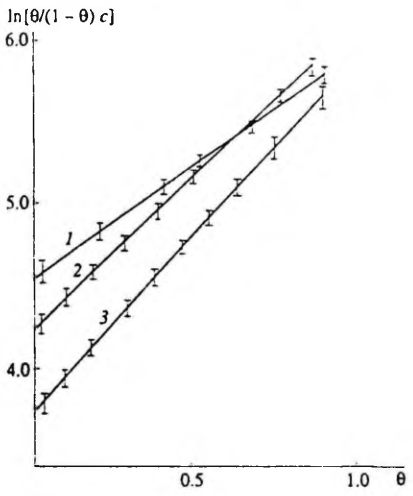

Fig. 5. Isotherms of the CH adsorption on (*1*) Sb($2\bar{1}\bar{1}$), (2) Sb(001), and (*3*) Sb(111).

ADSORPTION OF CYCLOHEXANOL ON A POLYCRYSTALLINE SURFACE OF ANTIMONIUM ELECTRODES

When studying the CH adsorption on polycrystalline antimonium electrodes (PC-Sb), we found that the shape of the adsorption–desorption peak on the C versus E-curve substantially depends on the preparational technique of a solid-drop antimonium electrode. According to the experimental data (Fig. 6), for a DAE with an additionally remelted surface (DAE-I), as in the case of a solid drop bismuth electrode with an additionally remelted surface (DBE-I) [12 - 14, 32 - 36], the effect of the splitting of the adsorption–desorption peaks is observed. This effect is most pronounced at concentrations c_{CH} = 0.02 - 0.05 M, while comparatively narrower and higher adsorption peaks are observed in more concentrated CH solutions ($c_{CH} \geq 0.1$ M). The maximum difference between the potentials of the splitted peak ΔE^{max} is observed at c_{CH} = 0.02 M and is 0.18 V, which is somewhat higher than the corresponding value for DBE, 0.14 V [36, 37]. This is indicative of a higher adsorption nonuniformity of the DAE-I surface as compared with the DBE-I surface, which is

Table 2. Parameters of the cyclohexanol adsorption on the faces of a Sb single crystal

Electrode	$a_m \pm 0.05$	C', μF/cm²	$c_\theta = 0.5$, mol/dm³	B_m, dm³/mol	$-\Delta G_A^m$, kJ/mol	$E^{max} - E_{q=0}$, V(0.1 M CH)
(001)	0.95	4.4 ± 0.1	0.0051 ± 0.0003	68 ± 3	20.1 ± 0.2	0.84 ± 0.01
(111)	1.10	3.9 ± 0.1	0.0071 ± 0.0002	41 ± 2	18.9 ± 0.2	0.93 ± 0.01
($2\bar{1}\bar{1}$)	0.70	3.6 ± 0.2	0.0049 ± 0.0004	86 ± 3	20.7 ± 0.2	0.99 ± 0.01

Table 3. Parameters of the CH adsorption on the polycrystalline surface of Sb electrodes

Electrode	$a_m \pm 0.1$	$C' \pm 0.2$, μF/cm²	$c_\theta = 0.5$, mol/dm³	B_m, dm³/mol	$-\Delta G_A^m$, kJ/mol	$E^{max} - E_{q=0}$, V(0.1 M CH)
DAE-I	1.0	5.0	0.007 ± 0.001	60 ± 5	19.9 ± 0.2	0.83 ± 0.01
DAE-II	0.6	5.4	0.009 ± 0.001	52 ± 5	19.6 ± 0.2	0.89 ± 0.02

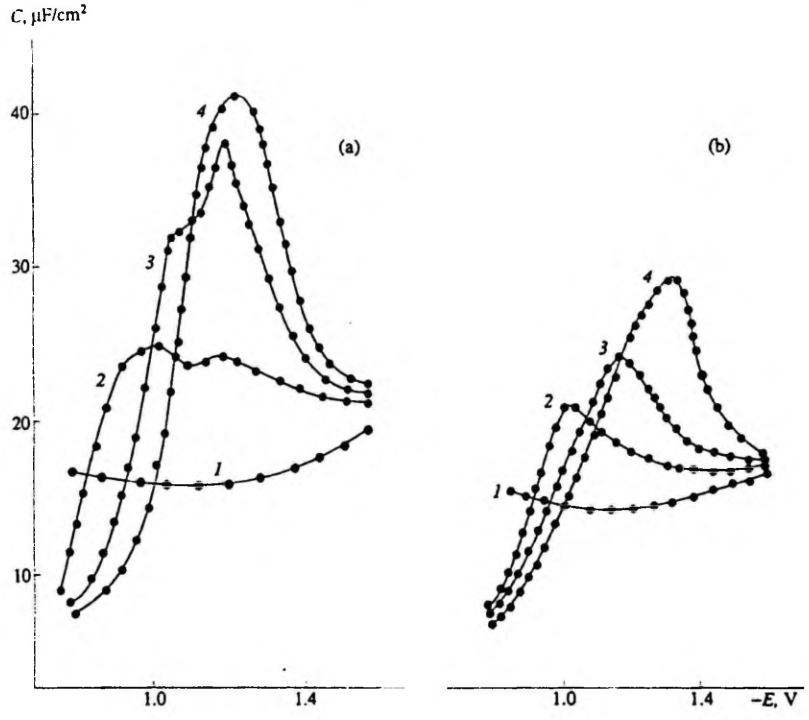

Fig. 6. *C* versus *E*-curves for (a) DAE-I and (b) DAE-II in (*1*) 0.1 M NaF and with CH additions: (*2*) 0.02; (*3*) 0.05; and (*4*) 0.1 M.

associated with the greater difference between the zero-charge potentials of different faces of an Sb single crystal as compared with the Bi crystal faces as well as the more pronounced dependence of the adsorption energy of the organic substance and water on the crystallographic structure of the surface in the case of Sb.

As in the case of electrochemically polished plane PC-Sb electrodes, solid-drop antimonium electrodes with heat-untreated surfaces (DAE-II) are characterized by deformed, low, and widened adsorption-desorption peaks. Optical and electronographic studies showed that, as in the case of DBE-I [33], along with defective polycrystalline regions consisting of numerous fine crystals, the DAE-I surface includes relatively large geometrically (energetically) uniform regions with surface characteristics (including the adsorption properties) approaching those of individual faces of an antimonium single crystal. However, the heat-untreated surface of DAE-II is characterized by a highly developed geometrical roughness ($f_{P-Z} \geq 1.30$; $f_v \geq 1.35$). Well-developed polycrystallinity and the energy non-uniformity associated with it encourage the appearance of a wide spectrum of adsorption interactions in the adsorption layer, and this leads not to the splitting of the adsorption peaks but to their widening [32 - 39]. According to [32 - 37, 39] and Fig. 6, the factor beneficial for the splitting of adsorption peaks is the microscopic nature of crystallographic heterogeneity (non-uniformly heterogeneous surface) of the DAE-I additionally remelted surface, which is characterized by the presence of relatively large geometrically and energetically uniform (single-crystal) regions with distinctly different adsorption properties.

Figure 7 compares $\log c$ versus $E^{max} - E_{q=0}$-curves for DAE-I and DAE-II with corresponding curves for faces Sb(001), Sb(111), and Sb($2\bar{1}\,\bar{1}$). As in the case of a solid-drop bismuth electrode [36, 37], the potentials of the less negative individual maximum of the split peak for DAE-I, with an accuracy of up to 5 - 10 mV, coincides with the potentials of the maxima on the *C* versus *E*-curve for face (001). However, the poten-

tials of the more negative maximum on the $E^{max} - E_{q=0}$ versus log$c$-curve for DAE-I do not coincide with the potentials on the corresponding dependences for Sb(111), Sb(2$\bar{1}\,\bar{1}$), or Sb(01$\bar{1}$) and, most probably, characterize the adsorption and desorption on the more active defective (single-crystal) regions of DAE-I.

According to Fig. 7, the $E^{max} - E_{q=0}$ versus log$c$-curve for the heat-untreated surface of DAE-II, like that of DBE-II, occupies an intermediate position between the corresponding dependences for Sb(001), Sb(111), and Sb(2$\bar{1}\,\bar{1}$). Most likely, the position of the $E^{max} - E_{q=0}$ versus log$c$-curve for DAE-II does not characterize the adsorption and desorption of CH in any actual surface site with definite crystallographic structure and adsorption energy. Therefore, the peak potential is determined by the overall adsorption–desorption process over the whole micropolycrystalline surface of DAE-II and is a mean (apparent) value.

Figure 8 compares the statistically processed isotherms of CH adsorption on DAE-I and DAE-II with the corresponding adsorption isotherms for Sb(111) and Sb(001). As in the case of DBE-I, with the additionally remelted surface [36, 37], the isotherm of CH adsorption on DAE-I is nonlinear at low surface coverages $\theta_{pc} \leq 0.1$ and bends towards lower values of $\ln[\theta_{pc}/(1 - \theta_{pc})c]$. This is associated with the preferential adsorption of CH on more active defective regions of the DAE-I surface at $\theta_{pc} \leq 0.1$. At surface coverages $0.1 < \theta_{pc} \leq 0.65$, the isotherm of CH adsorption on DAE-I is almost linear and coincides relatively well with the isotherm of CH adsorption on Sb(001). Table 3 shows the adsorption parameters determined from the linear region of the isotherm. The other parameters of CH adsorption on DAE-I and DAE-II are also given in this table. At surface coverages $0.65 < \theta_{pc} \leq 0.80$, a bend is observed in the isotherm. This is characteristic for a macropolycrystalline surface or for two-faced model polycrystalline electrodes [34 - 37, 40].

According to theoretical calculations and experimental data for two-faced model polycrystalline electrodes of bismuth [35 - 37, 40], the presence of linear regions and clearly pronounced bends in the isotherms of CH adsorption on DAE-I is indicative of the macroscopic nature of the surface crystallographic heterogeneity. On the basis of Tables 2 and 3, $E^{max} - E_{q=0}$ versus log$c$-dependences and adsorption isotherms, we can assume that uniform surface regions, the adsorption properties of which coincide with the characteristics of Sb(001), prevail on the DAE-I surface.

According to the experimental data of Fig. 8, the isotherms of CH adsorption on DAE-II are nonlinear at surface coverages $\theta_{pc} \leq 0.4$ and bend towards lower values of $\ln[\theta_{pc}/(1 - \theta_{pc})c]$. At surface coverages $0.4 \leq \theta_{pc} \leq 0.75$, the isotherm of CH adsorption on DAE-II is practically linear, and parameters of CH adsorption determined from this region are shown in Table 3.

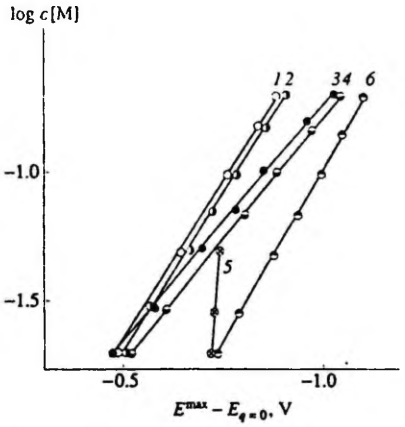

Fig. 7. The dependence of the adsorption-desorption peak potential on log$c$ CH for (*1*; *5*) DAE-I, (*3*) DAE-II, (*2*) Sb(001), (*4*) Sb(111), and (*6*) Sb(2$\bar{1}\,\bar{1}$).

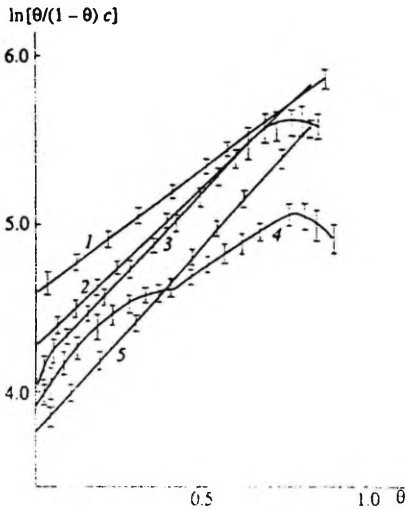

Fig. 8. Isotherms of the CH adsorption on (*3*) DAE-I, (*4*) DAE-II, (*1*) Sb(2$\bar{1}\,\bar{1}$), (*2*) Sb(001), and (*5*) Sb(111).

A comparison of Tables 2 and 3 shows that the B_m value for DAE-II occupies an intermediate position between the B_m values for faces (001) and (111), while the effective value a_m for DAE-II is substantially lower than that in the case of individual faces of an Sb single crystal. Similar isotherms are also observed for DBE-II and

chemically treated faces of Bi and Sb single crystals. As was shown by modelling, these isotherms are associated with the preferential adsorption of CH in more active defective surface sites (with sufficiently different adsorption energies) at $\theta_{pc} \leq 0.4$ and the preferential adsorption in less active (but energetically more uniform) surface sites at $\theta_{pc} \geq 0.4$ [34 - 40].

CONCLUSION

Our results point to a substantial dependence of the characteristics of the double-layer structure and CH adsorption on the crystallographic and energy factors of different faces of an Sb single crystal and a polycrystalline surface of Sb electrodes.

REFERENCES

1. Hamelin, A., Vitanov, T., Sevastyanov, E., and Popov, A., *J. Electroanal. Chem.*, 1983, vol. 145, p. 225.
2. Pal'm, U.V., Pärnoya, M.P., and Salve, M.A., *Elektrokhimiya*, 1977, vol. 13, p. 1074.
3. Lust, E.J. and Pal'm, U.V., *Elektrokhimiya*, 1985, vol. 21, p. 1381.
4. Lust, E.J., Lust, K.K., and Jänes, A.A.-J., *Elektrokhimiya*, 1990, vol. 26, p. 1627.
5. Lust, E. and Ehrlich, J., *Double Layer and Adsorption at Solid Electrodes, IX, Tartu*: Tartu Univ., 1991, p. 112.
6. Lust, E.J. and Jänes, A.A.-J., *Elektrokhimiya*, 1992, vol. 28, p. 802.
7. Jänes, A., Lust, E., and Pullerits, R., *Double Layer and Adsorption at Solid Electrodes, IX, Tartu*: Tartu Univ., 1991, p. 53.
8. Pearson, W., *The Crystal Chemistry and Physics of Metals and Alloys*, New York: Wiley, 1972.
9. Kelly, A. and Groves, G.W., *Crystallography and Crystal Defects*, Bristol: Longman, 1970.
10. Ashcroft, N.W. and Mermin, N.D., *Solid State Physics*, New York: Holt, Rinehart, and Winston, 1976.
11. Hamelin, A. and Stoicoviciu, L., *J. Electroanal. Chem.*, 1987, vol. 236, p. 283.
12. Palm, U., Past, V., and Pullerits, R., *Uchen. Zap. Tart. Gos. Univ.*, 1968, no. 219, p. 63.
13. Haga, M. and Past, V., *Elektrokhimiya*, 1969, vol. 5, p. 618.
14. Pullerits, R.Ya., Moldau, M.E., and Past, V.E., *Dvoinoi Sloi i Adsorbtsiya na Tverdykh Elektrodakh* (Double Layer and Adsorption at Solid Electrodes), IV, Tartu: Tart. Gos. Univ., 1975, p. 257.
15. Valette, G., *J. Electroanal. Chem.*, 1981, vol. 122, p. 285; 1982, vol. 138, p. 37; 1989, vol. 269, p. 191.
16. Hamelin, A. and Stoicoviciu, L., *J. Electroanal. Chem.*, 1989, vol. 271, p. 15.
17. Valette, G. and Hamelin, A., *J. Electroanal. Chem.*, 1973, vol. 45, p. 301.
18. Leiva, E. and Schmickler, W., *J. Electroanal. Chem.*, 1986, vol. 205, p. 323; 1987, vol. 229, p. 39.
19. Palm, U.V. and Pärnoya, M.P., *Elektrokhimiya*, 1978, vol. 14, p. 1070.
20. Pärnoya, M.P. and Palm, U.V., *Elektrokhimiya*, 1978, vol. 14, p. 1299.
21. Lust, E.J. and Palm, U.V., *Elektrokhimiya*, 1985, vol. 21, p. 1381.
22. Damaskin, B.B., Petrii, O.A., and Batrakov, V.V., *Adsorbtsiya Organicheskikh Soedinenii na Elektrodakh* (Adsorption of Organic Substances on Electrodes), Moscow: Nauka, 1968.
23. Damaskin, B.B., Frumkin, A.N., and Chizhov, A.V., *J. Electroanal. Chem.*, 1970, vol. 28, p. 93.
24. Ipatov, Yu.P., Batrakov, V.V., and Shalaginov, V.V., *Elektrokhimiya*, 1976, vol. 12, p. 786.
25. Khmelevaya, L.P., Chizhov, A.V., Damaskin, B.B., and Vainblat, T.I., *Elektrokhimiya*, 1980, vol. 16, p. 257.
26. Dobren'kov, G.A. and Shilotkach, G.D., *Elektrokhimiya*, 1970, vol. 5, p. 1416.
27. Alumaa, A.R. and Palm, U.V., *Elektrokhimiya*, 1972, vol. 8, p. 770.
28. Grigor'ev, N.B. and Bagotskaya, I.A., *Elektrokhimiya*, 1966, vol. 2, p. 1449.
29. Frumkin, A., Damaskin, B., Grigor'ev, N., and Bagotskaya, I., *Electrochim. Acta*, 1974, vol. 19, p. 69.
30. Frumkin, A.N., *Potentsialy Nulevogo Zaryada* (Potentials of Zero Charge), Moscow: Nauka, 1982, p. 153.
31. Vigdorovich, V.N., Ukhlinov, G.A., Marychev, V.V., and Shumyalov, V.P., *Sbornik Nauchnykh Trudov po Problemam Mikroelektroniki. Khimiko-Tekhnologicheskaya Seriya* (Collection of Scientific Papers on Microelectroniks. Ser. Chemical Technology), Moscow: Mosk. Inst. Elektronnoi Tekhniki, 1972, no. 8, p. 24.
32. Salve, M.A., Alumaa, A.R., and Palm, U.V., *Uchen. Zap. Tart. Gos. Univ.*, 1971, no. 289, p. 54.
33. Ehrlich, J.I., Pärnoya, M.P., Ehrlich, T.E., and Palm, U.V., *Dvoinoi Sloi i Adsorbtsiya na Tverdykh Elektrodakh* (Double Layer and Adsorption at Solid Electrodes), IV, Tartu: Tart. Gos. Univ., 1975, p. 342.
34. Alumaa, A.P., Lust, E.J., Paltusova, N.A., and Palm, U.V., *Elektrokhimiya*, 1983, vol. 19, p. 1582.
35. Alumaa, A. and Past, U., *Uchen. Zap. Tart. Gos. Univ.*, 1986, no. 757, p. 45.
36. Lust, E. and Palm, U., *Uchen. Zap. Tart. Gos. Univ.*, 1986, no. 757, p. 105.
37. Palm, U., *Acta Polytechnica Scandinavica. Chem. Technology and Metallurgy Series*, Helsinki, 1987, no. 178, p. 9.
38. Batrakov, V.V. and Sidnin, A.I., *Elektrokhimiya*, 1972, vol. 8, p. 743.
39. Batrakov, V.V. and Damaskin, B.B., *J. Electroanal. Chem.*, 1975, vol. 65, p. 361.
40. Lust, E.J. and Palm, U.V., *Elektrokhimiya*, 1986, vol. 22, p. 411.

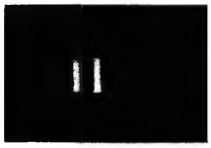

Reprinted from the *Russian Journal of Electrochemistry* 31, No. 6,
A. A.-J. Jänes, E. J. Lust, Adsorption of Cyclohexanon
on the Single Crystal Bismuth and Antimony Electrodes,
Russian J. of Electrochemistry, pages 648–651 31 (in Russian),

ЭЛЕКТРОХИМИЯ, 1995, том 31, № 6, с. 648 - 651

КРАТКИЕ СООБЩЕНИЯ

УДК 541.138.52:546.87-183

АДСОРБЦИЯ ЦИКЛОГЕКСАНОНА НА ГРАНЯХ МОНОКРИСТАЛЛА ВИСМУТА И СУРЬМЫ

© 1995 г. А. А. -Я. Янес, Э. Й. Луст

Тартуский университет, Эстония

Поступила в редакцию 20.07.94 г.

Для более глубокого понимания роли электронной и кристаллографической структуры поверхности и строения скелета углеводородного радикала в адсорбционных явлениях в продолжение работ [1 - 6] была исследована адсорбция циклогексанона (**ЦГН**) на сингулярных *F*-гранях (001) и (111) и на несингулярной *K*-грани $(2\bar{1}\bar{1})$ монокристаллов Bi и Sb. Методика измерений, подготовка электродов и очистка реактивов описаны ранее [3 - 6]. Электродом сравнения служил насыщенный каломельный электрод (нас. к. э.).

На рис. 1 приведены кривые зависимости емкости C от потенциала E на ранях Bi(111) – (а) и Sb(111) – (б) в присутствии ЦГН различных концентраций в 0.1 М водном растворе NaF. Из рис. 1 видно, что на грани (111) монокристалла Bi и Sb C,E-кривые имеют обычную форму с острыми катодными максимумами адсорбции–десорбции с потенциалом E^{max}, высота которых закономерно возрастает с ростом концентрации ЦГН. Согласно данным рис. 1, увеличение энергетической неоднородности поверхности сурьмяного электрода (по сравнению с висмутовым электродом) приводит к уменьшению высоты и расширению пиков адсорбции–десорбции. Наблюдается увеличение высоты катодных максимумов в ряду граней $(2\bar{1}\bar{1}) < (001) < (111)$. Подобная закономерность имеет место при адсорбции циклогексанола (**ЦГ**) на гранях монокристалла Bi и Sb [3, 5, 6].

Параметры адсорбции ЦГН были рассчитаны из C, E-кривых по методике расчета Фрумкина–Дамаскина [7], основывающейся на модели двух параллельных конденсаторов. Значения полученных параметров приведены в таблице, где они сопоставлены с соответствующими данными для Hg [2].

Как следует из приведенных в таблице параметров, грани (111) и $(2\bar{1}\bar{1})$ имеют весьма разные адсорбционные свойства, а грань (001) занимает промежуточное положение между гранями (111) и $(2\bar{1}\bar{1})$. Подобная тенденция наблюдается и при адсорбции ЦГ на разных гранях монокристаллов Bi и Sb [3, 5, 6, 8].

Различие в адсорбционных свойствах исследованных граней монокристаллов висмута и сурьмы особенно наглядно проявляется на рис. 2а, где представлены зависимости потенциалов максимума адсорбции–десорбции в рациональной шкале ($E^{max} - E_{\sigma=0}$) от логарифма концентрации ЦГН lgc для граней монокристаллов Bi и Sb. Согласно представлениям работ [9 - 11] и данным рис. 2а, гидрофильные свойства поверхности уменьшаются в ряду электродов Bi(111) > Bi(001) ≥ ≥ Bi$(2\bar{1}\bar{1})$ > Sb(111) > Sb(001) > Sb$(2\bar{1}\bar{1})$.

На рис. 2б приведены зависимости заряда поверхности в фоновом растворе электролита при потенциалах адсорбционно-десорбционных максимумов σ_0^{max} от логарифма концентрации ЦГН для граней монокристаллов Bi и Sb. Из рисунка следует, что обнаруженная в работах [9 - 11] закономерность, которая заключается в независимости заряда катодного максимума десорбции σ_0^{max} от природы металла, менее точно применима к граням монокристаллов Bi и Sb. Этот результат совпадает с выводами работы [12], где обнаружено, что энергия адсорбции органических соединений при отрицательных зарядах поверхности зависит от химической природы (гидрофильности) металла. Пониженная адсорбционная активность грани (111) обусловлена менее активным поверхностным состоянием, поскольку на поверхности этой грани все атомы химически насыщены и адсорбция циклогексанола носит чисто физический характер [6, 8, 13]. Согласно представлениям работ [10, 14] и данным рис. 2б, гидрофильные свойства поверхности электродов уменьшаются в ряду граней Bi(111) > Bi(001) > Bi$(2\bar{1}\bar{1})$ > Sb(111) > > Sb(001) > Sb$(2\bar{1}\bar{1})$.

На основе C, E-кривых для граней монокристаллов Bi и Sb в растворе фона методом обратного интегрирования были построены σ,E-кривые в присутствии ЦГН в растворе. Было найдено, что для небольших добавок органического соединения C,E-кривые в некоторой степени являются неравновесными. При $c_{орг} \geq 0.07$ М, σ,E-кривые сливаются с σ_0,E-кривой при потенциале E^{max}, что свидетельствует о равновесности C,E-кривых.

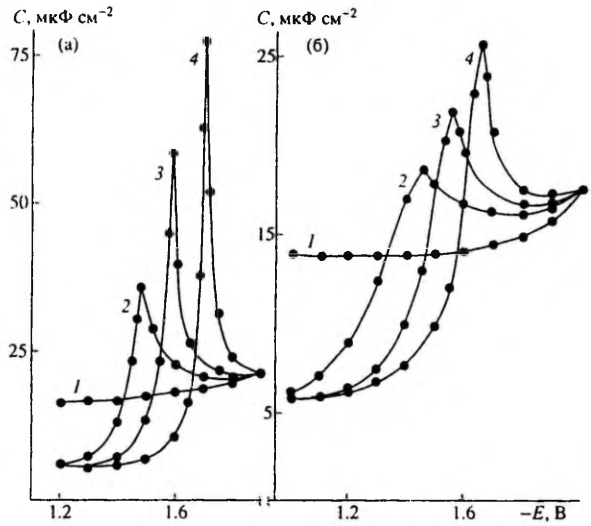

Рис. 1. C,E-кривые для граней Bi(111) (а) и Sb(111) (б) в 0.1 М растворе NaF (*1*) и с добавками ЦГН, М: *2* – 0.05; *3* – 0.1; *4* – 0.2.

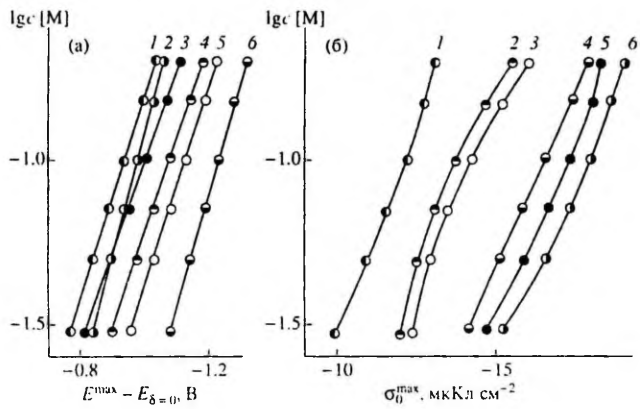

Рис. 2. Зависимость потенциала адсорбционно-десорбционных максимумов от lg*c* ЦГН (а) для электродов: *1* – Bi(111), *2* – Bi($2\bar{1}\bar{1}$); *3* – Bi(001); *4* – Sb(111); *5* – Sb(001); *6* – Sb($2\bar{1}\bar{1}$). Зависимость σ_0^{max} от lg*c* ЦГН (б) на гранях монокристалла: *1* – Bi(111); *2* – Sb(111); *3* – Sb(001); *4* – Sb($2\bar{1}\bar{1}$); *5* – Bi(001); *6* – Bi($2\bar{1}\bar{1}$).

По соотношениям, вытекающим из модели двух параллельных конденсаторов [7], на основе C,E-кривых были рассчитаны изотермы адсорбции при потенциале максимальной адсорбции $E = E^{max}$. Статистически обработанные изотермы адсорбции ЦГН представлены на рис. 3. Судя по значениям $B_м$, $-\Delta G_A^м$ и $c_{\theta=0.5}$, адсорбционная активность ЦГН растет в ряду граней (111) < (001) < < ($2\bar{1}\bar{1}$). Наибольшую адсорбционную активность среди изученных граней имеет грань ($2\bar{1}\bar{1}$), которая несингулярна и является энергетически неоднородной по кристаллографическим причинам [15, 16].

Параметры адсорбции циклогексанона на разных гранях монокристаллов Bi и Sb

Электрод	$a_м \pm 0.05$	C', мкФ/см^2	$c_{\theta=0.5}$, моль/дм^3	$B_м$, дм^3/моль	$-\Delta G_A^м$, кДж/моль	$E^{max} - E_{\delta=0}$, B (0.1 М ЦГН)
Bi(111)	1.04	4.8 ± 0.2	0.0060 ± 0.0003	60 ± 3	19.8 ± 0.2	0.94 ± 0.01
Bi(001)	0.99	6.6 ± 0.3	0.0058 ± 0.0003	68 ± 3	20.1 ± 0.2	1.01 ± 0.01
Bi(2$\bar{1}\bar{1}$)	0.92	6.4 ± 0.3	0.0028 ± 0.0005	174 ± 8	22.4 ± 0.2	0.97 ± 0.01
Sb(111)	1.02	5.4 ± 0.2	0.0040 ± 0.0003	98 ± 5	21.0 ± 0.2	1.09 ± 0.01
Sb(001)	0.83	7.0 ± 0.3	0.0020 ± 0.0004	200 ± 8	22.4 ± 0.2	1.12 ± 0.01
Sb(2$\bar{1}\bar{1}$)	0.64	6.6 ± 0.3	0.0022 ± 0.0005	239 ± 10	22.8 ± 0.2	1.23 ± 0.01
Hg[2]	0.574	–	0.00592	95.5	21.0	–

Видно, что адсорбционная активность ЦГН существенно выше на поверхности граней монокристалла сурьмы, чем на поверхности граней монокристалла висмута. Пониженная адсорбционная активность граней монокристалла висмута обусловлена более выраженной гидрофильностью. Сравнение с данными работ [3, 5, 6, 8] показывает, что адсорбционная активность ЦГН несколько выше, чем адсорбционная активность ЦГ. На рис. 4 приведены графики зависимости аттракционной постоянной a от E для граней Bi(111), Bi(001), Bi(2$\bar{1}\bar{1}$) и Sb(111). На гранях Sb(001) и Sb(2$\bar{1}\bar{1}$) эти зависимости не описываются теорией адсорбции Фрумкина–Дамаскина, поскольку a заметно меньше 1. По всей вероятности, это связано с менее выраженной гидрофильностью поверхности этих граней, а также влиянием кристаллографической структуры грани Sb(2$\bar{1}\bar{1}$).

Из рис. 4 видно, что зависимость a от E при адсорбции ЦГН на гранях Bi(001) и Bi(2$\bar{1}\bar{1}$) имеет

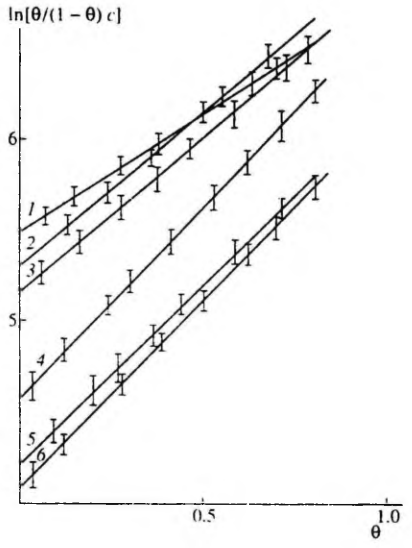

Рис. 3. Изотермы адсорбции ЦГН на гранях монокристалла: *1* – Sb(2$\bar{1}\bar{1}$); *2* – Sb(001); *3* – Bi(2$\bar{1}\bar{1}$); *4* – Sb(111); *5* – Bi(001); *6* – Bi(111).

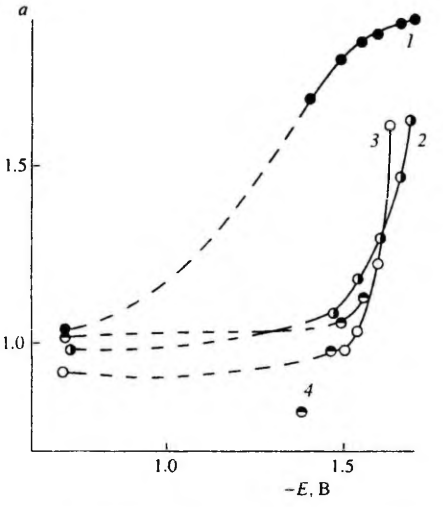

Рис. 4. Зависимость аттракционной постоянной a от E при адсорбции ЦГН на гранях монокристалла: *1* – Bi(111); *2* – Bi(001); *3* – Bi(2$\bar{1}\bar{1}$); *4* – Sb(111).

параболический вид. Подобная тенденция наблюдается и при адсорбции ЦГ на гранях монокристалла Bi и Sb [3, 5, 6, 8]. Причиной такой зависимости является уменьшение площади s, приходящейся на одну молекулу адсорбата, с ростом заполнения θ. Сравнение значений a, рассчитанных из ширины катодных максимумов для ЦГН и ЦГ [3, 6], показывает, что аттракционное взаимодействие адсорбированных молекул ЦГ несколько выше, чем при адсорбции ЦГН. Это обусловлено особенностями строения молекул ЦГ и ЦГН, а также различиями в структуре их адсорбционных слоев.

В заключение отметим, что результаты настоящей работы свидетельствуют о сильной зависимости закономерностей адсорбции органических соединений от кристаллографических и энергетических характеристик разных граней. Повышение адсорбционной активности граней монокристаллов Bi и Sb в ряду (111) < (001) < $(2\bar{1}\bar{1})$ в основном связано с уменьшением гидрофильных свойств в этом же ряду граней. Пониженная адсорбционная активность грани (111) может быть обусловлена кроме более выраженной гидрофильности ее менее активным поверхностным состоянием.

СПИСОК ЛИТЕРАТУРЫ

1. *Hamelin A., Vitanov T., Sevastyanov E., Popov A.* // J. Electroanal. Chem. 1983. V. 145. P. 225.
2. *Broadhead D., Hansen R., Potter G.* // J. Colloid Interface Sci. 1969. V. 31. P. 61.
3. *Луст Э.Й., Пальм У.В.* // Электрохимия. 1985. Т. 21. С. 1381.
4. *Луст Э.Й., Луст К.К., Янес А.А.-Я.* // Элктрохимия. 1990. Т. 26. С. 1627.
5. *Jänes A., Lust E., Pullerits R.* // Double Layer and Adsorption at Solid Electrodes, IX. Tartu, 1991. P. 53.
6. *Луст Э.Й., Янес А.А.-Я.* // Электрохимия. 1994. Т. 30. С. 357.
7. *Дамаскин Б.Б., Петрий О.А., Батраков В.В.* Адсорбция органических соединений на электродах. М.: Наука, 1968.
8. *Пальм У.В., Пярноя М.П.* // Электрохимия. 1978. Т. 14. С. 1070.
9. *Григорьев Н.Б., Багоцкая И.А.* // Электрохимия. 1966. Т. 2. С. 1449.
10. *Frumkin A., Damaskin B., Grigoryev N., Bagotskaya I.* // Electrochim. Acta. 1974. V. 19. P. 69.
11. *Фрумкин А.Н.* Потенциалы нулевого заряда. М.: Наука, 1982. С. 153.
12. *Pazzatini G., Moncelli M.R., Innocenti M., Guidelli R.* // J. Electroanal. Chem. 1990. V. 275. P. 295.
13. *Пярноя М.П., Пальм У.В.* // Электрохимия. 1978. Т. 14. С. 1229.
14. *Григорьев Н.Б.* // Двойной слой и адсорбция на твердых электродах, IV. Тарту, 1975. С. 78.
15. *Пирсон У.* Кристаллография и физика металлов и сплавов. Ч. 1. М.: Мир, 1977. С. 280.
16. *Келли А., Гровс Г.* Кристаллография и дефекты в кристаллах. М.: Мир, 1974. С. 130.

III

Reprinted from the *Russian Journal of Electrochemistry*, 31, No. 8,
E.J. Lust, K.K. Lust, A.A.-J. Jänes, Influence of the Crystallographic Structure
of the Electrode Surface on the Structure of the Electrical Double Layer and
Adsorption of Organic Molecules, pages 876–890 (in Russian),

ЭЛЕКТРОХИМИЯ, 1995, том 31, № 8, с. 876 - 890

УДК 541.135.52.183

ВЛИЯНИЕ КРИСТАЛЛОГРАФИЧЕСКОЙ СТРУКТУРЫ ПОВЕРХНОСТИ ЭЛЕКТРОДА НА СТРОЕНИЕ ДВОЙНОГО ЭЛЕКТРИЧЕСКОГО СЛОЯ И АДСОРБЦИЮ ОРГАНИЧЕСКИХ МОЛЕКУЛ

© 1995 г. Э. Й. Луст, К. К. Луст, А. А.-Я. Янес

Тартуский университет, Эстония

Поступила в редакцию 08.11.94 г.

Изложены результаты систематического исследования влияния кристаллического строения поверхности Bi-, Sb- и Cd-электродов на закономерности строения двойного электрического слоя в водном и неводном растворах поверхностно-неактивного электролита. Изучено влияние характеристик поверхности электрода на адсорбционное поведение различных органических молекул. Установлены общие закономерности влияния химической природы и кристаллографической структуры поверхности на строение двойного слоя и на адсорбцию органических соединений.

ВВЕДЕНИЕ

Вопрос о причинах зависимости межфазных характеристик от химической природы и энергетического состояния поверхности электрода стал обсуждаться, начиная с работ Борисовой, Эршлера и Фрумкина [1, 2], где было установлено, что двойнослойные характеристики в существенной мере зависят от предварительной обработки поверхности электрода. В 1967-м году А.Н. Фрумкин высказал мысль о кажущемся характере рассчитанных из экспериментальных данных двойнослойных и адсорбционных параметров в случае твердых электродов с поликристаллическим (**ПК**) строением поверхности и подчеркнул необходимость проведения прецизионных электрохимических измерений на отдельных гранях монокристаллических электродов [3]. Начиная с 1972 г. в лаборатории электрохимии Тартуского университета было начато систематическое исследование строения двойного электрического слоя (**ДЭС**), а также адсорбции ионов и молекул на разных гранях монокристалла висмута [4]. Необходимо отметить, что основные двойнослойные характеристики грани (111) монокристалла Bi были экспериментально изучены М. Пярноя, Н.Б. Григорьевым и У. Пальмом под руководством А.Н. Фрумкина в Институте электрохимии АН СССР [5]. С 1987 г. были начаты систематические исследования на гранях монокристалла Sb и Cd [6, 7]. Одной из главных целей данного исследования было дальнейшее развитие теоретико-модельных концепций строения ПК поверхности, распространенных в кинетике реальных электродов. Открытие эффекта расщепления максимумов адсорбции–десорбции органических соединений [8, 9] играло большую роль в развитии теории ДЭС и адсорбции на твердой ПК-поверхности. На основе этих данных А.Н. Фрумкиным, В.В. Батраковым, Б.Б. Дамаскиным с сотр. [9, 10] были развиты теоретические основы для количественного описания экспериментальных результатов по адсорбции органических молекул и ДЭС на поликристаллических электродах (**ПКЭ**). По существу физическое содержание современных теорий строения ПК поверхности твердого электрода заключается в модельном ее описании как совокупности различных граней монокристалла [10 - 13]. При этом в первом приближении эти модели могут быть разделены на две группы [13]: а) поверхность ПК электрода состоит из относительно больших по размерам монокристаллических областей ($x \gg 10$ нм – макрополикристалличность), в которых как плотные, так и диффузные слои на разных однородных участках могут считаться независимыми (так называемая модель независимых электродов – **МНЭ**) [10 - 12]; б) поликристаллическая поверхность состоит из мелких по размерам кристаллитов ($x < 10$ нм), размеры которых соизмеримы с параметрами двойного слоя [13]. В случае таких ПК-электродов плотные слои на разных монокристаллических участках считаются независимыми, а диффузный слой является единым по всей поверхности ПКЭ и является функцией среднего по поверхности ПКЭ заряда $\bar{\sigma}_{ПК} = \Sigma X_i \sigma_i$ (модель единого диффузного слоя – **МЕД**). В обеих моделях существенную роль играют как разность потенциалов нулевого заряда $E_{\sigma=0}$, так и их гидрофильность, т.е. емкость плотного слоя C_H [11 - 13]. Основным недостатком обеих концепций является пренебрежение ролью границ между отдельными монокристаллическими участками, их распределением на ПКЭ, поверхностной миграцией.

Посвящается столетию со дня рождения А.Н. Фрумкина.

Углубленное теоретическое обобщение этих первоначальных концепций было осуществлено в исследованиях М.А. Воротынцева [14].

Для определения истинных двойнослойных и адсорбционных характеристик в исследуемых системах, выяснения влияния кристаллографических эффектов и создания модельных ПК-поверхностей с заданными параметрами в лаборатории электрохимии ТУ проведен большой цикл работ по изучению двойного слоя и адсорбции на разных гранях монокристалла висмута, сурьмы и кадмия в водных и неводных растворах [15 - 20]. Данным проблемам посвящена настоящая работа.

МЕТОДИКА ПРОВЕДЕНИЯ ЭКСПЕРИМЕНТА

Для изготовления монокристаллических электродов были использованы массивные монокристаллы из Bi, Sb и Cd, выращенные по методу Чохральского (Bi) или по методу зонной плавки (Sb и Cd) в Институте проблем микроэлектроники и особо чистых веществ РАН. Методика вольтамперометрических и импедансных измерений, подготовка электродов и очистка растворителей, солей и органических соединений описаны ранее в [15 - 20]. В данном месте лишь отметим, что определение кристаллографической ориентации, по которой разрезался (методом анодного растворения) монокристалл, проводилось с помощью рентгеноструктурного метода. Для экспериментальных исследований были использованы электроды, для которых угол разориентации $\alpha < 0.2°$. В основном исследования были проведены на электрохимически полированных поверхностях Bi-, Sb- и Cd-электродов. В некоторых опытах были также исследованы монокристаллические поверхности граней Bi(111), Sb(111) и Cd(0001), полученные методом скалывания при температуре жидкого азота. Полученные поверхности были исследованы при помощи электронного микроскопа JEOL JSM-35 CF в режиме эмиссии секундарных электронов. Согласно данным рис. 1а, на уровне чувствительности электронной микроскопии электрохимически полированные, а также и полученные методом скалывания поверхности являются совершенно гладкими.

Для экспериментальной проверки соответствующих теоретических представлений об электрохимических свойствах ПК-поверхности электродов в работах [21 - 23] разработана методика изготовления двугранных модельных электродов. Исследуемые электроды были изготовлены вырезанием комбинации граней $(01\bar{1})$, (001), $(\bar{1}0\bar{1})$ или (111) из массивного куска монокристалла Bi и рабочими поверхностями служили боковые грани клина (клинообразные двугранные модельные электроды – КДМЭ). Модельные электроды типа КДМЭ имеют в области вершины стык двух граней, и электрохимическая полировка приводит к очень сложной (ступенчатой) топологии поверхности вершины электрода (рис. 1б). Поэтому в данной работе были проведены импедансные измерения и на модельных электродах,

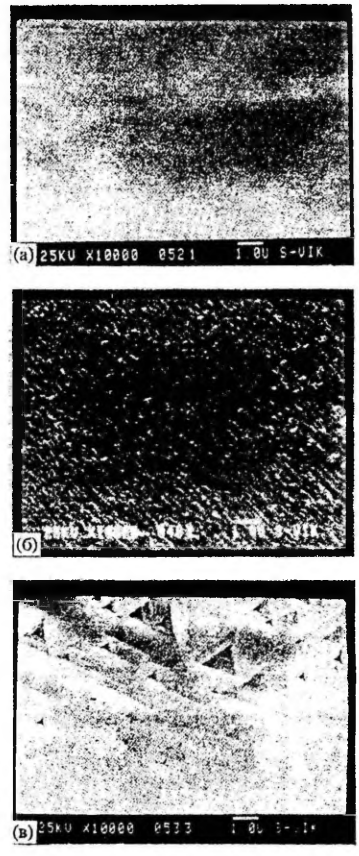

Рис. 1. Электронно-микроскопические снимки (JEOL, JSM-35 CF) поверхности электродов: а – электрохимически полированная поверхность грани Bi(111) (×10000); б – электрохимически полированная переходная область (стык двух граней) для КДМЭ (×10000); в – химически травленная поверхность грани Bi(111) (×10000).

состоящих из двух разделенных пространственно граней монокристалла висмута (двуэлектродные модельные электроды – **ДЭМЭ**). В случае ДЭМЭ отсутствует стык двух различных граней и грани находятся в электрическом контакте только через раствор электролита и через внешнюю цепь.

Для заметного увеличения доли переходной области между отдельными монокристаллическими участками (гранями) на поверхности электродов измерения были проведены и на электродах с ПК-поверхностью, полученных пересечением зоны (111) - $(01\bar{1})$ плоскостью, находящейся под углом 1, 3, 5, 10 и 15° относительно грани (111) (т.е. вицинальные или несингулярные электроды ВЭ-I), а также пересечением зоны (001) - $(01\bar{1})$, находящейся под углом 1, 3, 5, 10 и 15° относительно грани (001) (ВЭ-II). Электрохимическая полировка ВЭ-I или ВЭ-II приводит к очень сложной (ступенчатой) топологии поверхности, где каждая ступенька такой вицинальной или несингулярной плоскости (в атомарном масштабе) ограничена гранью с низким индексом.

На рис. 1в приведен фотоснимок химически травленной ($HNO_3 + NH_4NO_3$) поверхности грани Bi(111), на котором видны образованные при травлении треугольники с размерами меньше 10 мкм. Между ямками травления поверхность грани Bi(111) является практически гладкой.

СТРОЕНИЕ ДВОЙНОГО ЭЛЕКТРИЧЕСКОГО СЛОЯ НА ГРАНЯХ МОНОКРИСТАЛЛА Bi, Sb И Cd

Наиболее важной задачей при изучении строения двойного электрического слоя является определение с высокой точностью значения потенциала нулевого заряда $E_{\sigma=0}$, что, согласно А.Н. Фрумкину, является фундаментальной постоянной в электрохимии. С этой целью методами циклической вольтамперометрии и электрохимического импеданса сотрудниками лаборатории электрохимии ТУ были исследованы закономерности строения ДЭС на отдельных гранях монокристалла Bi, Sb и Cd в водных растворах поверхностно-неактивного электролита, а в случае граней Bi и в неводных растворах (в метаноле – MeOH; в этаноле – EtOH; в изопропаноле – *i*-PrOH и в ацетонитриле – ACN) [15 - 25]. Определенные основные характеристики ДЭС представлены в табл. 1, где $C_H^{\sigma=0}$ и $C_H^{\sigma\ll 0}$ – емкости плотного слоя по модели Грэма [26] при $E_{\sigma=0}$ и потенциале катодного минимума ($\sigma \ll 0$); $C_м^{min}$ – емкость металлической фазы по модели Амокрейна–Бадиали [27] при гипотезе, что емкость прослойки растворителя C_s = const; f_{P-Z} – фактор "шероховатости", определенный из графика Парсонса–Цобеля [28]; D – эффективная фрактальная размерность по модели [29]. Для исключения возможных случайных ошибок измерений в работах [18, 19] проведена статистическая обработка экспериментальных емкостных (C,E-) кривых, а также рассчитанных из них σ,E- и C_H,σ-кривых. Было установлено, что примененная методика изготовления монокристаллических электродов и проведения измерений позволяет определить величины C, σ и C_H с достаточно высокой точностью (относительные ошибки параметров не превышают 1 - 4%).

На основе циклической вольтамперометрии установлено, что в области идеальной поляризуемости поверхностная структура граней монокристалла Bi и Sb является более стабильной, чем в случае граней монокристалла Cd или Au [30, 31]. Обусловлено это тем, что в решетке Sb и Bi кроме металлических связей существуют также и ковалентные связи, повышающие стабильность кристаллической структуры Bi и Sb. Проблема возможного перестроения поверхности Cd- (Bi- и Sb-) электродов требует дальнейших всесторонних экспериментальных исследований методами STM и AFM.

Согласно данным [15 - 25], изменение частоты переменного тока ν от 110 до 1100 Гц сопровождается дисперсией емкости, не превышающей 3 - 4% для Bi(111) (т.е. $f_\nu = \dfrac{C_{110\ Гц}}{C_{1100\ Гц}}$ = 1.03 - 1.04), а для Bi(001), $(\bar{1}0\bar{1})$ и $(01\bar{1})$ f_ν = 1.05 - 1.07. Для граней монокристалла кадмия f_ν = 1.05 - 1.08, а для граней Sb f_ν = 1.04 - 1.12. По модели [29] нами были определены значения эффективной фрактальной размерности D, представленные в табл. 1. Согласно данным табл. 1, значения для граней Bi, Sb и Cd лишь несколько выше, чем для идеально гладкой поверхности (D = 2). Следовательно, изученные нами электроды на уровне чувствительности импедансного метода являются фактически гладкими и свободными от источников псевдоемкости.

Из приведенных в табл. 1 данных видно, что значения $E_{\sigma=0}$ граней монокристалла Bi, Sb и Cd зависят от кристаллографической структуры поверхности, от химической природы и электронных характеристик металла, а также от природы среды. Разность потенциалов нулевого заряда $\Delta E_{\sigma=0}$ граней монокристалла Sb существенно больше [6, 32, 33], чем в случае граней Bi [15, 16], что обусловлено повышением электронной и кристаллографической анизотропии при переходе от Bi к Sb. Подобная тенденция имеет место и в случае граней Zn ($\Delta E_{\sigma=0}$ = 90 мВ) [34] и Cd ($\Delta E_{\sigma=0}$ = 60 мВ) [7, 19].

Из табл. 1 видно, что в случае граней (001), $(01\bar{1})$ и $(2\bar{1}\bar{1})$ Sb и Bi зависимость $E_{\sigma=0}$ от ретику-

Таблица 1. Характеристики ДЭС для граней монокристаллов Bi, Sd и Cd

Растворитель	Электрод	$-E_{\sigma=0}$, В	$\Delta E^{H_2O-x}_{\sigma=0}$, В	$\frac{\delta E_{min}}{\delta \lg c}$ (мВ)	$C_H^{\sigma=0}$, $\frac{\text{мкФ}}{\text{см}^2}$	$C_H^{\sigma\neq0}$, $\frac{\text{мкФ}}{\text{см}^2}$	$C_м^{min}$, $\frac{\text{мкФ}}{\text{см}^2}$	f_{P-Z}	D
H_2O	Bi(111)	0.655	–	5	25.6	18.4	32	1.04	2.03
[15, 16, 19, 20, 38]	Bi($\bar{1}0\bar{1}$)	0.585	–	15	25.8	19.2	36	1.07	2.05
	Bi(001)	0.595	–	20	28.4	19.9	37	1.06	2.05
	Bi(01$\bar{1}$)	0.590	–	15	27.0	18.7	36	1.05	2.04
	Bi(2$\bar{1}\bar{1}$)	0.570	–	20	26.8	18.9	36	1.14	2.06
[6, 19, 20, 32, 33]	Sb(111)	0.46	–	10	23.6	15.2	24	1.06	2.04
	Sb(001)	0.37	–	20	26.2	16.4	27	1.04	2.04
	Sb(01$\bar{1}$)	0.39	–	30	25.9	15.8	26	1.18	2.08
	Sb(2$\bar{1}\bar{1}$)	0.34	–	50	25.0	15.4	26	1.25	2.10
[7, 19, 20]	Cd(0001)	0.95	–	20	38.0	17.0	59	1.09	2.05
	Cd(10$\bar{1}$0)	1.01	–	10	47.8	17.1	74	1.10	2.05
	Cd(11$\bar{2}$0)	1.00	–	10	44.6	16.9	68	1.12	2.07
ACN	Bi(111)	0.50	0.16	5	14.8	11.2	35	1.06	2.04
[18, 20]	Bi($\bar{1}0\bar{1}$)	0.42	0.16	15	15.3	10.8	38	1.01	2.04
	Bi(001)	0.41	0.19	10	17.4	12.8	40	0.98	2.03
	Bi(01$\bar{1}$)	0.42	0.17	15	16.3	12.0	38	1.08	2.06
	Bi(2$\bar{1}\bar{1}$)	0.41	0.16	20	16.2	11.9	38	1.03	2.05
MeOH	Bi(111)	0.52	0.14	10	19.8	8.2	26	1.05	–
[20]	Bi(001)	0.45	0.14	20	23.0	8.7	30	1.07	–
	Bi(01$\bar{1}$)	0.47	0.12	30	21.2	8.6	29	1.10	–
EtOH	Bi(111)	0.45	0.20	10	15.1	6.9	24	1.03	2.04
[17, 20, 24]	Bi(001)	0.42	0.18	20	16.4	7.9	29	1.08	2.07
	Bi(01$\bar{1}$)	0.44	0.15	20	15.8	7.5	29	1.07	–
	Bi(2$\bar{1}\bar{1}$)	0.46	0.11	25	15.8	7.2	30	1.12	–
[17, 20]	Sb(111)	0.26	0.20	15	11.0	6.7	19	1.01	–
	Sb(001)	0.19	0.18	20	13.4	7.3	21	1.04	–
i-PrOH	Bi(111)	0.45	0.20	10	15.9	6.0	–	1.02	–
[25]	Bi(001)	0.41	0.17	25	18.4	6.8	–	1.07	–
	Bi(01$\bar{1}$)	0.46	0.15	30	13.7	6.6	–	1.03	–

лярной плотности атомов сетки при одинаковой s^2p^3 электронной конфигурации незначительна и наблюдается лишь тенденция уменьшения отрицательного значения $E_{\sigma=0}$ при росте ретикулярной плотности сетки граней. Однако разность $E_{\sigma=0}$ для названных выше граней по сравнению с базисной гранью (111) составляет 70 - 120 мВ для Sb и 55 - 75 мВ для Bi, что, по всей вроятности, обусловлено различными поверхностными состояниями названных граней, т.е. у поверхностных атомов граней (001), ($\bar{1}0\bar{1}$), (01$\bar{1}$) и (2$\bar{1}\bar{1}$) существуют ненасыщенные ковалентные связи (s^2p^3-валентные состояния), а у поверхностных атомов грани (111) все ковалентные связи химически насыщены и они склонны к образованию связи при помощи гибридных sp^3d^2-орбиталей [35]. Подобная тенденция имеет место также и в случае неводных

растворителей. Из табл. 1 следует, что $\Delta E_{\sigma=0}$ возрастает в ряду *i*-PrOH ≈ EtOH < MeOH < H_2O < < ACN. Если в первом довольно грубом приближении допустить, что разность работы выхода электрона в раствор для граней Bi не зависит от природы растворителя, то нивелирование значений $E_{\sigma=0}$ указывает на заметное уменьшение различий в лиофильности различных граней Bi в *i*-PrOH или EtOH по сравнению с ACN или на более сильную адсорбцию анионов ClO_4^- на гранях $(01\bar{1})$ и $(2\bar{1}\bar{1})$ из EtOH или *i*-PrOH по сравнению с остальными гранями. Однако, к сожалению, прямое сопоставление абсолютных значений $E_{\sigma=0}$ для водной и неводной сред невозможно, поскольку $E_{\sigma=0}$ для неводной среды измерены относительно водного насыщенного каломельного электрода и значения $E_{\sigma=0}$ установлены лишь с точностью до не известного, но постоянного в пределах одного растворителя скачка потенциала жидкостного соединения. Поэтому в табл. 1 представлены величины скачка потенциала при переходе от H_2O к рассматриваемому растворителю *x*, т.е. величины $\Delta E_{\sigma=0}^{H_2O-x}$. Сопоставление данных табл. 1 с данными для Hg и Bi [24] показывает, что изменение лиофильности граней (001), $(\bar{1}0\bar{1})$ и (111) при переходе от H_2O к неводной среде практически совпадает с соответствующими изменениями для ПК-Bi и Hg. Наименьшие сдвиги $\Delta E_{\sigma=0}^{H_2O-x}$ для граней $(01\bar{1})$ и $(2\bar{1}\bar{1})$ обусловлены более сильной адсорбцией молекул растворителя (EtOH или *i*-PrOH), а также слабой специфической адсорбцией анионов ClO_4^- на поверхности химически более активных граней $(01\bar{1})$ и $(2\bar{1}\bar{1})$ Bi и Sb. В пользу последнего вывода говорят наиболее высокие значения коэффициента Есина–Маркова $(\partial E_{min}/\partial \lg c)$ в табл. 1 для $(01\bar{1})$ и $(2\bar{1}\bar{1})$ Sb и Bi.

Интересно отметим, что, как и в случае граней монокристалла Zn [34, 36], для Cd$(10\bar{1}0)$ и Cd$(11\bar{2}0)$ зависимость $E_{\sigma=0}$ от ретикулярной плотности сетки незначительна, а величины $E_{\sigma=0}$ для базисных граней Zn(0001) и Cd(0001) сдвинуты соответственно на 90 и 60 мВ в анодную сторону. Следовательно, повышение ретикулярной плотности сетки Zn- и Cd-электродов приводит к сдвигу $E_{\sigma=0}$ в анодную сторону.

На основе емкостных данных при различных σ = const были построены $C^{-1}, C_Д^{-1}$-зависимости, где $C_Д$ – емкость диффузного слоя, т.е. графики Парсонса–Цобеля [28]. Полученные зависимости (кроме Bi$(2\bar{1}\bar{1})$ и Sb$(2\bar{1}\bar{1})$) в интервале 0.003 М ≤ ≤ $c_{эл}$ ≤ 0.1 М являются линейными с котангенсом угла наклона f_{P-Z} = 1.01 - 1.12 [19]. Для электродов Bi$(2\bar{1}\bar{1})$ и Sb$(2\bar{1}\bar{1})$ графики Парсонса–Цобеля являются линейными при 0.007 ≤ $c_{эл}$ ≤ 0.1М. В данном месте необходимо отметить, что фактор f_{P-Z} является сложной комплексной величиной и в суммарном описывает отклонение реальной (экспериментальной) системы от идеальной системы с f_{P-Z} = 1.00 [11 - 22, 37, 38]. Отклонение $C^{-1}, C_Д^{-1}$-графиков от линейности может быть обусловлено также и экспериментальными погрешностями [37, 38], однако, на наш взгляд, различное поведение разных граней монокристалла Bi, Sb и Cd, по всей вероятности, в основном обусловлено слабой специфической адсорбцией анионов фона, а также геометрической и энергетической неоднородностью граней. Этот вывод подтверждается тем фактом, что при росте ν и отрицательного заряда поверхности наблюдается уменьшение f_{P-Z}.

На основе *C,E*-кривых по модели Гуи–Чапмена–Штерна–Грэма (**ГЧШГ**) [26] и методике работы [11] были рассчитаны C_H,σ-кривые, представленные для некоторых систем на рис. 2. Согласно данным рис. 2а и табл. 1, для водной среды величина $C_H^{\sigma=0}$ увеличивается в ряду Sb < Bi < Cd < Zn, что соответствует росту гидрофильности в приведенном ряду металлов [39, 40]. Величина емкости плотного слоя C_H при σ ≤ 0 увеличивается в ряду *i*-PrOH < EtOH < MeOH < ACN < H_2O (рис. 2), что соответствует возрастанию макроскопической диэлектрической проницаемости и уменьшению линейных размеров молекул растворителей (в первом приближении $C_H \sim \frac{\varepsilon\varepsilon_0}{d}$). В случае Sb- и Bi-электродов величина C_H (рис. 2б) увеличивается в ряду граней (111) < $(2\bar{1}\bar{1})$ < $(01\bar{1})$ < (001), т.е., за исключением грани (111), соблюдается основанное на модели жестких сфер правило [41], что более плотно упакованные грани имеют наибольшую емкость контакта металл/электролит. Аномальное расположение C_H,σ-кривой грани (111) по сравнению с гранями $(01\bar{1})$ и $(2\bar{1}\bar{1})$ монокристалла Sb и Bi как полуметаллов обусловлено различными металлическими свойствами отдельных граней [20, 42], т.е. значения C_H включают кроме истинной емкости плотного слоя C_s (C_s – емкость прослойки растворителя) также и емкость металлической фазы $C_м$ ($1/C_H = 1/C_s + 1/C_м$), зависящую от кристаллографической ориентации граней.

Для определения $C_м$ в работах [20, 42] были использованы различные модельные представления, однако в данной статье (табл. 1) приводятся лишь значения $C_м^{min}$, найденные по модели Амо-

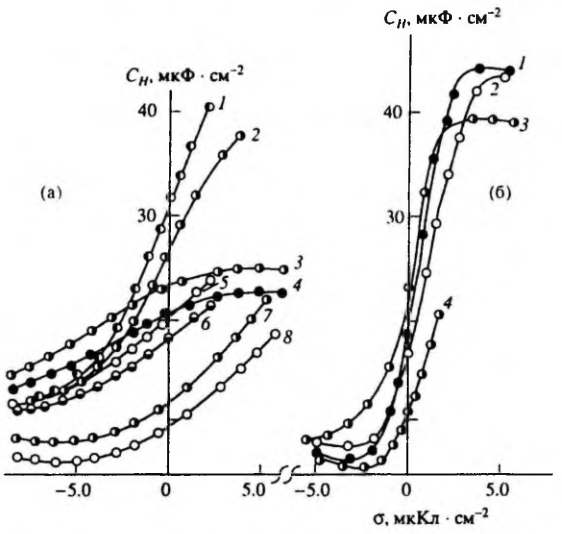

Рис. 2. C_H,σ-кривые в H_2O (*1* - *6*) и в ACN (*7*, *8*) для электродов: *1* – Cd(10$\bar{1}$0); *2* – Cd(0001); *3*, *7* – Bi(001); *4*, *8* – Bi(111); *5* – Sb(001); *6* – Sb(111) (а); для грани Bi(001) (*1* - *3*) и Sb(001) (*4*) для растворителей: *1* – *i*-PrOH; *2*, *4* – EtOH; *3* – MeOH (б).

крейна–Бадиали при допущении, что величина C_s определяется только свойствами растворителя (т.е. C_s является универсальной) и не зависит от природы металла и от кристаллографической структуры поверхности граней. На основе данных расчета (табл. 1) [20] величина $C_м^{min}$ увеличивается в ряду Sb < Bi < Hg < Cd, т.е. вклад металлической фазы в суммарную емкость C_H уменьшается при переходе от Sb к Cd. Величина $C_м^{min}$ для Sb(111) и Bi(111) существенно ниже, чем для остальных граней соответствующих металлов. Однако оказывается, что величина $C_м$ зависит от природы растворителя, и этот результат указывает на то, что допущение о универсальном характере C_s не выполняется. Следовательно, взаимодействие металлов с растворителями реально существует и игнорировать это явление необосновано.

АДСОРБЦИЯ ОРГАНИЧЕСКИХ МОЛЕКУЛ НА ГРАНЯХ МОНОКРИСТАЛЛА Bi, Sb И Cd

Адсорбция циклогексанола (**ЦГ**) [6, 7, 33, 43], *н*-гексанола (**НГ**) [44], циклогексанона (**ЦГН**) [45], циклогексанкарбоновой кислоты (**ЦГКК**) [46], бутилацетата (**БА**) [47], нормального (**НБС**), вторичного (**ВБС**), изобутилового (**ИБС**) [48] и третичного (**ТБС**) [49] спиртов исследовалась методом измерения импеданса в водном растворе поверхностно-неактивного электролита при T = = 293°K. Параметры адсорбции (табл. 2) были рассчитаны по методике Фрумкина–Дамаскина с применением модели обобщенного поверхностного слоя [50] (обозначения являются общепринятыми). Параметры обобщенной модели поверхностного слоя в общем мало отличаются от единицы, и, следовательно, адсорбция изученных соединений с хорошим приближением описывается в рамках теории Фрумкина–Дамаскина.

Значения адсорбционных параметров в табл. 2 свидетельствуют о существенной зависимости строения адсорбционного слоя как от химической природы и кристаллографической структуры поверхности электрода, так и от геометрического строения молекул адсорбата.

Согласно данным табл. 2, аттракционная постоянная a увеличивается при переходе от Sb к Bi, а также при переходе от Cd к Zn [43 - 49, 51], т.е. с ростом гидрофильности электродного металла в ряду Sb < Bi < Cd < Zn [39, 40].

При адсорбции органических молекул на гранях Sb и Bi a возрастает в ряду граней (2$\bar{1}\bar{1}$) < < (01$\bar{1}$) < ($\bar{1}$0$\bar{1}$) ≤ (001) < (111) [43 - 49, 51], т.е. с ростом гидрофильности граней в приведенном ряду и, за исключением грани (111), по мере снижения ретикулярной плотности упаковки. Низкие значения a для грани (2$\bar{1}\bar{1}$) обусловлены

Таблица 2. Параметры адсорбции органических соединений на гранях монокристаллов Bi, Sb и Cd

Система	Грань	a_0	C', $\frac{\text{мкФ}}{\text{см}^2}$	E_N, В	$\Gamma_м \times 10^{10}$, $\frac{\text{моль}}{\text{см}^2}$	B_0, $\frac{\text{дм}^3}{\text{моль}}$	$-\Delta G^\circ_A$, $\frac{\text{кДж}}{\text{моль}}$	$\Delta(-\Delta G^\circ_A)^{(111)}_{(z)}$
Bi/НБС	(111)	1.30	3.45	0.35	–	4.9	14.0	–
[48]	$(\bar{1}0\bar{1})$	1.38	4.76	0.28	–	5.9	14.44	0.44
	(001)	1.38	4.41	0.30	–	5.3	14.20	0.20
	$(01\bar{1})$	1.16	4.76	0.34	–	7.6	15.10	1.10
Bi/ИБС	(111)	1.60	3.57	0.34	–	3.0	12.66	–
[48]	$(\bar{1}0\bar{1})$	1.34	4.35	0.24	–	4.4	13.70	1.04
	(001)	1.68	4.44	0.32	–	3.0	12.70	0.04
	$(01\bar{1})$	1.23	4.81	0.32	–	6.1	14.52	1.80
	$(2\bar{1}\bar{1})$	1.20	4.72	0.32	–	5.3	14.20	1.54
Bi/ВБС	(111)	1.57	3.88	0.42	–	3.5	13.14	–
[48]	$(\bar{1}0\bar{1})$	1.42	4.76	0.26	–	4.8	13.95	0.81
	(001)	1.57	3.86	0.38	–	3.6	13.20	0.06
	$(01\bar{1})$	1.32	4.83	0.36	–	6.1	14.52	1.38
	$(2\bar{1}\bar{1})$	1.25	4.88	0.30	–	5.8	14.38	1.24
Bi/ТБС	(111)	1.53	4.03	0.49	4.6	2.6	12.2	–
[49]	$(\bar{1}0\bar{1})$	1.53	4.18	0.28	4.3	4.0	13.0	0.8
	(001)	1.26	4.40	0.46	4.7	3.1	12.6	0.4
	$(01\bar{1})$	0.85	4.48	0.36	4.4	4.6	13.6	1.4
Bi/БА	(111)	1.53	4.25	0.26	4.1	40	18.9	–
[47]	$(\bar{1}0\bar{1})$	1.53	4.60	0.29	4.0	104	21.3	1.4
	(001)	1.35	4.15	0.31	4.4	78	20.5	0.6
	$(01\bar{1})$	1.05	5.03	0.24	4.1	150	22.1	2.2
Bi/НГ	(111)	1.5	3.5	0.21	4.9	96	21.2	–
[44]	$(01\bar{1})$	1.3	3.3	0.19	4.4	132	22.0	0.8
	$(2\bar{1}\bar{1})$	1.3	3.6	0.18	4.1	113	21.7	0.3
Bi/ЦГ	(111)	1.83	4.0	0.49	5.5	20	17.1	–
[43, 51]	$(\bar{1}0\bar{1})$	1.65	4.1	0.34	5.1	43	19.0	1.9
	(001)	1.49	3.8	0.44	5.1	34	18.5	1.4
	$(01\bar{1})$	1.45	4.2	0.39	4.6	70	20.1	3.0
	$(2\bar{1}\bar{1})$	1.35	4.6	0.36	4.6	39	18.6	1.5
Sb/ЦГ	(111)	1.10	3.9	0.55	–	48	18.9	–
[32, 33]	(001)	0.95	4.4	0.50	–	68	20.1	1.2
	$(2\bar{1}\bar{1})$	0.70	3.6	0.42	–	86	20.7	1.8
Cd/ЦГ	(0001)	1.57	5.7	0.38	–	14	16.2	–
[7]	$(10\bar{1}0)$	1.40	5.4	0.28	–	22	17.4	1.2
	$(11\bar{2}0)$	1.37	5.2	0.27	–	21	17.3	1.1

Таблица 2. Окончание

Система	Грань	a_0	C', $\frac{\text{мкФ}}{\text{см}^2}$	E_N, В	$\Gamma_и \times 10^{10}$, $\frac{\text{моль}}{\text{см}^2}$	B_0, $\frac{\text{дм}^3}{\text{моль}}$	$-\Delta G_A^\circ$, $\frac{\text{кДж}}{\text{моль}}$	$\Delta(-\Delta G_A^\circ)_{(x)}^{(111)}$
Bi/ЦГН	(111)	1.04	4.8	0.55	–	60	19.8	–
[45]	(001)	0.99	6.6	0.51	–	68	20.1	0.3
	$(2\bar{1}\bar{1})$	0.92	6.4	0.45	–	174	22.4	2.6
Sb/ЦГН	(111)	1.02	5.4	0.65	–	98	21.0	–
[45]	(001)	0.83	7.0	–	–	200	22.4	1.4
	$(2\bar{1}\bar{1})$	0.64	6.6	–	–	293	22.8	1.8
Bi/ЦГКК	(111)	1.48	3.0	0.51	–	49	19.3	–
[46]	(001)	1.35	3.1	–	–	68	20.1	0.8
	$(2\bar{1}\bar{1})$	1.21	3.1	–	–	96	21.0	1.7
Sb/ЦГКК	(111)	1.31	3.1	0.55	–	105	20.8	–
[46]	(001)	0.92	3.5	–	–	143	21.6	0.8
	$(2\bar{1}\bar{1})$	0.70	3.6	–	–	166	22.3	1.5

ступенчатой топологией поверхности [43, 51]. В случае Cd- и Zn-электродов [52] притягательное взаимодействие увеличивается в ряду $(11\bar{2}0) <$ $< (10\bar{1}0) < (0001)$, т.е. с увеличением ретикулярной плотности упаковки граней. Из табл. 2 следует, что притягательное взаимодействие в адсорбционном слое зависит как от длины и строения углеводородного радикала, так и от расположения и химической природы функциональной группы. В общем a увеличивается в ряду НБС ≤ ВБС ≤ ≤ ИБС ≤ ТБС < ЦГКК < НГ < ЦГН < ЦГ, и этот ряд практически совпадает с увеличением стерических эффектов при переходе от НБС к НГ и далее к ЦГ [53].

Повышенные значения C' и пониженные величины $\Gamma_и$ и A на гранях $(\bar{1}0\bar{1})$, $(2\bar{1}\bar{1})$ и $(01\bar{1})$, а также уменьшение $E_п$ в ряду граней (111) > (001) > $> (01\bar{1}) > (2\bar{1}\bar{1}) > (\bar{1}0\bar{1})$ указывает на более выраженный горизонтальный компонент в расположении молекул на названных гранях по сравнению с гранью (111). Величина $E_п$ зависит также от строения углеводородного радикала и функциональной группы органического соединения и увеличивается в ряду НГ < ЦГКК ≤ ЦГ < ЦГН и в случае бутиловых спиртов в ряду ИБС ≤ НБС < < ВБС < ТБС [43 - 49, 51], т.е. с увеличением эффективного дипольного момента адсорбата.

Возрастание значений B_0 и $-\Delta G_A^0$ в ряду граней $(111) < (001) < (\bar{1}0\bar{1}) < (2\bar{1}\bar{1}) < (01\bar{1})$ указывает на возрастание адсорбционной активности изученных органических молекул в приведенном ряду граней, что связано с уменьшением гидрофильности поверхности Sb и Bi электродов в данном ряду. Пониженная адсорбционная активность грани (111) Sb и Bi может быть обусловлена кроме более выраженной гидрофильности также и менее активным состоянием грани (111) [43 - 49, 51].

Для оценки роли функциональной группы в адсорбционной связи молекулы адсорбата с поверхностью в табл. 2 включены разности изменения энергии адсорбции $[(-\Delta G_A^0)_{(x)} - (-\Delta G_A^0)_{(111)}]$ для изученной грани (x) и менее активной грани (111). Из табл. 2 следует, что разность $\Delta(-\Delta G_A^0)_{(x)}^{(111)}$ увеличивается с повышением адсорбционной активности адсорбата. Этот результат указывает на то, что хотя адсорбция органических молекул в основном обусловлена эффектом выжимания, некоторую роль играет также и химическое взаимодействие адсорбата с поверхностью. Этот вывод подтверждается данными рис. 3, на основе которого разность потенциала нулевого заряда $E_{\sigma=0}$ и катодного максимума адсорбции адсорбатов E^{max} при $c_{адс}$ = const увеличивается в ряду электродов $Zn(11\bar{2}0) <$ $< Zn(0001) < Cd(11\bar{2}0) \approx Cd(10\bar{1}0) < Cd(0001) <$ $< Bi(001) < Bi(\bar{1}0\bar{1}) < Bi(2\bar{1}\bar{1}) < Bi(111) < Bi(01\bar{1}) <$ $< Sb(001) < Sb(111) < Sb(2\bar{1}\bar{1})$, что, согласно модельным представлениям работ [39, 40], соответствует уменьшению гидрофильности электродов

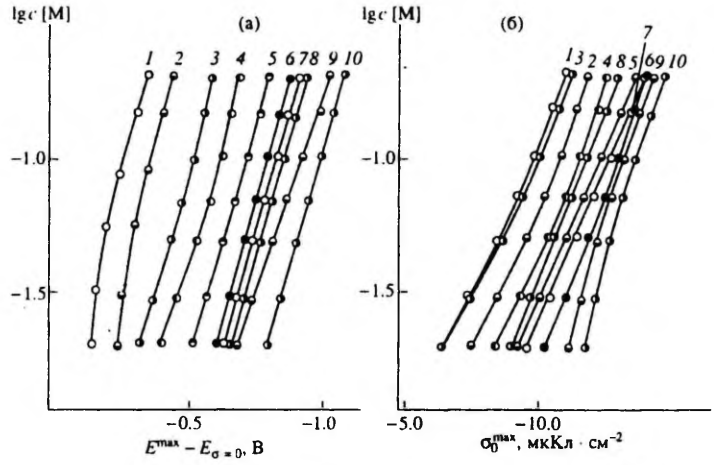

Рис. 3. ($E^{max} - E_{\sigma=0}$), lg$c$- (а) и σ_0^{max},lg$c$-кривые (б) при адсорбции ЦГ на электродах: *1* – Zn(11$\bar{2}$0); *2* – Zn(0001); *3* – Cd(11$\bar{2}$0); *4* – Cd(0001); *5* – Bi(001); *6* – Bi(111); *7* – Hg; *8* – Sb(111); *9* – Sb(001); *10* – Sb(2$\bar{1}\bar{1}$).

при переходе от Zn(11$\bar{2}$0) к Sb(2$\bar{1}\bar{1}$). Аномальное расположение ($E^{max} - E_{\sigma=0}$),lg$c$-кривых для граней Sb(111) и Bi(111) в основном связано с очень прочной структурой адсорбционного слоя (высокие значения a, A, $\Gamma_м$ и E_N), который разрушается при более высоких отрицательных потенциалах [43, 51]. На рис. 3б приведены зависимости заряда поверхности в фоновом растворе электролита при потенциалах адсорбционно-десорбционных максимумов σ_0^{max} от lg$c_{адс}$ [6, 7, 33, 51]. Выясняется, что величина σ_0^{max} зависит от химической природы металла и кристаллографической структуры поверхности, а также от адсорбата. По нашему мнению, этот результат является следствием того, что либо при $\sigma \ll 0$ разные металлы и грани имеют различные гидрофильности (см. табл. 1), либо взаимодействие органических молекул с поверхностью не является чисто физическим и включает в себя некоторую долю химического взаимодействия. Исследованиями кинетики адсорбции ЦГ установлено [51], что на гранях (001), (10$\bar{1}$) и (111) Bi адсорбция ЦГ носит чисто физический характер и лишь в случае химически более активных граней (2$\bar{1}\bar{1}$) и (01$\bar{1}$) некоторую роль играет частичный перенос заряда. Адсорбция изомеров бутилового спирта на гранях Bi контролируется стадией диффузии и, следовательно, адсорбция имеет в основном физический характер. В пользу этого говорит равновесность C,E-кривых.

СТРОЕНИЕ ДВОЙНОГО ЭЛЕКТРИЧЕСКОГО СЛОЯ НА ПОЛИКРИСТАЛЛИЧЕСКОЙ ПОВЕРХНОСТИ ВИСМУТОВОГО ЭЛЕКТРОДА

Для экспериментальной проверки соответствующих теоретических представлений о влиянии кристаллографической структуры поверхности электрода на строение ДЭС были проведены импедансные измерения на КДМЭ и **ХТВ** (химически травленном висмуте) (табл. 3). В табл. 3 $\Delta E_{\sigma=0}$ – разность $E_{\sigma=0}$ для отдельных граней КДМЭ; $E^{экс}_{мин,ПК}$ и $E^{расч}_{мин,ПК}$ – потенциалы минимума $C^{экс}_{ПК}$,E- и $C^{расч}_{ПК}$,E-кривых соответственно.

Сопоставлением экспериментальных $C^{экс}_{ПК}$,E-кривых с рассчитанными по модели МНЭ [$C^{расч}_{ПК} = \sum_i [f_i X_i C_{H,i} C_{д,i}/(C_{H,i} + C_{д,i})]$],$E$-кривыми в работах [21 - 23, 54, 55] было установлено их хорошее совпадение (рис. 4). Следовательно, $C^{экс}_{ПК}$,E-кривые для КДМЭ могут быть представлены в виде суммы $C_i^{ПК}$,E-кривых отдельных граней i при E-const и в хорошем приближении применима МНЭ, т.е. обе грани КДМЭ имеют собственные плотные ($C_{H,i}$) и диффузные ($C_{д,i}$) слои (X_i и f_i – доля поверхности и фактор неоднородности грани i, соответственно).

Таблица 3. Характеристики использованных висмутовых КДМЭ, ХТВ и КВВЭ и параметры ДЭС [15, 21 - 23, 54, 55]

Комбинация из граней	$\Delta E_{\sigma=0}$, мВ	c_{KF}, М	$-E^{экс}_{мин.ПК}$, В	$-E^{расч}_{мин.ПК}$, В	$f^{экс}_{P-Z}$, ±0.02	$f^{экс}_{C_{H,\bar{\sigma}}}$, ±0.02
0.6(001) + 0.4(111)	70	0.01	0.625	0.630	1.08	1.08
		0.001	0.610	0.620	1.14	1.28
0.3(01$\bar{1}$) + 0.7(111)	65	0.01	0.645	0.645	1.03	1.04
0.5(01$\bar{1}$) + 0.5(111)			0.635	0.620	1.09	10.6
0.8(01$\bar{1}$) + 0.2(111)			0.610	0.600	1.08	1.06
0.5(01$\bar{1}$) + 0.5(111)		0.001	0.605	0.615	1.15	1.26
0.3(01$\bar{1}$) + 0.7($\bar{1}$0$\bar{1}$)	15	0.01	0.605	0.605	1.02	1.03
0.4(01$\bar{1}$) + 0.6($\bar{1}$0$\bar{1}$)			0.600	0.605	1.03	1.02
0.8(01$\bar{1}$) + 0.2($\bar{1}$0$\bar{1}$)			0.600	0.595	1.03	1.04
0.4(01$\bar{1}$) + 0.6($\bar{1}$0$\bar{1}$)		0.001	0.590	0.590	1.07	1.12
0.55($\bar{1}$0$\bar{1}$) + 0.45(001)	5	0.01	0.610	0.615	1.04	1.03
		0.001	0.600	0.590	1.08	1.13
ХТВ-I	–	0.01	0.630	–	1.12	1.15
		0.001	0.610	–	1.20	1.25
ХТВ-II	–	0.01	0.610	–	1.18	1.20
		0.001	0.600	–	1.28	1.30
КВВЭ	80	0.01	0.625	0.620	1.02	1.10
		0.001	0.620	0.620	1.05	1.25

Согласно данным табл. 3, значения $E^{экс}_{мин.ПК}$ зависят от соотношения долей выхода граней X_1/X_2, причем наибольшая зависимость $E^{экс}_{мин.ПК}$ от соотношения X_1/X_2 наблюдается для КДМЭ с бо́льшей $\Delta E_{\sigma=0}$ [21, 22, 54, 55]. На основе $C^{экс}_{ПК}$,E-кривых при $E^{экс}_{мин.ПК}$ построены $(C^{экс}_{ПК})^{-1}$,$(C_{д,\bar{\sigma}})^{-1}$-зависимости, где значения $C_{д,\bar{\sigma}}$ рассчитаны по формулам теории Гуи–Чапмена в предположении, что при $E^{экс}_{мин.ПК}$ $\bar{\sigma} = \sum_i X_i\sigma_i = 0$. Анализ показывает, что величина котангенса $(C^{экс}_{ПК})^{-1}$,$(C_{д,\bar{\sigma}})^{-1}$-кривых $f^{экс}_{P-Z.ПК}$ зависит от $\Delta E_{\sigma=0}$, от соотношения X_1/X_2, а также и от $c_{эл}$, поскольку даже при умеренном $\Delta E_{\sigma=0}$ (60 - 80 мВ) $(C^{экс}_{ПК})^{-1}$,$(C_{д,\bar{\sigma}})^{-1}$-зависимости нелинейны и отклонение экспериментальных точек от прямой увеличивается по мере снижения $c_{эл}$ и с ростом $\Delta E_{\sigma=0}$ для КДМЭ. В работах [54, 55] показано, что использование значений $C_{д,\bar{\sigma}}$ для построения $(C^{экс}_{ПК})^{-1}$,$(C_{д,\bar{\sigma}})^{-1}$-графиков не корректно, поскольку при рассмотрении при кристаллографической неоднородности КДМЭ распределение ионов в диффузном слое принято также зависящим от координаты, направленной вдоль поверхности. Построенные в координатах $(C^{экс}_{ПК})^{-1}$,$(\sum C_д)^{-1}$-графики ($\sum_i C_д = \sum X_i C_{д,i}$ при E = const) практически прямолинейны, и величины котангенса угла наклона $f^{\sum C_i}_{P-Z}$ ($f^{\sum C_i}_{P-Z}$ = = 1.02 - 1.04) не зависят от типа КДМЭ (от $\Delta E_{\sigma=0}$), от $c_{эл}$, а также и от соотношения X_1/X_2.

Найденные по форме $C_{H,ПК}$,$\bar{\sigma}$-кривых значения фактора $f^{экс}_{C_{H,\bar{\sigma}}}$ также возрастают с разбавлением раствора и с ростом $\Delta E_{\sigma=0}$ для отдельных граней КДМЭ. В работах [54, 55] установлено, что так как различия в гидрофильных свойствах граней Bi незначительны и $\Delta C_{H,i}$ не зависят от $c_{эл}$, то наблюдаемые в случае КДМЭ эффекты кристаллографической и энергетической неоднородности в основном обусловлены различными значениями емкости диффузного слоя для разных граней КДМЭ вследствие различных значений σ_i для отдельных граней КДМЭ при E = const.

Более сложной задачей оказывается анализ строения ДЭС химически травленной поверхности граней (001) и (111), а также каплевидного висмутового электрода (**КВВЭ**), на поверхности

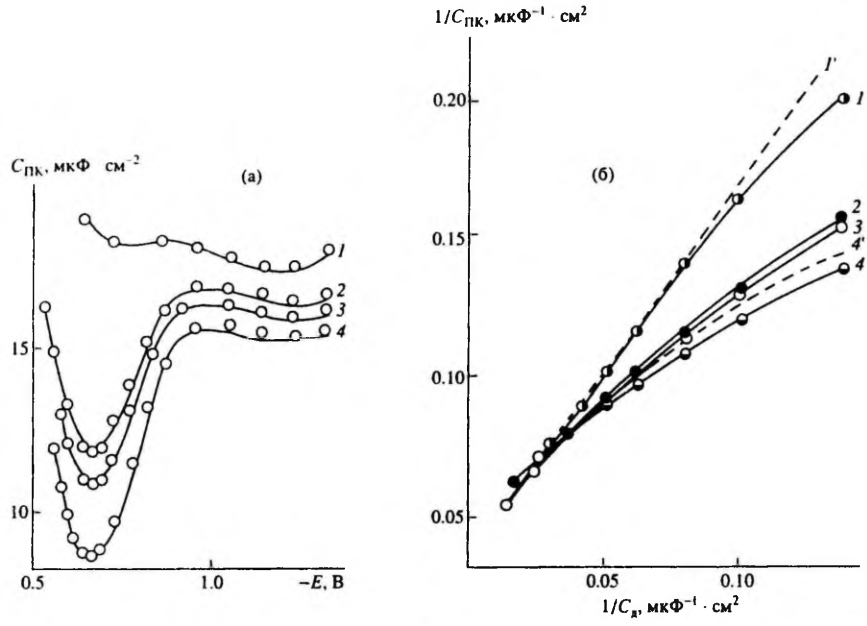

Рис. 4. $C_{ПК}$,E-кривые (а) для КДМЭ [0.5 Bi(111) + 0.5 Bi(01$\bar{1}$)] в водном растворе KF при c, М: *1* – 0.1; *2* – 0.01; *3* – 0.007; *4* – 0.003. Точки – эксперимент; сплошные линии – расчет по МНЭ. $C_{ПК}^{-1}$,$C_д^{-1}$-кривые (б) для КДМЭ: *1* – [0.5(01$\bar{1}$) + + 0.5($\bar{1}$0$\bar{1}$)]; *2* – [0.8(01$\bar{1}$) + 0.2(111)]; *3* – [0.3(01$\bar{1}$) + 0.7(111)] и *4* – [0.5(01$\bar{1}$) + 0.5(111)]. Кривая *1'* – расчет по МЭДС; *4'* – расчет по МНЭ.

которого представлена вся совокупность граней монокристалла, имеющих самые различные размеры и характеристики ДЭС, где однородные участки поверхности расположены не плоско и не равномерно относительно друг друга по всей поверхности КВВЭ. На основе проведенного анализа установлено [21, 22, 54, 55], что строение ДЭС на КВВЭ [53] или ХТВ описывается либо моделью единого диффузного слоя [13], либо уравнениями модели Воротынцева [14], при выдвижении которых были учтены эффекты нелинейности экранирования поля в диффузном слое, неплоское и неравномерное расположение однородных участков и другие эффекты, характерные для ПКЭ. В случае КВВЭ и ХТВ отмеченные выше модели являются неразличимыми [53], поскольку для граней монокристалла висмута наблюдается слишком слабая зависимость C_{Hi} от индекса грани при E = const. В случае КВВЭ графики Парсонса–Цобеля линейны [53], а эффективная фрактальная размерность D = 2.02 (т.е. поверхность КВВЭ является практически идеально гладкой). В случае ХТВ графики Парсонса–Цобеля не линейны [12, 21 - 23], а величина D = 2.20 - 2.30.

Следовательно, применимость той или иной модели для описания строения ДЭС на границе раздела ПКЭ / раствор электролита определяется анизотропией $E_{\sigma=0}$, $C_д$ и C_H разных граней, а также долей выхода X_i и размерами однородных монокристаллических участков.

АДСОРБЦИЯ ТРЕТИЧНОГО БУТИЛОВОГО СПИРТА, БУТИЛАЦЕТАТА И ЦИКЛОГЕКСАНОЛА НА ПОВЕРХНОСТИ ПКЭ ИЗ ВИСМУТА

С целью выяснения влияния кристаллографических и энергетических характеристик поверхности на адсорбцию органических соединений, а также применимости модели параллельных конденсаторов [9, 10] для описания адсорбции органических молекул на ПКЭ в работах [22, 23, 56, 57] была исследована адсорбция ЦГ, ТБС и БА на КДМЭ и ДЭМЭ, типы которых охарактеризова-

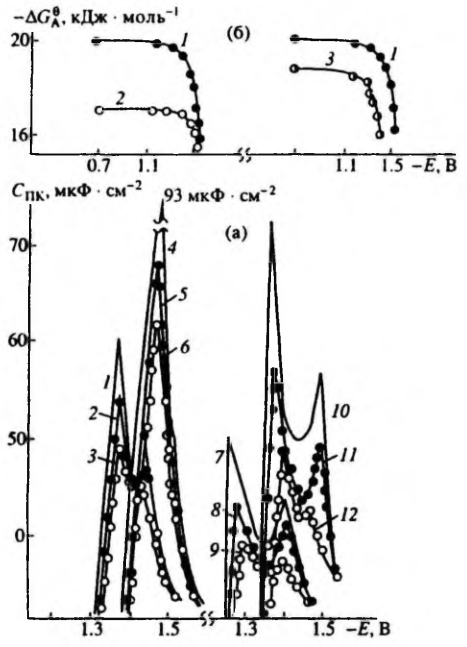

Рис. 5. $C_{ПК}$,E-кривые (а) в 0.05М водном растворе Na_2SO_4 с добавками 0.05 М ЦГ (*1* - *3*, *7* - *9*) и 0.1 М ЦГ (*4* - *6*, *10* - *12*) для ДЭМЭ-I [0.5(111) и 0.5(01$\bar{1}$)] – (*2*, *5*); для ДЭМЭ-II [0.5($\bar{1}$0$\bar{1}$) и 0.5(01$\bar{1}$)] – (*8*, *11*); для КДМЭ-I [0.5(101) + 0.5(01$\bar{1}$)] – (*3*, *5*) и для КДМЭ-II [0.5($\bar{1}$0$\bar{1}$) + 0.5(01$\bar{1}$)] – (*9*, *12*). Кривые *1*, *4*, *7*, *10* – расчет по МНЭ. ($-\Delta G_A^{\theta=0.5}$),E-кривые (б) при адсорбции ЦГ на Bi(01$\bar{1}$) – *1*; Bi(111) – *2* и Bi($\bar{1}$0$\bar{1}$) – *3*.

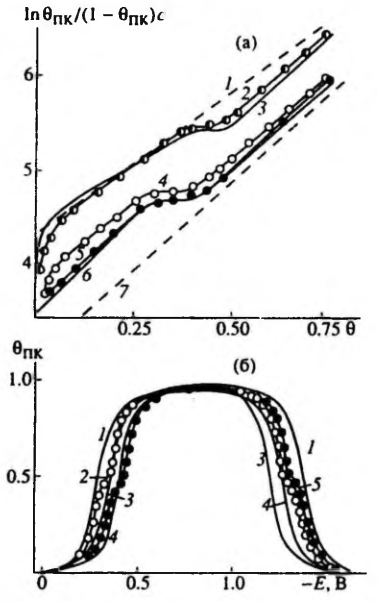

Рис. 6. Изотермы адсорбции ЦГ (а) на висмуте: *1* – (01$\bar{1}$); *2* – КДМЭ-I [0.7(01$\bar{1}$) + 0.3(111)]; *4* – КДМЭ-I [0.3(01$\bar{1}$) + 0.7(111)]; *5* – ДЭМЭ-I [0.5(01$\bar{1}$) и 0.5(111)] и *7* – грань (111). Кривая *3* – расчет при B_1^0 = 70 и B_2^0 = 20 дм^3/моль; a_1^0 = 1.45, a_2^0 = 1.82; X_1 = 0.68 и B_3' = 110 дм^3/моль; a_3' = 2.0 и X_3 = 0.04. Кривая *6* – расчет при B_1^0 = 70 и B_2^0 = 20 дм^3/моль; a_1^0 = 1.45; a_2^0 = 1.82 и X_1 = 0.3. Зависимость θ от E (б) при адсорбции ЦГ на электродах: *1* – Bi(01$\bar{1}$); *2* – КДМЭ-II; *3* – Bi($\bar{1}$0$\bar{1}$); *4* – Bi(111); *5* – КДМЭ-I.

ны в табл. 4. Индекс "1" обозначает более поверхностно-активную грань (см. табл. 2).

В работах [22, 23, 56, 57] было установлено, что характер энергетической неоднородности твердого электрода наиболее наглядно проявляется в форме адсорбционно-десорбционных максимумов $C_{ПК}$,E-кривых (расширение и расщепление максимумов), а также в форме (в виде задержек) $\sigma_{ПК}$,E-; $\theta_{ПК}$,E- и $\theta_{ПК}$,c-кривых ($\theta_{ПК}$ – степень заполнения ПКЭ) (рис. 5 и 6). Установлено, что с ростом адсорбционной неоднородности, мерой которой можно считать разность изменения свободной энергии адсорбции $\Delta(-\Delta G_A^{E,\theta})$ для отдельных граней КДМЭ или ДЭМЭ, отмеченные выше эффекты, характерные для ПКЭ, усиливаются. Согласно данным расчета, значение $\Delta(-\Delta G_A^{E,\theta})$ зависит от адсорбата и от E, поскольку $\Delta(-\Delta G_A^{E,\theta})$ связано с различными значениями C', E_N, $\Gamma_м$, a_0, B_0 и σ_0 для разных граней (табл. 2). Наибольший вклад в $\Delta(-\Delta G_A^{E,\theta})$ дают параметры B_0 и $\int \sigma_0 dE$, наименьший вклад C' [22, 23, 56, 57].

Экспериментально-теоретическим анализом установлено, что с ростом $\Delta(-\Delta G_A^{E,\theta})$ для отдельных граней увеличивается отклонение изучаемой системы от модели параллельных конденсаторов, связанное с перераспределением адсорбционного равновесия в процессе адсорбции [22, 23, 56]. При адсорбции органических молекул с замедленной стадией диффузии (ЦГ, БА) на КДМЭ или ДЭМЭ отдельные компоненты эквивалентной цепи переменного тока (в том числе значения импеданса

Таблица 4. Параметры адсорбции ЦГ, ТБС и БА на КДМЭ и ДЭМЭ [22, 23]

Адсорбат	Тип электрода	Комбинация граней	$X_1 \pm 0.05$	$X_2 \pm 0.05$	a_I'	B_I', $\frac{дм^3}{моль}$	a_{II}'	B_{II}', $\frac{дм^3}{моль}$
ЦГ	КДМЭ I	$(01\bar{1}) + (111)$	0.20	0.80	1.50	44.7	1.76	27.1
			0.40	0.60	1.46	48.0	1.68	29.0
			0.80	0.20	1.43	68.0	1.58	27.0
	ДЭМЭ I	$(01\bar{1})$ и (111)	0.50	0.50	1.47	63.0	1.70	25.0
	КДМЭ II	$(01\bar{1}) + (\bar{1}0\bar{1})$	0.35	0.65	1.68	64.0	1.42	46.0
			0.45	0.55	1.46	66.5	1.60	44.7
	ДЭМЭ II	$(01\bar{1})$ и $(\bar{1}0\bar{1})$	0.50	0.50	1.68	56.8	1.68	44.2
	КДМЭ III	$(\bar{1}0\bar{1}) + (001)$	0.55	0.45	1.6	43.0	1.72	33.1
ТБС	КДМЭ I	$(01\bar{1}) + (111)$	0.30	0.70	–	–	1.40	2.9
			0.50	0.50	1.46	3.7	1.30	3.3
			0.70	0.30	1.42	4.1	1.32	3.8
БА	КДМЭ I	$(01\bar{1}) + (111)$	0.35	0.65	–	–	1.34	84.8
			0.45	0.55	0.99	124	1.42	91.8
			0.75	0.25	1.06	134	–	–

Варбурга) различны на разных участках КДМЭ или ДЭМЭ, что приводит к отклонению исследуемой системы от простой модели параллельных конденсаторов.

Необходимо отметить, что использование изотермы адсорбции Фрумкина в координатах зависимости $\theta_{ПК}$ от $y = c/c_{\theta=0.5}$ для определения значений a_0 и B_0 не обосновано, поскольку величины $\theta_{ПК}$ и $c_{\theta=0.5}$ зависят от соотношения B_1^0/B_2^0 и a_1^0/a_2^0, а также от X_1/X_2 и являются усредненными, поэтому и рассчитанные адсорбционные параметры являются кажущимися [22, 23, 56, 57]. Для анализа изотерм адсорбции целесообразно применить выпрямляющие координаты зависимости $\ln[\theta_{ПК}/(1 - \theta_{ПК})c]$ от $\theta_{ПК}$. Согласно данным рис. 6, суммарная изотерма для КДМЭ или ДЭМЭ состоит из двух практически линейных областей, между которыми наблюдается загиб, начало которого зависит от соотношения X_1/X_2, а длина загиба увеличивается по мере роста адсорбционной неоднородности КДМЭ или ДЭМЭ. Найденные из первой линейной области изотермы эффективные значения B_I' и a_I', а также из второй линейной области изотермы B_{II}' и a_{II}' представлены в табл. 4. Видно, что значения B_I' увеличиваются с ростом доли X_1, а значения B_{II}' несколько выше, чем B_2^0, для менее активной грани КДМЭ или ДЭМЭ. Установлено, что наибольшая зависимость эффективных адсорбционных параметров от X_1 наблюдается для модельных электродов с большей адсорбционной неоднородностью поверхности.

В отличие от рассчитанных и экспериментальных изотерм для ДЭМЭ, изотермы для КДМЭ при низких $\theta_{ПК}^{эксп}$ ($\theta_{ПК}^{эксп} \leq 0.15$) не линейны и искривляются в направлении пониженных значений $\ln[\theta_{ПК}^{эксп}/(1 - \theta_{ПК}^{эксп})c]$ (рис. 6). Совпадения опытной и рассчитанной изотерм можно добиться только с учетом поправок на влияние границы раздела между отдельными монокристаллическими участками, а также на ступенчатость топологии поверхности в области вершины клинообразного электрода. Согласно расчетам, значения a_3' и B_3' должны превышать соответствующие параметры для граней модельных электродов, в доля X_3 находится в пределах 0.01 - 0.05 [23].

Исследованиями адсорбции ЦГ, БА и ТБС на вицинальных (несингулярных) поверхностях (**ВЭ**) установлено, что на кривых емкости ВЭ наблюдается четкое расщепление адсорбционно-десорбционных максимумов, а изотермы адсорбции состоят из двух практически линейных участков, между которыми обнаружены четко выраженные загибы (рис. 7). Сходство формы адсорбци-

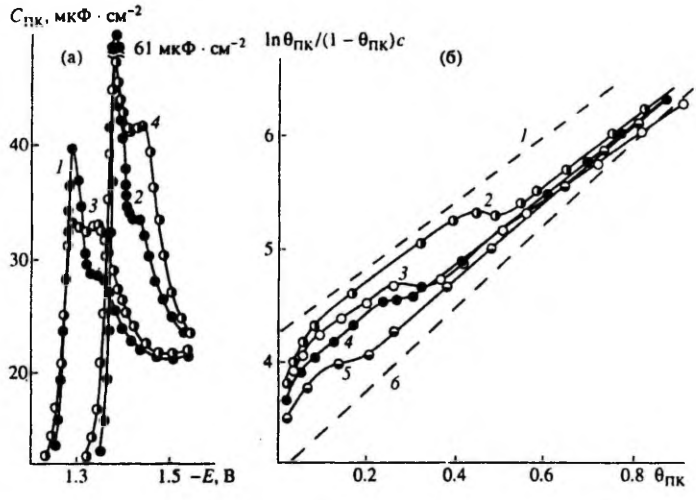

Рис. 7. $C_{ПК}$,E-кривые (а) с добавками ЦГ в растворе 0.05 М (*1*, *2*) и 0.1М (*3*, *4*) на (001) - $(01\bar{1})^{зоне}$. Плоскость пересечения 3° (*1*, *3*) и 10° (*2*, *4*) относительно грани (001). Изотермы адсорбции на висмуте (б): *1* – грань $(01\bar{1})$; *6* – грань (111); *2*, *3* – на (001) - $(01\bar{1})^{зоне}$ и *4*, *5* – на (111) - $(01\bar{1})^{зоне}$ при угле пересечения 10° (*2*, *4*) и 3° (*3*, *5*) относительно грани (001) и (111) соответственно.

онно-десорбционных максимумов, адсорбционных изотерм и найденных из них адсорбционных параметров позволяет предположить, что на поверхности ВЭ в основном превалируют адсорбционные центры двух типов, т.е. грани (111) и $(01\bar{1})$ на ВЭ-I и грани (001) и $(01\bar{1})$ на ВЭ-II. На кривых емкости адсорбции ЦГ, БА и ТБС на ХТВ наблюдаются относительно расширенные основные максимумы, а изотерма состоит из двух практически линейных участков. Переход от первой линейной области изотермы ко второму линейному участку происходит плавно и в широкой области $\theta_{ПК}^{экс}$ [22, 23, 56, 57].

Результаты исследования адсорбции ЦГ, ТБС и БА на ДЭМЭ, КДМЭ, ВЭ и ХТВ свидетельствуют о существенной зависимости формы изотермы адсорбции и явления расщепления адсорбционно-десорбционных максимумов от соотношения ряда адсорбционных параметров, а также от кристаллического состояния модельного электрода.

ЗАКЛЮЧЕНИЕ

На основе проведенного анализа установлено, что закономерности строения двойного электрического слоя и в адсорбции органических молекул в существенной мере зависят от химической природы и кристаллографической структуры поверхности электрода, а также от природы и молекулярной структуры молекул растворителя и адсорбата. Взаимное влияние электродного материала на поверхностное состояние молекул адсорбата и растворителя, а также влияние адсорбата и растворителя на энергетическое состояние электронного газа в приповерхностном слое реально существуют и игнорировать эти взаимодействия не обосновано. Проявление эффектов, характерных для поликристаллической поверхности, обусловлено, с одной стороны, анизотропией двойнослойных параметров энергетически однородных участков ПК поверхности и, с другой стороны, особенностями строения ПК поверхности (размерами однородных участков, их вицинальностью или несингулярностью, анизотропией энергетических характеристик и т.д.).

СПИСОК ЛИТЕРАТУРЫ

1. *Борисова Т.И., Эршлер Б.В., Фрумкин А.Н.* // Журн. физ. химии. 1948. Т. 22. С. 925.
2. *Борисова Т.И., Эршлер Б.В.* // Журн. физ. химии. 1950. Т. 24. С. 337.
3. *Frumkin A.* // J. Res. Inst. Hokkaido. 1967. V. 15. P. 61.
4. *Пальм У.* // Уч. зап. Тарт. гос. ун-та. 1986. Вып. 757. С. 3.

5. *Фрумкин А.Н., Пярноя М.П., Григорьев Н.Б., Пальм У.В.* // Электрохимия. 1974. Т. 10. С. 1130.
6. *Jänes A., Lust E., Pullerits R.* // Double Layer and Adsorption at Solid Electrodes. IX. Tartu Univ. 1991. P. 53.
7. *Lust E., Ehrlich J.* // Double layer and Adsorption t Solid Electrodes. IX. Tartu Univ. 1991. P. 112.
8. *Сальве М., Алумаа А., Пальм У.* // Уч. зап. Тарт. гос. ун-та. 1971. Вып. 289. С. 54.
9. *Frumkin A.N., Batrakov V.V., Sidnin A.I.* // J. Electroanalyt. Chem. 1972. V. 39. P. 225.
10. *Batrakov V.V., Damaskin B.B.* // J. Electroanalyt. Chem. 1975. V. 65. P. 361.
11. *Valette G., Hamelin A.* // J. Electroanalyt. Chem. 1973. V. 45. P. 301.
12. *Пальм У.В., Пярноя М.П., Григорьев Н.Б.* // Электрохимия. 1977. Т. 13. С. 1074.
13. *Bagotskaya I.A., Damaskin B.B., Levi M.D.* // J. Electroanalyt. Chem. 1980. V. 115. P. 189.
14. *Воротынцев М.А.* // Электрохимия. 1981. Т. 17. С. 197; С. 576; С. 1018.
15. *Пальм У.В., Пярноя М.П., Сальве М.А.* // Электрохимия. 1977. Т. 13. С. 873.
16. *Луст Э.Й., Пальм У.В.* // Электрохимия. 1985. Т. 21. С. 1256.
17. *Lust E., Anni K.* // Double Layer and Adsorption at Solid Electrodes. IX. Tartu Univ. 1991. P. 53.
18. *Луст Э.Й.* // Электрохимия. 1991. Т. 27. С. 424.
19. *Lust E., Jänes A., Lust K., Salve M.* // Trans. of Tartu Univ. 1993. V. 966. P. 63.
20. *Луст Э.Й., Янес А.А.-Я., Луст К.К., Эрлих Ю.Й.* // Электрохимия (в печати).
21. *Луст Э.Й., Салве М.А., Пальм У.В.* // Двойной слой и адсорбция на твердых электродах. VII. Тарту, 1985. С. 210.
22. *Луст Э.Й., Пальм У.В.* // Электрохимия. 1986. Т. 22. С. 411; С. 565.
23. *Луст Э.Й., Пальм У.В.* // Уч. зап. Тарт. гос. ун-та. 1986. Вып. 757. С. 105.
24. *Анни К.Л., Вяэртныу М.Г., Пальм У.В.* // Электрохимия. 1986. Т. 22. С. 992; 1988. Т. 24. С. 846.
25. *Pärsimägi P., Anni K., Väärtnõu M., Lust E.* // Double Layer and Adsorption at Solid Electrodes. IX. Tartu, 1991. P. 144.
26. *Grahame D.C.* // Chem. Rev. 1947. V. 41. P. 441.
27. *Amokrane S., Badiali J.P.* // J. Electroanalyt. Che. 1989. V. 266. P. 21; 1991. V. 297. P. 377.
28. *Parsons R., Zobel F.* // J. Electroanalyt. Chem. 1965. V. 9. P. 333.
29. *Nyikos L., Pajkossy T.* // Electrochim. Acta. 1985. V. 30. P. 1533.
30. *Ocko B.M., Wang J., Davenport A., Isaacs H.* // Phys. Rev. Lett. 1990. V. 65. P.1466.
31. *Hamelin A.* // J. Electroanalyt. Chem. 1992. V. 329. P. 247.
32. *Луст Э.Й., Янес А.А.-Я.* // Электрохимия. 1992. Т. 28. С. 802.
33. *Луст Э.Й., Янес А.А.-Я.* // Электрохимия. 1994. Т. 30. С. 357.
34. *Ипатов Ю.П., Батраков В.В.* // Электрохимия. 1975. Т. 11. С. 1717; 1976. Т. 12. С. 1174.
35. *Pearson W.B.* The Crystal Chemistry and Physics of Metals and Alloys. Wiley - Interscience, 1972. P. 280.
36. *Hamelin A., Vitanov T., Sevastyanov E., Popov A.* // J. Electroanalyt. Chem. 1983. V. 145. P. 225.
37. *Hamelin A., Stoicoviciu L.* // J. Electroanalyt. Chem. 1989. V. 271. P. 15.
38. *Луст Э.Й., Луст К.К., Янес А.А.-Я.* // Электрохимия. 1990. Т. 26. С. 1627.
39. *Frumkin A., Damaskin B., Grigoryev N., Bagotskaya I.* // Electrochim. Acta. 1974. V. 19. P. 69.
40. *Фрумкин А.Н.* Потенциалы нулевого заряда. М.: Наука, 1982. С. 153.
41. *Leiva E., Schmickler W.* // J. Electroanalyt. Chem. 1986. V. 205. P. 323; 1987. V. 229. P. 39.
42. *Луст Э., Пальм У.* // Уч. зап. Тарт. гос. ун-та. 1990. Вып. 905. С. 40.
43. *Пярноя М.П., Пальм У.В.* // Электрохимия. 1978. Т. 14. С. 1229.
44. *Тийдеберг М., Палтусова Н.* // Уч. зап. Тарт. гос. ун-та. 1984. Вып. 682. С. 151.
45, 46. *Янес А.А.-Я., Луст Э.Й.* // Электрохимия. 1995. Т. 31. С. 648.
47. *Луст Э.Й., Эрлих Ю.Й., Пальм У.В.* // Электрохимия. 1986. Т. 22. С. 695.
48. *Круусимяги А.Л., Луст Э.Й., Пальм У.В.* // Двойной слой и адсорбция на твердых электродах. VIII. Тарту, 1988. С. 198.
49. *Луст Э.Й., Пальм У.В.* // Электрохимия. 1986. Т. 22. С. 407.
50. *Дамаскин Б.Б.* // Электрохимия. 1970. Т. 6. С. 1135.
51. *Луст Э.Й., Пальм У.В.* // Электрохимия. 1985. Т. 21. С. 1381; 1988. Т. 24. С. 243.
52. *Ипатов Ю.П., Батраков В.В.* // Электрохимия. 1975. Т. 11. С. 1282; С. 1717.
53. *Тафт Р.В.* Пространственные эффекты в органической химии. М.: Изд-во иностр. лит., 1960. 719 с.
54. *Луст Э.Й., Салве М.А., Пальм У.В.* // Электрохимия. 1986. Т. 23. С. 561.
55. *Луст Э.Й., Пальм У.В.* // Электрохимия. 1988. Т. 24. С. 557.
56. *Алумаа А.Р., Луст Э.Й., Палтусова Н.А., Пальм У.В.* // Электрохимия. 1983. Т. 19. С. 1582.
57. *Луст Э.Й., Пальм У.В.* // Двойной слой и адсорбция на твердых электродах. VII. Тарту, 1985. С. 205.

IV

Reprinted from the *Russian Journal of Electrochemistry*, 32, No. 8,
A. A.-J. Jänes and E. J. Lust, Adsorption
of Cyclohexancarboxylic Acid on Facesof the Bismuth and
Antimony Single Crystals, pages 1020–1022 (in Russian),

ЭЛЕКТРОХИМИЯ, 1996, том 32, № 8, с. 1020–1022

КРАТКИЕ СООБЩЕНИЯ

УДК 541.135.52.183

АДСОРБЦИЯ ЦИКЛОГЕКСАНКАРБОНОВОЙ КИСЛОТЫ НА ГРАНЯХ МОНОКРИСТАЛЛОВ ВИСМУТА И СУРЬМЫ

© 1996 г. А. А.-Я. Янес, Э. Й. Луст

Тартуский университет, Эстония

Поступила в редакцию 14.06.95 г.

В электрохимической литературе накоплен обширный материал, свидетельствующий о влиянии кристаллографических характеристик поверхности электрода на адсорбцию органических соединений [1–8]. Настоящая работа посвящена изучению адсорбции циклогексанкарбоновой кислоты (**ЦГКК**) на сингулярных *F*-гранях (001) и (111) и на несингулярной *K*-грани $(2\bar{1}\bar{1})$ монокристаллов висмута и сурьмы. Методика измерений, подготовка электродов и очистка реактивов описаны ранее [2–8]. Электродом сравнения служил насыщенный каломельный электрод (нас. к. э.).

На рис. 1 приведены экспериментальные кривые зависимости емкости C от потенциала E на грани (111) монокристалла Bi и Sb в 0.1 М водном в растворе NaF в присутствии ЦГКК различных концентраций. Из рис. 1 видно, что на грани (111) C,E-кривые имеют обычную форму с острыми катодными максимумами адсорбции–десорбции с потенциалом E^{max}, высота которых закономерно возрастает с ростом концентрации ЦГКК. Согласно данным рис. 1 уменьшение гидрофильности поверхности сурьмяного электрода по сравнению с висмутовым электродом приводит к снижению высоты и к расширению пиков адсорбции–десорбции. Наблюдается увеличение высоты катодных максимумов в ряду граней $(2\bar{1}\bar{1}) < (001) < (111)$. Подобная закономерность имеет место при адсорбции циклогексанола (**ЦГ**) и циклогексанона (**ЦГН**) на гранях монокристалла Bi и Sb [2, 4–6], что обусловлено уменьшением энергетической неоднородности поверхности электрода в приведенном ряду граней.

Параметры адсорбции ЦГКК были рассчитаны из C,E-кривых по методике расчета Фрумкина–Дамаскина [9], основывающейся на модели двух параллельных конденсаторов. Значения полученных параметров приведены в таблице. Как следует из приведенных в таблице параметров, грани (111) и $(2\bar{1}\bar{1})$ имеют весьма разные адсорбционные свойства, а грань (001) занимает промежуточное положение между гранями (111) и $(2\bar{1}\bar{1})$. Подобная тенденция наблюдается и при адсорбции ЦГ и ЦГН на разных гранях монокристаллов Bi и Sb [2, 4–6].

Различие в адсорбционных свойствах исследованных граней монокристаллов висмута и сурьмы особенно наглядно проявляется на рис. 2а, где представлены зависимости потенциалов максимума адсорбции–десорбции в рациональной шкале $(E^{max}-E_{\sigma=0})$ от логарифма концентрации ЦГКК $\lg c$ для граней монокристалла Bi и Sb. Согласно представлениям работ [10, 11] и данным рис. 2а, гидрофильные свойства поверхности уменьшаются в ряду электродов Bi(111) > > Bi$(2\bar{1}\bar{1})$ > Sb(111) > Bi(001) > Sb(001) > Sb$(2\bar{1}\bar{1})$. Пониженная адсорбционная активность грани (111) обусловлена менее активным поверхностным состоянием, поскольку на поверхности этой грани все атомы химически насыщены и адсорбция носит чисто физический характер [2, 5, 6, 12].

На рис. 2б приведены зависимости заряда поверхности в фоновом растворе электролита при потенциалах адсорбционно-десорбционных максимумов σ_0^{max} от логарифма концентрации ЦГКК для граней монокристалла Bi и Sb. Этот результат совпадает с выводами работы [13, 14] и нашими предыдущими данными [2, 4–8, 12], где обна-

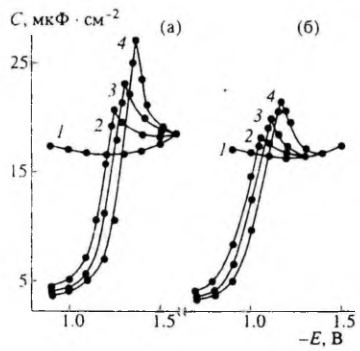

Рис. 1. C,E-кривые для граней Bi (111) – (а) и Sb (111) – (б) в 0.1 М растворе NaF (*1*) и с добавками ЦГКК, М: *2* – 0.015; *3* – 0.020; *4* – 0.025.

Параметры адсорбции циклогексанкарбоновой кислоты на гранях монокристалла Bi и Sb

Электрод	$a_м \pm 0.05$	C', мкФ/см^2	$c_{\theta=0.5}$, моль/дм^3	E_N, В	$B_м$, дм^3/моль	$-\Delta G_A^{м,*}$, кДж/моль	$E^{max}-E_{\sigma=0}$, В (0.02 М ЦГКК)
Bi (111)	1.48	3.0 ± 0.2	0.0034 ± 0.0002	0.51	49 ± 3	19.3 ± 0.2	0.65 ± 0.01
Bi (001)	1.35	3.1 ± 0.2	0.0032 ± 0.0002	0.48	68 ± 5	20.1 ± 0.2	0.78 ± 0.01
Bi ($2\bar{1}\bar{1}$)	1.21	3.1 ± 0.2	0.0030 ± 0.0002	0.46	96 ± 5	21.1 ± 0.2	0.82 ± 0.01
Sb (111)	1.31	3.1 ± 0.2	0.0028 ± 0.0002	0.55	105 ± 5	20.8 ± 0.2	0.73 ± 0.01
Sb (001)	0.92	3.5 ± 0.2	0.0026 ± 0.0002	0.51	143 ± 8	21.6 ± 0.2	0.81 ± 0.01
Sb ($2\bar{1}\bar{1}$)	0.70	3.6 ± 0.3	0.0024 ± 0.0003	0.47	166 ± 8	22.3 ± 0.2	0.86 ± 0.01

ружено, что энергия адсорбции органических соединений при отрицательных зарядах поверхности зависит от химической природы (гидрофильности) металлов.

На основе C,E-кривых для граней монокристалла висмута и сурьмы в растворе фона методом обратного интегрирования были построены σ,E-кривые в присутствии ЦГКК в растворе. Было найдено, что C,E-кривые для граней (001) и ($2\bar{1}\bar{1}$) в некоторой степени являются неравновесными. По соотношениям, вытекающим из модели двух параллельных конденсаторов [9], на основе C,E-кривых были рассчитаны изотермы адсорбции при потенциале максимальной адсорбции $E = E^{max}$. Статистически обработанные изотермы адсорбции ЦГКК представлены на рис. 3. Линейный характер зависимости $\ln[\theta/(1-\theta)c]$ от θ показывает, что адсорбционное поведение ЦГКК удовлетворительно описывается изотермой Фрумкина на всех исследованных гранях монокристалла висмута и сурьмы (рис. 3). Подобная закономерность имеет место при адсорбции ЦГ [2, 4, 5] и ЦГН [6] на гранях монокристалла Bi и Sb. Значения адсорбционных параметров в таблице свидетельствуют о существенной разнице адсорбционного поведения ЦГКК на изученных гранях монокристалла висмута и сурьмы. Возрастание значений $B_м$ и $-\Delta G_A^м$ в ряду граней (111) < (001) < ($2\bar{1}\bar{1}$) указывает на возрастание адсорбционной активности ЦГКК в этом же ряду граней. Наибольшую адсорбционную активность среди изученных граней имеет грань ($2\bar{1}\bar{1}$), которая несингулярна и является энергетически неоднородной по кристаллографическим причинам [15, 16]. Видно, что адсорбционная активность ЦГКК существенно выше на поверхности граней монокристалла сурьмы, чем на поверхности граней монокристалла висмута. Сравнение адсорбционных параметров $B_м$ и $-\Delta G_A^м$ с данными работ [2, 4–6, 12] показывает, что адсорбционная активность возрастает в ряду адсорбатов ЦГ < ЦГКК < ЦГН. Это различие обусловлено особенностями строения молекул ЦГ, ЦГКК и ЦГН, а также образованием различной структуры адсорбционного слоя.

Для выяснения специфики взаимодействия висмута и сурьмы с адсорбированными молекулами ЦГКК, ЦГ и ЦГН на рис. 4 сопоставлены изотермы двумерного давления на границах воздух/0.1 М NaF, Bi (111)/0.1 М NaF и Sb (111)/0.1 М NaF. Рисунок 4 показывает, что поверхностная активность ЦГКК, ЦГ и ЦГН на границе воздух/0.1 М NaF

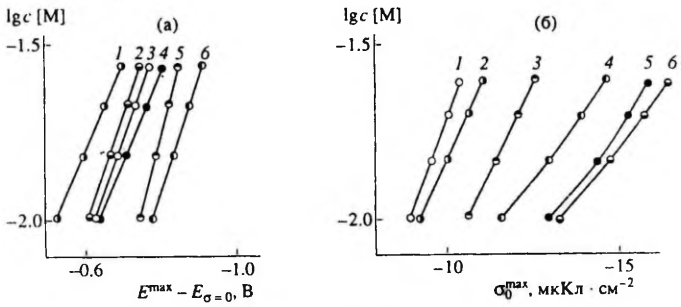

Рис. 2. Зависимость потенциала адсорбционно-десорбционных максимумов от lg c ЦГКК (а) для электродов: *1* – Bi (111); *2* – Bi($2\bar{1}\bar{1}$); *3* – Sb (111); *4* – Bi (001); *5* – Sb (001); *6* – Sb($2\bar{1}\bar{1}$) и зависимость σ_0^{max} от lg c ЦГКК (б) на гранях монокристалла: *1* – Sb (111); *2* – Bi (111); *3* – Sb (001); *4* – Sb($2\bar{1}\bar{1}$); *5* – Bi (001); *6* – Bi($2\bar{1}\bar{1}$).

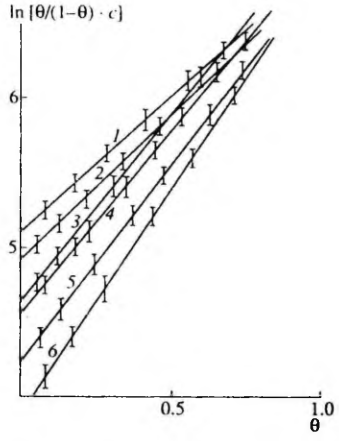

Рис. 3. Изотермы адсорбции ЦГКК на гранях монокристалла: *1* – Sb($2\bar{1}\bar{1}$); *2* – Sb (001); *3* – Sb (111); *4* – Bi($2\bar{1}\bar{1}$); *5* – Bi (001); *6* – Bi (111).

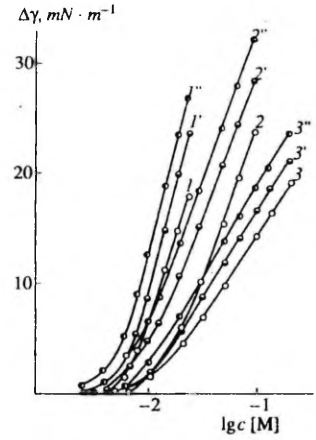

Рис. 4. Зависимость Δγ на границах раздела воздух/0.1 M NaF (*1*, *2*, *3*), Bi (111)/0.1 M NaF (*1'*, *2'*, *3'*) и Sb (111)/01 M NaF (*1"*, *2"*, *3"*) от lg*c* адсорбата: *1*, *1'*, *1"* – ЦГКК; *2*, *2'*, *2"* – ЦГ и *3*, *3'*, *3"* – ЦГН.

заметно ниже, чем на границе Bi (111)/0.1 M NaF и Sb (111)/0.1 M NaF. Величины Δγ в присутствии ЦГКК, ЦГ и ЦГН на границе Sb (111)/0.1 M NaF значительно выше, чем на границе Bi (111)/0.1 M NaF. Это различие обусловлено меньшей гидрофильностью сурьмяного электрода по сравнению с висмутовым. Повышение значений Δγ в ряду (111) < < (001) < ($2\bar{1}\bar{1}$) указывает на возрастание адсорбционной активности ЦГКК, ЦГ и ЦГН в этом же ряду граней. Более заметное специфическое взаимодействие ЦГКК с поверхностью Bi и Sb по сравнению с циклогексанолом [2, 4, 5] обусловлено более сильным взаимодействием –COOH группы как с поверхностью электрода, так и с адсорбированными на поверхности электрода молекулами воды.

В заключение отметим, что результаты настоящей работы свидетельствуют о существенной зависимости закономерностей адсорбции органических соединений от кристаллографических и энергетических характеристик разных граней. Превышение адсорбционной активности граней монокристалла Bi и Sb в ряду (111) < (001) < ($2\bar{1}\bar{1}$) в основном связано с уменьшением гидрофильных свойств в этом же ряду граней. Пониженная адсорбционная активность грани (111) может быть обусловлена кроме более выраженной гидрофильности менее активным поверхностным состоянием грани (111).

СПИСОК ЛИТЕРАТУРЫ

1. *Hamelin A., Vitanov T., Sevastyanov E., Popov A.* // J. Electroanalyt. Chem. 1983. V. 145. P. 225.
2. *Луст Э.Й., Пальм У.В.* // Электрохимия. 1985. Т. 21. С. 1381.
3. *Луст Э.Й., Луст К.К., Янес А.А.-Я.* // Электрохимия. 1990. Т. 26. С. 1627.
4. *Jänes A., Lust E., Pullerits R.* // Double Layer and Adsorption at solid electrodes, IX. Tartu. 1991. P. 53.
5. *Луст Э.Й., Янес А.А.-Я.* // Электрохимия. 1994. Т. 30. С. 357.
6. *Янес А.А.-Я., Луст Э.Й.* // Электрохимия. 1995. Т. 31. С. 648.
7. *Луст Э.Й., Пальм У.В.* // Электрохимия. 1986. Т. 22. С. 407.
8. *Луст Э.Й., Эрлих Ю.Й., Пальм У.В.* // Электрохимия. 1986. Т. 22. С. 695.
9. *Дамаскин Б.Б., Петрий О.А., Батраков В.В.* Адсорбция органических соединений на электродах. М.: Наука, 1968.
10. *Frumkin A., Damaskin B., Grigoryev N., Bagotskaya I.* // Electrochim. Acta. 1974. V. 19. P. 69.
11. *Фрумкин А.Н.* Потенциалы нулевого заряда. М.: Наука, 1982. С. 153.
12. *Пальм У.В., Пярноя М.П.* // Электрохимия. 1978. Т. 14. С. 1070.
13. *Григорьев Н.Б., Багоцкая И.А.* // Электрохимия. 1966. Т. 2. С. 1449.
14. *Pazzatini G., Moncelli M.R., Innocenti M., Guidelli R.* // J. Electroanalyt. Chem. 1990. V. 275. P. 295.
15. *Пирсон У.* Кристаллография и физика металлов и сплавов. Ч. I. М.: Мир, 1977. С. 280.
16. *Келли А., Гровс Г.* Кристаллография и дефекты в кристаллах. М.: Мир, 1974. С. 130.

V

Reprinted from the *Journal of Electroanalytical Chemistry*, Vol. 413,
E. Lust, A. Jänes, K. Lust and P. Miidla, Adsorption of Isomers of Butanol
on Bismuth Single Crystal Plane Electrodes, pages 175–185,

ELSEVIER

Journal of Electroanalytical Chemistry 413 (1996) 175–185

Adsorption of isomers of butanol on bismuth single crystal plane electrodes

E. Lust [a], A. Jänes [a], K. Lust [a], P. Miidla [b]

[a] *Institute of Physical Chemistry, University of Tartu, 2 Jakobi Street, EE-2400 Tartu, Estonia*
[b] *Institute of Applied Mathematics, University of Tartu, 2 Liivi Street, EE-2400 Tartu, Estonia*

Received 31 January 1996, revised 26 February 1996

Abstract

Cyclic voltammetry, impedance and chronocoulometry have been employed for quantitative study of normal butanol (*n*-BA), *iso*-butanol (*iso*-BA), *sec*-butanol (*sec*-BA) and *tert*-butanol (*tert*-BA) adsorption at the bismuth single crystal plane|aqueous Na_2SO_4 solution interface. The adsorption isotherms, Gibbs energies of adsorption, the surface excess and other adsorption parameters have been determined. As found, the adsorption characteristics of the isomers of butanol depend on the crystallographic structure of the electrodes, as well as on the geometrical structure of hydrocarbon chains of adsorbate. The adsorption characteristics obtained from the impedance and chronocoulometric measurements are in good agreement within the limits of surface charge densities $-24 < \sigma < 3\ \mu C\,cm^{-2}$. The adsorption of *n*-BA, *sec*-BA, *iso*-BA and *tert*-BA on Bi single crystal planes is physical and is limited by the rate of diffusion of organic molecules to the electrode surface. The adsorption activity of adsorbates at the bismuth|solution interface increases in the sequence *tert*-BA < *sec*-BA < *iso*-BA < *n*-BA as the adsorption at the air|solution interface increases. In the case of all compounds studied, the adsorption activity of planes increases in the sequence $(\bar{1}0\bar{1}) \leq (001) < (2\bar{1}\bar{1}) < (01\bar{1})$ as the superficial density of atoms increases. According to the values of the standard Gibbs energy of adsorption, it was established that the hydrophilicity of electrodes increases in the sequence $Sb(111) < Bi(01\bar{1}) < Bi(2\bar{1}\bar{1}) < Bi(\bar{1}0\bar{1}) \leq Hg < Bi(001) < Bi(111) < Cd(0001) < Zn(0001) < Ag(111) < Ag(100) < Ga$.

Keywords: Bismuth; Butanol; Adsorption

1. Introduction

This work is part of a project devoted to the study of the influence of the crystallographic structure of bismuth on the adsorption of neutral organic molecules at the Bi|solution interface [1–6]. Adsorption of various organic compounds at the polycrystalline bismuth solid drop electrode (BDE) has been described previously [6–10]. In the case of adsorption of pyridine [7], aliphatic ketones [8] and esters [9], the phenomenon of splitting of the adsorption–desorption maxima was discovered; however, if adsorption of aliphatic alcohols, carboxylic acids and amines [10–12] occurs, this effect was not observed. The previous investigations showed that the splitting of the maxima was due to the presence of different homogeneous monocrystalline surface segments (single crystal planes) on the solid electrode surface. This effect was rather sensitive to the characteristics of the polycrystalline nature of the surface, to the nature of both the adsorbing particle structure and the solvent, to surface charge density σ and to the base electrolyte and adsorbate concentration. The best verification of the crystallographic nature of the splitting of the adsorption–desorption maxima is the total absence of this effect on single crystal planes [1–6]. The results of electron diffraction studies [13] indicate that relatively large monocrystalline surface segments (dimensions of the order of 100 nm) with the Miller indices (001), (111), $(\bar{1}0\bar{1})$ and $(01\bar{1})$ exist at the BDEs. The statistical treatment of the electronograms and capacity data shows that the surface of the BDE consists mainly (ca. 60%) of homogeneous segments whose crystallographic, double layer and adsorption characteristics are similar to those for the (001) plane of bismuth [13–15].

The electrosorption behaviour of the same aliphatic compounds from electrolyte solutions on different metals under otherwise identical conditions may provide further useful information on the role played by metal–water and water–water interactions upon electrosorption. In fact, the

PII S0022-0728(96)04629-3

chemical nature and crystallographic structure of the single crystal plane electrode is known to affect the structuring of interfacial water molecules [1–6,12–15]. Such a structuring, which has been studied extensively from both experimental and theoretical points of view, is therefore used to exert an indirect influence upon the adsorption behaviour of the same aliphatic compound on different metals. Systematic adsorption measurements of *n*-aliphatic alcohols and their isomers from aqueous electrolyte solutions have been carried out on various sp-metals, such as Hg, Pb, Bi, Cd, Sn, Sb, Zn, In–Ga and Ga [16–23]. In general, these measurements indicate that the adsorption of aliphatic compounds is weaker the more hydrophilic is the metal. However, a further difficulty in comparing results from different laboratories lies in the fact that different experimental techniques are often used. In the specific case of organic adsorption on single crystal planes of various metals, there are three main approaches: (a) static capacitance measurements by means of a manually operated bridge; (b) dynamic capacitance measurements by means of a lock-in-amplifier; (c) charge measurements by potential steps (chronocoulometry). Dynamic measurements are not usually considered an equilibrium approach in view of the continuous potential scan, while full confidence is placed on chronocoulometric experiments [20,21].

Therefore, we have carried out systematic simultaneous impedance (capacity bridge) and chronocoulometric investigations of the adsorption of various organic substances on Bi single crystal planes. For a more profound understanding of the importance of the crystallographic structure of the electrode surface and the geometrical structure of the hydrocarbon chains of adsorbate in adsorption phenomena, in the present work we have studied the adsorption of normal butanol (*n*-BA), *iso*-butanol (*iso*-BA), *sec*-butanol (*sec*-BA) and *tert*-butanol (*tert*-BA) on singular faces (111), (001), $(01\bar{1})$ and $(01\bar{1})$, and the non-singular $(2\bar{1}\bar{1})$ plane of bismuth single crystals.

2. Experimental

The experimental procedure used in this work has been described in Refs. [1–6]. The crystallographic orientation was determined by X-ray analysis, using a special crystal holder and a goniometric head. The electrode was cut along the chosen crystallographic orientation with the precision $\pm 0.3°$. The isolation of the faces was carried out by a thin polystyrene film (dissolved in toluene) covering the part of no interest, and then the sample was placed into a Teflon holder [22,23]. The surface was polished to a mirror finish by using standard metallographic procedures. The final surface preparation was obtained by electrochemical polishing in an aqueous KI + HCl solution. Thereafter, the second X-ray diagram was used to determine the precise angle, and only the samples whose precision on the orientation was better than $\pm 0.15°$ were used for electrochemical investigations. After the last stage of surface preparation (electrochemical polishing), the electrodes were very well rinsed with ultra purified water and were polarized at -1.2 V vs. the saturated calomel electrode (SCE) in the working surface inactive solutions. In some cases, the basal plane (111) of Bi was prepared by cleaving the single crystal at the temperature of liquid nitrogen [Bi(111)^c].

For an additional characterization of the working surface of electrodes, electron microscopic analysis by JEOL-JSM-35CF at the SEI regime was made (40000 × max.). According to these measurements, the electrochemically polished surfaces of bismuth electrodes were smooth (understandably within the range of the sensitivity of electron microscopy). A few growth steps on the cut surface of [Bi(111)^c] were observed, but the distance between these steps was very large (of the order of millimetres).

2.1. Solutions

The water for preparing the solutions was purified by triple distillation (a quartz system was used for the last) and purified additionally by using the special method described in Refs. [22,24]. Solutions were prepared volumetrically using either NaF or Na_2SO_4 purified by triple recrystallization from water, followed by vacuum heating to dryness. NaF and Na_2SO_4 were calcined at 700°C immediately prior to the measurements. The change of the Na_2SO_4 solution pH in the range 4.0 to 6.0 was effected by the addition of a calculated amount of H_2SO_4 solution prepared from triply distilled concentrated sulphuric acid. The solution pH was determined with a pH-meter. Electrolytic hydrogen was bubbled for 1–2 h through the electrolyte before the submersion of the electrode in the solution. The temperature was kept at 298 K and an aqueous SCE was used as the reference electrode. The isomers of butanol were purified according to Ref. [25].

3. Results and discussion

3.1. Cyclic voltammograms (CVs)

The CVs were recorded in order to determine the quality of the surfaces investigated and the potential range in which the adsorption of butanol isomers occurred. The shape of the CV recorded for the supporting electrolyte was characteristic of the bismuth single crystal planes in accord with our previous studies [1–6]. The cyclic voltammetry curves also indicated that the bismuth single crystal planes investigated are ideally polarizable in the potential range of -1.8 to -0.45 V (SCE) in aqueous 0.05 M Na_2SO_4 or 0.1 M NaF solutions. In aqueous 0.04 M Na_2SO_4 + 0.01 M H_2SO_4 solution, bismuth electrodes are ideally polarizable in the range of -0.8 to -0.05 V (SCE).

3.2. Differential capacity vs. potential curves (C(E)-curves)

The $C(E)$-curves shown in Fig. 1 were recorded for the supporting electrolyte alone and with additions of *n*-BA. For accurate determination of the precision of the experimental data a statistical analysis was carried out [23]. The statistical analysis showed that in the case of electrochemically polished single crystal Bi electrodes, the values of C, surface charge density σ and surface tension $(\gamma - \gamma_0)$ can be determined sufficiently accurately by the measuring procedure used, and the error of these parameters is not greater than 2–5%. The values of the potential of maximum adsorption E_{max} and of the potential of adsorption–desorption maximum E^{max} can be established with accuracies of ± 25 mV and ± 5 to 7 mV accordingly.

All the $C(E)$-curves determined in the presence of isomers of butanol in the solutions investigated merge with the curve for the supporting electrolyte at -1.8 V (SCE), indicating that butanol and its isomers are completely desorbed from the bismuth surface at these negative polarizations. At less negative potentials the $C(E)$-curves display characteristic adsorption–desorption peaks. The height of the peak increases and its potential shifts in the negative direction with increasing butanol concentration. As we can see from Fig. 1 and Fig. 2, the shape (the height and width) of the adsorption–desorption maximum at c_{org} = const. depends on the geometrical structure of the adsorbate hydrocarbon chains. The height of peaks at c_{org} = const. increases and the width decreases in the sequence *tert*-BA > *sec*-BA > *iso*-BA > *n*-BA, which means that at $E < E_{\sigma=0}$ the attractive interaction between the adsorbed butanol molecules increases in the sequence *tert*-BA to *n*-BA. The potential of the adsorption–desorption maximum E^{max} at $E < E_{\sigma=0}$ (c_{org} = const.) depends on the geometrical structure of the adsorbate, and the adsorption activity of butanol isomers increases in the sequence of *tert*-BA to *n*-BA. The height and potential of the adsorption–desorption peaks depend on the geometrical structure of the electrode surface. One can see from Fig. 3 that these maxima increase in height in the range of faces $(2\bar{1}\bar{1}) < (01\bar{1}) < (111) < (\bar{1}0\bar{1}) \leq (001)$. Accordingly, the attractive interaction between adsorbed molecules increases as the superficial density of atoms decreases. Going further in the positive direction, the differential capacity decreases to a

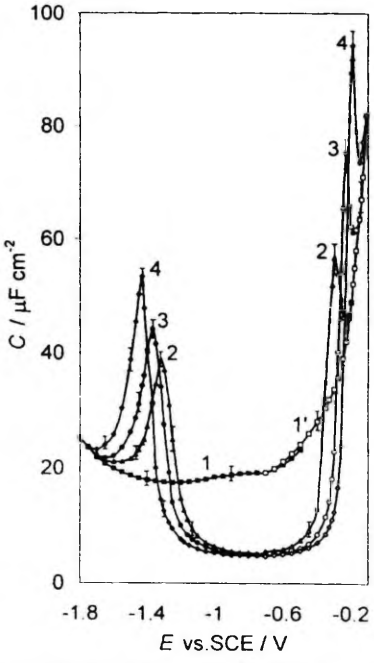

Fig. 1. $C(E)$-curves (ν = 210 Hz) for Bi(111) in 0.05 M Na_2SO_4 (1), in 0.04 M Na_2SO_4 + 0.01 M H_2SO_4 (1') and with different additions of *tert*-BA (M): (2) 0.4; (3) 0.6; (4) 1.0.

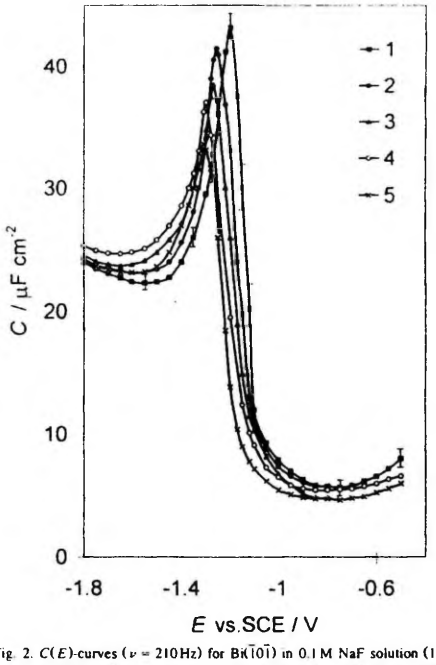

Fig. 2. $C(E)$-curves (ν = 210 Hz) for Bi($\bar{1}0\bar{1}$) in 0.1 M NaF solution (1) and for 0.2 M solutions of adsorbates: (2) *n*-BA; (3) *iso*-BA; (4) *sec*-BA; (5) *tert*-BA.

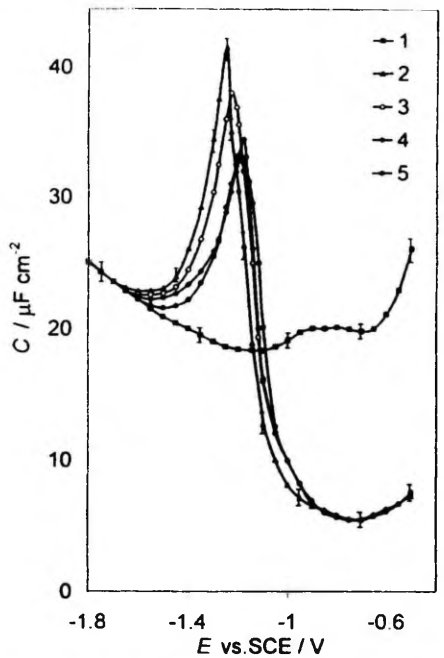

Fig. 3. $C(E)$-curves (ν = 210 Hz) for 0.05 M Na_2SO_4 + 0.25 M *sec*-BA for various electrodes: (1) Bi(001); (2) Bi($\bar{1}0\bar{1}$); (3) Bi(111); (4) Bi(01$\bar{1}$); (5) Bi(2$\bar{1}\bar{1}$).

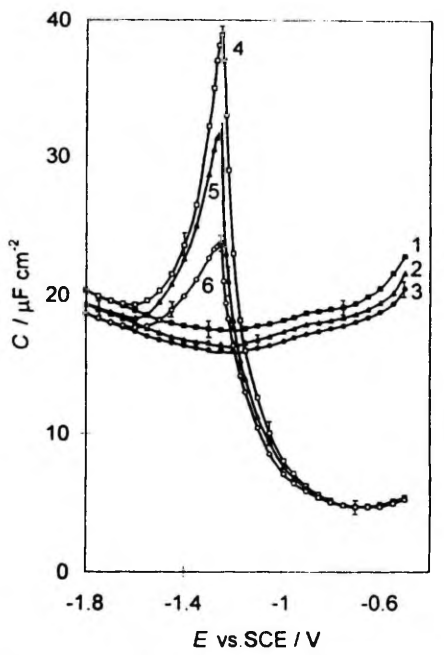

Fig. 4. $C(E)$-curves for Bi(111) in 0.1 M NaF (1)–(3) and with addition of 0.2 M *tert*-BA (4)–(6) at different ν (Hz): (1),(4) 110; (2),(5) 1100; (3),(6) 11 000.

value much smaller than that observed for the pure base electrolyte, indicating that butanol molecules are replacing water at the interface.

The adsorption–desorption maxima at $E > E_{\sigma=0}$ for *tert*-BA and *sec*-BA were found at $E \leq -0.1$ V (SCE) and only these curves were used for calculations. For more concentrated solutions of *iso*-BA and *n*-BA, the peaks for $c_{org} > 0.1$ M lie at very positive potentials $E > -0.1$ V (SCE) and are probably distorted by a slight specific adsorption of anions [3–6]; therefore, they were not used for the calculation of adsorption parameters.

3.3. Non-equilibrium differential capacity curves

The edl differential admittance was measured from 60 to 21 000 Hz. The capacity dispersion with frequency ν is small in the proximity of the differential capacity minimum (in the region of maximum adsorption), whereas it increases notably in the region of the adsorption–desorption peaks (Fig. 4). As shown in Refs. [16,26], if the rate of the adsorption of organic compounds is limited by diffusion, the equilibrium values of differential capacity at $\nu = 0$ can usually be found with a sufficient degree of accuracy by extrapolation of the $C_{add}(\omega^{1/2})$-curve ($\omega = 2\pi\nu$) to $\omega^{1/2} = 0$. As we can see from Fig. 5, in the region of $60 < \nu < 410$ Hz, the $C_{add}(\omega^{1/2})$-curves have a good linearity and, accordingly, we can obtain the equilibrium values of differential capacity. According to the

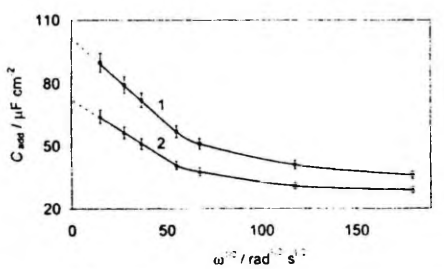

Fig. 5. $C(\omega^{1/2})$-curves for the 0.1 M NaF + 0.2 M *n*-BA system at the potential of adsorption–desorption peaks for (1) Bi(001) and (2) Bi(111).

method [26–28], the equilibrium values of differential capacity can be calculated by Eq. (1)

$$C_{add}(\omega = 0) = C^2_{add}(\omega) R^2_p(\omega) \omega^2 + 1/\{[C_{add}(\omega) R_p(\omega) \omega - 1] R_p(\omega) \omega\} \quad (1)$$

where $C_{add}(\omega)$ and $R_p(\omega)$ are the values of differential capacity and parallel resistance at ω = const.

The components of the adsorption impedance were calculated from the impedance data of the cell used for the measurements (series circuit), i.e. $C_S(\omega)$ and $R_S(\omega)$, following the procedure described in Refs. [16,17,26–29]. By extrapolating the $R_S(\omega)$-values to $\omega \to \infty$ we determined the solution resistance $R_S(\omega) = R_{sol}$. Since the amount of organic compounds added is small and does not affect the solution resistance, one can assume R_{sol} to be equal to the ohmic component R_S of the impedance in the pure base electrolyte solution. Then the series equivalents $R_S(\omega) - R_{sol}$ and $C_S(\omega)$ of impedance were converted into the parallel equivalents $C_P + C_{true}$ and R_P via the relations given in Refs. [16,17,26–28]. A more detailed discussion of the kinetics of butanol isomer adsorption on Bi electrodes will be published soon.

The equilibrium values of $C_{add}(\omega = 0)$ calculated by Eq. (1) are 82–85 μF cm^{-2} and 97–101 μF cm^{-2} for Bi(111) and Bi(001) respectively, and these values are in good agreement with the values obtained from Fig. 5 (83 ± 4.0 μF cm^{-2} for Bi(111) and 99 ± 5.0 μF cm^{-2} for Bi(001)).

3.4 Charge density–potential curves

A charge density–potential $\sigma_0(E)$-curve for base electrolyte solution was obtained by integration of the $C(E)$-curve, starting from the potential of zero charge (pzc) $E_{\sigma=0}$. The values of $E_{\sigma=0}$ for different Bi single crystal planes were obtained from the position of the diffuse layer minimum on independently measured differential capacity curves for dilute solutions of the base electrolyte. The established values of $E_{\sigma=0}$ were in good agreement with our previous data [30]. The charge density–potential curves for solutions with different additions of adsorbate were obtained by back integration of the $C(E)$-curves, starting from $E = -1.8$ V(SCE) and assigning the value of $\sigma(E = -1.8\,V)$ equal to $\sigma_0(E = -1.8\,V)$, because there is no adsorption at $E = -1.8$ V (SCE). The shape of $\sigma(E)$-curves is typical of the behaviour observed for the adsorp-

Table 1
Adsorption parameters of butanol isomers on Bi single crystal planes (ν = 60 Hz)

System	Plane	a_m ±0.1	C_1/ μF cm^{-2} ±0.15	E_N/ V ± 0.04 (SCE)	10^{10} Γ_{max}/mol cm^{-2} ±0.4	S_{max}/ nm^2	B_m/ dm^3 mol^{-1} ±0.2	$-\Delta G^0_{ads}$/ kJ mol^{-1} ±0.2	$\Delta(-\Delta G^0_{ads})$/ kJ mol^{-1}
n-BA	(111)	1.3	3.45	0.35	4.7	0.35	4.9	13.9	—
	$(\bar{1}0\bar{1})$	1.4	4.76	0.28	4.7	0.35	5.9	14.4	0.4
	(001)	1.4	4.41	0.33	5.3	0.31	5.3	14.2	0.2
	$(01\bar{1})$	1.2	4.76	0.34	3.7	0.45	7.6	15.1	1.1
iso-BA	(111)	1.6	3.57	0.34	4.9	0.34	3.0	12.7	—
	$(\bar{1}0\bar{1})$	1.3	4.35	0.24	4.4	0.37	4.4	13.7	1.0
	(001)	1.7	4.44	0.32	5.6	0.30	3.0	12.7	0.0
	$(01\bar{1})$	1.2	4.81	0.32	4.4	0.38	6.1	14.5	1.8
	$(2\bar{1}\bar{1})$	1.2	4.72	0.32	5.0	0.33	5.3	14.2[a]	1.5
sec-BA	(111)	1.6	3.88	0.42	4.3	0.39	3.5	13.1	—
	$(\bar{1}0\bar{1})$	1.4	4.76	0.26	4.1	0.41	4.8	14.0	0.9
	(001)	1.6	3.86	0.38	4.4	0.38	3.6	13.2	0.1
	$(01\bar{1})$	1.3	4.83	0.36	4.2	0.40	6.1	14.5	1.4
	$(2\bar{1}\bar{1})$	1.3	4.88	0.30	4.2	0.40	5.8	14.4	1.3
tert-BA	(111)	1.5	4.03	0.49	5.4	0.31	2.6	12.2	—
	$(\bar{1}0\bar{1})$	1.5	4.18	0.28	4.2	0.40	4.0	13.0	0.8
	(001)	1.3	4.40	0.46	5.3	0.31	3.1	12.6	0.4
	$(01\bar{1})$	0.9	4.48	0.36	5.7	0.29	4.6	13.6	1.4
	$(2\bar{1}\bar{1})$	0.8	4.52	0.31	4.2	0.37	4.4	13.4	1.2
tert-BA[a]	(111)	1.6	4.00	0.39	5.2	0.32	2.4	12.0	—

[a] Obtained from chronocoulometry.

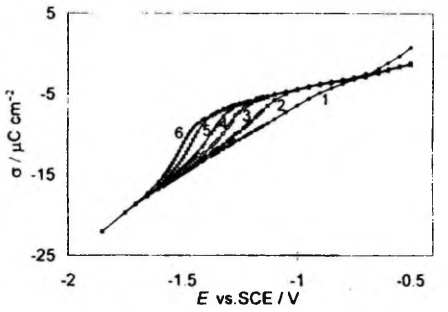

Fig. 6. $\sigma(E)$-curves (ν = 210 Hz) for Bi(111) in 0.05 M Na_2SO_4 (1) and with addition of *tert*-BA (M): (2) 0.2; (3) 0.4; (4) 0.6; (5) 1.0; (6) 1.5.

tion of neutral organic molecules at ideally polarizable electrodes.

The $\sigma(E)$-curves for different concentrations of *n*-BA and its isomers investigated intersect the curve obtained for the base electrolyte. The potential at which the curves intersect is the potential of maximum adsorption E_{max}. As we can see from Fig. 6, E_{max} is practically independent of c_{ads} and the nearly linear segments are observed on the $\sigma(E)$-curves around E_{max}. By linear extrapolation of these fragments of the curve to $\sigma = 0$, one can determine the pzc corresponding to the surface covered by adsorbate molecules. The difference between these experimental values and the value of $E_{\sigma=0}$ for the pure base electrolyte solution is equal to the change in the surface potential due to the displacement of a monolayer of water molecules by a monolayer of adsorbate (E_N). The established values of E_N are presented in Table 1, and we can see that the values of E_N increase in the sequence of Bi planes $(\bar{1}0\bar{1}) < (01\bar{1}) \leq (2\bar{1}1) < (001) < (111)$. Accordingly, the effective dipole moment of the adsorbate at E_{max} increases in the same direction of planes. According to the data of Table 1, E_N depends on the geometrical structure of the hydrocarbon chains of adsorbate, and the effective dipole moment increases from *iso*-BA to *tert*-BA.

3.5. Potential step measurements

The values of the initial and final potentials for the potential step experiments were chosen with the help of the $C(E)$-and $j(E)$-curves. The initial potential E_i was varied from −0.50 to −1.80 V (SCE). The final potential E_f was equal to −1.60 V (SCE) for $c_{org} \leq 0.01$ M and −1.80 V (SCE) for $c_{org} > 0.01$ M. Its value was chosen carefully in order to: (1) achieve the complete desorption of isomers of butanol; (2) keep the current of hydrogen evolution small enough so that the faradaic reaction would not interfere with the determination of the electrode charge density σ.

Five series of step experiments were made for concentrations from 1×10^{-3} to 2.0 M of *tert*-BA. The results were practically similar and so the results of one experiment were analysed thereafter. Representative current transients determined in the potential step experiments for the pure base electrolyte and a solution containing *tert*-BA had the traditional form. The time window (from 10 to 150 ms) in which the transients were recorded was the same for both the base electrolyte and solutions containing *tert*-BA.

The chronoamperometric curves were integrated digitally to obtain the charge transients. The chronocoulometric curves display an initial fast-rising section, corresponding to the charging of the edl followed by a quasi-plateau in which the charge varies slowly and linearly with time. The slope of this segment is small (owing to a very slight hydrogen evolution reaction). These linear segments of the transients were extrapolated to zero time to obtain the relative charge densities $\Delta\sigma$. In this way, the faradaic contribution from hydrogen evolution was minimized. The relative charge densities $\Delta\sigma$ were determined from these step measurements:

$$\Delta\sigma(E) = \sigma(E_i) - \sigma(E_f) \quad (2)$$

In Eq. (2) $\sigma(E_i)$ and $\sigma(E_f)$ are the charge densities at the metal side of the interface at potentials E_i and E_f respectively. Knowing the value of $E_{\sigma=0}$, determined by impedance measurements in the dilute solutions of base electrolyte [30], the absolute charge densities were calculated for each value of E by using the formula

$$(E) = \Delta\sigma(E) - \Delta\sigma(E_{\sigma=0}) \quad (3)$$

The precision of charge measurements is about 2–4%. A plot of charge density vs. potential for the surface inactive electrolyte and for three concentrations of *tert*-BA is shown in Fig. 7(a). The shape of these curves is typical, and all the curves merge at −1.8 V (SCE). Accordingly, a complete desorption of adsorbate takes place at E = −1.8 V (SCE).

Starting from E = −1.8 V (SCE) and going in the positive direction, a sharp rise in the charge density is observed if *tert*-BA is present in the bulk of the solution. The increase in σ slows quickly, and the charge becomes nearly dependent on the potential. The $\sigma(E)$ curves for different concentrations of *tert*-BA intersect the $\sigma_0(E)$-curve at the potential of maximum adsorption E_{max}. At E = const. the values of σ are practically independent of the direction of potential step measurements, which means that the adsorption of *tert*-BA is practically reversible. The same conclusions are valid in the case of the adsorption of other butanol isomers at bismuth single crystal electrodes.

Fig. 7(b) shows that the charge–potential data from capacitance and potential step measurements do not differ significantly ($\Delta\sigma = \pm 0.5\,\mu C\,cm^{-2}$). A particularly good agreement can be seen between −24 and $3\,\mu C\,cm^{-2}$, where the analysis of the experimental adsorption data of *tert*-BA and other butanol isomers was carried out.

3.6. Surface tension and film pressure curves

Capacitance curves were back-integrated twice to obtain a surface tension ($\gamma - \gamma_0$) decrease as a function of the electrode potential and adsorbate concentration [20]. The second integration was performed from the same negative charge at first, assigning the value of zero to the surface tension at the pzc in the base solution. Our data show a progressive decrease in surface tensions as c_{org} increases. The shape of the surface tension–potential ($\gamma - \gamma_0$)–(E) curve is typical of organic adsorption. A good agreement between the data obtained from impedance and chronocoulometry ($\Delta(\gamma - \gamma_0) = \pm 0.3\,\mu J\,cm^{-2}$) was established at $-12 < (\gamma - \gamma_0) < +2.0\,\mu J\,cm^{-2}$ where the thermodynamic analysis takes place. The adsorption activity of bismuth single crystal electrodes increases in the sequence of adsorbates *tert*-BA < *iso*-BA < *sec*-BA < *n*-BA as the adsorption activity of organic molecules at the air|solution interface increases. The adsorption activity of bismuth electrodes increases in the sequence of planes (111) < (001) ≤ ($\bar{1}0\bar{1}$) < ($2\bar{1}\bar{1}$) < ($01\bar{1}$) as the surface density of atoms increases (except Bi(111) and Bi($2\bar{1}\bar{1}$)). These deviations are evidently determined by the competitive adsorption of water and the organic substance, as well as by the crystallographic and electronic structure of electrodes. Just as in the case of cyclohexanol [3], *n*-hexanol [23] and butyl acetate [6] adsorption, the basal plane (111), where the surface atoms are chemically saturated (electron configuration sp^3d^2), has the lowest adsorption activity. The most active one is the singular face ($01\bar{1}$), where unsaturated covalent bonds are distributed uniformly over the entire surface (s^2p^4). The lower adsorption energy of butanol isomers at the Bi($2\bar{1}\bar{1}$) plane is mainly caused by the non-singular geometrical structure of the electrode surface, which induces the irregular orientation of the adsorbed molecules (and therefore the non-compact adsorbed layer at the stepped Bi($2\bar{1}\bar{1}$) surface), as well as by the higher adsorption energy of water molecules on the stepped Bi($2\bar{1}\bar{1}$) surface compared with Bi($01\bar{1}$) plane.

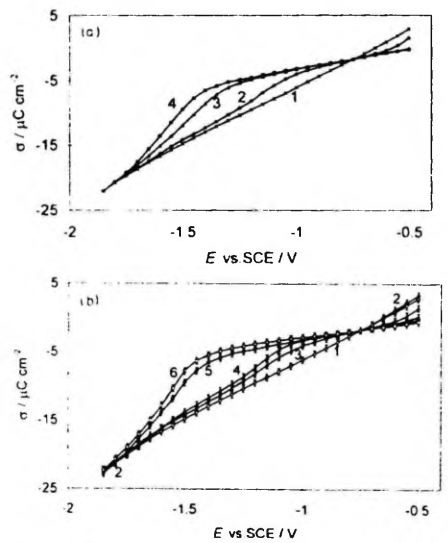

Fig. 7. $\sigma(E)$-curves for Bi(111). (a) Obtained by chronocoulometry in 0.1 M NaF (1) and with addition of *tert*-BA (M): (2) 0.2; (3) 1.0; (4) 2.0. (b) Obtained by impedance (1),(4),(6) and chronocoulometry (2),(3),(5) in 0.1 M NaF (1),(2) and with additions of *tert*-BA (M): (3),(4) 1.0; (5),(6) 2.0.

Fig. 4 and Fig. 7(b) indicate that the departure from equilibrium is probably very small under the peak at negative rational potentials. Thus, thermodynamic analysis is still possible in the negative rational potential range; however, capacitance at the minimum of the curves should be substantially reliable, since no noticeable frequency effects are expected in that potential range (Fig. 4). The pressure of the film of adsorbate π can be determined as

$$\pi(E) = \gamma_{c=0} - \gamma_c = \int_{E_0}^{E} \sigma_c \,dE - \int_{E_0}^{E} \sigma_{c=0} \,dE \qquad (4)$$

where subscripts c and $c = 0$ indicate the presence and absence of adsorbate in the bulk of the electrolyte respectively, and γ is the surface tension. The calculated $\pi(E)$-curves are plotted in Fig. 8. For each concentration the curve displays a maximum, the potential E_{max} of which is practically independent of c_{org}. The film pressure of the adsorbate increases in the sequence of compounds *tert*-BA < *sec*-BA < *iso*-BA < *n*-BA and in the sequence of planes (111) < (001) ≤ ($\bar{1}0\bar{1}$) < ($2\bar{1}\bar{1}$) < ($01\bar{1}$).

3.7. Gibbs excess–potential and Gibbs excess–log c_{org} curves

The film pressure data were used to calculate the relative Gibbs surface excess Γ. First the film pressure was plotted against log c_{org} at E = const. (Fig. 9). The curves display a long linear section, its slope giving the limiting value of Γ_{max}

$$\Gamma = \frac{1}{RT}\left(\frac{\partial \pi}{\partial \ln c}\right)_{E,T,p} \qquad (5)$$

The values of Γ_{max} obtained are presented in Table 1 and show that Γ_{max} increases in the sequence of adsorbates: *sec*-BA < *n*-BA < *iso*-BA < *tert*-BA as the size and solubility of organic compounds increases.

As in the rising part of the curves, the slope changes dramatically; therefore, the related Gibbs excesses for the intermediate coverages were determined from the electrode charge densities using the well-known formula

$$\Gamma = \frac{\sigma_\Gamma - \sigma_{\Gamma=0}}{\sigma_{\Gamma_{max}} - \sigma_{\Gamma=0}} \Gamma_{max} \qquad (6)$$

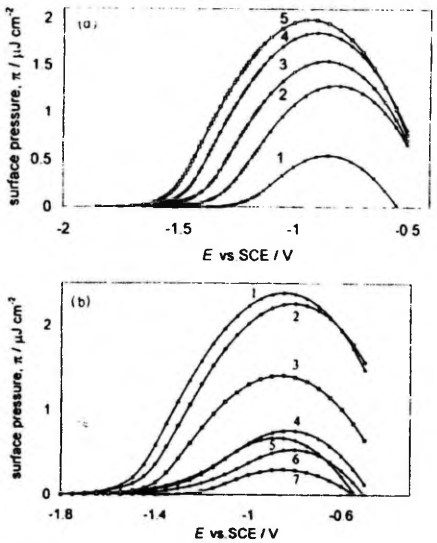

Fig. 8. $\pi(E)$-plots for Bi(111). (a) (ν = 60 Hz) 0.1 M NaF with additions of *tert*-BA (M): (1) 0.2; (2) 0.4; (3) 0.6; (4) 1.0; (5) 1.5. (b) 0.1 M NaF with additions of different adsorbates (c_{org} = 0.5 M (1)–(3) and c_{org} = 0.1 M (4)–(7)): (1),(4) *n*-BA; (2),(6) *iso*-BA; (3),(7) *tert*-BA; (5) *sec*-BA.

The values of $(\sigma_{\Gamma_{max}} - \sigma_{\Gamma=0})$ were obtained by the extrapolation of the linear sections of the $\sigma(E)$-curves. The shape of the $\Gamma(E)$-curves for different c_{org} and of the $\Gamma(\ln c)$-curves (Fig. 10 and Fig. 11) suggest that the relative maximum of the adsorption of butanol isomers on all the planes investigated is reached at $-0.7 < E < -1.1$ V (SCE) and it depends on the crystallographic structure of the surface, as well as on the hydrocarbon chain structure.

3.8. Adsorption isotherms

The differential capacity C_1 at the maximum coverage was obtained by extrapolating $1/C$ vs. $1/c_{org}$ plots to

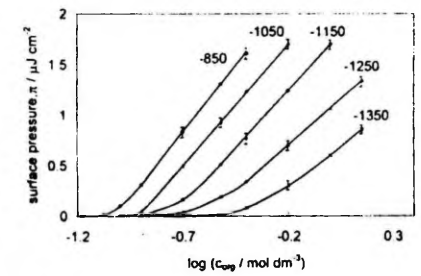

Fig. 9. $\pi(\log c)$-curves (ν = 60 Hz) for Bi(111) at different electrode potentials (mV), noted by numbers.

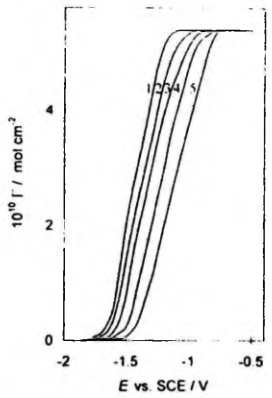

Fig. 10. $\Gamma(E)$-curves (ν = 60 Hz) for Bi(111) at different additions of *tert*-BA (M): (1) 2.0; (2) 1.5; (3) 1.0; (4) 0.5; (5) 0.2.

$(1/c_{org}) \rightarrow 0$. The data taken at the potential of maximum adsorption E_{max} lie satisfactorily on a straight line. This is proof that the capacitance in the region of maximum adsorption is negligibly affected by problems of reversibility. Thus, the C_1 values obtained are reported in Table 1.

Since the surface pressure data are to some degree not quantitatively reliable, the surface coverage at $E = E_{max}$ was first estimated from Eq. (7) based on Frumkin's two parallel condensers model [16,17]

$$\theta = (C_0 - C_\theta)/(C_0 - C_1) \quad (7)$$

where C_0 and C_1 are the capacitances at $\theta = 0$ and $\theta = 1$ respectively. The next step is the test of the Frumkin

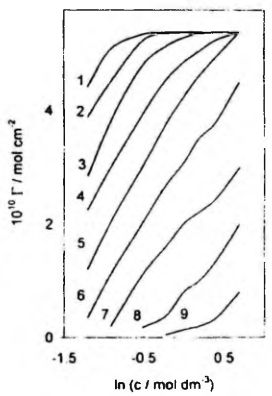

Fig. 11. $\Gamma(\ln c)$-curves (ν = 60 Hz) for *tert*-BA adsorption on Bi(111) at different electrode potentials (V): (1) −0.8; (2) −0.9; (3) −1.0; (4) −1.1; (5) −1.2; (6) −1.3; (7) −1.4; (8) −1.5; (9) −1.6.

isotherm ($\log[\theta/(1-\theta)c]$ vs. θ plot) to derive the adsorption parameters. Fig. 12 shows that the plots have a good linearity for all the systems investigated. Thus, the slope gives the molecular interaction parameter a_m and the intercept provides the adsorption equilibrium constant B_m at E_{max} accordingly. The standard Gibbs energy of adsorption ΔG^0_{ads} at E_{max} was obtained by Eq. (8)

$$-\Delta G^0_{ads} = RT\ln(55.5B_m) \quad (8)$$

The adsorption data of isomers of butanol on the Bi single crystal planes are collated in Table 1, which shows that the adsorption activity of isomers of butanol increases in the sequence of planes (111) < (001) < $(\bar{1}0\bar{1})$ < $(2\bar{1}\bar{1})$ < $(01\bar{1})$ as the superficial density of atoms increases (except Bi(111) and $(2\bar{1}\bar{1})$). The surface activity of adsorbates increases in the sequence of *tert*-BA < *sec*-BA ≤ *iso*-BA < *n*-BA as the adsorption at the air|solution interface increases.

The adsorption isotherms at various E = const. and σ = const. were calculated by the methods described in Refs. [16–21]. The adsorption isotherms at σ = const. show larger deviations from the Frumkin isotherm behaviour than those at E = const. where the deviations in the region $-0.6 < E < -1.0$ V(SCE) are small. The plots of ΔG^0_{ads} vs. E for all the systems investigated are roughly parabolic.

A good agreement can be seen between the values of a_m and B_m (Table 1) obtained from impedance and chronocoulometric measurements.

3.9. Analysis of the adsorption–desorption peaks

If the Frumkin–Damaskin model [16,17] is accepted, further information on adsorption parameters can be obtained from an analysis of the adsorption–desorption peaks. The following analysis is not unquestionable per se. First, frequency effects are included; secondly, the validity of the formulae entails in particular a congruence of isotherms with respect to the potential and constants C_0 and C_1.

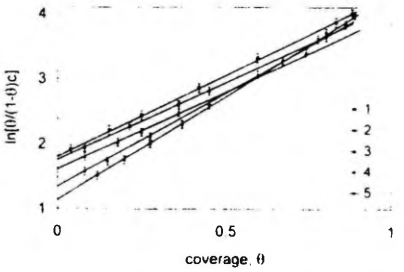

Fig. 12. Frumkin adsorption isotherms (ν = 60 Hz) for *iso*-BA adsorption on Bi single crystal electrodes: (1) $(01\bar{1})$, (2) $(2\bar{1}\bar{1})$; (3) $(\bar{1}0\bar{1})$, (4) (001); (5) (111).

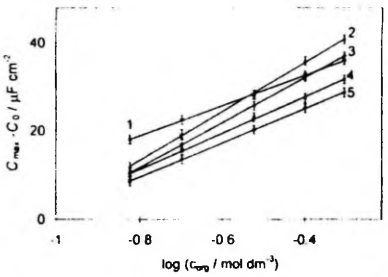

Fig. 13. $(C^{max} - C_0)$/log c)-plots at the negative potentials of *iso*-BA adsorption–desorption peaks for Bi single crystal electrodes: (1) $(01\bar{1})$; (2) $(2\bar{1}\bar{1})$; (3) $(\bar{1}0\bar{1})$; (4) (111); (5) (001).

However, the analysis is carried out in order to compare the adsorption of the same compound at the various planes of the same metal, using the same experimental variable. Therefore, the relevance of the conclusions reached with the aid of the present analysis is believed to be incontestable. Fig. 13 shows that the variation of $(C^{max} - C_0)$ with log c_{org} is linear for all the systems studied. The values of C^{max} at E^{max} were obtained by using Eq. (1) and the value of C_0 was obtained by extrapolation of $C_0(\omega^{1/2})$-dependence to $\omega \to 0$. The slope of the plot in Fig. 13 is given by [16,17]

$$d(C^{max} - C_0)/d\log c_{org} = 2.3(C_0 - C_1)/2 - a) \quad (9)$$

Since C_0 and C_1 are known independently, a value of a at $E = E^{max}$ can be obtained from Eq. (9). The established values of a for the Bi single crystal planes are in good agreement with the values of a obtained from the width of the adsorption–desorption peaks according to the conception [16,17]. The intercept of the plots in Fig. 13 is given by

$$\text{intercept} = \text{slope}(\log B_m + a/2.3) + (C_0 + C_1)/2 \quad (10)$$

By using the values of a obtained from Eq. (9), and a value of log B_m, the adsorption equilibrium constant at E_{max} can be obtained from Eq. (10). From the experimental data analogous to Fig. 13, we obtained log B_m values for the single crystal Bi electrodes which are in agreement with the values of log B_m obtained directly from adsorption isotherms.

According to Frumkin's model, $(E^{max} - E_{max})^2$ should be linearly related to log c with a slope given by

$$d(E^{max} - E_{max})^2/d\log c = 4.6RT\Gamma_{max}/(C_0 - C_1) \quad (11)$$

Since C_0 and C_1 are known, Γ_{max} can be estimated from Eq. (11). Fig. 14 shows that the plots are satisfactorily linear. The values of Γ_{max} obtained on the basis of Eq. (11) are in a satisfactory agreement with the values obtained from Fig. 9 and Fig. 10. According to these data it may be assumed that at the first approximation in the case

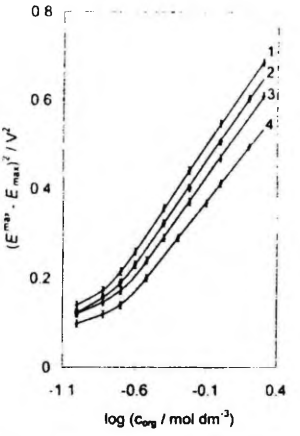

Fig. 14. $(E^{max} - E_{max})^2$(log c)-plots for *tert*-BA adsorption on Bi electrodes: (1) $(01\bar{1})$; (2) (001); (3) (111); (4) $(2\bar{1}\bar{1})$.

of weak physical adsorption of organic compounds the Frumkin–Damaskin adsorption theory [16,17] is valid.

4. Summary

The present results indicate that the adsorption parameters of the butanol isomers depend on the crystallographic structure of the Bi surface, as well as on the geometrical structure of the hydrocarbon chains of adsorbate. The adsorption parameters derived from the capacitance data at $-24 < \sigma \leq +3\,\mu C\,cm^{-2}$ are in good agreement with the data obtained from the chronocoulometric measurements. In the region of cathodic adsorption–desorption maxima, as well as in the region of maximum adsorption, the kinetics of adsorption of butanol isomers are determined by the rate of diffusion of adsorbate molecules to the electrode surface. In all cases the data indicate that the maximum adsorption occurs at small negative charges between -0.5 and $-2.0\,\mu C\,cm^{-2}$. Thus, the adsorption of butanol isomers on Bi shifts $E_{\sigma=0}$ to more positive values. The adsorption activity of bismuth planes increases in the sequence $(111) < (001) \leq (\bar{1}0\bar{1}) < (2\bar{1}\bar{1}) < (01\bar{1})$ as the superficial density of surface atoms increases (except Bi(111) and Bi$(2\bar{1}\bar{1})$). The same tendency is valid for silver single crystal electrodes [18,20,21,27,31,32]. The lower adsorption activity of Bi(111) is caused mainly, in addition to the more pronounced hydrophilicity, by a less active surface state of the Bi(111) surface [2–6]. The lower adsorption activity of Bi$(2\bar{1}\bar{1})$ is caused mainly by the non-singular surface structure and by the higher hydrophilicity of the non-singular surface structure compared with the singular Bi$(01\bar{1})$ plane. The higher values of Γ_{max} and the lower values of C'' and S_{max}, as well as the decrease of E_N in the sequence of faces $(111) > (001) > (01\bar{1}) > (2\bar{1}\bar{1}) > (\bar{1}0\bar{1})$ point to a more pronounced horizontal component in the distribution of molecules on the above listed faces than on the Bi(111) face.

The maximum surface concentration of *iso*-BA or *n*-BA for Bi electrodes is practically the same as it is for Ag and Hg [16,21,28,31]. The lower values of Γ_{max} and higher values of S_{max} for *n*-BA at Bi, Hg and Ag electrodes, compared with the Γ_{max} and S_{max} values obtained in the case of adsorption of higher normal aliphatic compounds on Hg, forming condensed films at the interface (S_{max} = 0.21 nm^2; where S_{max} is the surface area, engaged by one absorbed molecule at Γ_{max}) [16], would indicate the existence of a tilted orientation or unsaturated adsorbed monolayer on the surface of Bi electrodes, as well as on Ag, Zn(0001) and Hg electrodes [16,19–21,31,32].

The standard Gibbs energy of adsorption ΔG^0_{ads} of a neutral compound, weakly interacting with the metal surface, can also be used as a measure of its hydrophilicity [16–21]. The main differences in the values of ΔG^0_{ads}, when passing from one electrode (metal) to another, can then be ascribed to the difference in the energy required for desorption of the water molecules, which must make room for the adsorbing compound. According to the data of Table 1, the differences between the adsorption energies for the faces *X* studied and the less active Bi(111) face $(-\Delta G^0_{ads})_X - (-\Delta G^0_{ads})_{(111)}$ to some degree depend on the geometrical structure of the hydrocarbon chain of the adsorbate, but the arrangement of the Bi planes is independent of the geometrical structure of the hydrocarbon chain of butanol isomers studied. Therefore, it may be summarized that the hydrophilicity of electrodes increases in the sequence Sb(111) < Bi$(01\bar{1})$ < Bi$(2\bar{1}\bar{1})$ < Bi$(\bar{1}0\bar{1})$ ≤ Hg ≤ Bi(001) < Bi(111) < Cd(0001) < Zn(0001) < Ag(111) < Ag(001) < Ga [16,19–21,31,32].

References

[1] A.R. Alumaa, E.J. Lust, N.A. Paltusova and U.V. Palm, Sov. Electrochem., 19 (1983) 1420.
[2] A.R. Alumaa, E.J. Lust and U.V. Palm, Sov. Electrochem., 20 (1984) 919.
[3] E.J. Lust and U.V. Palm, Sov. Electrochem., 21 (1985) 1304.
[4] E.J. Lust and U.V. Palm, Sov. Electrochem., 22 (1986) 378.
[5] E.J. Lust and U.V. Palm, Sov. Electrochem., 22 (1986) 383.
[6] E.J. Lust, J.J. Ehrlich and U.V. Palm, Sov. Electrochem., 22 (1986) 695.
[7] M. Salve, A. Alumaa and U. Palm, Trans. Tartu State Univ., 289 (1971) 54.
[8] J.J. Ehrlich and U.V. Palm, Elektrokhimiya, 10 (1974) 1866.
[9] J.J. Ehrlich, T.E. Ehrlich and U.V. Palm, Elektrokhimiya, 11 (1975) 1009.
[10] R.J. Pullerits, Elektrokhimiya, 5 (1969) 886.
[11] U.V. Palm, V.E. Past, J.J. Ehrlich and T.E. Ehrlich, Elektrokhimiya, 9 (1973) 1399.
[12] U.V. Palm, Trans. Tartu State Univ., 757 (1986) 3.

[13] J.J. Ehrlich, M.P. Pärnoja, T.E. Ehrlich and U.V. Palm, Proc. 4th Symp. on Double Layer and Adsorption on Solid Electrodes, Tartu, 1975, p. 342.
[14] E.J. Lust, M.A. Salve and U.V. Palm, Sov. Electrochem., 23 (1987) 520.
[15] E. Lust and U.V. Palm, Trans. Tartu State Univ., 757 (1986) 105.
[16] B.B. Damaskin, O.A. Petrii and V.V. Batrakov, Adsorption of Organic Compounds on Electrodes, Plenum, New York, 1971, p. 35.
[17] A.N. Frumkin, Potentsialy Nulevogo Zaryada, Nauka, Moskva, 1979, p. 206.
[18] S. Trasatti, Electrochim. Acta, 37 (1992) 2137.
[19] G. Pezzatini, R. Moncelli, M. Innocenti and R. Guidelli, J. Electroanal. Chem., 295 (1990) 275.
[20] L.M. Doubova, S. Valcher and S. Trasatti, J. Electroanal. Chem., 376 (1994) 73.
[21] M.L. Foresti, M. Innocenti and R. Guidelli, J. Electroanal. Chem., 376 (1994) 85.
[22] A.N. Frumkin, M.P. Pärnoja, N.B. Grigoryev and U.V. Palm, Elektrokhimiya, 10 (1974) 1130.
[23] E. Lust, K. Lust and A. Jänes, Russ. J. Electrochem., 31 (1995) 876.
[24] U.V. Palm, M.P. Pärnoja and M.A. Salve, Elektrokhimiya, 13 (1977) 1074.
[25] D.D. Perrin and W.L.F. Armanego, Purification of Laboratory Chemicals, Pergamon, Oxford, 3rd edn., 1986.
[26] G.A. Tedoradze and R.A. Arakelyan, Dokl. Akad. Nauk SSSR, 156 (1964) 1170.
[27] E.J. Lust and U.V. Palm, Sov. Electrochem., 24 (1988) 227.
[28] R.P. Armstrong, W.P. Race and H.R. Thirsk, J. Electroanal. Chem. 16 (1968) 517.
[29] K. Takashasi, Electrochim. Acta, 13 (1968) 1609.
[30] E.J. Lust and U.V. Palm, Sov. Electrochem., 21 (1985) 1186.
[31] T. Vitanov and A. Popov, Elektrokhimiya, 12 (1976) 319.
[32] V.V. Batrakov and B.B. Damaskin, J. Electroanal. Chem., 65 (1975) 361.

VI

Reprinted from the *Electrochimica Acta,* Vol. 42, No. 5,
E. Lust, A. Jänes, K. Lust and M. Väärtnõu,
Electric Double Layer Structure and Adsorption of Cyclohexanol
on Single Crystal Cadmium, Antimony and Bismuth Electrodes, pages 771–783,

Pergamon

Electrochimica Acta, Vol. 42, No. 5, pp. 771–783, 1997

PII: S0013-4686(96)00339-8
0013-4686/97 $17.00 + 0.00

Electric double layer structure and adsorption of cyclohexanol on single crystal cadmium, antimony and bismuth electrodes

E. Lust, A. Jänes, K. Lust and M. Väärtnõu

Institute of Physical Chemistry, University of Tartu, 2 Jakobi Str., EE2400 Tartu, Estonia

(Received 1 October 1995)

Abstract—The electric double layer structure in aqueous and non-aqueous surface inactive electrolyte solutions and the adsorption of cyclohexanol on the electrochemically polished Sb, Bi and Cd electrodes were studied by using cyclic voltammetry, impedance and chronocoulometry. The limits of ideal polarizability, the potentials of zero charge and the values of capacity of inner layer were established. As found, the differences between the zero charge potential for various planes depend on the chemical nature and crystallographic structure of the electrode surface, as well as on the chemical nature of the solvent studied. The inner layer capacity at negative surface charges depends on the crystallographic orientation of the single crystal planes and on the electronic properties of the electrode metal. The inner layer capacity increases in the sequence of metals Sb < Bi < Hg < Cd < Zn, as the hydrophility of electrodes increases and as the contribution of metal phase decreases. The values of capacity of metal phase and the effective thickness of the thin metal surface layer were calculated by using various theoretical approximations. The effective thickness of the thin layer of metal surface increases in the sequence of metals Ga < Zn < Cd < Hg < Bi < Sb as the metallic properties of electrodes decrease. The adsorption parameters of cyclohexanol were established by using Frumkin–Damaskin adsorption theory. It was found that the adsorption characteristics depend on the chemical nature and crystallographic structure of electrode surface. The adsorption activity of cyclohexanol increases in sequence of metals Zn < Cd < Bi < Hg < Sb as the adsorption energy of solvent decreases.

Key words: Double layer, capacity of metal layer, organic adsorption, hydrophility, lyophility.

INTRODUCTION

The electrical double layer is fundamental for electrochemistry, because the rate and mechanism of the various electrochemical reactions (hydrogen, evolution, corrosion and corrosion inhibition by surfactants, metal deposition and dissolution, *etc*) depend on the metal–electrolyte phase boundary structure.

During several decades the quantitative analysis of the *edl* structure, adsorption of ions and molecules on the ideally polarizable solid electrodes was carried out on the basis of relationships, developed for the liquid mercury surface without any consideration of the peculiarities of the solid surface. But the theoretical analysis of the electrochemical characteristics for the polycrystalline solid electrodes, even for simple metals, is considerably complicated in comparison with that for liquid metals and alloys. One of the reasons is due to both the differences between the properties of individual faces of the metal and the influence of various defects of the surface structure [1, 2]. In the beginning of the seventies by a careful experimental study of the adsorption of pyridine on the solid bismuth drop electrode of known polycrystalline surface structure [3, 4] and of tetra-alkylammonium ions on the polycrystalline surface of a zinc electrode [5], the phenomenon of splitting of the cathodic adsorption–desorption maxima was discovered. Already the first investigations showed that splitting of the maxima was due to the polycrystalline nature of the surface, also to the nature of the adsorbing particle and the solvent, to the surface charge density σ and the solution concentration. On account of that the *edl* and adsorption parameters (for example, the values of zero charge potential, interaction parameters in the Frumkin's isotherm, adsorption equilibrium constants, *etc*), obtained for the PC electrodes, often may be apparent [6, 7].

Secondly, the real solid surfaces are not flat and their geometrical surface area does not coincide with the "true" one. Therefore, it is senseless for the sake of further applications, to have unnormalized values.

A. N. Frumkin was the first to point out the necessity to realize the experimental investigations on the single crystal planes of various metals and to account for the crystallographic structure of the solid PC metal surface in the quantitative interpretation of the elements of the differential capacity (C, E)—curves [8] and other experimental results.

Recently, much attention has been paid to the research and development of new methods for the investigation of the electrochemical interface *in situ* based on the modern advances in surface science. However, classical impedance (capacity) measurements remain one of the major tools for studying the interfacial properties. Indeed, the capacitance and related characteristics are sensitive to the specific properties of the contact region when the electric potential charges in a distance are comparable with its "thickness". The rapid drop of the potential near to the electrochemical interface is provided by the field in the electrolyte. For typical ionic concentrations, the depth of the field penetration into the electrolyte solution is comparable to the dimensions of the interfacial region. Thus, the electrical properties of the electrochemical interface (the capacitance, in the equilibrium case) are very sensitive to its structure. Therefore, the adequate interpretation of capacitance data is one of the central points in electrochemistry.

This article concentrates on comprehensive experimental and theoretical studies of the influence of the surface structure of Bi, Sb and Cd single crystal planes on the electric double layer parameters in the aqueous and non-aqueous solutions of surface inactive electrolyte, as well as of the influence of the crystallographic effects on the adsorption characteristics of organic molecules.

Bismuth and antimony being the electron analogues, are considered as semi-metals, which crystallize in the same rhombohedral system, and are characterized by the existence of two types of bonds (covalent and metallic) in the lattice. As shown before [15, 18–20], the existence of two types of bonds in the lattice causes considerable differences in the semimetallic properties of different single crystal planes of Bi and Sb electrodes and in this case the metallic side of the interface has an important effect on the properties and structure of the "inner" part of *edl* [7, 9].

Unlike the zinc single crystal electrodes [1, 2, 10, 11], up to now only a few studies have been devoted to the influence of the crystallographic orientation on the *edl* and adsorption of ions and organic compounds on the Cd single crystal faces [12–15]. Zn and Cd are electronanalogues and they are crystallized in the same hexagonal close-packed system. In the case of the Cd single crystal planes the semi-metallic nature of electrodes must be expressed less noticeably in comparison with Sb or Bi electrodes.

ELECTRODES, CHEMICALS AND TECHNIQUES

The electrodes were bismuth, antimony and cadmium single crystals, grown in the Institute of Problems of Microelectronics Technology and Superpure Materials (Russian Academy of Sciences) by a modified Czochralski vertical Bridgman method (Bi) [16] or by the Horizontal Bridgman (zone refiring) method (Sb, Cd) [16]. The crystal growth, the characterization techniques and other experimental problems have already been described in [15–20]. The chemicals and solvents—water, methanol (MeOH), ethanol (EtOH), isopropanol (*i*-PrOH) and acetonitril (AN) were purified according to [18–22].

The *edl* differential admittance was measured in the range from 60 to 21,000 Hz by using an impedance bridge P-568. The cyclic voltammetric curves were recorded by the polarographic analyzer PA-2. Chronocoulometry was performed with a system characterized in [23]. Pulses were recorded from variable E (-0.95 to -1.70 V) as the starting potential, where the electrode was held for 5–60 sec before each step to $E_T = -1.7$ V. Charge–time curves with a time scale in a 100 ms range were extrapolated to $t = 0$ as described elsewhere [23–25].

EXPERIMENTAL RESULTS AND DISCUSSION

Cyclic voltammograms (CVs)

The CVs for different single crystal Bi, Sb and Cd electrodes were recorded in neutral aqueous NaF, $LiClO_4$ and acidified $LiClO_4$ solutions and non-aqueous $LiClO_4$ solutions. In the NaF aqueous solutions the Bi single crystal electrodes are ideally polarizable in the range of potentials $-1.60\ V < E < -0.50\ V$ [26], and the single crystal Sb electrodes are ideally polarizable in the range of $-1.45\ V < E < -0.45\ V$ [27]. The Cd planes are ideally polarizable in the range of $-1.70\ V < E < -0.90\ V$ [28]. In the aqueous $LiClO_4$ solutions the anodic limit of ideal polarizability is shifted ~ 200 mV to the positive direction. In the acetonitrilic and methanolic $LiClO_4$ solutions the single crystal Bi electrodes are ideally polarizable in the range of $-1.80\ V < E < -0.25\ V$ [29] and in the ethanolic and isopropanolic solutions in the limits $-1.60\ V < E < -0.05\ V$ (*sce*). It must be noted that the continuous cycling of the potential in these limits does not evoke noticeable changes in the shape of CVs and capacity–potential curves and does not affect the limits of ideal polarizability of electrochemically polished Bi, Sb and Cd electrodes. The continuous cycling of Bi, Sb and Cd electrode on a larger range of E causes noticeable transformations in

the shape of CVs, differential capacity curves (values of zero charge potential $E_{\sigma=0}$ and values of differential capacity at $E_{\sigma=0}$), in the limits of ideal polarizability and in the values of adsorption parameters of Sb, Bi and Cd electrode. Accordingly the charge-induced (it means induced by the oxidation and reduction of the surface) surface reconstruction is possible, but these problems were not an object of this work and will be discussed in the next paper.

Precision of experimental capacity data

For the accurate determination of the precision of the experimental data the statistical treatment of the data was carried out for the single crystal Cd, Bi and Sb electrodes in the surface inactive electrolyte solution. The geometrical surface area was established by using optical methods to a precision of ±2%. The total number of independent experiments $n > 8$ and four electrodes with the same indexes were used. Thereafter the mean values of differential capacity, $\bar{C}$, charge density $\bar{\sigma}$, Helmholtz layer capacity $\bar{C}_H$ and their standard deviations $\bar{S}$, standard error of the mean $S_{\bar{C}}(C_x)$ and the coefficient of variation V at the fixed E = const (or at σ = const) and at the fixed c = const were calculated by using a HP-85 computer and General Statistics Pac.

The statistical analysis shows [15, 26–29] that in the case of electrochemically polished single crystal Bi, Sb and Cd electrodes, the value of C, σ and C_H can be determined sufficiently accurately by the measuring procedure used (the relative error of the parameters determined is not over 2–5%). For the pzc ($E_{\sigma=0}$) the measuring accuracy is ±5 mV for Bi(111) and ±15 mV for Sb(2$\bar{1}\bar{1}$) and Sb (01$\bar{1}$). For the other single crystal electrodes the measuring accuracy of $E_{\sigma=0}$ is ±10 mV.

As follows from experimental results and Fig. 1, in moderate surface inactive electrolyte solutions ($c_{NaF} \geq 0.03$ M), the experimental values of C can be established better than ±3% for the whole region of σ. But the precision of experimental C decreases as the concentration of the solution decreases, and for the dilute solutions ($c_{NaF} < 0.01$ M) the maximum values of error (5–8%) can be established in the region of σ where the derivation dC/dE is large. In the region of surface charge densities $\sigma < 0.5$ μC cm^{-2}, the error of C (2–4%) is only somewhat higher than for the more concentrated solutions. Comparison of the statistically treated $\bar{C}(E)$- and $\bar{C}(\sigma)$-curves (Figs 1 and 2) shows that the $\bar{C}(E)$-curves are more erratic than the $\bar{C}(\sigma)$-curves calculated at σ = const. The main reason for this effect is the slight variation of $E_{\sigma=0}$ (±10 mV) from one experiment to another.

As we can see from Figs 1 and 2, the experimental values of $\bar{C}$ in the region of the diffuse minimum are constantly higher than those calculated by the

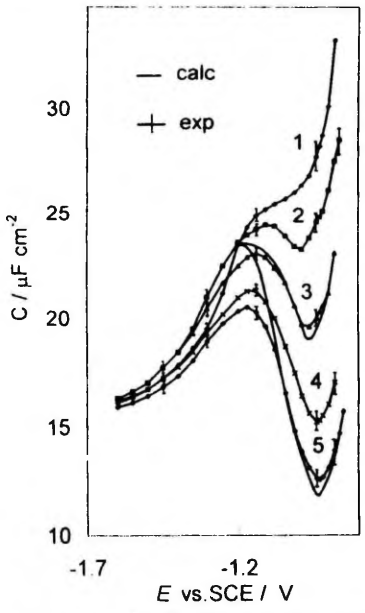

Fig. 1. $C(E)$-curves for Cd(0001) in aqueous solutions of NaF. M: 1, 0.1; 2, 0.05; 3, 0.02; 4, 0.07 and 5, 0.0045.

Gouy–Chapman Stern Grahame (GCSG) theory [15–18].

$$1/C = 1/C_d + 1/C_H, \quad \text{i.e.} \quad C_H = 1/(1/C - 1/C_d), \quad (1)$$

where C_d and C_H are the values of the differential capacity of the diffuse part and of the inner part of

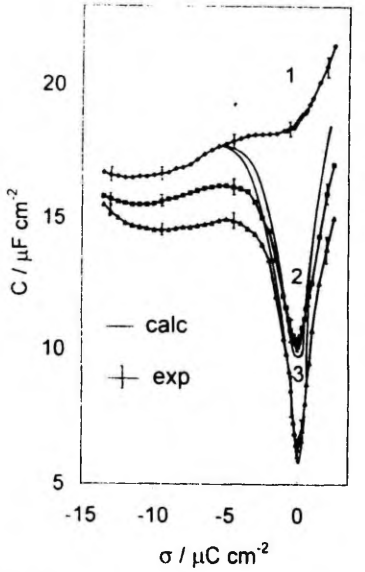

Fig. 2. $C(\sigma)$-curves for Bi(111) in aqueous solutions of NaF. M: 1, 0.1; 2, 0.005 and 3, 0.001.

the double layer. As shown in [1–12, 15–20] at the potential of the diffuse minimum, the differential capacity of a polycrystalline (for the real monocrystalline electrode with surface defects) and for a two-plane model electrode in the dilute solutions is higher than on the perfect single crystal faces at $E_{\sigma=0}$. For more detailed discussion see [19, 26–33].

Electric double layer in the surface inactive electrolyte solution

The *edl* differential admittance was measured in the *ac* frequency ν interval from 60 to 21,000 Hz. For the electrochemically polished single crystal Bi, Sb and Cd electrodes as well as for polycrystalline Bi, Sb and Cd (PC-Bi, PC-Sb, PC-Cd) [34–36], a very slight variation of capacity (3–6%) as a function of frequency ν was observed. Therefore, the measured admittance at the first approximation was identified with the differential capacitance C.

According to the experimental data (Table 1) the values of zero charge potential $E_{\sigma=0}$, the difference $\Delta E_{\sigma=0}^{H_2O-X} = E_{\sigma=0}^{H_2O} - E_{\sigma=0}^{X}$ (where $E_{\sigma=0}^{X}$ is $E_{\sigma=0}$ for non-aqueous solutions), the values of Essin–Markov coefficient $(\partial E_{min}/\partial \lg c)$, the values of the fitting (roughness) coefficient $f_{P\text{-}Z}$ and the values of inner layer capacity at $\sigma = 0$ ($C_H^{\sigma=0}$) and at $\sigma \ll 0$ ($C_H^{\sigma<0}$) are dependent on the crystallographic structure and chemical nature of electrodes, as well as on the chemical nature and geometrical structure of solvents. The large deviation of values of the basal Bi(111), Sb(111), Cd(0001) and Zn(0001) planes in comparison with values of $E_{\sigma=0}$ for other Bi, Sb, Cd and Zn planes is caused mainly by the specific surface state of these basal planes. The differences in electric double layer properties for different Bi and Sb planes decreases in the direction of solvents AN > H_2O > MeOH > EtOH ≥ *i*-PrOH and in the sequence of metals Zn > Sb > Cd > Bi. According to [34–43] the lyophility of the electrodes increases in the sequence Sb(2$\bar{1}\bar{1}$) < Sb(01$\bar{1}$) < Sb(111) < Sb(001) < Bi(2$\bar{1}\bar{1}$) < Bi(01$\bar{1}$) < Bi(111) < Bi(001) < Cd(0001) < Cd(10$\bar{1}$0) < Cd(21$\bar{1}$0) < Zn(0001) < Zn(10$\bar{1}$0) < Zn(21$\bar{1}$0). A more detailed discussion of experimental data is presented in [15, 18–20].

Table 1.
Electric double layer characteristics for Bi, Sb and Cd electrodes

Solvent	Electrode	$-E_{\sigma=0}$ (V)	$\Delta E_{\sigma=0}^{H_2O-X}$ (V)	$\frac{\partial E_{min}}{\partial \log c}$ (mV)	$l_H^{\sigma=0}$ (nm)	$l_H^{\sigma<0}$ (nm)	$\frac{C_H^{\sigma=0}}{C_H^{\sigma<0}}$	f_{P-Z}	D
H_2O	Bi(111)	0.655	—	5	0.035	0.048	1.39	1.04	2.03
	Bi(1$\bar{1}$0)	0.585	—	15	0.034	0.046	1.34	1.07	2.05
	Bi(001)	0.595	—	20	0.031	0.044	1.43	1.06	2.05
	Bi(01$\bar{1}$)	0.590	—	15	0.033	0.047	1.44	1.05	2.04
	Bi(2$\bar{1}\bar{1}$)	0.570	—	20	0.033	0.047	1.42	1.14	2.06
	Sb(111)	0.46	—	10	0.038	0.058	1.55	1.06	2.04
	Sb(001)	0.37	—	20	0.034	0.054	1.60	1.04	2.04
	Sb(01$\bar{1}$)	0.39	—	30	0.034	0.056	1.64	1.18	2.08
	Sb(2$\bar{1}\bar{1}$)	0.34	—	50	0.035	0.057	1.62	1.25	2.10
	Cd(001)	0.95	—	20	0.023	0.052	2.24	1.09	2.05
	Cd(1$\bar{1}$0)	1.01	—	10	0.019	0.052	2.79	1.10	2.05
	Cd(11$\bar{2}$0)	1.00	—	10	0.018	0.052	2.94	1.12	2.07
AN	Bi(111)	0.50	0.16	5	0.059	0.079	2.32	1.06	2.04
	Bi(1$\bar{1}$0)	0.42	0.16	15	0.058	0.087	1.42	1.01	2.04
	Bi(001)	0.41	0.19	10	0.051	0.069	1.36	0.98	2.03
	Bi(01$\bar{1}$)	0.42	0.17	15	0.054	0.074	1.36	1.08	2.06
	Bi(2$\bar{1}\bar{1}$)	0.41	0.16	20	0.055	0.074	1.36	1.03	2.05
MeOH	Bi(111)	0.52	0.14	10	0.045	0.108	2.41	1.05	—
	Bi(001)	0.45	0.14	20	0.038	0.102	2.64	1.07	—
	Bi(01$\bar{1}$)	0.47	0.12	30	0.042	0.103	2.47	1.10	—
EtOH	Bi(111)	0.45	0.20	10	0.059	0.128	2.28	1.03	2.04
	Bi(001)	0.42	0.18	20	0.052	0.116	2.23	1.08	2.07
	Bi(01$\bar{1}$)	0.44	0.15	20	0.053	0.118	2.14	1.07	—
	Bi(2$\bar{1}\bar{1}$)	0.46	0.11	25	0.056	0.123	2.20	1.12	—
	Sb(111)	0.26	0.20	15	0.080	0.132	1.64	1.01	—
	Sb(001)	0.19	0.18	20	0.07	0.137	1.84	1.04	—
i-PrOH	Bi(111)	0.45	0.20	10	0.056	0.147	2.65	1.02	—
	Bi(001)	0.41	0.17	25	0.048	0.130	2.70	1.07	—
	Bi(01$\bar{1}$)	0.46	0.15	30	0.053	0.134	2.53	1.03	—

Electrical double layer and fractal structure of electrode surface

For a long time the dependence of C on ν in the case of ideally polarizable electrodes was left unexplained and was only described in a phenomenological way [36, 44]. The phenomenological description of the frequency dependence of impedance Z_{CPE} (CPE = constant phase element) is given as [45, 46]

$$Z_{CPE} \approx (i\omega)^{-\alpha} \qquad (0 < \alpha < 1). \tag{2}$$

The CPE angle φ is related to α by

$$\varphi = \frac{\pi}{2}(1 - \alpha). \tag{3}$$

Obviously, $\alpha = 1$ corresponds to normal capacitive behaviour. Recently, some new ideas have been put forward to explain the so-called constant phase element CPE, because it affects the frequency-independent phase-shift between the applied *ac* voltage and its current response in a satisfactory way [45, 46]. The main idea is that the deviations from ideal behaviour are caused by surface roughness of a special kind, nowadays commonly denoted by the term "fractal" [45, 46]. The so-called fractal dimension D is a formal quantity introduced by Mandelbrot [46] which attains a value between 2 and 3 for a fractal structure and reduces to 2 when the surface is flat. D is related to α by

$$\alpha = 1/(D - 1). \tag{4}$$

The established values of D, presented in Table 1, show that the surface of electrochemically polished Bi, Sb and Cd electrodes is practically flat and free from components of pseudocapacity. The somewhat higher values of D for the cut electrodes indicate that the surface of electrodes, cleaved at the temperature of liquid nitrogen, is to some extent geometrically and energetically inhomogeneous. But the surfaces of cut Bi, Sb and Cd electrodes are relatively flat and homogeneous, in comparison with the surface of mechanically polished electrodes.

Capacity of metal phase at Bi, Sb and Cd electrodes

The $I_H(\sigma)$-curves ($I_H = 1/4\pi C_H$) were calculated according to the Grahame model (concerning the existence of the compact layer with concentration-independent properties) and by the Valette–Hamelin method [47] from the well-known equation applicable to the *edl* model in the absence of specific adsorption of ions

$$\frac{1}{C} = \frac{1}{FC_H} + \frac{1}{FC_D}, \tag{5}$$

where F is the fitting coefficient. As shown in Table 1 and Fig. 3, the thickness of the inner layer I_H at $\alpha \ll 0$ depend on the chemical nature and crystallographic structure of electrodes. According to the modern conception [33, 48, 51–53] this is caused mainly by the different potential drops at the thin layer of metal

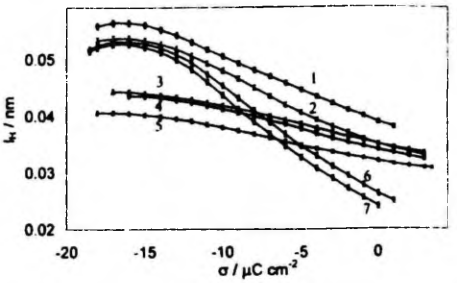

Fig. 3. $I_H(\sigma)$-curves in aqueous solution of NaF for different electrodes: 1, Sb(111); 2, Sb(001); 3, Bi(111); 4, Bi(01$\bar{1}$); 5, Bi(001); 6, Cd(0001) and 7, Cd(21$\bar{1}$0).

surface (capacities) of various electrodes. Therefore, the experimental inner layer capacity values contain not only the value of compact layer capacitance C_s (solvent monolayer contribution), but also the contribution of capacitance of the metal phase C_M [51–53]:

$$\frac{1}{4\pi C_H} = \frac{1}{4\pi C_M} + \frac{1}{4\pi C_S}. \tag{6}$$

The first attempt to derive the capacity of metal phase was done by Rice [33–54], who utilized the Sommerfeld's quantum theory of metals and applied it to the problem of the capacitance of an electrochemical interface. Rice's approach was analogous to a simple linearized Thomas–Fermi model with a sharp boundary for electrons at the surface.

According to the experimental data of [56, 57] it may be assumed that in the case of Bi(111) the value of $\varepsilon_M = \varepsilon_{33} = \varepsilon_\perp \approx 78$ and for Bi(01$\bar{1}$) and Bi(2$\bar{1}\bar{1}$) $\varepsilon_M = \varepsilon_{11} = \varepsilon_{22} = \varepsilon_\parallel \approx 100$. Using the value of $(k_{TF})^{-1} = 0.38$ nm, there were obtained values of $I_M = 1/4\pi C_M$ which are presented in Table 2. For aqueous and methanolic solutions the experimental inner layer thickness I_H is smaller than calculated thickness of the thin layer of metal surface. So the sharp boundary model for electrons at the metal–electrolyte interface in the case of Bi–electrolyte interface is wrong. For EtOH, *i*-PrOH and AN the values of $I_H > I_M$ and therefore for these solvents the Rice's paradox was not observed [33].

The influence of the solvent nature to the charging process of the metal–electrolyte interface (to the interfacial characteristics) is very well detectable in

Table 2.
Thickness and capacity of thin metal layer for Bi electrodes, calculated by Rice model [54]

Plane	C_M (μF cm^{-2})	I_M (nm)
Bi(111)	20.5	0.043
Bi(01$\bar{1}$)	23.5	0.038
Bi(2$\bar{1}\bar{1}$)	23.5	0.038

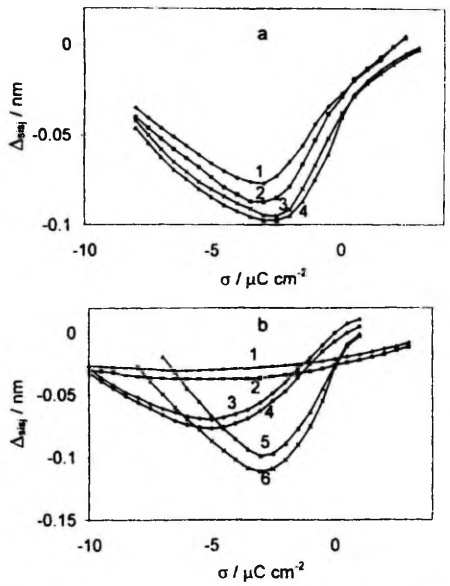

Fig. 4. $\Delta_{S_i S_j}(\sigma)$-curves (a) for solvents $S_i = H_2O$ and S_j = EtOH (1–4) for various electrodes: 1, Bi(001); 2, Bi(111); 3, Sb(001) and 4, Sb(111). $\Delta_{S_i S_j}(s)$-curves (b) for Bi(001), (1, 3, 5) and Bi(111), (2, 4, 6) for $S_i = H_2O$ and different solvents S_j: AN, (1, 2); MeOH, (3, 4) and *i*-PrOH, (5, 6).

Fig. 4, where the dependence of the quantity $\Delta_{S_i S_j} = [1/(4\pi C_H)]^{S_i} - [1/(4\pi C_H)]^{S_j}$ on σ for various solvents is presented (S_i-H_2O; S_j-non-aqueous solution). As we can see the $\Delta_{S_i S_j}$ is dependent on the structure and chemical nature of solvent.

During the last few years there were different models constructed in which the interfacial properties of metal and solution are described by various theoretical approximations. In one of the more successful and simplest of these models, the metal is represented as a "jellium" (with and without a pseudo-potential *at* lattice) and the electrolyte solution is described as an ensemble of hard sphere ions and dipoles [48].

According to the above-mentioned model, the capacity of the thin surface layer of Bi, Sb and Cd single crystal electrodes was calculated by using the equation

$$\frac{1}{4\pi C_M} = \frac{1}{4\pi C_H} - \frac{1}{4\pi C_S}, \tag{7}$$

where

$$\frac{1}{4\pi C_S} = \frac{\delta_s}{2\lambda} + \frac{\delta_i - \delta_s}{2\varepsilon}. \tag{8}$$

In equations (7) and (8) C_M and C_S are the differential capacities of the metal phase and the solvent monolayer, accordingly; δ_i and δ_s are the hard sphere diameters of the ions and solvent molecules, respectively; λ is a parameter related to the bulk dielectric constant ε through the equation $\lambda^2(1 + \lambda)^4 = 16\varepsilon$. It must be noted that equation (8) was derived in the mean spherical approximation and is valid at $\sigma \approx 0$. The values of C_M at $\sigma = 0$ ($C_M^{\sigma=0}$) were calculated at $\delta_i = \delta_{ClO_4^-} = 0.472$ nm. For H_2O: $\delta_S = 0.272$ nm, $\lambda = 2.65$, $I_s = 1/4\pi C_S = 0.052$ nm and $C_S = 17.2\ \mu$F cm^{-2}; for MeOH: $\delta_S = 0.335$ nm, $\lambda = 2.21$, $I_s = 0.081$ nm and $C_S = 10.9\ \mu$F cm^{-2}; for EtOH: $\delta_S = 0.385$ nm, $\lambda = 2.08$, $I_s = 0.095$ nm and $C_S = 9.34\ \mu$F cm^{-2}; for *i*-PrOH: $\delta_S = 0.58$ nm, $\lambda = 2.01$, $I_s = 0.1436$ nm and $C_S = 6.162\ \mu$F cm^{-2}; and for AN: $\delta_S = 0.472$ nm, $\lambda = 2.28$, $I_s = 0.105$ nm and $C_S = 9.51\ \mu$F cm^{-2}. Established at $\sigma = 0$ values of C_M are presented in Table 3. As we can see from Table 3, in the case of AN, MeOH and EtOH the values of I_M are practically independent of the chemical nature of the solvent if we use the values of δ_S (hard sphere parameters) obtained in three state models for the interpretation of experimental Hg/EtOH and Hg/MeOH systems [17]. If we use the MSA parameters obtained for gas phase

Table 3.
Thickness and capacity of thin metal layer for Cd, Sb and Bi electrodes, calculated by Levia–Schmickler model [48] (I_M in nm and C_M in μF cm^{-2})

	H_2O		MeOH		EtOH		i-PrOH		AN	
Solvent	$-I_M$	$-C_M$	$-I_M$	$-C_M$	$-I_M$	$-C_M$	$-I_M$	$-C_M$	$-I_M$	$-C_M$
Metal										
Bi(111)	0.020	44	0.034	26	0.036	25	0.087	10	0.033	27
Bi(001)	0.023	39	0.039	23	0.041	22	0.095	9	0.039	23
Bi($\bar{1}0\bar{1}$)	0.018	49	—	—	—	—	—	—	0.036	25
Bi($01\bar{1}$)	0.022	41	0.035	25	0.038	23	0.090	10	0.039	23
Bi($2\bar{1}\bar{1}$)	0.022	42	—	—	0.038	23	—	—	0.038	23
Sb(111)	0.013	71	—	—	0.018	50	—	—	—	—
Sb(001)	0.017	51	—	—	0.027	33	—	—	—	—
Sb($01\bar{1}$)	0.017	52	—	—	—	—	—	—	—	—
Sb($2\bar{1}\bar{1}$)	0.016	57	—	—	—	—	—	—	—	—
Cd(0001)	0.033	27	—	—	—	—	—	—	—	—
Cd($10\bar{1}0$)	0.036	25	—	—	—	—	—	—	—	—
Cd($11\bar{2}0$)	0.038	24	—	—	—	—	—	—	—	—

(δ_{EtOH} = 0.44 nm; δ_{MeOH} = 0.37 nm), the negative value of I_M decreases in the sequence of solvents H_2O > MeOH > AN > EtOH > *i*-PrOH. As shown in Table 3 the negative values of the capacity of the thin layer of metal surface for aqueous solutions decrease in the sequence of electrodes: Sb(111) > Bi(111) > Sb(001) ≥ Sb(01$\bar{1}$) > Bi(01$\bar{1}$) > Bi(001) > Hg > Cd(0001) > Cd(10$\bar{1}$0) > Cd(11$\bar{2}$0) > Ga if the metallic nature of electrodes increases.

As we know [51–55] the hard sphere model is not a very good approximation for the aqueous solutions of surface inactive electrolytes, therefore the capacities of the thin metal surface layer at Cd, Sb and Bi were calculated by the theory developed in [52, 53, 58]. In this theory the metal is described according to the density functional formalism and the metal–solvent interaction as the sum of an attractive term due to dispersion forces (Van der Waals) and a repulsion simulating the exclusion of metal electrons from the electron cloud of the solvent molecule. Taking into account the difficulties connected with the theoretical estimation of the values of capacity C_M for Sb, Bi and Cd electrodes, in this work we used a few simplifications of the theory [52, 53]. At first we calculated the $C_S(\sigma)$-curves according to equation (6) by using the hypothesis that C_M is "universal" and is independent of the electronic and crystallographic structure of the electrode. Therefore, at the first approximation, in the calculations we have used the $C_M(\sigma)$-curve for the Ag(111) [58]. The established $C_S(\sigma)$-curves are presented in Figs 5 and 6. As we can see, the value of C_S increases in the sequence of Sb(111) < Sb(2$\bar{1}\bar{1}$) < Sb(01$\bar{1}$) < Sb(001) < Bi(111) < Bi(01$\bar{1}$) < Bi(2$\bar{1}\bar{1}$) < Bi(001) < Hg < Cd(0001) < Cd(10$\bar{1}$0) < Cd(11$\bar{2}$0) since the lyophility of electrodes increases. The value of σ^{max} increases and C_S^{max} decreases in sequence of solvents H_2O > MeOH > EtOH > *i*-PrOH > AN, if the specific adsorption energy of solvents decreases.

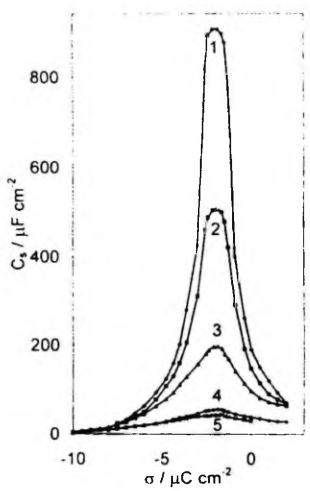

Fig. 5. $C_S(\sigma)$-curves, calculated by Amokrane Badiali model (at C_M = const) for H_2O on different electrodes: 1, Cd(11$\bar{2}$0); 2, Cd(10$\bar{1}$0); 3, Cd(0001); 4, Bi(001) and 5, Sb(001).

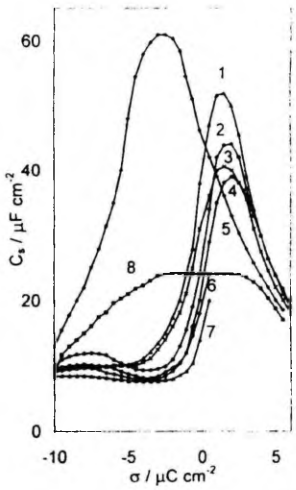

Fig. 6. $C_S(\sigma)$-curves at C_M = const on Bi(001), (1, 2, 4, 8); Bi(111), (3, 5); Sb(001), (6) and Sb(111), (7) for various solvents: 1, H_2O; 2, 4, MeOH; 3, 5, 6, 7, EtOH; and 8, AN.

It is obvious from Figs 5 and 6 that as a direct consequence of the difference in the experimental C_H curves (Fig. 3), C_S values are different and each one strongly differs from its related C_H. However, all C_S curves have similar shape (except AN) symmetry with respect to the position of the maximum σ^{max} and a monotonic delay to an almost common value. These conclusions are in good agreement with the works of [52, 53, 58].

It must be noted that the approximation, that the capacity of metal phase is independent of the electronic properties of the metal and crystallographic structure of planes, may be incorrect in the case of Ag, Cd, Bi, Sb, Hg and Ga, because these metals have very different zone structures and "electronic" properties [33, 48–53, 55–58]. Therefore the second hypothesis of works [52, 53] that C_S is "universal" and is independent of the chemical nature of electrodes, was used for the calculation of the capacity of the metal phase of Cd, Sb and Bi electrodes. The obtained $I_M(\sigma)$-curves are presented in Figs 7 and 8. According to these data, the value of effective thickness of the thin metal surface layer l_M^{max} increases in sequence of Ga < Cd < Hg ≤ Bi < Sb, if the metallic nature of electrodes decreases and the superficial density of atoms increases. The effective thickness of the thin layer of metal surface is somewhat higher and capacity C_M^{min} is lower for Bi(111) and Sb(111) than for other Bi and Sb faces. This is caused mainly by the different electronic properties (ε_M, k_{TF}^{-1}) of planes in the crystallographic direction [111] and other directions. In the case of Cd

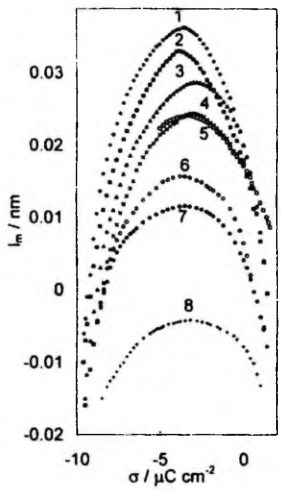

Fig. 7. $I_M(\sigma)$-curves, calculated by Amokrane–Badiali model (at C_S = const) for aqueous solution on different electrodes: 1, Sb(111); 2, Sb(001); 3, Bi(111); 4, Hg; 5, Bi(001); 6, Cd(0001); 7, Cd ($11\bar{2}0$) and 8, Ga.

electrodes the value of I_M^{max} decreases if the superficial density of atoms decreases.

Analyzing the capacity data for single crystal Bi electrodes for various solvents it was established that the obtained values of I_M^{max} noticeably depend on the chemical nature and geometrical structure of the solvent (Fig. 8). According to the model described in [52, 53], a slight dependence of I_M^{max} on solvent nature is possible. In spite of this it seems that the dividing of the inner layer capacity into two components, independent of one another, is a very rough approximation and in the analysis of the *edl* properties in various solvents a more complicated model must be used [59].

Adsorption of cyclohexanol on the single crystal Sb, Bi and Cd electrodes

The electrosorption behaviour of the same organic compound on different metals and on different single crystal planes of the same metal under all the rest identical conditions can help to establish a scale of metal–water and water–water interactions for these various electrode materials. To this end the organic compounds must satisfy the requirement of being weakly physisorbed on the metal surface. Whereas monofunctional aliphatic compounds (alcohols, amines, ethers, esters, ketones and carboxylic acids) are usually convenient candidates for this purpose [49, 60, 61]. Pyridine and other organic compounds with conjugated double bonds or sulphide groups are not suitable for this purpose, since they tend to form weak chemical bonds with the metal surface. A further difficulty in comparing results from different laboratories lies in the fact that different experimental techniques are often used [60–62]. Therefore, we have carried out a systematic simultaneous impedance and chronocoulometric investigation of the adsorption of organic substances on Bi, Sb and Cd single crystal planes. In particular, in this work we present the data for cyclohexanol adsorption, since the adsorption data of this compound already exists in the literature for a number of sp metals [63–65].

Capacity–potential curves (C,E-curves)

The $C(E)$-curves shown in Fig. 9 were recorded for the supporting electrolyte and for that with additions of cyclohexanol (CH). All the $C(E)$-curves deter-

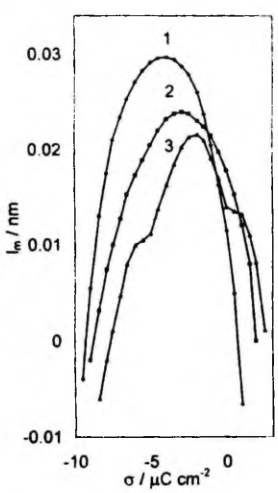

Fig. 8. $I_M(\sigma)$-curves, calculated by Amokrane–Badiali model (at C_S = const) for Bi(001) for various solvents: 1, MeOH; 2, H_2O; 3, AN.

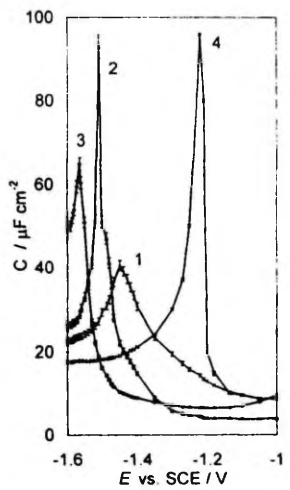

Fig. 9. $C(E)$-curves for aqueous 0.05 M Na_2SO_4 + 0.15 M CH on different electrodes: 1, Cd(0001); 2, Bi(111); 3, Sb(111) and 4, Zn(0001) [64].

mined in the presence of CH in the systems investigated merge with the curves for the supporting electrolyte at negative potentials, indicating that CH molecules are completely desorbed from the electrode surface at these negative polarizations. At less negative potentials the $C(E)$-curves display characteristic adsorption–desorption peaks. The height of this peak increases and its potential shifts to the more negative direction with the increasing CH concentration. According to Fig. 9, the shape (the height and width) of the adsorption–desorption maximum at c_{org} = const depends on the chemical nature of metal, as well as on the cystallographic structure of electrode surface. The height of peaks at c_{org} = const increases and their width decreases in the sequence of Sb < Cd < Zn < Bi, which means that at $E < E_{\sigma=0}$ the attractive interaction between the adsorbed CH molecules increases going from Sb to Bi. According to experimental results the height of the maxima increase in the sequence of planes $(2\bar{1}\bar{1}) < (01\bar{1}) < (001) < (\bar{1}0\bar{1}) < (111)$ as the hydrophilic properties of electrodes increase in the same sequence. A similar relationship is observed for Cd and Zn single crystal electrodes, where the attractive interaction constant a_0 increases from $(11\bar{2}0)$ to (0001) [14, 16]. On metals that differ in their hydrophility a_0 increases in the sequence Sb < Hg < Bi < Cd < Zn < Ga [66].

The frequency dispersion of C is very small in the proximity of the potential of maximum adsorption E_{max} whereas it increases notably in the region of the adsorption–desorption peaks. As shown in [67, 68], if the rate of the adsorption of organic compounds is limited by diffusion, the equilibrium values of differential capacity at $v = 0$ can usually be found to a sufficient degree of accuracy by the extrapolation of the $C_{add}(\omega^{1/2})$-curve to $\omega^{1/2} = 0$ ($\omega = 2\pi\nu$). According to the experimental data, in the region of 60 Hz < ν < 410 Hz, the $C_{add}(\omega^{1/2})$-curves have a good linearity and, accordingly, we can obtain the equilibrium values of differential capacity and use the Frumkin–Damaskin adsorption theory [67]. According to the method described in [69], the equilibrium values of differential capacity can be calculated by the equation

$$C_{add}(\omega = 0) = C^2_{add}(\omega)R^2_p(\omega)\omega^1 + 1/\{[C_{add}(\omega)R_p(\omega)\omega - 1]R_p(\omega)\omega\} \quad (9)$$

where $C_{add}(\omega)$ and $R_p(\omega)$ are the values of differential capacity and solution resistance, respectively, at ω = const.

The equilibrium values of $C_{add}(\omega = 0)$ calculated by equation (9) are in good agreement with the values obtained from $C_{add}(\omega^{1/2})$-curves. As shown in [67–69], the various parameters of the adsorption of CH can be obtained by using the experimental $C(E)$-curves and the Frumkin–Damaskin adsorption theory [67].

Charge density–potential curves [$\sigma(E)$-curves]

The charge density–potential [$\sigma(E)$]-curves were obtained by the back integration of $C(E)$-curves. The shape of these curves is typical for the behaviour observed for the adsorption of neutral organic molecules at metals and all the curves merge at $E \leq -1.8$ V (Fig. 10).

The potential at which the curves intersect the $\sigma_0(E)$-curve is the potential of maximum adsorption E_{max}. In the case of Bi and Cd single crystal electrodes, the value of E_{max} is practically independent of c_{ads}, accordingly the adsorption of CH is approximately equilibrium.

The chronocoulometric investigations of the adsorption of CH were carried out by using the system described in [23]. The values of the initial and final potentials were chosen with the help of $C(E)$- and $i(E)$-curves. The initial potential was varied from −0.50 V to −1.80 V for Bi, from −0.45 V to −1.50 V for Sb and from −0.70 V to −1.80 V for Cd single crystal planes. The final potential value was chosen carefully in order to: (1) achieve the complete desorption of CH; (2) keep the current of hydrogen evolution small enough so that the faradaic reaction would not interfere with the determination of electrode charge density (σ). Five series of potential step experiments were made for $5 \cdot 10^{-4}$ M < c_{CH} < $2 \cdot 10^{-1}$ M. The precision of the charge measurements was good (2–4%). The strategy of the interpretation of the chronocoulometric curves is described thoroughly in [24, 25, 60, 61].

Figure 10 shows that the charge–potential data from the capacitance and chronocoulometric measurements do not differ significantly. A particularly good agreement is seen between −18 and 3 μC cm^{-2}, where the analysis of experimental adsorption data of CH was carried out. Thus, in the case of Bi, Sb and Cd electrodes the existence of problem of non-equilibrium adsorption–desorption peaks is probable but not dramatic.

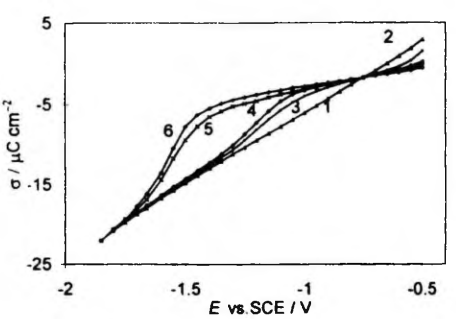

Fig. 10. $\sigma(E)$-curves for Bi(111) in aqueous solution of 0.05 M Na_2SO_4 (1, 2) and with addition of 0.05 M CH (3, 4) and 0.1 M CH (5, 6) obtained from $C(E)$-curves (1, 3, 5) and from chronocoulometry (2, 4, 6).

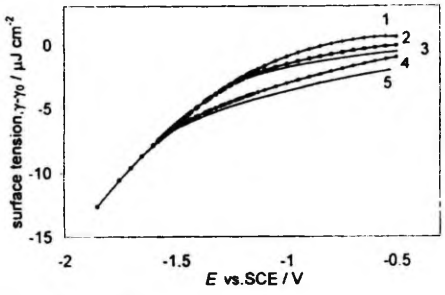

Fig. 11. $[\gamma - \gamma^0](E)$-curves for Bi(111) in aqueous solution of 0.05 M Na_2SO_4 (1) and with addition of 0.05 M CH (2, 3) and 0.1 M CH (4, 5) obtained from $C(E)$-curves (1, 2, 4) and from chronocoulometry (3, 5).

Surface tension, film pressure and Gibbs excess curves

The $\sigma(E)$-curves were back-integrated to obtain the surface tension and film pressure curves. Figure 11 shows that the difference between the surface tension–charge curves, obtained from the capacity and chronocoulometric measurements, is very small, and therefore, the thermodynamic analysis is still possible in the negative rational potential range, since no noticeable frequency effects are expected in that potential range. The film pressure π of the adsorbate was determined by

$$\pi(E) = \gamma_{c=0} - \gamma_c = \int_{E_0}^{E} \sigma_{M,c} dE - \int_{E_0}^{E} \sigma_{M,c=0} dE \quad (10)$$

where subscripts c and $c = 0$ indicate the presence or absence of CH in the bulk of the electrolyte, respectively, and γ is the interfacial tension. For each concentration the curve displays a maximum, the potential of which (E_{max}) is practically independent of c_{CH}.

The film pressure data were used to calculate the relative Gibbs surface excess (Γ). First the film pressure was plotted against log c_{CH} at E = const. The curves display a long linear section, with the slope giving the limiting value of Γ_{max}

$$\Gamma = \frac{1}{RT}\left(\frac{\partial \pi}{\partial \ln c}\right)_{E,T,P}. \quad (11)$$

As in the rising part of the curves, the slope changes drastically, therefore, the related Gibbs excesses for the intermediate coverages were determined from the electrode charge densities using the well-known formula

$$\Gamma = \frac{\sigma_{M,\Gamma} - \sigma_{M,\Gamma=0}}{\sigma_{M,\Gamma_{max}} - \sigma_{M,\Gamma=0}} \Gamma_{max}. \quad (12)$$

The values of $(\sigma_{M,\Gamma_{max}} - \sigma_{M,\Gamma=0})$ were obtained by the extrapolation of the linear sections of the $\sigma_M(E)$-curves. The shape of the $\Gamma(E)$-curves for different c_{CH} suggests that the relative maximum of the adsorption of CH on all planes investigated is reached at $0.7 < E < 1.1$ V and is dependent on the crystallographic structure of the surface. The obtained values of Γ_{max} are presented in Table 4. The Γ_{max} increases in the sequence of metals Zn < Cd < Sb < Bi. In the case of Sb and Bi electrodes Γ_{max} increases in the sequence of planes $(2\bar{1}\bar{1}) \leq (01\bar{1}) < (\bar{1}0\bar{1}) < (001) < (111)$ as the hydrophility of planes increases. In the case of Cd and Zn electrodes [64] the Γ_{max} increases in the sequence $(11\bar{2}0) < (10\bar{1}0) < (0001)$ as the reticular density of planes increases and hydrophility of electrodes decreases.

The differences in the adsorption properties of Sb, Bi, Cd and Zn [10, 64] single crystal electrodes studied become particularly evident if we compare the dependence of potentials of the adsorption–desorption peaks (E^{max}) in the relative scale ($E^{max} - E_{\sigma=0}$)

Table 4.
Adsorption parameters of cyclohexanol on Bi, Sb and Cd electrodes

Electrode	a_0	C' (μF cm^{-2})	E_N (V)	$\Gamma_m \cdot 10^{10}$ (mol cm^{-2})	B_m (dm^3 mol^{-1})	$-\Delta G_A^0$ (kJ mol^{-1})	$\Delta(-\Delta G_A^0)_{(x)}^{(111)}$ (kJ mol^{-1})
Bi(111)	1.83	4.0	0.49	5.5	20	17.1	—
Bi($\bar{1}0\bar{1}$)	1.65	4.1	0.34	5.1	43	19.0	1.9
Bi(001)	1.49	3.8	0.44	5.1	34	18.5	1.4
Bi($01\bar{1}$)	1.45	4.2	0.39	4.6	70	20.1	3.0
Bi($2\bar{1}\bar{1}$)	1.35	4.6	0.36	4.6	39	18.6	1.5
Bi(111)^{Ch}	1.78	—	0.45	5.3	18	16.8	—
Bi(001)^{Ch}	1.44	—	0.42	4.8	31	18.1	1.3
Sb(111)	1.10	3.9	0.55	5.1	48	18.9	—
Sb(001)	0.95	4.4	0.50	4.6	68	20.1	1.2
Sb($2\bar{1}\bar{1}$)	0.70	3.6	0.42	3.5	86	20.7	1.8
Cd(0001)	1.57	5.7	0.38	4.6	14	16.2	—
Cd($10\bar{1}0$)	1.40	5.4	0.28	4.2	22	17.4	1.2
Cd($11\bar{2}0$)	1.37	5.2	0.27	4.1	21	17.3	1.1
Cd(000)^{Ch}	1.53	—	0.34	4.5	12	15.8	—

^{Ch} These parameters are calculated from chronocoulometric data.

on the logarithm of cyclohexanol concentration log c_{CH} for different Sb [70], Bi [63], Cd [14] and Zn [64] faces. According to the conception of works [49–50] the hydrophilic properties of surface decrease in the following sequence of electrodes Zn(11$\bar{2}$0) ≥ Zn(10$\bar{1}$0) > Zn(0001) > Cd(11$\bar{2}$0) ≥ Cd(10$\bar{1}$0) > Cd(0001) > Bi(0$\bar{1}$1) ≥ Bi(001) > Bi(111) > Bi(2$\bar{1}\bar{1}$) ≥ Bi(01$\bar{1}$) > Hg > Sb(001) > Sb(2$\bar{1}\bar{1}$) > Sb(01$\bar{1}$).

Adsorption isotherms

From $C(E)$-curves, using the relationships that follow from the model of two parallel capacitors, were calculated the CH adsorption isotherms (Fig. 12) at the potential of the maximum adsorption $E = E_{max}$. The limiting electrode capacitance C' at the surface coverage $\theta = 1$ was found by extrapolating the dependence of $1/C$ on $1/c_{CH}$ at $E = E_{max}$ to $1/c_{CH} = 0$. The other parameters of the CH adsorption were found using the technique of Frumkin–Damaskin [67] and are shown in Table 4, which uses the generally accepted symbols.

In Table 4, the values of the adsorption parameters point to a substantial difference in the adsorption behaviour of CH on the studied Sb, Bi, Cd and Zn faces. According to the data of Table 4 the difference between the adsorption parameters, obtained from the capacity and chronocoulometric measurements, is small. The values of E_N and Γ_M which are high relative to those found at other electrodes, indicated that the CH molecules have the pronounced vertical orientation on the face (111) of Bi and Sb single crystal. Lower values of Γ_M found for Sb and Bi faces (001), (0$\bar{1}$0), (2$\bar{1}\bar{1}$) and (01$\bar{1}$), and adsorption potential drops E_N decreasing in the order of (001) > (01$\bar{1}$) > (2$\bar{1}\bar{1}$) > (0$\bar{1}$0) indicate that the orientation of the CH molecules has a more distinct horizontal component on these faces, as compared to the basal plane (111) of Sb or Bi, respectively. This in all likelihood is the result of interaction of the OH-group in the CH molecules with the electrode surface. According to the values of B_m, $-\Delta G_A^m$ and $c_{\theta=0.5}$, the adsorption activity of CH increases in the sequence of metals Zn < Cd < Bi ≤ Hg < Sb. The adsorption activity of CH in the case of Bi and Sb electrodes increases in the sequence of planes (111) < (001) < (0$\bar{1}$0) < (2$\bar{1}\bar{1}$) < (01$\bar{1}$), *ie* except the face (111), the adsorption activity of CH increases as the reticular density of planes increases. Higher adsorption activity of the planes (001), (0$\bar{1}$0), (2$\bar{1}\bar{1}$) and (01$\bar{1}$) than (111) is mainly determined by stronger interaction between adsorbed CH molecules and the bismuth or antimony surface atoms, having unsaturated covalent bonds [38]. In the conditions of equal saturation of bonds of the surface atoms, the adsorption activity of CH increases by the increase of the superficial atom density of planes. The adsorption activity of CH at Cd electrodes increases in the sequence of Cd(0001) < Cd(10$\bar{1}$0) ≤ Cd(11$\bar{2}$0).

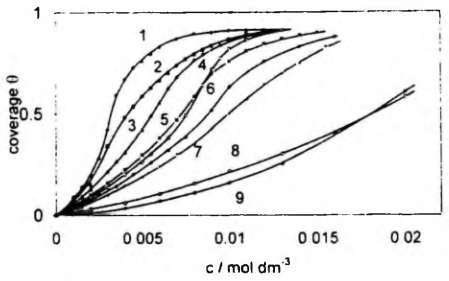

Fig. 12. Isotherms of the CH adsorption on different electrodes: 1, Sb(01$\bar{1}$); 2, Sb(001); 3, Sb(111); 4, Bi(111); 5, Bi(001); 6, Cd(11$\bar{2}$0); 7, Cd(0001); 8, Zn(11$\bar{2}$0) and 9, Zn(0001).

CONCLUSIONS

The results presented above indicate that the inner layer structure, as well as adsorption properties of Bi, Sb and Cd electrodes depend sufficiently on the crystallographic structure of electrode surface, as well as on the chemical nature of metals. According to experimental results the differences between the zero charge potentials for various planes depend on the chemical nature and crystallographic structure (electronic properties) of electrode surface, as well as on the chemical nature of solvent. In all solvents studied the basal Bi(111) and Sb(111) planes have the more negative values of $E_{\sigma=0}$, and the basal plane of Cd(0001) and Zn(0001) [6, 7, 37] has the more positive values of $E_{\sigma=0}$ than other planes investigated. The values of zero charge potential of polycrystalline electrodes are intermediate of these two groups of planes.

The differences between values of $E_{\sigma=0}$ for (001), (01$\bar{1}$), (2$\bar{1}\bar{1}$) and (0$\bar{1}$0) planes for Bi and Sb do not exceed 20 and 50 mV, respectively, but the values of $E_{\sigma=0}$ for Bi(111) and Sb(111) are 60 and 80 mV respectively more negative, than those for the other Bi and Sb planes. This is mainly caused by the specific surface state (electronic properties) of the bismuth and antimony atoms of the basal face (111) in the lattice. The maximum difference in $E_{\sigma=0}$ for various Bi planes is 90 mV for AN, and the difference decreases in the sequence of solvents AN > H_2O > MeOH > *i*-PrOH > EtOH as the anisotropy of the specific adsorption of solvents on various planes diminishes.

The applicability of Grahame theory has been tested by various methods. At the first approximation the double layer can be described by Grahame's model concerning the existence of compact layer with concentration-independent properties. The inner layer capacity increases in the sequence of metals Sb < Bi < Hg < Cd < Zn, as the capacity of thin metal surface layer or lyophility of electrodes increases. For the single crystal planes (001), (01$\bar{1}$) and (2$\bar{1}\bar{1}$) of Bi and Sb and for (0001), (10$\bar{1}$0) and (11$\bar{2}$0) of Cd in all solvents and in all regions of σ the

most compact principal plane has the smallest and the most open plane has the largest interfacial capacity. This conclusion is in good agreement with the theoretical calculations, where metal is represented as a "jellium" and the electrolyte has an ensemble of hard sphere ions and dipoles. The lower values of C_H for Sb(111) and Bi(111) can be explained mainly by the specific state of atoms at the surface of these Bi and Sb planes, *ie* by the lower hydrophility of Bi(111) and Sb(111) or by the higher contribution of metal phase to the values of C_H in the case of Bi(111) and Sb(111) than in the case of other Bi and Sb planes. These conclusions are in good agreement with the data of cyclohexanol adsorption at Sb, Bi, Hg, Cd and Zn electrodes according to which the adsorption activity of cyclohexanol decreases and the adsorption energy of solvent (water) increases in the sequence of electrodes $Sb(2\bar{1}\bar{1}) < Sb(001) < Sb(111) < Bi(01\bar{1}) < Bi(2\bar{1}\bar{1}) < Bi(\bar{1}0\bar{1}) < Bi(001) < Bi(111) < Cd(0001) < Cd(10\bar{1}0) < Cd(11\bar{2}0) < Zn(0001) < Zn(10\bar{1}0)$.

According to the classical conception the specific interaction of solvent dipoles with Bi single crystal planes increase in the sequence of solvents An < H_2O < MeOH < EtOH < *i*-PrOH as the relation $C_H^{\varphi=0}/C_H^{\varphi<0}$ increases.

The values of capacity and thickness of the metal layer, obtained by using various theoretical approximations, give different absolute values of C_M and l_M, but the direction on metals and planes is independent of the approximation used. As it seems to us the more realistic values of metal phase capacity are possible to establish using the model developed by Amokrane, Badiali, Goodisman *et al.* According to this model the effective thickness increases in the sequence of electrodes Cd < Hg < Bi < Sb.

In all solvents studied the capacity of metal layer increases in sequence of $Bi(111) < Bi(\bar{1}0\bar{1}) < Bi(2\bar{1}\bar{1}) < Bi(01\bar{1}) < Bi(001)$. The same tendency seems to be valid in the case of Sb electrodes. But a noticeable dependence of l_M on the chemical nature of solvent takes place and probably the dividing of the inner layer capacity into two components, independent of each other, is a very rough approximation. In the future, for analysis of the electric double layer properties in various solvents, a more complicated model must be elaborated and researched.

REFERENCES

1. A. Hamelin, T. Vitanov, E. Sevastyanov and A. Popov, *J. Electroanal. Chem.* **145,** 225 (1983).
2. A. Hamelin, in *Modern Aspects of Electrochemistry* (Edited by J. O'M. Bockris, B. E. Conway and R. E. White), Vol. 16, Ch. 1, p. 1. Plenum Press, New York (1985).
3. M. Salve, A. Alumaa and U. Palm, *Trans. Tartu State Univ.* **289,** 54 (1971).
4. J. J. Ehrlich, M. P. Pärnoja, T. E. Ehrlich and U. V. Palm, *Proceedings 4th Symp. on Double Layer and Adsorption on Solid Electrodes. Tartu*, p. 342 (1975).
5. A. N. Frumkin, V. V. Batrakov and A. I. Sidnin, *J. Electroanal. Chem.* **39,** 225 (1972).
6. A. R. Alumaa, E. J. Lust, N. A. Paltusova and U. V. Palm, *Soviet Electrochem.* **19,** 1420 (1983).
7. E. Lust and U. V. Palm, *Trans. Tartu State Univ.* **757,** 105 (1986).
8. A. N. Frumkin, *J. Res. Inst. Catal. Hokkaido Univ.* **15,** 61 (1967).
9. U. V. Palm, *Trans. Tartu State Univ.* **757,** 3 (1986).
10. V. V. Batrakov and B. B. Damaskin, *J. Electroanal. Chem.* **65,** 361 (1975).
11. V. V. Batrakov, B. B. Damaskin and Yu. P. Ipatov, *Elektrokhimiya* **10,** 144 (1974).
12. A. P. Korotkov, E. B. Bezlepkina, B. B. Damaskin and E. F. Golov, *Elektrokhimiya* **22,** 1298 (1985).
13. R. Naneva, T. Vitanov, N. Dimitrov, V. Bostanov and A. Popov, *J. Electroanal. Chem.* **274,** 179 (1989); **328,** 287 (1992).
14. E. Lust and J. Ehrlich, *Proceedings 9th Symp. on Double Layer and Adsorption on Solid Electrodes, Tartu*, p. 112 (1991).
15. E. Lust, K. Lust and A. Jänes, *Russian J. of Electrochem.* **31,** 803 (1995).
16. V. N. Vigdorovich, G. A. Ukhlimov, V. V. Marychev and V. P. Shumyalov, Sbornik Nauchnykh Trudov po Problemam Mikroelektroniki. Khimiko-Tekhnologicheskaya Seriya. Collection of Scientific Papers on Microelectronics. Ser. Chemical Technology. *Mosk. Inst. Elektronnoi Tekhniki.* **8,** 24 (1972).
17. W. R. Fawcett, R. C. Rocha Filho and L. M. Doubova, *J. Chem. Soc., Faraday Trans.* **87,** 2967 (1991).
18. E. J. Lust and U. V. Palm, *Soviet Electrochem. Engl. Tr.* **21,** 1256 (1985).
19. E. J. Lust and A. A.-J. Jänes, *Russian J. of Electrochem.* **30,** 357 (1994).
20. E. J. Lust, A. A.-J. Jänes, K. K. Lust and J. J. Ehrlich, *Russian J. of Electrochem.* (1996) (accepted).
21. D. D. Perrin and W. L. F. Armarego, *Purification of Laboratory Chemicals*, 3rd edition. Pergamon Press, Oxford, New York (1986).
22. A. J. Zara and L. O. S. Bulhoes, *Anal. Lett.* **15,** 775 (1982).
23. V. Semevsky, P. Pärsimägi, M. Väärtnõu and A. Alumaa, *Proceedings 9th Symp. on Double Layer and Adsorption at Solid Electrodes, Tartu*, p. 175 (1991).
24. J. Richer and J. Lipkowski, *J. Electroanal. Chem.* **251,** 217 (1988).
25. A. Hamelin, S. Morin, J. Richer and J. Lipkowski, *J. Electroanal. Chem.* **285,** 249 (1990).
26. E. J. Lust, A. A.-J. Jänes and K. K. Lust, *Soviet Electrochem. Engl. Tr.* **26,** 1448 (1990).
27. E. Lust and A. Jänes, *Soviet Electrochm. Engl. Tr.* **28,** 650 (1992).
28. E. Lust, A. Jänes, K. Lust and J. Ehrlich, *Russian J. of Electrochem.* **32,** 597 (1996).
29. E. Lust, *Soviet Electrochm. Engl. Tr.* **27,** 432 (1991).
30. A. Hamelin and L. Stoicoviciu, *J. Electroanal. Chem.* **236,** 267 (1987).
31. A. Hamelin and L. Stoicoviciu, *J. Electroanal. Chem.* **271,** 15 (1989).
32. D. C. Grahame, *J. Am. Chem. Soc.* **76,** 4819 (1954); **79,** 2093 (1957).
33. A. A. Kornyshev and M. A. Vorotyntsev, *Elektrokhimiya* **20,** 3 (1984).
34. M. Salve and U. Palm, *Trans. Tartu State Univ.* **332,** 71 (1974).
35. V. Past, R. Pullerits and M. Moldau, *Trans. Tartu State Univ.* **757,** 140 (1986).
36. D. I. Leikis, K. V. Rybalka and E. S. Sevastyanov, *Adsorption and Electric Double Layer in Electrochemistry* (Edited by A. N. Frumkin and B. B. Damaskin) p. 5. Nauka, Moscow (1972).
37. V. V. Batrokov, A. I. Sidnin, M. M. Melomed and A. A. Predvoditelev, *Elektrokhimiya* **9,** 864 (1973).

38. E. Lust, A. Jänes, K. Lust and M. Salve, *Trans. Tartu Univ.* **966**, 63 (1993).
39. E. Lust and K. Anni, *Proceedings 9th Symp. on Double Layer and Adsorption at Solid Electrodes, Tartu*, p. 109 (1991).
40. P. Pärsimägi, K. Anni, M. Väärtnõu and E. Lust, *Proceedings 9th Symp. on Double Layer and Adsorption at Solid Electrodes, Tartu*, p. 144 (1991).
41. M. Väärtnõu and U. Palm, *Elektrokhimiya* **24**, 553 (1987).
42. K. K. Lust and E. J. Lust, *Soviet Electrochm. Engl. Tr.* **26**, 1453 (1990); **27**, 469 (1991).
43. K. Annia, M. Väärtnõu and U. Palm, *Elektrokhimiya* **22**, 1673 (1986); **23**, 526 (1987).
44. M. A. Vorotyntsev, in *Modern Aspects of Electrochemistry* (Edited by J. O'M. Bockris, B. E. Conway and R. E. White), Vol. 17, p. 131. Plenum Press, New York (1986).
45. L. Nyikos and T. Pajkossy, *Electrochim. Acta* **30**, 1533 (1985).
46. B. B. Mandelbrot, *The Fractal Geometry of Nature*. Freeman, San Francisco (1982).
47. G. Valette and A. Hamelin, *J. Electroanal. Chem.* **45**, 301 (1973).
48. E. Leiva and W. Schmickler, *J. Electroanal. Chem.* **205**, 323 (1986); **227**, 39 (1987).
49. A. N. Frumkin, *Potentsialy Nulevogo Zaryada* (*Potentials of Zero Charge*), p. 206. Nauka, Moscow (1979).
50. A. Frumkin, B. Damaskin, N. Grigor'ev and I. Bagotskaya, *Electrochim. Acta* **19**, 69 (1974).
51. A. A. Kornyshev, *Electrochim. Acta* **36**, 1660 (1991).
52. J. P. Badiali, M. L. Rosenberg, F. Vericat and L. Blum, *J. Electroanal. Chem.* **158**, 253 (1983).
53. S. Amokrane and J. P. Badiali, *J. Electroanal Chem.* **266**, 21 (1989).
54. O. K. Rice, *Phys. Rev.* **31**, 1051 (1928).
55. P. M. Plazman and P. A. Wolf, *Waves and Interactions in Solid State Plasmas, Solid State Physics*, Suppl. 13. Academic Press, New York (1973).
56. V. S. Edelman, *Uspekhi Fizicheskikh Nauk* **129**, 257 (1972).
57. V. S. Kulakovski and V. D. Jegorov, *Fizika Tverdogo Tela* **15**, 2053 (1973).
58. S. Amokrane, V. Russier and J. P. Badiali, *Surf. Sci.* **217**, 425 (1989).
59. V. V. Emets, B. B. Damaskin and V. E. Kazarinov, *Elektrokhimiya* **31**, 787 (1995).
60. M. L. Foresti, M. Innocenti and R. Guidelli, *J. Electroanal. Chem.* **376**, 85 (1994).
61. L. M. Doubova, S. Valcher and S. Trasatti, *J. Electroanal. Chem.* **376**, 73 (1994).
62. A. Iannelli, J. Merza and J. Lipkowski, *J. Electroanal. Chem.* **376**, 49 (1994).
63. E. J. Lust and U. V. Palm, *Soviet Electrochem.* **21**, 1304 (1985).
64. Yu. P. Ipatov, V. V. Batrakov and V. V. Shalaginov, *Elektrokhimiya* **12**, 786 (1976).
65. G. N. Dobrenkov and G. D. Shilotkach, *Elektrokhimiya* **5**, 1416 (1970).
66. N. B. Grigor'ev and I. A. Bagotskaya, *Elektrokhimiya* **2**, 1449 (1966).
67. B. B. Damaskin, O. A. Petrii and V. V. Batrakov, *Adsorption of Organic Compounds on Electrodes*. Plenum Press, New York (1971).
68. R. D. Armstrong, W. P. Race and H. R. Thirsk, *J. Electroanal. Chem.* **16**, 517 (1968).
69. G. A. Tedoradze and R. A. Arakelyan, *Dokl. Akad. Nauk SSSR* **156**, 1170 (1964).
70. E. J. Lust and A. A.-J. Jänes, *Russian J. of Electrochemistry* **30**, 321 (1994).

VII

Reprinted from the *Journal of Electroanalytical Chemistry*, Vol. 425,
E. Lust, A. Jänes, P. Miidla and K. Lust, Adsorption of Pyridine
on the (111), (001) and ($01\bar{1}$) Faces of Bismuth, pages 25–37,

ELSEVIER

Journal of Electroanalytical Chemistry 425 (1997) 25–37

Adsorption of pyridine on the (111), (001) and (01$\bar{1}$) faces of bismuth

E. Lust [a], A. Jänes [a], P. Miidla [b], K. Lust [a]

[a] *Institute of Physical Chemistry, University of Tartu, 2 Jakobi Street, EE-2400 Tartu, Estonia*
[b] *Institute of Applied Mathematics, University of Tartu, 2 Liivi Street, EE-2400 Tartu, Estonia*

Received 15 May 1996; revised 17 September 1996

Abstract

The adsorption of pyridine (PY) on Bi(111), Bi(001) and Bi(01$\bar{1}$) single crystal electrodes has been studied in 0.1 M aqueous NaF solution for concentrations of PY ranging from 1 to 200 mM. In the range of potentials explored, adsorption maximum coverage of the surface and the desorption of PY at $E = -1.8$ V (SCE) have been observed. At the negative potentials and polarization close to the potential of zero charge, PY molecules at bismuth single crystal planes assume a tilted orientation, with the hydrocarbon ring facing the metal. The saturation coverage Γ_{max} and the limiting capacity C_1 decrease, and the shift of zero charge potential E_N, due to the displacement of surface water by a monolayer of PY, rises in the sequence of planes Bi(01$\bar{1}$) < Bi(001) < Bi(111) as the vertical component of the orientation of the PY molecules increases. Adsorption isotherms, values of the attraction constant a and standard Gibbs energy of adsorption ΔG^0_{ads} have been determined. As in the case of other organic compounds studied, the activity of Bi planes increases in the sequence of planes Bi(111) < Bi(001) < Bi(01$\bar{1}$). The partial change transfer from PY to Bi electrodes increases in the same direction of planes. The attractive interaction between the adsorbed molecules rises in the sequence of planes Bi(01$\bar{1}$) < Bi(111) < Bi(001) as the superficial density of atoms decreases.

The absolute value of the Gibbs energy of adsorption of PY increases in the sequence of electrodes Ag < Bi(111) < Hg < Bi(001) < Bi(01$\bar{1}$) < Au(111) < Au(100) < Au(311). As the adsorption activity of aliphatic compounds on Au is lower than on Bi or on Hg we can conclude that there is a weak chemical interaction of PY molecules with Au surface atoms. The Gibbs energy of adsorption of PY on Ag is somewhat lower (3 to 5 kJ mol^{-1}) than for Bi and Hg electrodes; this is caused mainly by the higher hydrophilicity of Ag electrodes. The values of Gibbs energy of PY adsorption on Bi and Hg are comparable and, accordingly, the differences between the metal–adsorbate interaction are not large and the adsorption activity of PY increases, when the hydrophilicity of electrodes decreases in the sequence Bi(111) > Hg > Bi(001) > Bi(01$\bar{1}$).

Keywords: Bismuth single crystals; Pyridine adsorption

1. Introduction

This work is a part of the project which is devoted to the study of the influence of the crystallographic structure of bismuth on the adsorption of neutral organic molecules at the Bi|aqueous solution interface [1–5]. Adsorption of pyridine (PY) at the polycrystalline bismuth solid drop electrode (BDE) was described in Ref. [6], and the phenomenon of solutions of the adsorption–desorption maxima was discovered. Already the first investigations have showed that the splitting of the maxima was due to the presence of different homogeneous monocrystalline surface segments (single crystal planes) on the solid electrode surface. This effect was rather sensitive to the characteristics of the polycrystalline nature of the surface, to the nature of the adsorbing particle structure and of the solvent, to the surface charge density σ and to the solution concentration. The results of electron diffraction studies [7,8] indicate that relatively large monocrystalline surface segments (dimensions of the order of 100 nm) with Miller indices (001), (101) and (01$\bar{1}$) exist at the BDE surface. The statistical treatment of the electronograms and capacity data shows that the surface of the BDE consists mainly of homogeneous segments whose crystallographic, double layer and adsorption characteristics are similar to those for the (001) plane of bismuth [5,7–10]. To this end we undertook experimental investigations of PY adsorption at singular Bi(001), Bi(01$\bar{1}$) and Bi(111) single crystal plane electrodes from aqueous surface inactive electrolyte solutions.

PII S0022-0728(96)04962-5

The PY and pyrazine molecules are known to be weakly chemisorbed at different (Au, Ag, Bi, Zn) metals [11–18]. A large number of spectroscopic investigations of PY and pyrazine at silver, gold and copper have been performed [14–18]. The chemisorption involves the non-bonding molecular orbitals (n) localized at the nitrogen heteroatom and/or π and π^* orbitals of the aromatic ring [14–18]. Consequently, the adsorbed PY molecules may assume either a vertical upright position with the aromatic ring or nitrogen attached to the metal surface, or a flat-lying orientation with the aromatic ring horizontal with respect to the metal surface. Moreover, the adsorption from electrolyte solution at electrodes is complicated by the presence of the electric field and solvent molecules. In this case, comparison of the adsorption of PY at different single crystal plane|solution and at metal|gas interfaces has provided a means of assessing the role of the electronic interaction in the adsorption of organic molecules from solution at bismuth surfaces.

In this work we have carried out systematic simultaneous impedance (capacity bridge) and chronocoulometric investigations of adsorption of PY on the singular bismuth single crystal planes (111), (001) and (01$\bar{1}$).

2. Experimental

The experimental procedures used in this work have been described in Refs. [1–7]. The crystallographic orientation was determined by X-ray diffraction, using a special crystal holder and goniometric head. The massive bismuth single crystal was cut along the chosen crystallographic orientation with a precision of $\pm 0.2°$. The isolation of the faces was carried out by a thin polystyrene film (dissolved in toluene) covering the part of no interest, and then the sample was placed into a Teflon holder [1–5]. The surface was polished to a mirror finish by using standard metallographic procedures. The final surface preparation was obtained by electrochemical polishing in the aqueous KI + HCl solution. Thereafter, a second X-ray diagram was undertaken to determine the precise angle; only those samples whose precision on the orientation was better than $\pm 0.15°$ were used for the electrochemical investigations. After the last stage of surface preparation (electrochemical polishing), electrodes were very well rinsed with ultrapurified water and polarized at -1.2 V (SCE) in the working surface-inactive electrolyte solution.

For an additional characterization of the working surface of the electrodes, an electron microscopic analysis (Jeol JSM-35CF) in the SEI regime was made (40 000 ×). According to these investigations the electrochemically polished surfaces of Bi(111), Bi(01$\bar{1}$) and Bi(001) are ideally smooth (understandably in the range of sensitivity of electron microscopy) [5].

PY was purified according to the methods described in Ref. [19].

3. Results and discussion

3.1. Cyclic voltammograms (CVs)

The CVs and impedance curves were recorded in order to determine the quality of the surfaces investigated and the potential range in which PY adsorption occurred. The shape of the CV recorded for the supporting electrolyte was characteristic of the Bi(111), Bi(01$\bar{1}$) and Bi(001) planes in accord with our previous studies [1–7]. The cyclic voltammetry $j(E)$ curves also indicate that the bismuth single crystal planes investigated are ideally polarizable in the potential range between -1.8 and -0.4 V (SCE) in the aqueous surface-inactive electrolyte solution. A small cathodic current due to hydrogen evolution was observed at the most negative potentials when PY was added to the solution. Neglecting the current due to hydrogen evolution slightly catalysed by the presence of PY, the CVs can be considered as nearly symmetrical.

3.2. Differential capacity vs. potential C(E) curves

The $C(E)$ curves shown in Figs. 1 and 2 were recorded for the pure base electrolyte and with the additions of PY from 1×10^{-3} to 2×10^{-1} M. All the $C(E)$ curves determined in the presence of PY in the solutions investigated merge with the curve for the supporting electrolyte at -1.8 V (SCE), indicating that PY molecules are com-

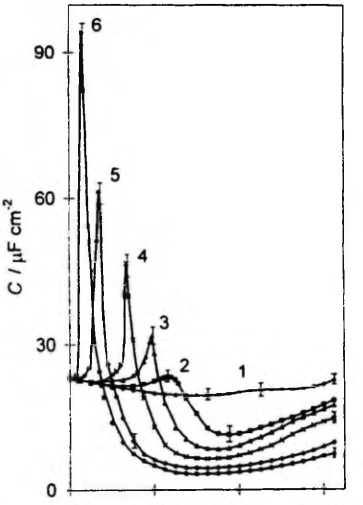

Fig. 1. $C(E)$ curves (ν = 210 Hz) for Bi(111) in 0.1 M NaF (1) and with addition of PY: (2) 0.05; (3) 0.07; (4) 0.1; (5) 0.15; (6) 0.2 M.

pletely desorbed from the bismuth surface at these negative polarizations. At less negative potentials the curves display characteristic adsorption–desorption peaks. The height of the peak increases, and its potential shifts in the negative direction with increasing PY concentration. The adsorption–desorption maxima for Bi(001) are higher and straighter ($c_{PY} > 0.05$ M) than for Bi(111) and Bi(01$\bar{1}$). Accordingly, at these concentrations the attractive interaction between the adsorbed PY molecules on Bi(001) is higher than the Bi(111) and Bi(01$\bar{1}$). The adsorption–desorption maxima at the negative potential scale ($E^{max} - E_{\sigma=0}$) for Bi(01$\bar{1}$) lie at more negative potentials than for Bi(111) or Bi(001). The same order of the adsorption activity of Bi planes was observed in the case of adsorption of cyclohexanol [2] and butylacetate [4] on the single crystal bismuth electrodes. Going further in the positive direction, the differential capacity decreases to a value much smaller than that observed for the pure base electrolyte, indicating that PY molecules are replacing water at the interface. The value of the differential capacity for a solution containing PY remains lower than the value observed for the pure base electrolyte at the positive limit of the potentials investigated. Apparently, no desorption of PY molecules takes place at the polarization $E < -0.4$ V (SCE) applied in this work. As seen from Figs. 1 and 2, the potential of maximum adsorption E_{max} of PY on Bi(001) is practically independent of c_{PY} (± 0.025 V), but for Bi(01$\bar{1}$) and for Bi(111) a noticeable decrease of E_{max}

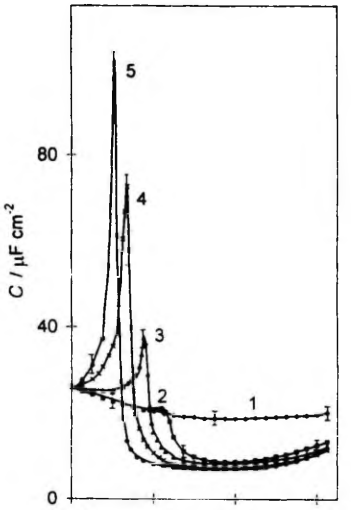

Fig. 2. $C(E)$ curves (ν = 210 Hz) for Bi(001) in 0.1 M NaF (1) and with addition of PY: (2) 0.07; (3) 0.1; (4) 0.15; (5) 0.2 M.

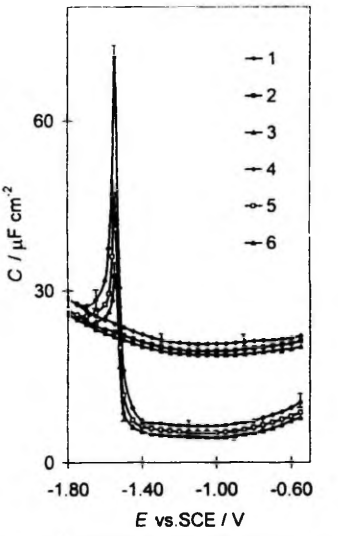

Fig. 3. $C(E)$ curves for Bi(001) in 0.1 M NaF (1–3) and with addition of 0.15 M PY (4–6) at different ν: (1, 4) 210; (2, 5) 2100; (3, 6) 21 000 Hz.

with increasing of c_{PY} was found ($\Delta E_{max} \leq 0.3$ V) for intermediate PY concentrations ($0.005 \leq c_{PY} \leq 0.1$ M). For more concentrated PY solutions ($c_{PY} \geq 0.1$ M) the value of E_{max} is practically independent of c_{PY}.

3.3. Non-equilibrium differential capacity curves

The edl differential admittance was measured from 60 to 21 000 Hz. The capacity dimension with frequency ν is small in the proximity of the differential capacity minimum (in the region of maximum adsorption), whereas it increases noticeably in the region of the adsorption–desorption peaks (Fig. 3). As shown in Refs. [20–22], if the rate of the adsorption of organic compounds is limited by diffusion, the equilibrium values of differential capacity at $\nu = 0$ can usually be found to a sufficient degree of accuracy by the extrapolation of the C_{add} vs. $\omega^{1/2}$ ($\omega = 2\pi\nu$) curve to $\omega^{1/2} = 0$. As we can see from Fig. 4, in the region of $60 < \nu < 410$ Hz the C_{add} vs. $\omega^{1/2}$ curves are practically linear ($\Delta C = \pm 4\ \mu F cm^{-2}$) and, accordingly, to a first approximation we can obtain the equilibrium values of differential capacity by extrapolation of the C_{add} vs. $\omega^{1/2}$ curves to $\omega^{1/2} = 0$ [20–22]. According to the model [20,22], the equilibrium values of differential capacity can be calculated by Eq. (1)

$$C_{add}(\omega = 0) = C^2_{add}(\omega) R^2_p(\omega) \omega^2 + 1/\left[C_{add}(\omega) R_p(\omega) \omega - 1\right] R_p(\omega) \omega \quad (1)$$

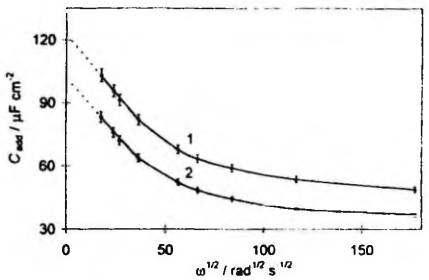

Fig. 4. $C(\omega^{1/2})$ curves for 0.1 M NaF+0.2 M PY at the potential of adsorption–desorption peaks for Bi(001) (1) and Bi(111) (2).

where $C_{add}(\omega)$ and $R_p(\omega)$ are the values of differential capacity and solution resistance at ω = const.

The components of the adsorption impedance were calculated from the impedance data of the cell used for the measurements (series circuit), i.e. $C_S(\omega)$ and $R_S(\omega)$, following the procedure described in Refs. [20–25]. By extrapolating the $R_S(\omega)$ values to $\omega \to \infty$ we determined the solution resistance $R_S(\omega) = R_{sol}$. Since the amount of organic compounds added was small and did not affect the solution resistance, one can assume R_{sol} equal to the ohmic component R_S of impedance in the pure base electrolyte solution. Then the series equivalents $R_S(\omega) - R_{sol}$ and $C_S(\omega)$ of impedance were converted into the parallel equivalents $C_P + C_{true}$ and R_p via the relations given in Refs. [20–25]. A more detailed discussion of the kinetics of PY adsorption on Bi electrodes will be published soon.

The equilibrium values of $C_{add}(\omega = 0)$ calculated by Eq. (1) are 105 to 110 μF cm^{-2} and 126 to 134 μF cm^{-2} for Bi(111) and Bi(001) respectively. These values are in good agreement with the values obtained from Fig. 4 (108 ± 4 μF cm^{-2} for Bi(111) and 128 ± 5 μF cm^{-2} for Bi(001)). Accordingly, as shown in Refs. [20–25], to a first, very rough, approximation the parameters of PY adsorption can be obtained by using the experimental $C(E)$ curves extrapolation to $\omega = 0$.

3.4. Charge density–potential curves

The charge density–potential $\sigma(E)$ curves for base electrolyte solution were obtained by the integration of the $C(E)$ curve, starting from the zero charge potential $E_{\sigma=0}$. The values of $E_{\sigma=0}$ for different Bi single crystal planes were obtained from the position of the diffuse layer minimum on an independently measured differential capacity curve for a dilute solution of the base electrolyte (0.002 to 0.001 M NaF). The established values of $E_{\sigma=0}$ were in good agreement with our previous data published in Refs. [1–5]. The charge density–potential curves for solutions with different additions of PY were obtained by back integration of $C(E)$ curves, starting from $E = -1.8$ V (SCE), and asserting the value of surface charge density σ at $E = -1.8$ V (SCE), equal to σ_0 at $E = -1.8$ V (SCE), because there is no adsorption of PY at this potential.

The shape of the curves obtained is typical of the behaviour observed for the adsorption of neutral organic molecules at metals (Fig. 5). The $\sigma(E)$ curves for different concentrations of PY intersect the $\sigma_0(E)$ curve, obtained for the base electrolyte, at the potential of maximum adsorption E_{max}. Contrary to the cyclohexanol [2] and butanol isomers [21], in the case of PY adsorption at Bi(111) and Bi(01$\bar{1}$) for the intermediate PY concentrations ($0.005 \le c \le 0.1$ M), the E_{max} decreases with increasing of c_{PY} (Fig. 5(b)). For solutions with additions of PY $c_{PY} \ge 0.1$ M, the dependence of E_{max} on c_{PY} is significant. The pronounced dependence of E_{max} on c_{PY} for solutions $0.005 \le c_{PY} \le 0.1$ M indicates that the orientation of PY molecules adsorbed on Bi(111) and Bi(01$\bar{1}$) depend noticeably on the surface coverage θ. At higher surface coverages the PY molecules would have a more stable orientation than the intermediate θ values. The dependence of E_{max} on c_{PY} for Bi(001) is not over 0.1 V (Fig. 5(a)). These results are in good agreement with the data of Figs. 1 and 2.

3.5. Potential step measurements

The values of the initial and final potentials for the potential step experiments were chosen with the help of the $C(E)$- and $j(E)$-curves. The initial potential E_i was varied from -0.40 to -1.8 V (SCE). Usually the electrode was held at initial potential E_θ for 60 s, during which PY adsorption occurred and equilibrium between the interface and the bulk of the solution was established. The final potential E_f was equal to -1.60 V (SCE) for $c_{PY} \le 0.01$ M and -1.80 V (SCE) for $c_{PY} > 0.01$ M. Its value was chosen carefully in order to: (1) achieve complete desorption of PY; (2) keep the current of hydrogen evolution small enough so that the faradaic reaction would not interfere with determination of the electrode charge density σ.

Five series of step experiments were made for concentrations from 1×10^{-3} to 2×10^{-1} M of PY. The precision of charge measurements was 2–5%; therefore, the result of just one experiment was analysed thereafter. The time window in which the transients were recorded was the same for both the base electrolyte and solutions containing PY (10–150 ms).

The chronoamperometric curves were integrated digitally to obtain the charge transients. The charge–potential plots obtained by the integration of the chronoamperometric curves are shown in Figs. 6 and 7. The chronocoulometric curves display an initial fast-rising section corresponding to the charging of the edl followed by a quasi-plateau, in which the charge varies slowly and linearly with time. The slope of this segment is small due to a slight hydrogen evolution reaction. These linear segments

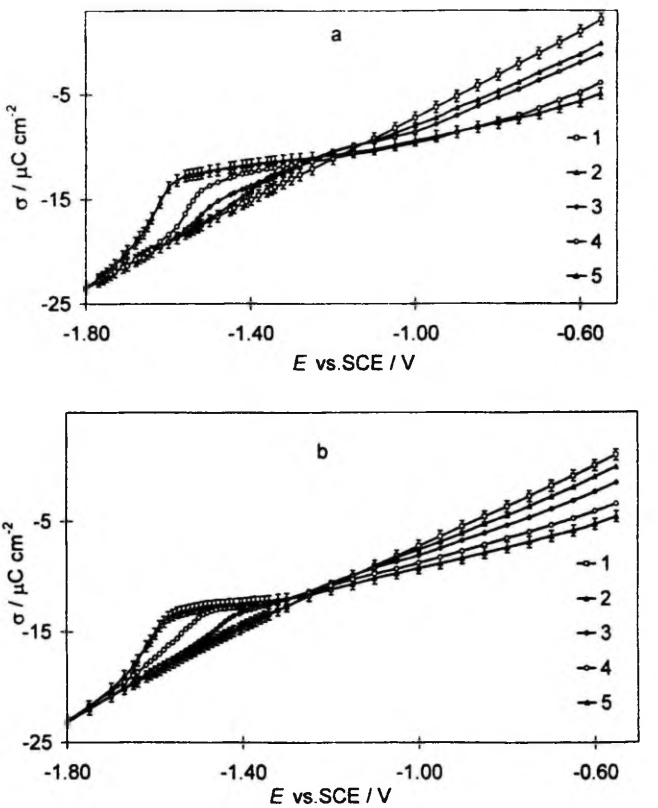

Fig. 5. $\sigma(E)$ curves for Bi(001) (a) and for Bi(111) (b) obtained from impedance data ($\nu = 60$ Hz) for 0.1 M NaF (1) and with addition of PY: (2) 0.07; (3) 0.1; (4) 0.15; (5) 0.2 M.

of the transients were extrapolated to zero time to obtain the relative charge densities $\Delta\sigma$. In this way, the faradaic contribution from hydrogen evolution was minimized. The relative charge densities $\Delta\sigma$ were determined from these step measurements according to the relation

$$\Delta\sigma(E) = \sigma(E_t) - \sigma(E_\theta) \quad (2)$$

In Eq. (2) $\sigma(E_t)$ and $\sigma(E_\theta)$ are the charge densities at the metal side of the interface at potentials E_t and E_θ respectively. Knowing the value of $E_{\sigma=0}$ determined by impedance measurements [5] the absolute charge densities were calculated for each value of E using the formula

$$\sigma(E) = \Delta\sigma(E) - \Delta\sigma(E_{\sigma=0}) \quad (3a)$$

The precision of charge measurements was about 2–5%. Plots of charge density vs. potential for the surface-inactive electrolyte and for some concentrations of PY are shown in Figs. 6 and 7. The shape of these curves is typical and all the curves merge at potentials more negative than -1.8 V (SCE), which indicates that PY is desorbed completely from the Bi surface in this range of E.

Starting from $E = -1.8$ V (SCE) and going in the positive direction, a sharp rise in the charge density is observed if PY is present in the bulk of the solution. The increase in σ slows quickly and the charge becomes nearly linearly dependent on the potential. The $\sigma(E)$ curves for different concentrations of PY intersect the $\sigma_0(E)$ curve at E_{max} and, according to the experimental data, the potential E_{max} for Bi(001) is practically independent (± 0.035 V) of the PY concentration. In the case of Bi(111) (Figs. 6 and 7) and for Bi(01$\bar{1}$) the value of E_{max} depends slightly on the concentration of PY in solution ($\Delta E_{max} \approx \pm 0.1$ V). The slight dependence of E_{max} on c_{PY} is valid for Ag and Au electrodes [11–17].

In some experiments the initial potential E was fixed at

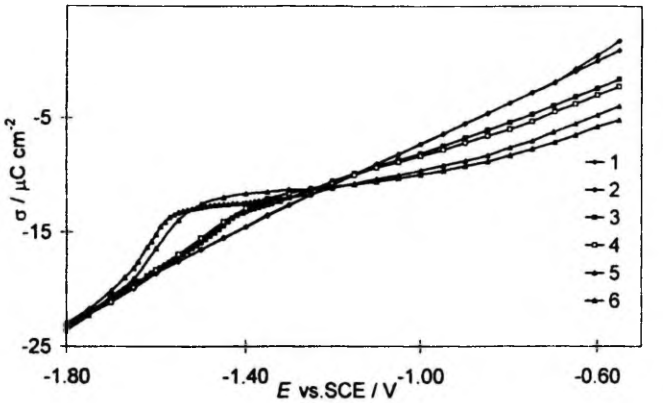

Fig. 6. $\sigma(E)$ curves obtained from impedance (1, 3, 5) and from chronocoulometry (2, 4, 6) in 0.1 M NaF (1, 2) and with additions of PY. (3, 4) 0.1; (5, 6) 0.2 M.

$E = -1.8$ V (SCE) and the final potential E_f was varied from -1.75 to -0.40 V (SCE). The absolute charge densities were calculated according to the Eqs. (2) and (3a).

$$\sigma(E) = \sigma_0(E = -1.8\,\text{V (SCE)}) - \Delta\sigma(E) \qquad (3b)$$

where $\sigma_0(E = -1.8$ V (SCE)) is the surface charge density obtained for the base electrolyte solution at $E = -1.8$ V (SCE). The values of σ are practically independent of the direction of potential step measurements ($\Delta\sigma = \pm 0.5\,\mu\text{C cm}^{-2}$) (Fig. 7), which means that the adsorption of PY is practically reversible.

Unlike with the Au and Ag electrodes [14–19], Fig. 6 shows that the charge–potential data from capacitance and potential step measurements for Bi electrodes do not differ very significantly ($\Delta\sigma = \pm 0.8\,\mu\text{C cm}^{-2}$). The values of σ obtained from chronocoulometry are always higher than the values of σ obtained from impedance data. Therefore, the $\sigma(E)$ curves obtained from impedance data, to some degree, indicate a non-equilibrium condition. Comparison of the $\sigma(E)$ data for Bi(001) and Bi(01$\bar{1}$) planes, as well as for isomers of butanol [21] and cyclohexanol [26], shows that increasing adsorption activity of planes or adsorbates results in an increasing difference between the $\sigma(E)$ curves obtained from impedance and chronocoulometry.

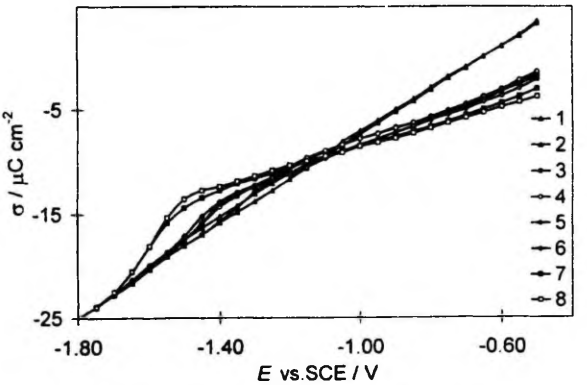

Fig. 7. $\sigma(E)$ curves (chronocoulometry) in 0.1 M NaF (1, 2) and with additions of PY: (3, 4) 0.07; (5, 6) 0.1; (7, 8) 0.2 M (1, 3, 5, 7) started from $E = -1.8$ V (SCE); (2, 4, 6, 8) started from $E = -0.5$ V (SCE).

As we can see from Figs. 5–7, the nearly linear segments were observed on the $\sigma(E)$ curves around E_{max}. By linear extrapolation of these fragments to $\sigma = 0$ one can determine the potential of zero charge corresponding to the surface covered by PY molecules. The difference between this value and the value of $E_{\sigma=0}$ for the pure base electrolyte solution is equal to the change of the surface potential due to the displacement of a monolayer of water molecules by a monolayer of PY, E_N. According to the data of Figs. 5–7, a very slight dependence of E_N on c_{PY} (± 0.05 V) has been observed for Bi(001); however, for Bi(111) and for Bi(01$\bar{1}$) the dependence of E_N on c_{PY} is noticeable (± 0.15 V). The values of E_N presented in Table 1 were found in the limits of c_{PY} from 0.15 to 0.20 M. According to the data of Table 1, in the case of all faces studied, $E_N > 0$ and increases in the sequence of planes Bi(01$\bar{1}$) < Bi(001) < Bi(111).

With the help of the (unrationalized) Helmholtz formula, E_N can be expressed as

$$E_N = 4\pi\Gamma_{max}(\mu^{org} - n\mu^{w})/\varepsilon \quad (4)$$

where Γ_{max} is the limiting surface concentration of PY, μ^{org} and μ^{w} are the components of the dipole moment normal to the surface of the electrode for the organic and water molecules respectively; n is the number of H_2O molecules displaced by one adsorbed PY molecule, and ε is the permittivity of the inner layer. The positive sign of E_N indicates that either (1) $|\mu^{org}| > |n\mu^{w}|$ and $\mu^{org} > 0$ ($0 < \mu^{w} < 0$) or (2) $|\mu^{org}| < |n\mu^{w}|$ and $\mu^{w} < 0$ ($0 < \mu^{org} < 0$). In the first case μ^{org} is positive, which means that PY molecules are oriented with their aromatic hydrocarbon ring facing the Bi surface at $E_{\sigma=0}$. In the second case the PY molecules may be oriented with the aromatic hydrocarbon ring facing the electrode surface ($\mu^{org} > 0$), as well as the nitrogen atom facing the electrode surface ($\mu^{org} < 0$). In these two latter cases, the very large positive value of E_N would suggest a strong preferential orientation of water with oxygen atoms toward the electrode surface at the E_{max} ($\mu^{w} < 0$), which for Bi planes is in contradiction with the data of our previous work [1–5,24,25]. As the maximum adsorption of PY takes place at the noticeably negatively charged surfaces ($\sigma_{max} \approx -9$ to $-11\,\mu C\,cm^{-2}$), it seems to us that the first possibility is more plausible. Therefore, the effective dipole moment of the organic molecules must be positive. Accordingly, in the region of potentials of maximum adsorption, PY molecules on bismuth single crystal planes are oriented with the aromatic hydrocarbon ring facing the bismuth surface and the nitrogen atom facing the solution side of the interface. The same conclusions are valid in the case of adsorption of PY [6], benzene and toluene ($E_N > 0$; $\mu^{org} > 0$) on the BDE [8,27] and on Hg [28]. However, the pronounced dependence of E_{max} and E_N on c_{PY} would seem to indicate that the orientation of PY dipoles depends noticeably on the surface coverage θ; with increasing θ the PY molecules will assume a more pronounced vertical orientation than at low surface coverages.

3.6. Interfacial tension and film pressure curves

Capacitance curves were back-integrated twice to obtain the interfacial tension decrease ($\gamma - \gamma^0$) as a function of the potential and PY concentration. The second integration was performed from the same negative charge at first, equalizing the value of zero to the surface tension value at the $E_{\sigma=0}$ in the blank solution. A progressive decrease of surface tension was found as c_{PY} increased. The shape of the interfacial tension–charge density curve is typical of an organic adsorption. The $\sigma(E)$ curves obtained from chronocoulometric curves were integrated from the same negative charge as the $\sigma(E)$ curves obtained from impedance measurements. The comparison of $(\gamma - \gamma^0)(E)$ curves obtained from impedance and chronocoulometric measurements shows that, in the case of PY adsorption at Bi(111) and Bi(001) planes, there are no big differences between the two collections of $(\gamma - \gamma^0)(E)$ curves ($\Delta(\gamma - \gamma^0)_{max} = \pm 0.3\,\mu J\,cm^{-2}$), but the decrease of interfacial tension is always bigger in the case of chronocoulometry. According to the interfacial tension–potential curves, the adsorption activity of the Bi planes increases in the sequence Bi(111) < Bi(001) < Bi(01$\bar{1}$).

Table 1
Adsorption parameters of PY on Bi single crystal planes

Plane	$a \pm 0.05$	$C_1 \pm 0.4$/ $\mu F\,cm^{-2}$	$c_{\sigma=0} \pm 0.002$/ $mol\,dm^{-3}$	$10^{10}\,\Gamma_{max} \pm 0.4$/ $mol\,cm^{-2}$	$E_N \pm 0.1$/ V (SCE)	$B \pm 20$/ $dm^3\,cm^{-2}$	$\Delta G^0_{ads} \pm 0.3$/ $kJ\,mol^{-1}$
From impedance measurements							
(111)	1.10	3.0	0.048	5.4	1.05	137	22.1
(001)	1.05	3.4	0.049	5.1	0.89	385	24.7
(01$\bar{1}$)	1.00	3.6	0.025	4.9	0.75	515	25.4
From chronocoulometric measurements							
(111)	1.20	—	—	5.5	0.69	325	24.3
(001)	1.05	—	—	5.2	0.65	460	25.1
(01$\bar{1}$)	0.90	—	—	5.1	0.63	710	26.2

The Gibbs energies of adsorption have been calculated using the following standard states: unit mole fraction of the organic species in the bulk of the solution and monolayer coverage ($\theta = 1$) of the 'ideal non-interacting' adsorbate. For more detailed analysis see Ref. [14].

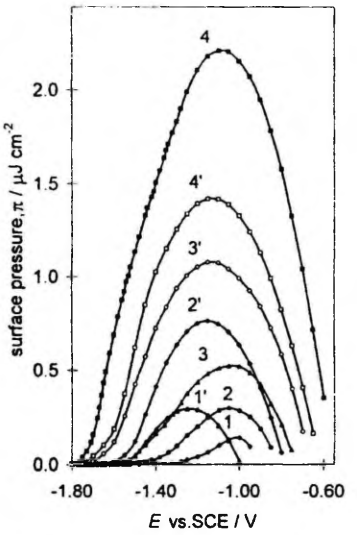

Fig. 8. $\pi(E)$ plots for Bi(001) (1, 2, 3, 4) and for Bi(111) (1', 2', 3', 4') obtained from impedance ($\nu = 60$ Hz) in 0.1 M NaF with addition of PY: (1, 1') 0.05; (2, 2') 0.1; (3, 3') 0.15; (4, 4') 0.2 M.

The surface pressure π of the film of adsorbed PY can be determined as

$$\pi(E) = \gamma_{c=0} - \gamma_c = \int_{E_0}^{E} \sigma_{M,c}\, dE - \int_{E_0}^{E} \sigma_{M,c=0}\, dE \quad (5)$$

where subscripts c and $c = 0$ indicate the presence and absence of PY in the bulk of the electrolyte respectively, and γ is surface tension. The calculated $\pi(E)$ curves are plotted in Fig. 8. For each concentration the curve displays a maximum, the E_{max} of which shifts negatively as c_{PY} increases. The dependence of E_{max} and E_N on c_{PY} indicates that the orientation of the adsorbed PY molecules at Bi(111), Bi(01$\bar{1}$) and Bi(001) single crystal planes depends on the concentration of PY (surface coverage). Comparison of $\pi(E)$ curves for single crystal bismuth planes with the corresponding data for Ag and Au electrodes [11–16] shows that the adsorption activity of bismuth electrodes is noticeably lower than the activity of Au electrodes, but it is comparable with the adsorption activity of Ag planes [11–16]. According to the $\pi(E)$ curves the adsorption activity of PY increases in the sequence of planes Bi(111) < Bi(001) < Bi(01$\bar{1}$). The comparison of the $\pi(E)$ curves obtained from chronocoulometry with the $\pi(E)$ curves calculated from the impedance data shows that the values of π (at E = const., c = const.) from chronocoulometry are always higher than the values of π obtained from impedance ($\Delta\pi = \pm 0.1\ \mu J\ cm^{-2}$) (Fig. 9).

3.7. Gibbs excess–potential and Gibbs excess–log c_{PY} curves

The film pressure data obtained from chronocoulometry, as well as from impedance, were used to calculate the relative Gibbs surface excess Γ. First the film pressure was plotted against log c_{PY} at E = const. The curves display a long linear section, its slope giving the limiting value of Γ_{max}

$$\Gamma = \frac{1}{RT}\left(\frac{\partial\pi}{\partial \ln c}\right)_{E,T,P} \quad (6)$$

the values of which are presented in Table 1. As in the rising part of the curves, the slope changes noticeably; therefore, the related Gibbs excesses for the intermediate coverages were determined from the electrode charge densities using the well-known formula

$$\Gamma = \frac{\sigma_\Gamma - \sigma_{\Gamma=0}}{\sigma_{\Gamma_{max}} - \sigma_{\Gamma=0}}\Gamma_{max} \quad (7)$$

The values of $(\sigma_{\Gamma_{max}} - \sigma_{\Gamma=0})$ were obtained by the extrapolation of the linear sections of the $\sigma(E)$ curves. The shapes of the $\Gamma(E)$ curves for different c_{PY} (Fig. 10) suggest that the relative maximum of the adsorption of PY on Bi(001) is reached for $c_{PY} \geq 0.03$ M at $-0.9 < E < -1.2$ V (SCE). At the base of Bi(111) the relative maxi-

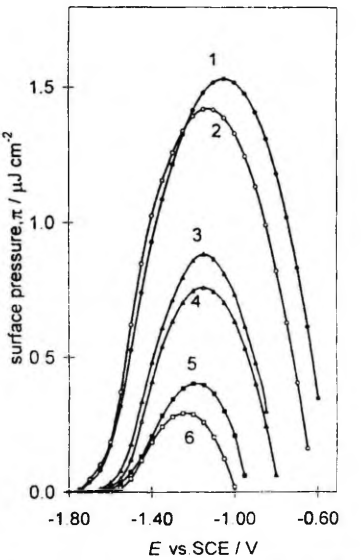

Fig. 9. $\pi(E)$ plots for Bi(111) obtained from chronocoulometry (1, 3, 5) and from impedance (2, 4, 6) ($\nu = 60$ Hz) in 0.1 M NaF with additions of PY: (1, 2) 0.2; (3, 4) 0.1; (5, 6) 0.05 M.

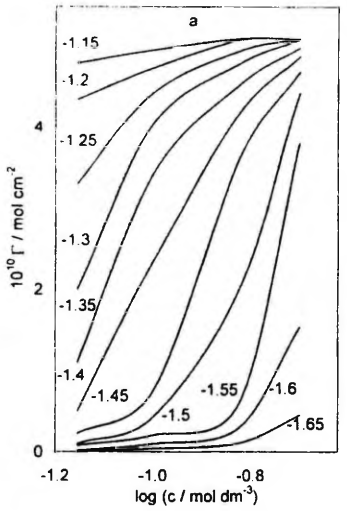

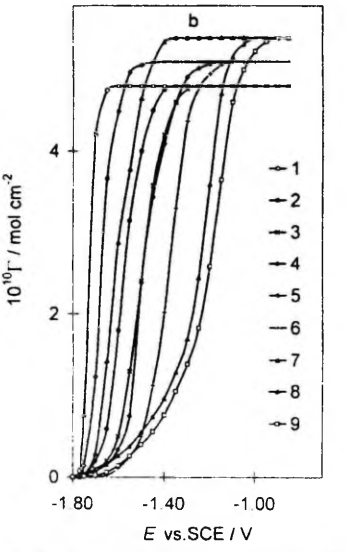

Fig. 10. (a) $\Gamma(\log c)$ curves obtained from impedance ($\nu = 60$ Hz) for Bi(001) at different electrode potentials as noted; (b) $\Gamma(E)$ curves for Bi(01$\bar{1}$) (1, 2, 3); Bi(001) (4, 5, 6) and Bi(111) (7, 8, 9) with different additions of PY (1, 4, 7) 0.2; (2, 5, 8) 0.1; (3, 6, 9) 0.07 M.

mum of PY adsorption is reached for $c_{PY} \geq 0.05$ M at the potentials $-1.0 < E < -1.3$ V (SCE) and for Bi(01$\bar{1}$) at $-0.9 < E < -1.4$ V (SCE).

According to the data of Table 1, in the case of Bi electrodes, the values of Γ_{max} obtained from impedance data are only a little lower than the values of Γ_{max} obtained from chronocoulometry. The value of Γ_{max} at E_{max} increases in the sequence of planes Bi(01$\bar{1}$) < Bi(001) < Bi(111) as the surface activity of planes decreases.

The maximum value of Γ_{max} for Bi(001) is 5.2×10^{-10} mol cm^{-2}, for Bi(01$\bar{1}$) Γ_{max} is 5.1×10^{-10} mol cm^{-2} and for Bi(111) Γ_{max} is 5.5×10^{-10} mol cm^{-2} (chronocoulometry data). These values correspond to an area for one molecule $S_{max} \approx 0.32$ nm^2 for Bi(001) and Bi(01$\bar{1}$), and $S_{max} \approx 0.30$ nm^2 for Bi(111). Packing densities calculated for the flat and for the vertical orientations of PY molecules correspond to 4.7×10^{-10} mol cm^{-2} and 6.5×10^{-10} mol cm^{-2} respectively [14–16]. These values of Γ_{max} correspond to the effective molecular areas S_{max}(flat) ≈ 0.35 nm^2 and S_{max}(vert) ≈ 0.25 nm^2 [14–18]. As found, the values of Γ_{max} and S_{max} for Bi(01$\bar{1}$), Bi(001) and Bi (111) (Table 1) are intermediate between the values expected for the flat and vertical orientations. Accordingly, the PY molecules are tilted on the surface of bismuth single crystal planes.

The $\Gamma(E)$ and $\Gamma(\log c_{PY})$ plots are presented in Fig. 10. The sharp rise of $\Gamma(\log c_{PY})$ plots suggests a possible phase transition indicating strong lateral interaction between adsorbed PY molecules at negative potentials ($E < -1.1$ V (SCE)). The values of Γ_{max} for Bi(01$\bar{1}$) and Bi(001) planes are somewhat lower than the corresponding value for Bi(111). Therefore, a more pronounced flat orientation of PY dipoles on Bi(01$\bar{1}$) and Bi(001) surface is possible. This conclusion is in good agreement with the noticeable decrease of E_N in the sequence of planes Bi(111) ≥ Bi(001) > Bi(01$\bar{1}$).

3.8. Gibbs energy–potential curves

The energetics of PY adsorption are characterized by the magnitude of the Gibbs energy of adsorption. Fig. 11 shows the $\Delta G^0_{ads}(E)$ curves determined from the tangent of the initial slope of $\pi(\ln c)$ curves at E = const. (following the Henry isotherm) for the various Bi single crystal planes investigated. The $\Delta G^0_{ads}(E)$ curves display a quasi-parabolic shape. The absolute values of ΔG^0_{ads} progressively increase (at E_{max}) when moving from the Bi(111) to Bi(01$\bar{1}$) surface. The value of the potential of the maximum of these curves corresponds very well with the value of the potential of maximum adsorption of $C(E)$ curves. According to Fig. 11, the absolute values of ΔG^0_{ads} obtained from the impedance data (from π vs. ln c curves) are somewhat lower than the absolute values of ΔG^0_{ads} obtained from chronocoulometry. Thus, at the low PY concentrations the $C(E)$ curves are, to some degree, not in equilibrium; therefore, to establish the 'true' values of ΔG^0_{ads} the chronocoulometric data (π vs. ln c curves) [14–16] must be used. The precision of ΔG^0_{ads} is improved by avoiding the differentiation of $\pi(\ln c)$ curves, as the

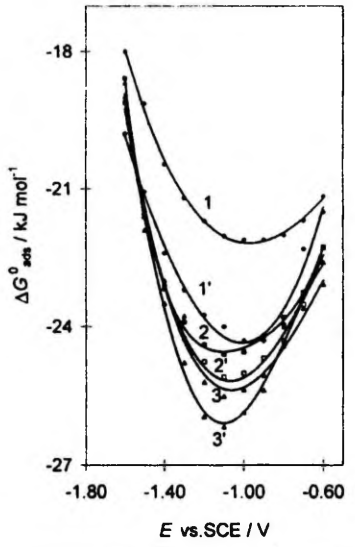

Fig. 11. The $\Delta G^0_{ad,s}(E)$ curves for PY adsorption obtained from impedance (1–3) and from chronocoulometry (1′–3′) for Bi single crystal electrodes: (1, 1′) (111); (2, 2′) (001); (3, 3′) (01$\bar{1}$).

values of Γ_{max} obtained from the linear part of the $\pi(\ln c)$ plots are quite precise. Thus the precision of the film pressure data must be very high in order to obtain meaningful values of ΔG^0_{ads}. Therefore, in addition to the previously described method, the equation of the Frumkin isotherm

$$Bc = \frac{\theta}{1-\theta}\exp(-2a\theta) \quad (8)$$

was fitted to the data presented in Figs. 9 and 10. In Eq. (8) B is the adsorption equilibrium constant, θ is the surface coverage ($\theta = \Gamma/\Gamma_{max}$) and a is the lateral interaction parameter. B is related to the Gibbs energy of adsorption by

$$\Delta G^0_{ads} = RT\ln(55.5B) \quad (9)$$

A good fit to Eq. (8) was achieved with the parameter a weakly dependent on the electrode potential (Fig. 12). The agreement of the Gibbs energies of PY adsorption obtained from the Henry and Frumkin isotherms is good, indicating that the data are free from major systematic errors.

The Gibbs energy of adsorption is given by the sum of the differences between the partial molar chemical potentials of the adsorbate μ^0_A and n water molecules $n\mu^0_W$ at the surface (s) and in the bulk (b), i.e.

$$\Delta G^0_{ad,s} = \left(\mu^0_{A,s} - n\mu^0_{W,s}\right) + \left(n\mu^0_{W,b} - \mu^0_{A,b}\right)$$

where the second term is surface independent. In the case of adsorption of aliphatic molecules the interaction between the hydrocarbon tails and the metal surface must have the character of dispersive forces and is, therefore, weak; hence, the dependence of ΔG^0_{ads} on the crystallographic structure essentially displays changes in the energy of Bi–H_2O interactions, i.e. the surface hydrophilicity. In the case of PY adsorption the interaction of bismuth surface atoms with PY may be noticeably stronger than that with water. Therefore, the change in the Gibbs energy of adsorption with crystallographic orientation to some degree reflects the difference between PY interaction with the surface atoms of various single crystal planes of Bi. As in the case of adsorption of cyclohexanol [2], butylacetate [4] and butanol isomers [21], the adsorption activity increases in the sequence of planes Bi(111) < Bi(001) < Bi(01$\bar{1}$). Thus, the most active is the singular Bi(01$\bar{1}$) plane, where unsaturated covalent bonds are distributed uniformly over the entire surface; the most inactive is the basal plane Bi(111), where the surface atoms are chemically saturated. Unlike the aliphatic compounds, where the adsorption activity of aliphatic compounds on Ag and Au is lower than on Bi [14–16], in the case of PY the gold electrodes are noticeably more active than the Bi electrodes; this means that the chemical interaction of PY with Au is noticeably higher ($\Delta(-\Delta G^0_{ad,s}) \sim 15$ to 20 kJ mol^{-1}) than with Bi electrodes [14–16]. The absolute value of ΔG^0_{ads} of PY adsorption on Ag is somewhat lower (3 to 5 kJ mol^{-1}) than for Bi and Hg electrodes, which is caused mainly by the higher hydrophilicity of the Ag electrodes [29,30]. The absolute values of the Gibbs energy of PY adsorption on Bi [8,27] and Hg [28] are comparable; accordingly, the differences between the metal–adsorbate interactions are not large, and the adsorption activity of PY

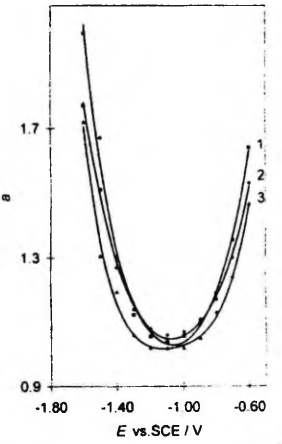

Fig. 12. $a(E)$ curves for Bi(001) (1), Bi(111) (2) and Bi(01$\bar{1}$) (3).

increases when the hydrophilicity of the electrodes decreases in the sequence Bi(111) > Hg > Bi(001) > Bi(01$\bar{1}$).

The lateral interaction constants a are positive (Fig. 12 and Table 1) and their values decrease as the surface charge density decreases. According to Fig. 12, the attractive interaction increases in the sequence of planes Bi(01$\bar{1}$) < Bi(001) < Bi(111) as the superficial density of surface atoms decreases (except Bi(111)). In the case of adsorption of organic compounds at metal surfaces from solution, a can be expressed in terms of different particle–particle interactions at the interface [14–16,20,28]

$$2a = (2Z_{WA} - Z_{AA} - Z_{WW})/RT \quad (10)$$

where Z_{ij} are the particle–particle interaction energies, W stands for water and A for adsorbate. The positive values of a mean that $2Z_{WA} > Z_{AA} + Z_{WW}$, i.e. the adsorbate–adsorbate and water–water interactions are much more attractive than the adsorbate–water interactions. The same conclusions are valid in the case of adsorption of PY on a BDE and Hg [8,27,28].

3.9. Adsorption isotherms

According to the data of Fig. 3, there are no noticeable frequency effects in the region of potential of maximum adsorption. Therefore, the differential capacity C_1 at the maximum coverage was obtained by the usual method, i.e. by extrapolating $1/C$ vs. $1/c_{PY}$ plots to $(1/c_{PY}) \rightarrow 0$. The data taken at $E = -1.0$ V (SCE) lie satisfactorily on a straight line. This is proof that the capacitance is affected negligibly by problems of reversibility in the region between the adsorption–desorption peaks. Thus, the C_1 values obtained are reported in Table 1.

The surface coverage was estimated from Eq. (11) based on Frumkin's two parallel condenser model [20]

$$\theta = (C_0 - C_\theta)/(C_0 - C_1) \quad (11)$$

where C_0 and C_1 are the capacitances at $\theta = 0$ and $\theta = 1$ respectively. The next step is the test of the Frumkin isotherm in the semi-logarithmic co-ordinates ($\log[\theta/(1-\theta)c]$ vs. θ plot) to derive the adsorption parameters. According to the experimental data, the $\log[\theta/(1-\theta)c](\theta)$ plots are linear in the region of $0.3 < \theta < 0.85$. The slope of the semi-logarithmic isotherms gives the molecular interaction parameter a and the intercept provides the adsorption equilibrium constant B at E_{max}. The $\Delta G^0_{ad_s}$ values obtained show that the adsorption activity of the Bi planes increases in the order Bi(111) < Bi(001) < Bi(01$\bar{1}$). However, the absolute values of $\Delta G^0_{ad_s}$ obtained by using Eq. (11) are systematically lower than the absolute values of $\Delta G^0_{ad_s}$ obtained from chronocoulometric data ($\Delta(-\Delta G^0_{ad_s}) \leq 1.5$ kJ mol^{-1}).

The non-linear character of the adsorption isotherms at the low surface coverages ($\theta < 0.3$) is probably caused by the weak dependence of E_{max} on c_{PY}, because in the case of low c_{PY} the dependence of C on E is noticeable, and a small deviation of potential of capacity minimum from E_{max} causes a very large deviation of C and therefore a large error on θ. At the higher PY concentrations ($c_{PY} \geq 0.003$) the dependence of C on E (in the region of $E_{max} = -1.0$ V (SCE)) is small, and at $c_{PY} \geq 0.003$ M the adsorption isotherms in the semi-logarithmic co-ordinates are linear. It must be noted that, in the case of PY adsorption at Bi electrodes, changes in the dipole orientation at the electrode surface with electrode potential are possible; therefore, the use of the two parallel condenser model is, to some degree, incorrect.

3.10. Electrosorption valency

The first derivative of $\Delta G^0_{ad_s}$ vs. E is equal to the electrosorption valence γ' [14,16,28]. The $\Delta G^0_{ad_s}(E)$ data obtained from the Henry or Frumkin isotherms were fitted by a fourth-order polynomial and numerically differentiated. The established $\gamma'(E)$ curves show that the value of γ' (in the region of E_{max}) increases in the sequence of planes Bi(111) < Bi(001) < Bi(01$\bar{1}$) as the adsorption activity of PY on bismuth planes increases. Accordingly, the partial charge transfer from PY to bismuth electrodes increases in the same direction of planes.

3.11. Analysis of the adsorption–desorption peaks

If the Frumkin model is accepted, further information on adsorption parameters can be obtained from an analysis of the adsorption–desorption peaks. The following analysis is not unquestionable per se. First, frequency effects are included; secondly, the validity of the formulae entails, in particular, a congruence of isotherms with respect to the potential and constants C_0 and C_1. However, the analysis is carried out in order to compare adsorption of the same compound at the three different planes of the same metal, using the same experimental variable. Therefore, the relevance of the conclusions reached with the aid of the present analysis is believed to be incontestable. Fig. 13 shows that the variation of $(C^{max} - C_0)$ with $\log c_{PY}$ is

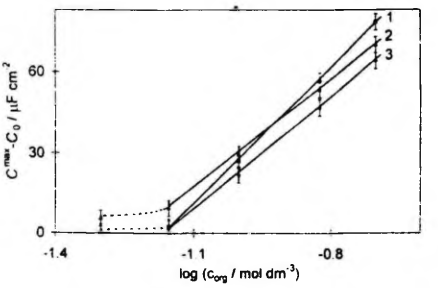

Fig. 13. $(C^{max} - C_0)\log c$) plots ($\nu = 0$ Hz) at negative potentials of PY adsorption–desorption peaks for Bi planes: (1) (001); (2) (111); (3) (01$\bar{1}$).

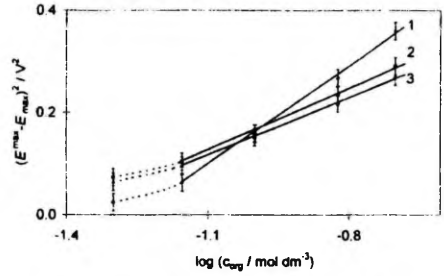

Fig. 14. $(E^{max} - E_{max})^2(\log c)$ plots for PY adsorption on Bi planes: (1) (111); (2) (001); (3) (01$\bar{1}$).

linear for both faces at $c_{PY} \geq 0.05$ M (the values of C^{max} at $\omega = 0$ have been determined from $C^{max}(\omega^{1/2})$ dependences). The slope of the plot in Fig. 13 is given by [19]

$$d(C^{max} - C_0)/d\log c_{PY} = 2.3(C_0 - C_1)/(2 - a) \quad (12)$$

Since C_0 and C_1 are known independently, a value of a can be obtained from Eq. (12). From our results, $a = 1.84$, 1.70 and 1.75 for Bi single crystal planes (001), (01$\bar{1}$) and (111) respectively; these values are in good agreement with the data of Fig. 12.

According to the Frumkin model, the value of $(E^{max} - E_{max})^2$ should be linearly related to $\log c$ with a slope given by [20,30]

$$d(E^{max} - E_{max})^2/d\log c = 4.6RT\Gamma_{max}/(C_0 - C_1) \quad (13)$$

Since C_0 and C_1 are known, Γ_{max} can be estimated from Eq. (13). Fig. 14 shows that the $(E^{max} - E_{max})^2$ vs. $\log c$ plots are satisfactorily linear for the Bi electrodes investigated. On the basis of Eq. (12) it was found that $\Gamma_{max} = (5.3 \pm 0.5) \times 10^{-10}$ mol cm^{-2} for Bi(001), $\Gamma_{max} = (6.5 \pm 0.6) \times 10^{-10}$ mol cm^{-1} for Bi(111) and $\Gamma_{max} = (5.0 \pm 0.6) \times 10^{-10}$ mol cm^{-1} for Bi(01$\bar{1}$). The somewhat higher values of Γ_{max} obtained in the region of the adsorption–desorption peaks, compared with the values of Γ_{max} obtained at E_{max}, indicate that with increasingly negative polarization (surface charge density) the vertical component of the orientation of PY molecules increases.

4. Summary

Data presented for the adsorption of PY on single crystal electrodes indicate that the adsorption characteristics of PY depend noticeably on the crystallographic structure of the Bi electrode surface. To summarize, it is convenient to compare the adsorption data of this compound on single crystal bismuth electrodes with the adsorption data for Hg, Ag and Au electrodes.

The comparison of the data obtained from the impedance measurements with those obtained from chronocoulometry shows that the capacity values at low PY concentrations are, to some degree, not in equilibrium; therefore, the adsorption parameters obtained from chronocoulometry measurements at Bi electrodes have been used for the quantitative analysis of PY adsorption on various electrodes.

The experimental investigations indicate that the shape of the differential capacity curves is very sensitive to the crystallographic structure of electrode surface studied. As in the case of the cyclohexanol [1–5] and butanol isomers [21] studied, the heights of the adsorption–desorption maxima increase in the order of planes Bi(01$\bar{1}$) < Bi(111) < Bi(001) as the superficial density of surface atoms decreases. The values of attractive coefficient a obtained from the heights or widths of these adsorption–desorption maxima are in a good agreement with one another, and the values of a increase in the sequence of planes Bi(01$\bar{1}$) < Bi(111) < Bi(001), i.e. with decreasing interfacial density of atoms.

As for the Hg electrode [28], the maximum adsorption of PY on Bi single crystal planes takes place at the noticeably negatively charged electrode surface ($-\sigma \approx 9$ to 11 μC cm^{-2}). The potential of maximum adsorption E_{max} shifts towards more and more negative values of E as c_{PY} increases. The same tendency is valid for Hg electrodes [28]. If the PY adsorption at Ag or Au electrodes takes place, the E_{max} with increasing c_{PY} shifts towards the more positive values of E [11–16]. The opposite sign of E_{max} for these two groups of metals suggest that the PY molecules assume opposite orientations at the noble metal (Au, Ag) and Hg-like (Hg, Bi) metal surfaces. The values obtained for the shift of zero charge potential E_N, owing to the displacement of a surface water monolayer by PY molecules, are positive for Hg and Bi electrodes, indicating that the PY molecules are oriented with the aromatic hydrocarbon ring towards the electrode surface. The same orientation of benzene and toluene molecules is valid at polycrystalline bismuth [2,27] and Hg [28] electrodes. The limiting capacity C_1 decreases and the maximum surface coverage Γ_{max} increases in the sequence of metals Bi ≤ Hg < Ag < Au [8,11–16,28] if the adsorption activity of the electrode increases. The higher value of Γ_{max} for Bi(111), compared with the values of Γ_{max} for Bi(001)and Bi(01$\bar{1}$) planes, indicates that at this plane the PY molecules have a more pronounced vertical orientation than at the Bi(001) and Bi(01$\bar{1}$) planes. The values of Γ_{max} for Bi(111), Bi(001) and Bi(01$\bar{1}$) are intermediate between the values expected for the flat ($\Gamma_{max} = 4.5 \times 10^{10}$ mol cm^{-2}) and for the vertical ($\Gamma_{max} = 6.5 \times 10^{10}$ mol cm^{-2}) orientation of PY [14]; therefore, it may be assumed that PY molecules have a tilted orientation at the surface of Bi single crystal planes.

The orientation of the adsorbate at the metal|solution interface is a result of competition between interactions of the functional group with the metal and the solution phase. The adsorption activity of aliphatic compounds increases

in the sequence of metals Au < Ag < Bi ≤ Hg, as the hydrophilicity of the electrodes decreases. Therefore, as the absolute value of Gibbs energy of adsorption of PY on Au planes is noticeably higher (15 to 20 kJ mol^{-1}) than for Bi, Hg and Ag, we can conclude that there is a weak chemical interaction of PY molecules with Au surface atoms [14–16]. The absolute value of the Gibbs energy of adsorption of PY on Ag is somewhat lower (3 to 5 kJ mol^{-1}) than for Bi and Hg electrodes; this is caused mainly by the higher hydrophilicity of the Ag electrodes. The absolute values of the Gibbs energy of PY adsorption on Bi [8,27] and Hg [28] are comparable and, accordingly, the differences between the metal–adsorbate interaction are not large and the adsorption activity of PY increases when the hydrophilicity of the electrodes decreases in the sequence Bi(111) > Hg > Bi(001) > Bi(01$\bar{1}$). The adsorption activity of PY on bismuth planes increases (except Bi(111)) if the superficial density of atoms increases. Just as in the case of cyclohexanol [1], butyl acetate [4] and butanol isomers [21] adsorption, the basal plane Bi(111), where the surface atoms are chemically saturated, has the lowest adsorption activity of PY, and the most active one is the singular Bi(01$\bar{1}$) plane, where unsaturated covalent bonds are distributed uniformly over the whole surface. Decreasing a and Γ_{max} values with decreasing negative charge density of the metal show that the orientation of PY molecules becomes less vertical and, therefore, that the nitrogen atoms are moving towards the electrode surface if σ increases. In the case of positively charged Bi electrodes a weak chemical interaction ($-\Delta G^0_{Me-PY} \approx 2$ to 3 kJ mol^{-1}) is possible; however, this is very weak in comparison with the PY–Au interaction ($-\Delta G^0_{Me-PY} = 15$ to 20 kJ mol^{-1}). A more detailed analysis of the dependence of ΔG^0_{Me-org} on the chemical nature of the adsorbate will be published elsewhere [31].

References

[1] U.V. Palm and M.P. Pärnoja, Sov. Electrochem., 14 (1978) 1070.
[2] E.J. Lust and U.V. Palm, Sov. Electrochem., 21 (1985) 1304.
[3] E.J. Lust and U.V. Palm, Sov. Electrochem., 22 (1986) 383.
[4] E.J. Lust, J.J. Ehrlich and U.V. Palm, Sov. Electrochem., 22 (1986) 695.
[5] E.J. Lust, K.K. Lust and A.A.-J. Jänes, Russ. J. Electrochem., 31 (1995) 807.
[6] M. Salve, A. Alumaa and U. Palm, Trans. Tartu State Univ., 289 (1971) 54.
[7] J.J. Ehrlich, M.P. Pärnoja, T.E. Ehrlich and U.V. Palm, Proc. 4th Symp. on Double Layer and Adsorption on Solid Electrodes, Tartu, 1975, p. 342.
[8] B.B. Damaskin and U.V. Palm, Itogi Nauki Tekh. Elektrokhim., 14 (1977) 99.
[9] E.J. Lust, M.A. Salve and U.V. Palm, Sov. Electrochem., 23 (1987) 520.
[10] J.J. Ehrlich, T.E. Ehrlich and E.J. Lust, Proc. 7th Symp. on Double Layer and Adsorption on Solid Electrodes, Tartu, 1985, p. 385.
[11] A. Hamelin, S. Morin, J. Richer and J. Lipkowski, J. Electroanal. Chem., 272 (1989) 241.
[12] A. Hamelin, S. Morin, J. Richer and J. Lipkowski, J. Electroanal. Chem., 285 (1990) 249.
[13] A. Hamelin, S. Morin, J. Richer and J. Lipkowski, J. Electroanal. Chem., 304 (1991) 195.
[14] J. Lipkowski and L. Stolberg, in J. Lipkowski and P.N. Ross (Eds.), Molecular Adsorption at Metal Electrodes, VCH, New York, 1992.
[15] A. Iannelli, J. Merza and J. Lipkowski, J. Electroanal. Chem., 376 (1994) 49.
[16] J. Lipkowski, L. Stolberg, P.-F. Yang, B. Pettinger, S. Mirwald, F. Henglein and D.M. Kolb, Electrochim. Acta, 39 (1994) 1057.
[17] J.H. Fock, J. Schmidt-May and E.E. Koch, J. Electron Spectrosc. Relat. Phenom., 34 (1984) 225.
[18] A. Otto and B. Reihl, Surf. Sci., 178 (1986) 635.
[19] A. Weissberger, Organic Solvents: Physical Properties and Methods of Purification, Vol. 2.: John Wiley, New York, 1986.
[20] B.B. Damaskin, O.A. Petrii and V.V. Batrakov, Adsorption of Organic Compounds on Electrodes, Plenum, New York, 1971.
[21] E. Lust, K. Lust and A. Jänes, J. Electroanal. Chem., 413 (1996) 175.
[22] G.A. Tedoradze and R.A. Arakelyan, Dokl. Akad. Nauk SSSR, 156 (1964) 1170.
[23] R.P. Armstrong, W.P. Race and H.R. Thirsk, J. Electroanal. Chem., 16 (1968) 517.
[24] K. Takashaki, Electrochim. Acta, 13 (1968) 1609.
[25] E.J. Lust and U.V. Palm, Sov. Electrochem., 24 (1988) 227.
[26] E. Lust, A. Jänes, K. Lust and M. Väärtnõu, Electric double layer structure and adsorption of cyclohexanol on single crystal cadmium, antimony and bismuth electrodes, Electrochim. Acta, in press.
[27] A.P. Alumaa and U.V. Palm, Elektrokhimiya, 8 (1972) 471.
[28] D. Rolle and J.W. Schultze, J. Electroanal. Chem., 229 (1987) 141.
[29] M.L. Foresti, M. Innocenti and R. Guidelli, J. Electroanal. Chem., 376 (1994) 85.
[30] L.M. Doubova, S. Valcher and S. Trasatti, J. Electroanal. Chem., 376 (1994) 73.
[31] E. Lust, A. Jänes, K. Lust, J. Ehrlich and R. Pullerits, Adsorption of organic compounds and hydrophilicity of bismuth and antimony electrodes, in preparation.

VIII

Reprinted from the *Electrochimica Acta*, Vol. 42, No. 19,
E. Lust, A. Jänes, K. Lust, V. Sammelselg and P. Miidla,
Influence of Surface Pretreatment of Bismuth and
Cadmium Electrodes to the Electric Double Layer and
Adsorption Characteristics of Organic Compounds, pages 2861–2879,

Pergamon

Electrochimica Acta, Vol. 42, No. 19, pp. 2861–2879, 1997

Printed in Great Britain
PII: S0013-4686(97)00107-2
0013-4686/97 $17.00 + 0.00

Influence of surface pretreatment of bismuth and cadmium electrodes to the electric double layer and adsorption characteristics of organic compounds

E. Lust,[a]* A. Jänes,[a] K. Lust,[a] V. Sammelselg[b] and P. Miidla[c]

[a]Institute of Physical Chemistry, University of Tartu, 2 Jakobi Street, EE-2400 Tartu, Estonia
[b]Institute of Physics, Estonian Academy of Sciences, 142 Riia Street, EE-2400 Tartu, Estonia
[c]Institute of Applied Mathematics, University of Tartu, 2 Liivi Street, EE-2400 Tartu, Estonia

(Received 1 September 1996; in revised form 19 December 1996)

Abstract—Influence of the surface structure of electrodes on the electric double layer properties, as well as on the adsorption characteristics of various organic compounds has been investigated by cyclic voltammetry, impedance and electron microscopic methods at variously prepared Bi, Sb and Cd electrodes. The systematic trends of the influence of surface roughness and energetic inhomogeneity on the electric double layer characteristics (value of differential capacity, potential of diffuse minimum, Parsons–Zobel factor, inner layer capacity, roughness function) have been established. The dependencies of the shape of adsorption–desorption maxima of organic compounds and other adsorption parameters (values of attraction interaction, adsorption equilibrium constant, shape of adsorption isotherm) on the electrode surface structure have been investigated. The Debye–length dependent roughness function has been calculated. The approximate values of the linear parameter of homogeneous regions, which prevail at the surface of polycrystalline electrodes have been calculated using various theoretical models. The established values of linear parameters of homogeneous regions have been compared with the characteristics obtained from the electron microscopic studies. © 1997 Published by Elsevier Science Ltd

Key words: Bi, Sb, Cd, polycrystal, monocrystal, surface treatment, surface roughness, organic adsorption.

1. INTRODUCTION

The phase boundary structure and adsorption properties, as well as the kinetics of various interfacial reactions at solid surfaces significantly depend not only on the chemical composition of electrode material, but also on the morphology of the surface studied [1–5]. The atomic level STM investigations at quasi-perfect silver single crystal planes, electrolytically grown in glass or Teflon capillaries [6, 7], show that at the surface of quasi-perfect Ag(001) plane the monoatomic steps exist. At the surface of so-called real single crystal macro- and micro-electrodes (prepared either by thermal, chemical or electrochemical pretreatment, by vapor deposition techniques) a great density of crystal imperfections exists, especially emergence points of edge and screw dislocations, which lead to the appearance of mono- and multi-atomic steps and a relatively high surface corrugation [8–10]. Accordingly, no matter how careful the surface preparation of a solid electrode is, the surface of real solid electrode is always to some extent inhomogeneous. The surface roughness of solid material is a universal phenomena and it exists always and everywhere. As a consequence the electric double layer (*edl*) and adsorption parameters (for example, the values of zero charge potential, capacity of inner layer, interaction parameter in adsorption isotherm, adsorption equilibrium constant, maximum surface excess, Gibbs energy of adsorption, *etc*) obtained for polycrystalline (PC) electrodes have intermediate or apparent values [1–5, 11–12]. Some of the *edl* and electrochemical kinetic parameters, being

*Author to whom correspondence should be addressed.

extensive quantities, have to be referred to the geometric unit area of the surface, in the case of inhomogeneous solid surfaces, and have apparent values. Therefore the question of obtaining the "true" working surface area of electrodes will have a great importance.

In electrochemistry three main *in situ* methods for obtaining the surface roughness $R = S_{real}/S_{geom}$ (where S_{real} and S_{geom} are the working surfaces and geometrical areas determined, respectively) have been used [13]: (1) differential capacity measurements in the region of ideal polarizability of electrodes, applied in Parsons–Zobel [14], Valette–Hamelin [15] and other methods [16]; (2) mass transfer process under diffusion control with assumption of homogeneous current distribution [13, 17]; (3) adsorption of radio-active organic compounds (radio tracer adsorption technique) or reactant monolayer (H_2, O_2 or metals) at electrode surface and following electrochemical reaction [13, 18, 19]. According to [1–5, 13–19], the value of R depends on the method used, and therefore more systematic investigations are indispensable.

In many cases the experimental data cannot be rationalized only in terms of surface roughness and energetic inhomogeneity, as the roughness can be the reason of new characteristic lengths, which may compete with other typical lengths, inducing the rise of new functional dependences for charge carrier concentration and potential distribution. The determination of the solvent and ionic concentration (charge carriers) distribution, as well as the electron density profile at metal–electrolyte, metal–semiconductor–electrolyte and semiconductor–electrolyte phase boundaries is an important step towards a complete description of the interfacial phenomena.

Up to now the physical content of the modern theories on the PC structure of solid electrode surface involves its modeling description as a combination of different monocrystalline faces [15, 20–27]. Thus, the differential capacity of a PC electrode is obtained by the superposition of the corresponding $C(E)$-curves for individual faces exposed at the surface of PC electrode:

$$C_{PC}^{app}(E) = R\Sigma X_i C_i(E). \tag{1}$$

where $C_i(E)$ refer to unit area of the true surface and C_{PC}^{app} refer to unit area of the apparent surface of the electrode. As shown in [1–4, 15, 20–28], the coefficient R can characterize the geometric roughness, with which the size of the surface area and differential capacity have been measured. But for solid electrodes, R also reflects the energetic inhomogeneity of the surface caused by the fact that crystallographically different grains (single crystal planes), grain boundaries and other crystallographic defects are exposed at the surfaces of solid polycrystalline electrodes, as well as at the surface of real single crystal planes.

It must be noted that in the general case it is useful to distinguish the microscopic and macroscopic values of roughness factor R and the share of planes X at a polycrystalline (PC) electrode surface [25]. The microscopic value of R would characterize the "true" geometrical roughness and the share of ideally flat single crystal planes at the surface of a PC electrode $R = \Sigma_i X_i f_i$, where f_i and X_i are the roughness and share of the ideally smooth single crystal plane i, respectively. If we at the first approximation assume that the PC electrode surface consists only of the homogeneous regions, of which the *edl* characteristics are similar to the real monocrystalline planes (not ideally smooth), then the values of macroscopic roughness factor $f_{macr}^{PC} = \Sigma_i X_i$. The methods for obtaining the R and X values have been discussed in [25].

As a first approximation, the *edl* models for PC electrodes may be classified in two groups [15, 21–26]. The first group considers the PC electrode surface as one consisting only of relatively large monocrystalline regions with linear parameter $y^* \gg 10$ nm (y^*, so-called characteristic length), which corresponds to macropolycrystallinity. Within these regions both the compact and the diffuse layers at different homogeneous areas can be viewed as independent ones, and accordingly

$$C_{PC}^{app} = R\Sigma_i X_i C_{H,i} C_{D,i}/(C_{H,i} + C_{D,i}), \tag{2}$$

where $C_{H,i}$ and $C_{D,i}$ are the inner layer and diffuse layer capacities for the plane i, respectively. Therefore this is the so-called model of independent diffuse layers (IDL). In terms of the second group of models, the polycrystalline surface consists only of very small crystallites with linear parameter y^*, which sizes are comparable with the *edl* parameters in moderate electrolyte concentrations [22–25]. In the case of such electrodes, compact layers at different monocrystalline areas are considered to be independent, but the diffuse layer is common for the entire surface of a PC electrode and depends on the total charge density $\bar{\sigma}_{PC} = R\Sigma_i X_i \sigma_i$, averaged over the PC electrode surface, and capacitance C_{PC}^{app} can be obtained by the equation:

$$C_{PC}^{app} = \frac{C_D(\bar{\sigma}) R\Sigma_i X_i C_{H,i}}{C_D(\bar{\sigma}) + R\Sigma X_i C_{H,i}}. \tag{3}$$

This model is known as the model of the common diffuse layer (CDL) [22]. As shown in [23, 24], both models can describe only some limiting cases and the exposition for the total capacity of the PC electrode (equivalent circuit) investigated depends on the relationship among the three lengths:

(1) the characteristic size of the individual planes at a PC electrode surface y^*;

(2) the effective screening length in the bulk of the diffuse layer near the face i ($l_{D,i}(\sigma_i)$)

$$l_{D,i} \equiv l_D(\sigma_i) = l_D/[1 + (\sigma_i/\sigma^*)^2]^{1/2}, \tag{4}$$

where l_D is the Debye screening length and $\sigma^* = \varepsilon RT/2\pi Fl_D$;

(3) ε/l_{H_i}, where ε is the bulk dielectric constant of the solvent and the length $l_{H_i} = 1/4\pi C_{H_i}$ is determined by the capacity of the compact layer of the face i.

According to the theoretical analysis [23, 24] the CDL model is valid for PC electrodes with very small grains ($y^* < 5 \div 10$ nm) first of all with a moderate difference of $(E_{\sigma=0})_i$ for the faces ($\Delta E_{\sigma=0} = 0.1 \div 0.15$ V) and for very dilute electrolyte solutions ($c \leq 0.01$ M) near the point of total zero charge, *ie* if the value of y^* is much less than two of the three lengths: $y^* \ll \varepsilon/l_{H1} \sim \varepsilon/l_{H2}$, l_{D1}, l_{D2}. For other cases the model of IDL would be valid.

According to the results of electron diffraction studies [27–29], the surface of solid bismuth drop electrode with the remelted surface $(Bi_{DE})^R$ consists of the comparatively large homogeneous surface regions with Miller indexes (001), (111) and (101). The analysis shows that 70–90% of the whole surface of $(Bi_{DE})^R$ is covered by the segments, of which the linear parameter $y^* > 10$ nm. But between the large homogeneous areas there are aggregates, which consist of many very small crystallites, of which the size is probably smaller than the effective Debye screening lengths. Therefore, the structure of the *edl* at such segments of $(Bi_{DE})^R$ is described by the CDL model and the total capacity of $(Bi_{DE})^R$ at $E = \text{const.}$ can be expressed by the relations

$$C_{PC}^{app} = R \sum_{i=1}^{n} \frac{X_i C_{H_i} C_{D_i}}{C_{H_i} + C_{D_i}} + X_{m+1} \left[\frac{C_D(\bar{\sigma}) R \sum_{i=n+1}^{m} X_i C_{H_i}}{C_{D_i}(\bar{\sigma}) + R \sum_{i=n+1}^{m} X_i C_{H_i}} \right], \quad (5)$$

$$X_{m+1} + \sum_{i=1}^{n} X_i = 1, \qquad \sum_{i=n+1}^{m} X_i = 1, \qquad m > n.$$

The results of computer simulation [27] of many experimental $C_{PC}^{exp}(E)$-curves for various $(Bi_{DE})^R$ show that the standard deviation $\bar{\Delta}(\Delta C)$ of $C_{PC}^{exp}(E)$-curves from $C_{PC}^{app}(E)$-curves is smaller, if we use equation (5) instead of (2) or (3). According to the computer simulation of C(E)-curves, it must be noted that 10–30% of the whole surface of $(Bi_{DE})^R$ is covered with small crystallites ($y^* < 10$ nm). The experimental investigations and computer simulation of experimental $C(E)$-curves for the wedge-shape two-plane model PC electrode (*wme*) show that the share of small crystallites at the surface of *wme* is not over 5–10% [26, 28]. The influence of the base boundaries between the individual monocrystalline regions at a PC electrode surface on the *edl* capacity has been theoretically discussed in [24].

A new approach to the double layer capacity properties on rough electrodes was given in the papers of A. A. Kornyshev, M. Urbakh and L. I. Daikhin [30, 31]. In this theory the conception of Debye-length dependent roughness factor, *ie* the roughness function which determines the deviation of capacitance from the Gouy–Chapman result for a flat interface, has been worked out. It was shown that an analytical expression for the roughness is available in the case of weak Euclidean roughness and two parameters—mean square height and the correlation length are important in this theory. The effect of anisotropy of the roughness profile has been investigated in [31]. This method is based on the double layer capacity measurements in the solutions where the Debye-length is varied by the change of electrolyte concentration, as well as by variation of surface charge density of the electrode. It is evident that the new method [30, 31] for studying surface roughness might be most reliably tested by electron microscopy in *uhv*, *in situ* STM or some optical methods, based on the recent advances in surface science. However, the classical impedance (capacity) measurements remain one of the major tools in studying the interfacial properties. Indeed, the capacity and related characteristics are very sensitive to the specific properties on the contact region when the electric potential changes in a distance comparable with *edl* thickness. For typical ionic concentrations, the depth of the field penetration into the electrolyte solution at the potential of diffuse minimum of $C(E)$-curves is comparable to the dimensions of the interfacial region. Thus, the electrical properties of the electrochemical interface (the capacitance in the equilibrium case) are very sensitive to its structure. Therefore the adequate interpretation of impedance data is one of the central points in electrochemistry.

This article concentrates on the comprehensive experimental studies of the influence of the surface structure (pretreatment) of Bi, Sb and Cd electrodes on the electric double layer (*edl*) parameters in aqueous and nonaqueous surface inactive electrolyte solutions and of the influence of the crystallographic effects on the adsorption characteristics of organic molecules.

2. EXPERIMENTAL

The electrodes for single crystal experiments were bismuth, antimony and cadmium single crystals, grown in the Institute of Problems of Microelectronics Technology and Superpure Materials (Russian Academy of Sciences) by a modified Czochralski (Vertical Bridgman) method (Bi) [32] or by the Horizontal Bridgman method (Sb, Cd) [32, 33]. The crystal growth, the characterisation techniques and other experimental problems have already been discussed in [21, 22, 32–34]. The chemicals and solvents—water, methanol (MeOH), ethanol (EtOH)

and acetonitril (AN) were purified according to [4, 34, 35].

The *edl* differential admittance was measured in the range from 60 to 21,000 Hz by using an impedance bridge P-568. The cyclic voltammetric curves were recorded by the polarographic analyzer PA-2. Chronocoulometry was performed with a system characterized in [4, 34]. Pulses were recorded from variable E (−0.95 to −1.70 V) as the starting potential, at which the electrode was held for 5–60 s before each step to $E_T = -1.7$ V. The charge–time curves with a time scale in a 100 ms range were extrapolated to $t = 0$ as described elsewhere [36, 37].

For additional characterization of the working surface of electrodes, an electron microscopic analysis using a JEOL-JSM-35CF at the SEI regime was carried out (40,000 × max).

According to Fig. 1(a), the surface of electrochemically polished (EP) single crystal plane electrodes is practically smooth within the range of sensitivity of electron microscopy. The same conclusion is valid in the case of electrochemically polished non-singular (stepped at the atomic level) single crystal planes of Bi(2$\bar{1}\bar{1}$), Sb(2$\bar{1}\bar{1}$), Cd(11$\bar{2}$1) and Cd(1$\bar{1}$01) planes. The surfaces of these electrodes consist of small terraces with linear parameter $y^* \sim 1$–10 nm and from atomic steps (1–3 atomic layers). The surface of the nonsingular plane is a typical example of a weakly disorbed solid surface. In some experiments the planes Bi(111)^c, Sb(111)^c and Cd(0001)^c cleaved at the temperature of liquid nitrogen were investigated. According to the data of Fig. 1(b), on the cut surface of Bi(111)^c and Sb(111)^c there are thinly scattered break steps, the distance between which is very large. In the case of Cd(0001)^c, the distance between these break steps is somewhat smaller. In some experiments the *edl* properties at electrochemically etched surfaces of Bi(111)^{ECE}, Bi(001)^{ECE}, Cd(0001)^{ECE} and Sb(111)^{ECE} were investigated. The electrochemical etching of Bi(111)^{ECE} and Sb(111)^{ECE} was carried out in KJ–HCl aqueous solution at anodic currents $i > 1.5$ A cm^{-2}. The analysis of many experiments shows that for the etching times $\tau < 2$ minutes, the *edl* and adsorption parameters depend on this time, but at $\tau > 2$ minutes, the influence of the time of etching to the *edl* and adsorption characteristics is very weak. The main aim of the electrochemical etching was to produce a weakly disordered surface, *ie* to prepare the polycrystalline surface with self-similar fractals at the electrode surface. According to the electron microscopic studies, there are surface pittings (triangles) with linear parameter $x \sim 1$ μm at the surface of Bi(111)^{ECE}. Between the pittings the surfaces of Bi(111)^{ECE} and Sb(111)^{ECE} seem to be practically smooth. The statistical analysis of many electrodes, prepared by the electrochemical etching at high anodic currents, shows that 3–5% of the whole surface is covered by the pittings. To increase the concentration of defects at the electrode surface, the self-made massive single crystal Bi and Sb electrodes, grown by the Horizontal Bridgman method in Tartu, have been used. At the surface of electrochemically treated self-made Bi(111)^{ECE} and Sb(111)^{ECE} electrodes there are 5–25% of surface defects (Fig. 1(c)).

In some experiments the *edl* and adsorption characteristics of organic compounds at chemically etched in the mixture $HNO_3 + NH_4NO_3 + H_2O$ Bi(111)^{CE}, Sb(111)^{CE}, Bi(001)^{CE}, Cd(0001)^{CE}, Cd(10$\bar{1}$0)^{CE} and Cd(11$\bar{2}$0)^{CE} have been investigated. According to Fig. 1(d), additionally to the surface pittings (triangles) with linear parameter $x \sim 1$ μm, a great number of various surface defects at the surface of chemically treated Bi, Sb and Cd (self-made massive Bi and Sb monocrystals) electrodes exists. In some experiments, the mechanically polished (with Al_2O_3) and thereafter chemically etched PC Bi $(Bi_{DE})^{MP\,CE}$ electrodes have been investigated (Fig. 1(e)). At the first approximation, the surface of a PC electrode prepared in such a way can be described as a uniformly inhomogeneous surface.

The experimental *edl* and adsorption characteristics for variously prepared electrodes have been compared with the data for solid bismuth drop electrodes with remelted surface $(Bi_{DE})^R$ [2], as well as with the data for wedge shape two-plane model polycrystalline PC-Bi electrodes (*wme*) with conceded and therefore to some extent known crystallographic and energetic inhomogeneity of surface [26–28]. In some experiments the solid Bi drop electrodes without any additional remelting of the surface $(Bi_{DE})^{WR}$ have been used. According to the electron microscopic studies, at the surface of $(Bi_{DE})^{WR}$, the homogeneous areas are smaller and the concentration of surface defects is noticeably higher than at $(Bi_{DE})^R$.

3. RESULTS AND DISCUSSION

3.1. Cyclic voltammograms (CVs)

The CVs for different single crystal Bi, Sb and Cd electrodes were recorded in neutral aqueous NaF, $LiClO_4$ and acidified $LiClO_4$ solutions and non-aqueous $LiClO_4$ solutions. In the NaF aqueous solutions the Bi single crystal electrodes are ideally polarizable in the range of potentials -1.60 V $< E < -0.50$ V [4, 38, 39], and the single crystal Sb electrodes are ideally polarizable in the range of -1.45 V $< E < -0.45$ V [39]. All potential values presented in this work are measured in the scale of saturated calomel electrode (*sce*). The Cd planes are ideally polarizable in the range of -1.70 V $< E < -0.90$ V [38]. In the aqueous $LiClO_4$ solutions the anodic limit of ideal polarizability is shifted ~200 mV to the positive direction. In the acetonitrilic and methanolic $LiClO_4$ solutions the single crystal Bi electrodes are ideally polarizable in the range of -1.80 V $< E < -0.25$ V [34, 38, 39] and in the ethanolic and isopropanolic solutions in the limits -1.60 V $< E < -0.05$ V. The potential range of ideal polarizability of cut and electrochemi-

cally etched electrodes is practically the same as for the electrochemically polished electrodes. The positive limit of the ideal polarizability of the chemically etched Bi, Sb and Cd electrodes is shifted ~ 50 mV towards the negative direction and the negative limit is shifted $\sim 50 \div 75$ mV toward the less negative

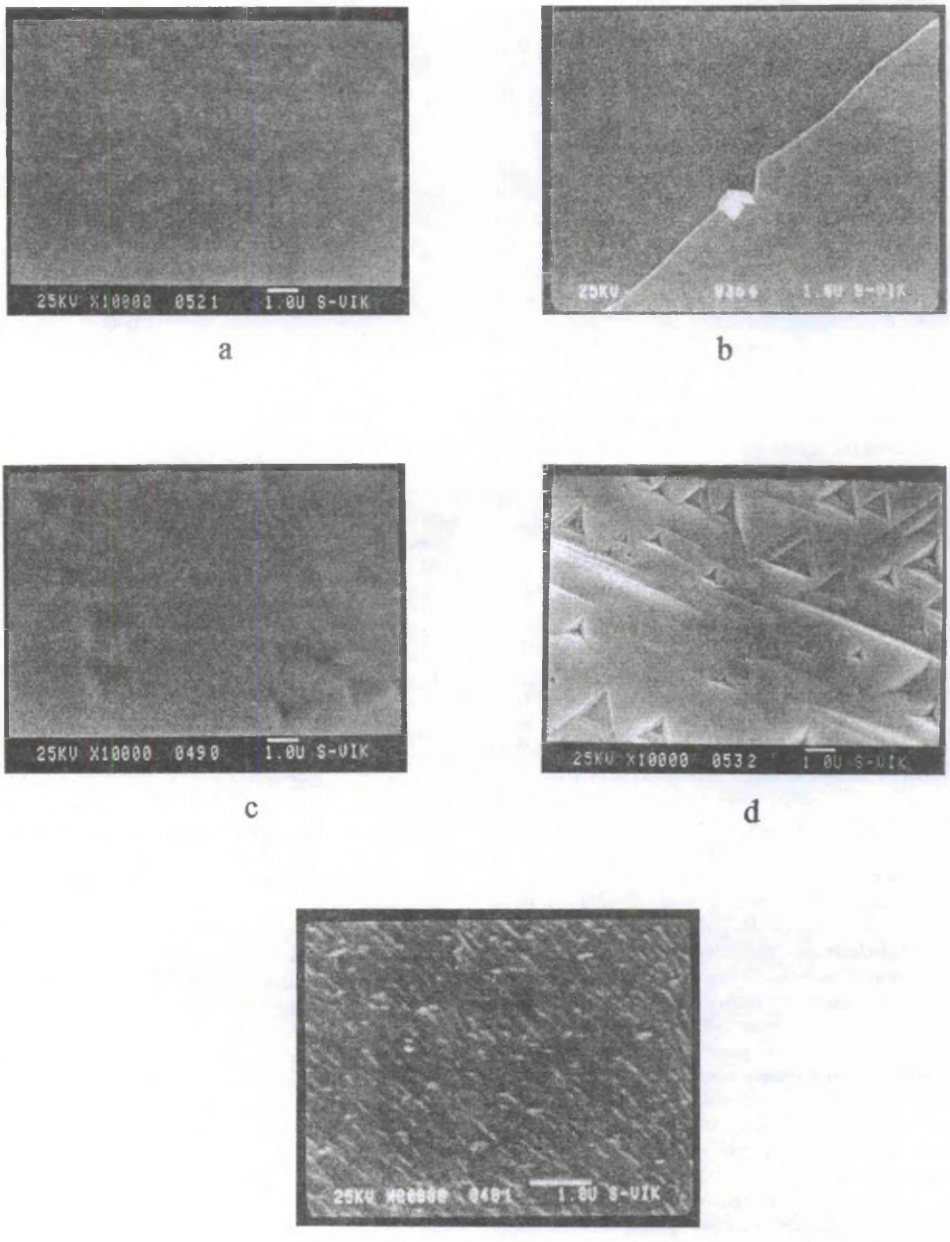

Fig. 1. Photomicrographs of electrode surfaces obtained using JEOL JSM-35CF electronmicroscope ($\times$ 10,000, $\times$ 20,000): (a) electrochemically polished $Bi(111)^{EP}$; (b) cleaved at temperature of liquid nitrogen $Bi(111)^{C}$; (c) electrochemically etched at high anodic currents ($i > 1.5$ A cm^{-2}) $Bi(111)^{ECE}$; (d) chemically etched in solution $HNO_3 + NH_4NO_3 + H_2O$ $Bi(111)^{CE}$ ($\tau_{etching} > 2$ min); (e) mechanically polished with Al_2O_3 and thereafter chemically etched $(Bi_{PC})^{MP\,CE}$.

potentials. The values of current density at E = const. are 20–30% higher than for EP Sb, Bi and Cd electrodes. This effect is probably caused by the increase of the working surface area of treated electrodes, as well as by the more active surface state of modified electrodes. The continuous cycling of the potential in these limits of ideal polarizability does not evoke noticeable changes in the shape of CVs and capacity–potential curves and does not affect the limits of ideal polarizability of electrochemically polished Bi, Sb and Cd electrodes. The continuous cycling of Bi, Sb and Cd electrodes on a larger range of E causes noticeable transformations in the shape of CVs, differential capacity curves (values of zero charge potential $E_{\sigma=0}$ and values of differential capacity at $E_{\sigma=0}$), in the limits of ideal polarizability and in the values of adsorption parameters of Sb, Bi and Cd electrodes. According to the impedance and cyclic voltammetry measurements, the tendency of surface reconstruction increases in order of electrodes $(Bi_{DE})^R \leq Bi^{EP} < (Bi_{DE})^{WR} < Bi^{ECE} < Bi^{CE} < Cd^{EP} < Cd^{ECE}$. Accordingly, the charge-induced (*ie* induced by the oxidation and reduction of the surface) surface reconstruction is possible, but these problems have not been an object of this work and will be discussed in the next paper after obtaining STM and AFM data bases.

3.2. Precision of experimental capacity data

For the accurate determination of the precision of the experimental data the statistical treatment of the data was carried out. The geometrical surface area was established by using optical methods to a precision of $\pm 2\%$. The mean values of differential capacity $\bar{C}$, charge density $\bar{\sigma}$, Helmholtz layer capacity $\bar{C}_H$ and their standard deviations $S_{\bar{C}}$, standard error of the mean $S_{\bar{C}}(C_d)$ and the coefficient of variation V at fixed E = const. (or at σ = const.) and at fixed c = const. were calculated using a HP-85 computer and General Statistics Pac [4, 26–28].

The statistical analysis shows [4, 26–28] that in the case of electrochemically polished single crystal Bi, Sb and Cd electrodes, the value of C, σ and C_H can be determined sufficiently exactly by the measuring procedure used (the relative error of the parameters determined is not over 2–5%). For ECE electrodes the relative error of parameters is not more than 4–8% and for CE electrodes 5–12%. For EP and cut Bi(111), the measuring precision of the p.z.c. ($E_{q=0}$) is ± 5 mV, and ± 15 mV for ECE and ± 20 mV for CE electrodes. For the other EP single crystal electrodes the measuring exactness of $E_{\sigma=0}$ is 10 mV.

As follows from the experimental results, in moderate surface inactive electrolyte solutions ($c_{NaF} \geq 0.03$ M), the experimental values of C for EP Sb, Cd and Bi can be established better than $\pm 3\%$ for the whole region of σ. But the precision of experimental values of C decreases when the concentration of the solution decreases, and for the dilute solutions ($c_{NaF} < 0.01$ M) the maximum values

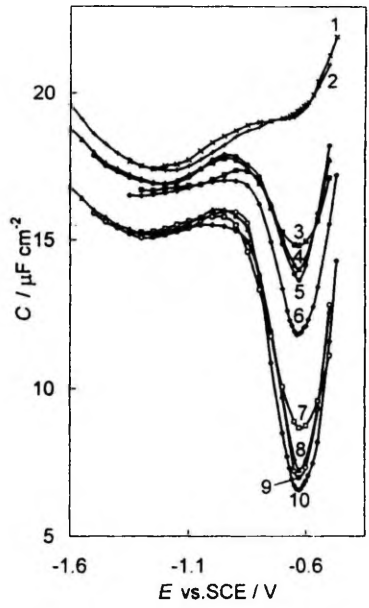

Fig. 2. $C(E)$-curves (ν = 210 Hz) for $(Bi_{DE})^R$ (1, 4, 8), $Bi(111)^{EP}$ (2, 6, 10), $(Bi_{PC})^{MP\,CE}$ (3, 7) and $Bi(111)^{CE}$ (5, 9) in aqueous solution of NaF, M: 1, 2: 0.1; 3–6: 0.01; 7–10: 0.002.

of error (5–8%) can be established in the region of σ where the derivation dC/dE is large. For ECE and CE electrodes, the error in the region of high dC/dE is very big ($\sim 20\%$). In the region of surface charge densities $\sigma < 0.5\,\mu C\ cm^{-2}$, the error of C for EP electrodes (2–4%) is only somewhat higher than for more concentrated solutions. For ECE and EC electrodes the error of C is ~ 5–8% Comparison of the statistically treated $\bar{C}(E)$- and $\bar{C}(\sigma)$-curves shows that the $\bar{C}(E)$-curves are more erratic than the $\bar{C}(\sigma)$-curves calculated at σ = const. The same conclusions have been made in review articles [2, 41] analyzing the capacity data for Hg and other liquid electrodes, as well as for various PC electrodes. In the case of PC electrodes investigated in this work the main reason for this effect is the variation of E_{min} (max ± 20 mV) from one experiment to another.

The experimental values of $\bar{C}$ in the region of the diffuse minimum are constantly higher than those calculated by the Gouy–Chapman–Stern–Grahame (GCSG) theory [15–18] for ideally smooth electrodes:

$$1/C = 1/C_D + 1/C_H, \quad ie \quad C_H = 1/(1/C - 1/C_D), \qquad (6)$$

where C_D and C_H are the values of the differential capacities of the diffuse part and of the inner part of the double layer.

Comparison of $C(E)$-curves for various electrodes at E = const. and c_{el} = const. shows that C increases in order of electrodes $Bi(111)^{EP} \leq Bi(111)^{C} < Bi(111)^{ECE} < Bi(111)^{CE} <$

$(Bi_{PC})^{MP}$ (Fig. 2). The same conclusion is valid in the case of differently prepared Bi(001), Sb(111) and Cd electrodes (Fig. 3). According to the experimental results, this deviation depends on the concentration of surface inactive electrolyte and the value of ΔC increases with dilution of electrolyte solution. This effect is in accordance with the calculations by the IDL model.

The potential of the minimum of $C(E)$-curves depends on the surface pretreatment and E_{min} moves to the direction of less negative potentials in the order $Bi(111)^{EP} > Bi(111)^{C} > (Bi_{DE})^{R} > (Bi_{DE})^{WR} > Bi(111)^{ECE} > Bi(111)^{CE} > (Bi_{PC})^{MP} > (Bi_{PC})^{MP\,CE}$ (Table 1). The same order of E_{min} values is valid for modified Sb(111) electrodes. Accordingly, with increasing of the concentration of surface defects (other planes than Bi(111) or Sb(111) at the modified Bi(111) and Sb(111) surface), having less negative values of $E_{q=0}$ than Bi(111) or Sb(111) plane, E_{min} moves to the direction of less negative E. As shown in Fig. 2, in the case of modified $Bi(111)^{EPE}$ and $Bi(111)^{CE}$, the value of E_{min} moves to the direction of less negative potential with decrease of concentration of electrolyte. Such dependence is characteristic for the electrodes with polycrystalline surface structure and can be explained by the increase of the adsorption activity of anions at defect surface regions [1–5]. But the main reason of this effect is the fact that $C(E)$-curves for single crystal plane electrodes are non-symmetrical with respect to potential of capacitance minimum [2, 4, 20–29, 41]. The derivative dC/dE is always higher in the region of positive surface charge densities ($\sigma > 0$) than in the region of negative surface charge densities ($\sigma < 0$). Therefore, the value of E_{min} does not correspond to the condition of $\bar{\sigma} = 0$ ($\bar{\sigma} = R\Sigma_i X_i \sigma_i$) for polycrystalline electrode [15, 20–23].

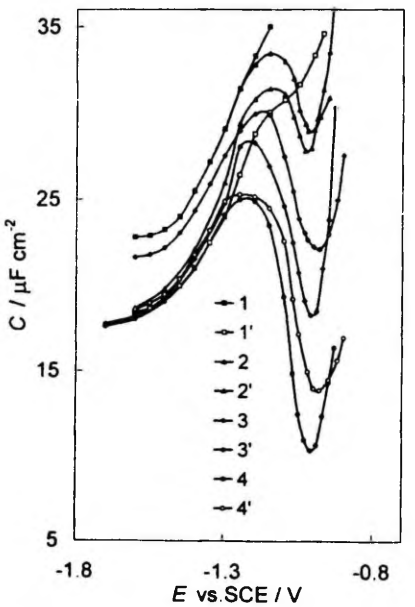

Fig. 3. $C(E)$-curves (ν = 210 Hz) for $Cd(11\bar{2}1)^{EP}$ (1–4) and for $Cd(11\bar{2}1)^{ECE}$ (1'–4'') in aqueous solution of NaF. M: 1, 1': 0.1; 2: 0.05; 2': 0.03; 3, 3': 0.01 and 4, 4': 0.002.

In the case of monocrystalline Sb and Bi electrodes, having less negative values of $E_{\sigma=0}$ than Bi(111) or Sb(111), the surface etching shifts the values of E_{min} to the negative direction. For example, the negative values of E_{min} for Sb(001), Bi(001) and Cd(0001) electrodes increase in the order $(Sb^{DE})^{R} < Sb(001)^{ECE} < Sb(001)^{CE} < Bi(001)^{C} < Bi(001)^{EP}$, *ie* towards increasing the inhomogeneity of the electrode surface.

These results are in very good accordance with the experimental data for $(Bi_{PC})^{MP\,CE}$ and *wme* and with results of simulation by the IDL model [20–28]. As found, with increasing the share of plane having more negative values of $E_{\sigma=0}$ at the surface of $(Bi_{PC})^{MP}$ or *wme*, the value of E_{min} shifts toward the more negative potentials [26–28].

3.3. Electric double layer and fractal structure of electrode surface

The *edl* differential admittance was measured in the *ac* frequency (ν) interval from 60 to 21,000 Hz. For the electrochemically polished single crystal Bi, Sb and Cd, as well as for cut Bi(111) and Sb(111) electrodes, a very slight variation of capacity (3–6%) as a function of ν was observed [4, 34]. For $(Bi_{DE})^{R}$ the dependence of C from ν is somewhat lower (1–3%) [21, 25] than for $Bi(111)^{EP}$ or $Bi(111)^{C}$. For $(Bi_{DE})^{WR}$ this dependence is in the same order as for electrochemically etched single crystal Bi, Sb and Cd electrodes (5–8%). A more pronounced dependence of C on ν was found for chemically treated (5–10%) and mechanically polished (10–25%) electrodes. According to the experimental results the "true" roughness factor values at E = const. ($f_\nu = C_{210\,Hz}/C_{2100\,Hz}$), have been calculated and presented in Table 1. According to the data of Table 1, the values of f_ν are practically independent of the solvent properties and, in the region of ideal polarizability, the values of f_ν for different electrodes increase in the order $(Bi_{DE})^{R} < Bi(111)^{EP} < Bi(111)^{C} < Bi(001)^{EP} \leq Bi(01\bar{1})^{EP} < (Bi_{DE})^{WR} < Bi(2\bar{1}\bar{1})^{EP} < Bi(111)^{ECE} < Bi(001)^{ECE} < Bi(111)^{CE} < Bi(111)^{MP} < (Bi_{PC})^{MP}$. The same order of the influence of the surface pretreatment to f_ν values is valid for Sb and Cd electrodes. The very low values of f_ν for $(Bi_{DE})^{R}$ and Bi, Sb and Cd single crystal planes indicate that these surfaces are smooth and the values of C are free from components of pseudocapacity.

The phenomenological description of the frequency dependence of impedance Z_{CPE} (CPE = constant phase element) is given as [42, 43]

$$Z_{CPE} \approx (i\omega)^{-\alpha} \qquad (0 < \alpha < 1). \tag{7}$$

Table 1.
Electric double layer characteristics for Sb, Bi and Cd electrodes

Solvent	Electrode	$-E_{min}$ (*sce*) (V)	$f_v = \frac{C_{210\,Hz}}{C_{2100\,Hz}}$	$f_{P,Z}$	D	$C_H^{E_{min}}$ (μF cm^{-2})
H_2O	$Bi(111)^{EP}$	0.655	1.04	1.04	2.03	25.6
	$Bi(111)^{C}$	0.650	1.06	1.06	2.04	28.9
	$Bi(111)^{ECE}$	0.630	1.09	1.08	2.05	29.1
	$Bi(111)^{CE}$	0.620	1.11	1.10	2.07	33.8
	$Bi(111)^{MPCE}$	0.625	1.15	1.20	2.11	32.0
	$(Bi_{DE})^{R}$	0.625	1.02	1.01	2.01	25.8
	$(Bi_{DE})^{WR}$	0.620	1.08	1.11	2.05	25.5
	$Bi(001)^{EP}$	0.595	1.07	1.06	2.05	28.4
	$Bi(001)^{ECE}$	0.610	1.16	1.13	2.07	29.1
	$Bi(001)^{CE}$	0.615	1.20	1.15	2.08	28.8
	$Cd(0001)^{EP}$	0.95	1.04	1.09	2.05	38.0
	$Cd(0001)^{C}$	0.97	1.06	1.11	2.07	37.0
	$Cd(0001)^{ECE}$	0.97	1.09	1.20	2.06	37.1
	$Cd(0001)^{CE}$	1.00	1.11	1.25	2.10	35.0
	$Cd(11\bar{2}0)^{EP}$	1.02	1.06	1.14	2.06	48.6
	$Cd(11\bar{2}0)^{ECE}$	0.99	1.08	1.28	2.09	59.6
	$Sb(111)^{EP}$	0.46	1.06	1.06	2.04	23.6
	$Sb(111)^{C}$	0.45	1.08	1.09	2.06	38.9
MeOH	$Bi(111)^{EP}$	0.52	1.03	1.05	2.03	19.8
	$Bi(001)^{EP}$	0.45	1.05	1.07	2.04	23.0
	$(Bi_{DE})^{R}$	0.49	1.01	1.03	2.01	22.2
AN	$Bi(111)^{EP}$	0.50	1.05	1.06	2.04	14.8
	$Bi(001)^{EP}$	0.42	1.02	0.98	2.01	17.4
	$(Bi_{DE})^{R}$	0.47	1.01	1.15	—	15.0

D, fractal dimension, dimensionless parameter.
^{EP}, electropolished surface.
^{C}, cleaved at the temperature of liquid nitrogen surface.
^{ECE}, electrochemically etched surface.
^{CE}, chemically etched surface.
^{MPCE}, mechanically polished and thereafter chemically etched surface.
$(Bi_{DE})^{R}$, remelted solid drop Bi electrode.
$(Bi_{DE})^{WR}$, solid drop Bi electrode without additional remelting of surface.

The CPE angle φ is related to α as:

$$\varphi = \frac{\pi}{2}(1 - \alpha). \tag{8}$$

The value $\alpha = 1$ corresponds to normal capacitive behaviour. Recently some new ideas have been put forward to explain the so-called constant phase element CPE [42, 43]. The main position is that the deviations from the ideal behaviour are caused by surface roughness of a special kind, today commonly denoted by the term "fractal" [42, 43]. The so-called fractal dimension D introduced by Mandelbrot [43] is a formal quantity which attains a value between 2 and 3 for a fractal structure and reduces to 2 when the surface is flat. D is related to α by

$$\alpha = 1/(D - 1). \tag{9}$$

The established values of D, presented in Table 1, show that the surfaces of $(Bi_{DE})^{R}$ and electrochemically polished Bi, Sb and Cd single crystal electrodes are practically smooth. The slightly higher values of D for the cut electrodes indicate that the surface of electrodes, cleaved at the temperature of liquid nitrogen, is to some extent geometrically and energetically inhomogeneous. Somewhat higher values of D have been established for ECE electrodes. The surfaces of ECE Bi, Sb and Cd electrodes are relatively flat in comparison with the surfaces of chemically treated and mechanically polished electrodes.

3.4. Parsons–Zobel plots

The Parsons–Zobel $[C_{PC}^{-1}(C_D^{-1})]$ plots [14] at $\nu = 210$ Hz, represented in Figs 4–6 for the various electrodes studied, were calculated at the potential of diffuse minimum $(E_{min})_{PC}$ of differential capacity curves, and also at various surface charge densities $\tilde{\sigma} = \text{const.}$, from the experimental $C_{PC}(E)$- or $C_{PC}(\tilde{\sigma})$-curves. The values of C_d were calculated according to Gouy–Chapman theory under the assumption that for $(E_{min})_{PC}$ the overall surface charge density $\tilde{\sigma}_{PC} = 0$. At the first approximation, according to the data of Figs 4–6 the Parsons–Zobel

plots for EP electrodes can be considered linear in the concentration range of electrolyte c_{el} from 0.01 M to 0.1 M. But for the ECE and CE Cd, Bi and Sb electrodes, the Parsons–Zobel plots can be considered linear in the very narrow concentration range of solution. The values of the fitting (roughness) coefficient, $f_{P\text{-}Z}$, estimated from the inverse slope of nearly linear segments of these dependencies, reflecting the geometrical roughness of surface, the exactness of the determination of the surface area and electrolyte concentration c_{el} [34, 38–40, 44–46] as well as the crystallographic heterogeneity ($\Delta E_{\sigma=0}$, $\Delta C_H^{\sigma=0}$), are given in Table 1. Meanwhile, in the absence of these two mentioned components of the errors, the fitting coefficient $f_{P\text{-}Z}$ would correspond to RF, where F represents the crystallographic heterogeneity and R the geometrical roughness of the surface, respectively. As shown theoretically in [20–23] and proposed from the experiments for *wme* [26–28], the coefficient F depends on the differences of the zero charge potential $\Delta E_{\sigma=0}$ of the individual planes and on c_{el}, *ie* on the differences of differential capacity ΔC for individual planes at E = const. The values of F increase if the $\Delta E_{\sigma=0}$ and $\Delta C_{E=\text{const}}$ increase and c_{el} decreases. Nonlinearity of the Parsons–Zobel plots is also an indication that the Grahame model is not valid in the case of *wme* and for other PC electrodes investigated, since the values of charge density at different homogeneous regions

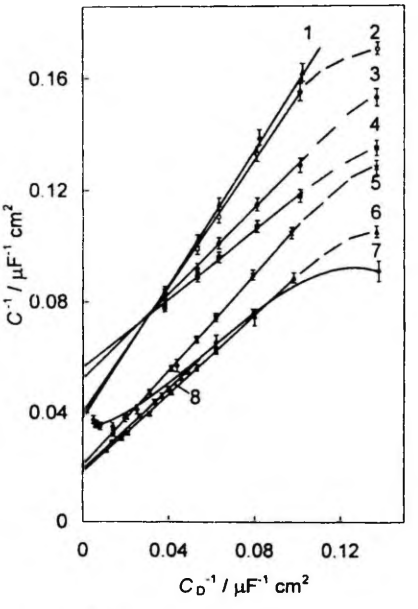

Fig. 4. Parsons–Zobel plots (ν = 210 Hz) at σ = 0 (1–7) and at $\sigma = -1$ μC cm^{-2} (8) for $(Bi_{DE})^R$. 1: WME-Bi[0.4(01$\bar{1}$) + 0.6($\bar{1}$0$\bar{1}$)]. 2: WME-Bi[0.8(01$\bar{1}$) + 0.2(111)]. 3: *wme*-Bi[0.5(01$\bar{1}$) + 0.5(111)]. 4: Bi(111)^{EP}. 5, Bi(111)^{ECE}. 6, 8 and Bi(111)^{CE}. 7.

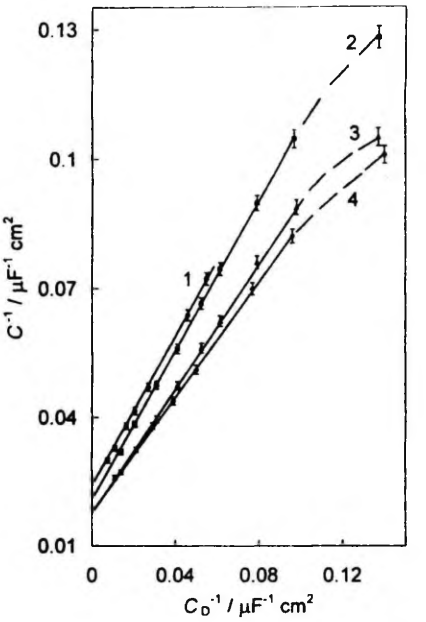

Fig. 5. Parsons–Zobel plots (ν = 210 Hz) for Cd(0001)^{EP}, (1, 2); Cd(0001)^{ECE}, 3 and Cd(11$\bar{2}$1)^{ECE}, 4 at σ = 0 (2–4) and at $\sigma = -1$ μC cm^{-2}, 1.

depends on $E_{\sigma=0}$ of plane, *ie* the charge density is distributed in an non-equal manner over the macropolycrystalline surface. Therefore, for PC electrodes with $\gamma^* > 10$ nm, the one-dimensional Gouy–Chapman model is not applicable [20–28].

If the model of IDL is valid [15, 20, 21], the partial charge densities σ_i of the faces found for *wme*[0.5 Bi(001) + 0.5 Bi(111)] at $(E_{min})_{PC}$ differ from zero, and for 0.01 M KF solutions have values of $\sigma_{(001)} = -0.15$ and $\sigma_{(111)} = +0.39$ μC cm^{-2}. The calculated values at $(E_{min})_{PC}$ are found to be equal to $(C_D)_{(111)} = 24.11$ and $(C_D)_{(001)} = 23.09$ μF cm^{-2}, while calculated from the Gouy–Chapman model for $\bar{\sigma}_{PC} = 0$ gives $C_D(\bar{\sigma}) = 22.90$ μF cm^{-2}. For the (111) face in 0.01 M KF the dispersion of $\Delta C_D = C_{d(111)} - C_D(\bar{\sigma})$ is ~5% of $C_D(\bar{\sigma})$, and increases with the step of dilution (in 0.001 M KF $\Delta C_D / C_D(\bar{\sigma}) \approx 20\%$). The difference $\Delta C_H = (C_H)_1 - (C_H)_2$ does not depend on c_{KF} and the relative values $(C_H)_1$, $(C_H)_2 > (C_D)_1$, $(C_D)_2$. Thus, the convexity of the Parsons–Zobel plots is mainly caused by the dependence of ΔC_D on c_{el}. The values of $(E_{min})_{PC}$ depend on X_i, from hence the values of σ_i and $(C_D)_i$ at $(E_{min})_{PC}$ also depend on X_i, even though the $\Delta E_{\sigma=0}$ and $(\Delta C_H)_i$ for the *wme* faces remain unchanged. The values of $f_{P\text{-}Z}$ found for *wme* and PC electrodes are apparent values, even though they characterize to a certain extent the crystallographic (energetic) heterogeneity of the *wme* surfaces [28]. As shown in [28] the plot of $1/C_{PC}$ against $1/\Sigma C_d$ which was obtained by summing up the partial $(C_D)_i$ and $(C_D)_2$ values at $(E_{min})_{PC}$, depart less from

linearity, and the obtained values of $f_{\Sigma C_D}$ insignificantly differ from unity ($f_{\Sigma C_D} = 1.01–1.03$). In the case of ECE and CE electrodes, this procedure is very complicated, because only very approximate values of the share of various planes exposed at the PC surface can be established by the computer simulation of the experimental $C_{PC}(E)$-curves.

The whole $C^{-1}(C_D^{-1})$-curve can be described by the third order power function with the correlation coefficient R^2 varying from 0.9975 to 0.9999 for *CE* electrodes and for EP single crystal planes, accordingly. The obtained values of constant term $\equiv C_H^{exp}$ at $C_D^{-1} = 0$ are presented in Table 1. According to the data of Table 1, the inner layer capacity C_H^{exp} for electrodes investigated is always > 0 and increases in order of solvents EtOH < MeOH ≤ ACN < H_2O. The deviation from linearity of the Parsons–Zobel plots (in the same electrolyte solution) increases in order of the electrodes $(Bi_{DE})^R \leq Bi^{EP} < (Bi_{DE})^{WR} < Bi^{ECE} < Bi^{CE} < (Bi_{PC})^{MP} < (Bi_{PC})^{MP\,CE}$.

3.5. Fitting (roughness) coefficient—Debye length plots

The third order power functions have been used to obtain the fitting (roughness) coefficient $f_{P\text{-}Z}$ at the various electrolyte concentrations, *ie* at the various values of length l_D. The values of $f_{P\text{-}Z}$ have been calculated by differentiation of $C^{-1}(C_D^{-1})$-plots by an IBM-486 DX-2 computer using the Mathcad 4.0 Standard Pac. The values of l_D at $\sigma = 0$ have been calculated according to the Debye–Hückel theory [47] and at $\sigma \neq$ const. by the following equation [30, 31]:

$$(l_D)_{eff}(\sigma) = (l_D^2 + 4\pi\sigma^2 L_B^3/e^2)^{1/2}, \qquad (10)$$

where L_B = the Bjerrum length, e = elementary charge.

The established $f_{P\text{-}Z}(l_D)$-plots ($l_D \equiv \kappa^{-1}$) are presented in Fig. 7. According to these data for $(Bi_{DE})^R$, for EP single crystal electrodes, *wme* and ECE Bi and Sb electrodes, the values of $f_{P\text{-}Z}$ increase when l_D increases. This is mainly caused by the fact that for *wme*, $(Bi_{DE})^R$ and for EP single crystal planes, the concentration of surface defects is small and most of the surface area is covered by homogeneous regions which linear parameter $r^* \gg l_D$. For these electrodes the IDL model is valid.

For CE Sb, Cd and Bi electrodes and for ECE Cd electrodes, in the region of small concentrations ($l_D > 2.0$ nm), the values of $f_{P\text{-}Z}$ increase if the concentration of the electrolyte decreases. This result is in contradiction with the theoretical predictions of a new model [30, 31].

In Fig. 8 the dependence of the experimental thickness of the electric double layer l^{exp} ($l^{exp} = 1/4\pi C^{exp}$) on the Debye length l_D are presented. According to these data, the thickness of the double layer increases as the dielectric constant of solvents

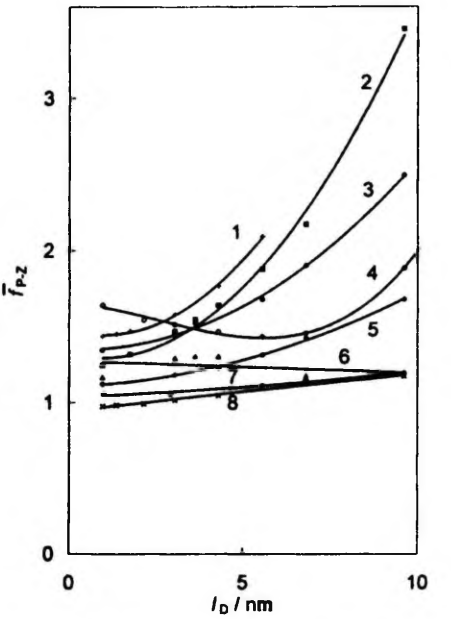

Fig. 7. Parsons–Zobel factor–Debye length plots for different electrodes: 1, Bi(111)^{CE}; 2, Cd(11$\bar{2}$0)^{CE}; 3, *wme*-Bi[0.5(01$\bar{1}$) + 0.5(111)] ($\Delta E_{\sigma=0} = 0.08$ V); 4, *wme*-Bi[0.8(01$\bar{1}$) + 0.2(111)] ($\Delta E_{\sigma=0} = 0.08$ V); 5, Cd(11$\bar{2}$0)^{EP}; 6, Bi(001)^{EP}; 7, $(Bi_{DE})^R$; 8, *wme*-Bi[0.4(01$\bar{1}$) + 0.6(1$\bar{0}$1)] ($\Delta E_{\sigma=0} = 0.015$ V).

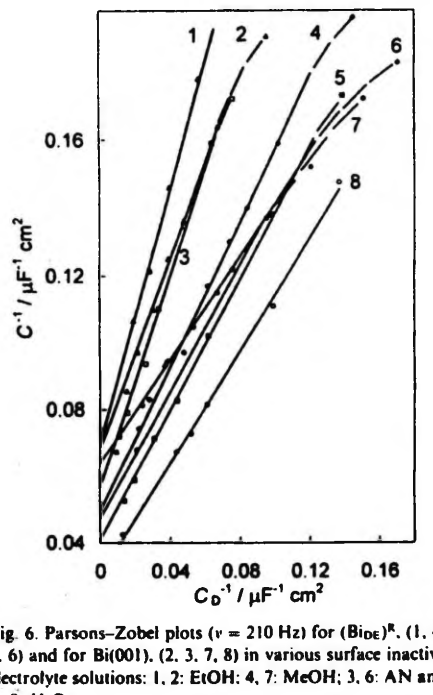

Fig. 6. Parsons–Zobel plots ($\nu = 210$ Hz) for $(Bi_{DE})^R$. (1, 4, 5, 6) and for Bi(001). (2, 3, 7, 8) in various surface inactive electrolyte solutions: 1, 2: EtOH; 4, 7: MeOH; 3, 6: AN and 5, 8: H_2O.

diminishes and the linear length of solution molecules grows. Differently from the theoretically calculated $l(l_D)$-plots [30, 31] the experimental $l^{exp}(l_D)$-plots are convex curves, *ie* not concave curves as predicted theoretically.

3.6. Roughness function—inverse Debye length plots

For a more accurate interpretation of the experimental data, the roughness function–inverse Debye length [$\tilde{R}(x),\kappa$] plots have been constructed by using equation 11:

$$\tilde{R}(x) \sim \left(\frac{1}{C_{tot}} - \frac{1}{C_H}\right)^{-1} \cdot C_{GC}^{-1} \qquad (11)$$

The dependencies found for various electrodes are presented in Fig. 9. According to the experimental data, the values of roughness function (at κ = const.) increase in order of the electrodes $(Bi_{DE})^R$ < EP Bi single crystals < $Bi(111)^C$ < $(Bi_{DE})^{WR}$ < $Bi(111)^{ECE}$ < $Bi(111)^{CE}$ < $Bi(111)^{MP}$ < $(Bi_{PC})^{MP\,CE}$ < $Sb(111)^C$. The nonlinearity of $\tilde{R}(x),\kappa$-plots is very small for $(Bi_{DE})^R$ and for EP single crystal Bi and Cd electrodes. But the deviation from linearity of $\tilde{R}(x),\kappa$-plots increases in the same order of electrodes as the value of $\tilde{R}(x)$. Thereafter, the nonlinear regression analysis has been done according to the equations (13)–(15) presented in [30, 31] to obtain the roughness parameters of electrode surface.

According to the data of nonlinear regression analysis, in the moderate electrolyte solutions ($c_{el} \geq 0.05$ M), where the influence of the energetic inhomogeneity ($\Delta E_{\sigma=0}$) of PC electrode surface on the total *edl* capacity is relatively weak, the values of R increase in order of the planes $(Bi_{DE})^R \leq$ EP Bi single crystals ≤ $Bi(111)^C$ < EP Cd single crystals ≤ EP Sb single crystals < ECE Bi and Sb single crystals < CE Bi single crystals < MP CE Bi single crystals < MP CE $Bi_{PC} \leq (Sb_{PC})^{MP}$. In the case of more dilute solutions (c_{el} < 0.05 M), the experimental and theoretical $\tilde{R}(x),\kappa$-plots are going in the opposite directions, and thus in solutions, where the influence of crystallographic inhomogeneity on the *edl* capacity of PC electrodes has a more pronounced effect, the new theory [30, 31] is inadequate.

According to the data of computer simulation of experimental $\tilde{R}(x),\kappa$-plots, in the case of weak roughness of electrode surface, it is impossible to select out the "true" theoretical model for surface roughness and therefore the future experimental and theoretical investigations are inevitable.

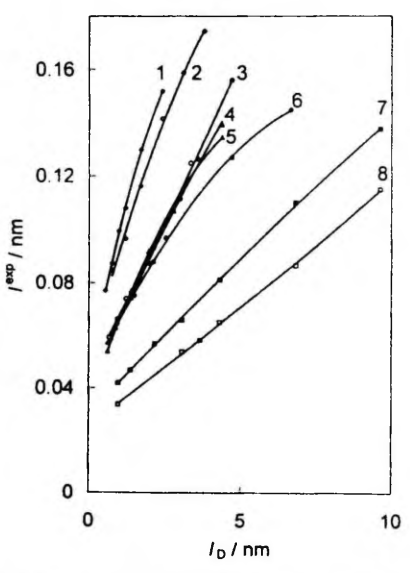

Fig. 8. Experimental double layer thickness–Debye length plots for $(Bi_{DE})^R$, (1, 5, 6, 7) and for $Bi(001)^{EP}$, (2, 3, 4, 8) in various surface inactive electrolyte solutions: 1, 2: EtOH; 3, 6: AN; 4, 5: MeOH and 7, 8: H_2O.

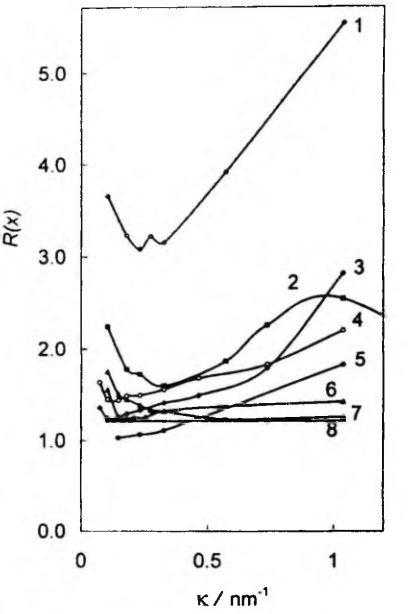

Fig. 9. Roughness function–Gouy length plots for various electrodes: 1, $Sb(111)^C$; 2, $Bi(111)^{CE}$; 3, $Cd(11\bar{2}0)^{ECE}$; 4, $Cd(0001)^{ECE}$; 5, $Bi(001)^{EP}$; 6, $Sb(111)^{EP}$; 7, $Cd(11\bar{2}0)^{EP}$ and 8, $(Bi_{DE})^R$.

According to the data of computer simulation of experimental $\tilde{R}(x),\kappa$-plots, in the case of weak roughness of electrode surface, it is impossible to select out the "true" theoretical model for surface roughness and therefore the future experimental and theoretical investigations are inevitable.

3.7. Differential capacity—potential curves in the presence of organic compounds

The adsorption behavior of cyclohexanole (CH), propylacetate (PA), butylacetate (BA) and pyridine (PY) on the electrochemically polished single crystal Bi, Sb and Cd electrodes; on the cleaved at the temperature of liquid nitrogen $Bi(111)^C$, $Cd(0001)^C$ and $Sb(111)^C$; on the electrochemically etched $Bi(111)^{ECE}$, $Bi(001)^{ECE}$, $Cd(0001)^{ECE}$; on chemically

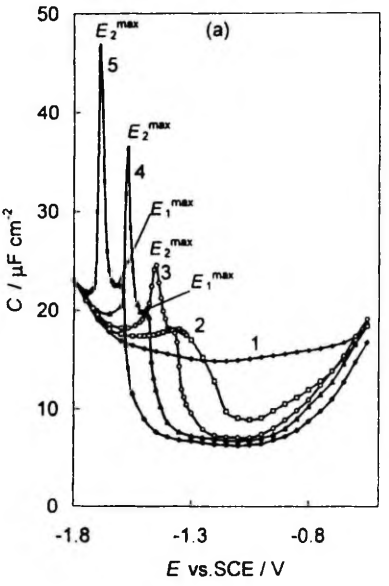

Fig. 10(a)

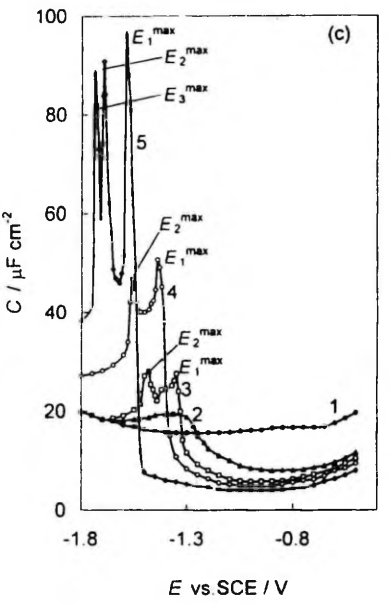

Fig. 10(c)

Fig. 10. $C(E)$-curves (ν = 210 Hz) for Bi(111)^{C} (a); Bi(111)^{ECE} (b) and Bi(111)^{CE} (c) in 0.1 M NaF (1) and with additions of pyridine, M: 2: 0.05; 3: 0.07; 4: 0.1 and 5: 0.2.

etched Bi(111)^{CE}, Cd(11$\bar{2}$0)^{CE}, and on the mechanically polished (using Al_2O_3) and thereafter chemically etched (Bi$_{PC}$)$^{MP\,CE}$ electrodes, have been investigated by impedance, chronocoulometry and cyclic voltammetry methods. The obtained results have been compared with the data for (Bi^{DE})^{R}, (Bi^{DE})^{WR} and *wme* [4, 49, 50]. The experimental investigations indicate that the shape of the differential capacity–potential curves is very sensitive to the Bi(111) surface structure, *ie* to the pretreatment of electrode surface (Figs 10–12). The $C(E)$-curves for EP single crystal electrodes have their usual shape with one very high, sharp and narrow cathodic adsorption–desorption maximum at negative potentials [4, 50, 51]. For Bi(111)^{C} at $c_{Py} > 0.1$ M, besides the main adsorption–desorption maximum, there are some steps on the $C(E)$-curves at the more positive potentials than the potential of the main maximum (Figs 10(a), 13(a)). From the $C(E)$-curves for single crystal planes of Bi, Sb and Cd, at the first approximation, it is possible by computer simulation to obtain the share of energetically various, but geometrically homogeneous surface regions, adsorption properties of which are similar to the adsorption characteristics for single crystal planes [4, 12, 49–52]. This method is based on the conception that at every homogeneous surface region of a *PC* electrode the adsorption process of organic compound studied can be described by the Frumkin–Damaskin adsorption theory [53], and the capacity of a *PC* electrode can be described by the superposition of $C(E)$-curves (at E = const.) for different homogeneous regions (single crystal electrodes) [11, 12]. The last presumption is valid only at the potential of maximum adsorption $E = E_{max}$, but as shown in [48, 49], at the first very rough approximation it is possible to use the shape of adsorption–desorption maxima to establish the share of various planes at a PC electrode surface. The

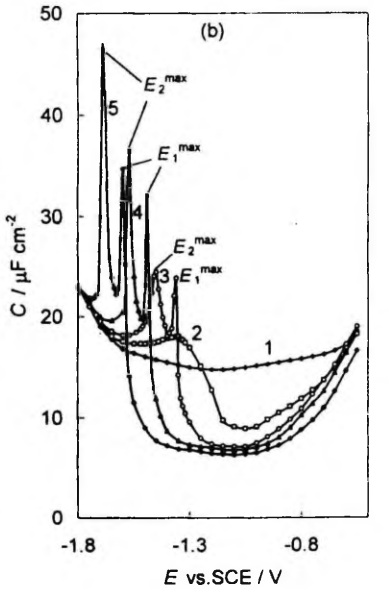

Fig. 10(b)

more correct method was given in [54]. According to the results of a computer simulation, the share of plane Bi(001) at the cut surface $Bi(111)^{C}$ is 3–8% ($\Delta = \pm 5\%$).

As follows from the data of Figs 10–12, studying the adsorption of PY and CH at $(Bi_{DE})^{R}$, $Bi(111)^{ECE}$, $Bi(001)^{ECE}$, $Cd(12\bar{2}0)^{ECE}$ and $Bi(111)^{CE}$ the effect of the splitting of the adsorption–desorption maxima has been established [52]. It must be noted that the shape of adsorption–desorption maxima depends on the duration of the electrochemical etching of electrodes, τ. The height of additional maximum (at c_{org} = const.) increases and the height of the main maximum decreases, when τ increases. But at $\tau_{ECE} \geq 3$ min, the increase of τ has very weak influence on the shape of the adsorption–desorption maxima at the $C(E)$-curves. The potentials of the main more-negative maximum E_2^{max}, as well as of the additional maximum E_1^{max}, are practically independent of the values of τ_{ECE} and are in very good agreement with the potentials of E^{max} for individual planes (Fig. 13(b)). The computer simulation of the prepared $Bi(111)^{EPE}$ shows that the share of plane Bi(001) at $Bi(111)^{EPE}$ surface, X_2, is approximately from 0.2 to 0.4. Thus, with the increasing of τ_{ECE}, the share of homogeneous surface regions, adsorption characteristics of which are similar to the Bi(001) plane, increases. The same tendency is valid in the case of adsorption of CH, PA and BA at $Bi(111)^{ECE}$ and $Cd(11\bar{2}0)^{ECE}$ (Fig. 11(b), 13(e)). The same conclusion is valid for $Bi(001)^{ECE}$ where the increase of τ_{ECE} causes the increase of the share of Bi(111) plane at $Bi(001)^{ECE}$ surface ($\tau_{ECE} \geq 3$ min, $X_{(111)} \sim 15$–30%).

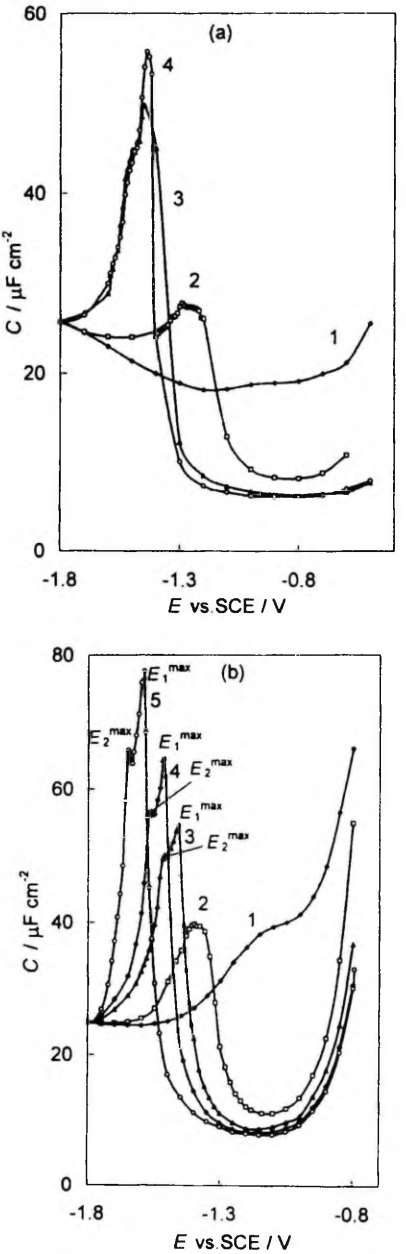

Fig. 11. $C(E)$-curves (ν = 210 Hz) for $(Bi_{PC})^{MP}$ (a) and for $Cd(11\bar{2}0)^{ECE}$ (b) in 0.1 M NaF (1) and with additions of cyclohexanole, M: 2: 0.02; 3: 0.07; 4: 0.1 and 5: 0.2.

According to the data of Fig. 10(c), at $c_{PY} \geq 0.1$ M the adsorption–desorption maximum for chemically etched $Bi(111)^{CE}$ electrode is split into the three independent adsorption–desorption maxima with the values of potentials very close to the individual planes of Bi: $E_1^{max} \sim E_{Bi(001)}^{max}$, $E_2^{max} \sim E_{Bi(111)}^{max}$ and $E_1^{max} \sim E_{Bi(01\bar{1})}^{max}$ (Fig. 13(c)). As in the case of an ECE, the shape of adsorption–desorption maxima depends on the time of chemical etching τ_{CE}, but at $\tau_{CE} \geq 2$ min the transformations in the shape of adsorption–desorption maxima are comparatively small. For τ_{CE} = 3 min, the share of various planes at $Bi(111)^{CE}$ is: $X_{Bi(111)} \sim 50$–40%, $X_{Bi(001)} \sim 25$–30% and $X_{Bi(01\bar{1})} \sim 25$–30%.

As shown in Fig. 11(a), a very low and wide adsorption–desorption maximum for $(Bi_{PC})^{MP\,CE}$ has been found and the potential of E^{max} is intermediate between the E^{max} values for Bi(111), $Bi(01\bar{1})$ and Bi(001) planes. The values of attraction constant obtained from the width of these maxima according to the calculation method [12, 13] are approximately 2.5 times lower than for single crystal planes [4, 48, 49]. Therefore, at the surface of $(Bi^{PC})^{MP\,CE}$, not very large homogeneous surface segments exist. At the first moment it seems that by MP and CE of Bi_{PC} it is possible to prepare the more uniformly inhomogeneous surface for which the CDL electrode model would be valid.

The adsorption studies at $(Bi_{DE})^{R}$ show (Figs 12(a), 13(d)) that there are exposed three (sometimes four) energetically different homogeneous surface regions, adsorption properties of which are similar to those

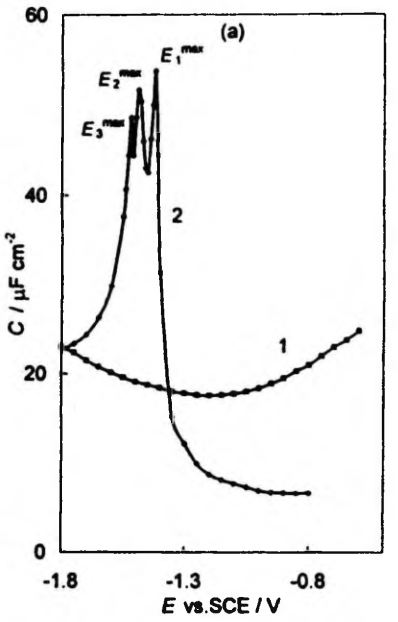

Fig. 12(a)

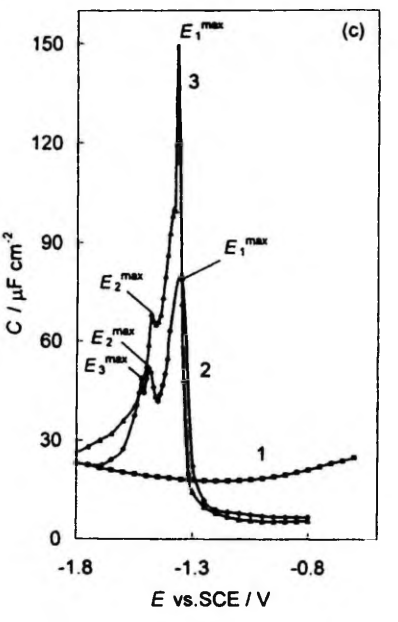

Fig. 12(c)

Fig. 12. $C(E)$-curves (ν = 210 Hz) for $(Bi_{DE})^R$ (a) and for $(Bi_{DE})^{WR}$ (b, c) in 0.1 M, (a, b) and in 1 M (c) aqueous NaF solutions, (1) and with addition of cyclohexanole, M: 2: 0.07 and 3: 0.1.

for Bi(001), Bi(111) and Bi(01$\bar{1}$) planes. The statistical analysis of many experiments with PA, BA, CH, PY and alkanes [12, 49] shows that mainly at the surface of $(Bi^{DE})^R$ there are homogeneous regions, the adsorption properties of which are similar to Bi(001)

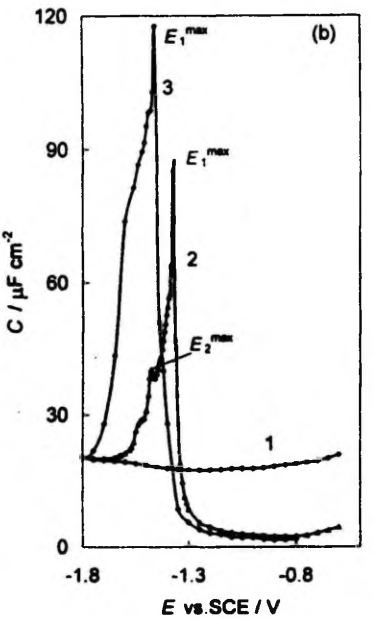

Fig. 12(b)

($X_{(001)} = 0.4 \div 0.6$), Bi(111) ($X_{(111)} = 0.3 \div 0.2$) and Bi(01$\bar{1}$) ($X_{(01\bar{1})} = 0.3 \div 0.2$).

$C(E)$-curves in the presence of CH for bismuth solid drop electrode, prepared without additional remelting of surface, are presented in Figs 12(b) and (c). According to the experimental data of many experiments (c_{el} = 0.1 M), there is only one low but not very wide adsorption–desorption maximum at the $C(E)$-curves, potential of which (E_{ik}^{max}) is practically same as the E_{max} value for Bi(001). The values of interaction parameter (a), obtained from the height or width of these maxima, are approximately 1.5 times lower than for the single crystal planes. In some cases only a very small additional adsorption–desorption peak at the potentials more negative than E^{max} for the main maximum can be found.

3.8. Influence of surface inactive electrolyte concentration on the shape of adsorption–desorption maxima

Experimental investigations at $(Bi_{DE})^R$ and $(Bi_{DE})^{WR}$ in various surface inactive electrolyte solutions show (Fig. 12) that the shape of $C(E)$-curves depend on the concentration of surface inactive electrolyte. According to the data of Fig. 11(a), in 0.1 M NaF, as well in 0.05 M Na_2SO_4 aqueous solutions, there is only one very low and wide adsorption–desorption peak and small steps at more positive or more negative potentials than the

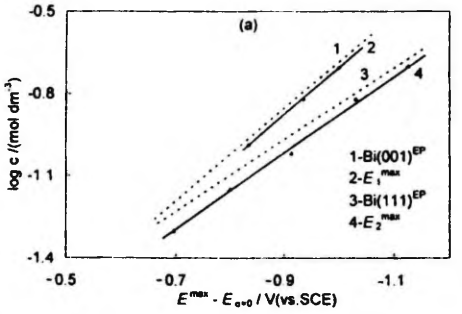

Fig. 13(a)

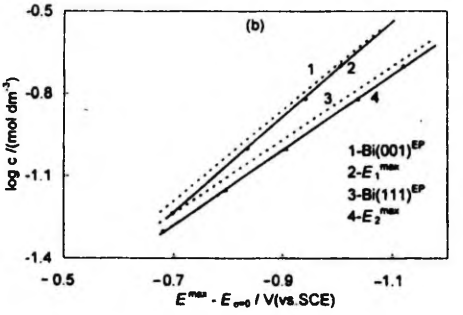

Fig. 13(b)

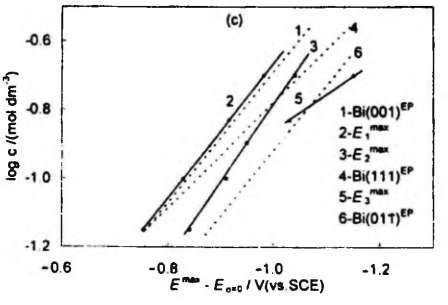

Fig. 13(c)

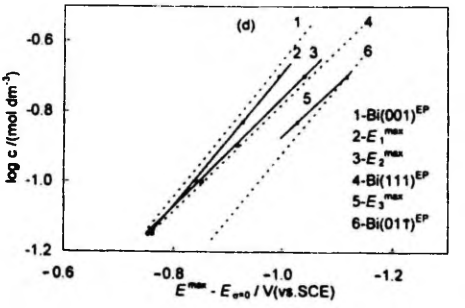

Fig. 13(d)

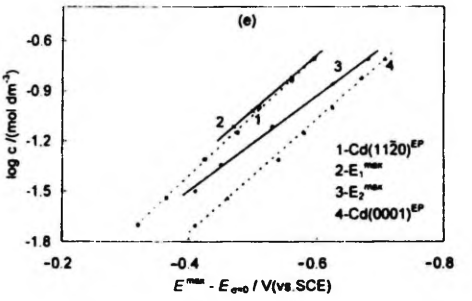

Fig. 13(e)

Fig. 13. lgc(E^{max})-curves of PY adsorption (a, b, c) and CH adsorption (d, e) at Bi(111)^{C}, a; Bi(111)^{ECE}, b; Bi(111)^{CE}, c; (Bi$_{DE}$)*, d and Cd(11$\bar{2}$0)^{ECE}, e. Notations of planes are given in figure and in text.

main maximum. The increase of c_{NaF} from 0.1 M to 1.0 M, as well $c_{Na_2SO_4}$ from 0.05 M to 0.5 M results in splitting of the adsorption–desorption maximum to three separate adsorption–desorption maxima (Fig. 12(c)) with the potential values very close to the E^{max} values for individual plane Bi(001) (main maximum), Bi(111) (central maximum) and Bi(01$\bar{1}$) (maximum at more negative potential). This effect can be explained by the dependence of effective Debye screening length $l_{D,eff}$ on the surface inactive electrolyte concentration

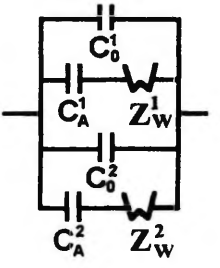

a

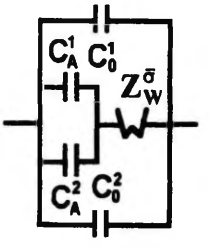

b

Fig. 14. Equivalent circuits of *ac* for PC electrodes for the independent diffuse layer model (a) and for the common diffuse layer model (b). C_0 = true capacity; C_A = pseudocapacity; Z_W = Warburg impedance.

(at $\sigma = 0$, in 0.1 M NaF $l_D = 0.96$ nm and in 1.0 M NaF $l_D = 0.22$ nm). Therefore, the linear parameters of surface regions, exposed additionally to the large Bi(001) planes at the surface of $(Bi_{DE})^{WR}$ must be in the same order (~0.5 nm) as the effective Debye screening length (calculated by equation (10)) at which the CDL model replaces the IDL. The same conclusion is valid for the adsorption of CH at $(Bi_{PC})^{MP}$ electrodes. In the case of $(Bi^{DE})^{R}$ and EP single crystal Bi, Cd and Sb electrodes, as well as for *wme* and $(Bi_{PC})^{ECE}$, the influence of surface inactive electrolyte concentration to the shape of adsorption–desorption maxima is weak and the effects established are in good correspondence with the theoretical predictions of [53, 54].

3.9. Influence of the frequency on the shape of adsorption–desorption maxima and on the linear parameters of homogeneous regions at a PC electrode surface

As shown in [54], if the diffusion of an organic compound is slow and thus the rate determining process of adsorption of organic compound at the electrode surface, the adsorption process at two different types of PC electrode surface can be described by the models presented in Fig. 14. In Fig. 14: $(C_i)_i = (\partial\sigma/\partial E)_\Gamma$ = true capacity of the double layer of homogeneous region i; $(C_A)_i$ = adsorption pseudocapacity (additional capacity) of region i; $(Z_W)_i$ = Warburg impedance for the region i, and $(Z_W)^{el}$ = common Warburg impedance of the mi-

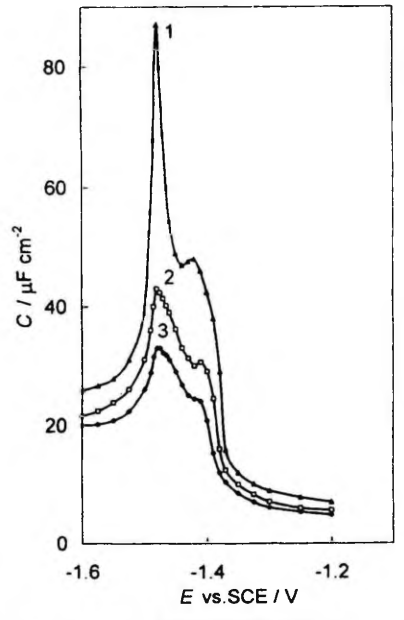

Fig. 15. $C(E)$-curves of cyclohexanole (0.08 M) adsorption at *wme*-Bi[0.8(01$\bar{1}$) + 0.2($\bar{1}$0$\bar{1}$)] at different v, Hz: 1: 110; 2: 2100 and 3: 11,000.

Table 2.
Adsorption parameters of CH at wedge shape electrode (*wde*) and bismuth solid drop electrode $(Bi_{DE})^{R}$

	$\Gamma_c \cdot 10^5$ cm	
v (Hz)	Bi[0.8(01$\bar{1}$) + 0.2($\bar{1}$0$\bar{1}$)]	$(Bi_{DE})^{R}$
60	1.80	1.95
210	1.68	1.82
510	1.58	1.78
1100	1.49	1.79
5100	1.40	1.64
11,000	1.29	1.50
21,000	1.20	1.30

cropolycrystalline surface, obtained by the average charge density of a PC electrode. In the case of *ac*, the concentration penetration depth of organic compound can be obtained as $L = (2D_i/\omega)^{1/2}$. At high values of v the characteristic length of homogenous regions $y^* \gg L$ and the model of independent diffuse layer (IDL) is valid, *ie* the diffusion of organic compound to the homogeneous region i is independent of the adsorption process of organic compound to the other surface regions. At very low values of v, $L < y^*$, and the model of common diffuse layer (CDL) is valid, *ie* the adsorption of organic compound at every inhomogeneous surface depends on the adsorption characteristics of all the very small crystallites. The critical frequency at which the IDL model is replaced by the CDL electrode model is in the same order as the characteristic length y^* of the homogeneous surface regions which prevail and determine the adsorption characteristics of the whole PC electrode surface.

As shown in [54], the more sensitive (experimental) parameter is $\Gamma_c = (\partial\Gamma_c/\partial c)_E$ obtained by methods described in [53–56]. If the IDL electrode model is valid, then $\Gamma_c = f(v)$, and if the CDL model is valid then $\Gamma_c \neq f(v)$ (Γ_c = const.).

As established in [55], the rate of adsorption process of CH at bismuth single crystal planes is determined mainly by the rate of diffusion of CH molecules to the electrode surface, and therefore the adsorption data at different v can be used for obtaining y^* for *wme* and other PC electrodes.

The experimental $C(E)$-curves for 0.8 Bi(01$\bar{1}$) + 0.2 Bi(101) at various v are presented in Fig. 15 and the obtained values of Γ_c are given in Table 2. According to the data for *wme*, in the whole region of v investigated, the value of $\Gamma_c = f(c)$, and probably $y^* > 5 \cdot 10^{-4}$ cm. For more accurate estimation of y^*, the investigations at a larger region of v are inevitable. The adsorption data of CH on $(Bi^{DE})^{R}$ show (Table 2) that in the region of 510 Hz $< v <$ 2100 Hz $\Gamma_c \sim$ constant, and therefore, the values of $y^* \sim 10^{-5}$ cm. The same order of y^* was obtained from the data for *p*-toluidine adsorption at

$(Bi^{DE})^{R}$ [54]. The experimental investigations of CH adsorption at $Bi(111)^{ECE}$, $Bi(111)^{CE}$ and $(Bi_{PC})^{MP}$ are in progress now and the results will be discussed in our next publications.

3.10. The shape of adsorption isotherms and the approximate share of various homogeneous regions at a PC electrode surface

As established in [4, 12, 48, 49], the shape of an adsorption isotherm is very sensitive to the crystallographic structure of the electrode surface. To obtain the share of various single crystal planes at a PC surface it is useful to present the adsorption isotherm in the linearized Frumkin isotherm coordinates $\ln[\theta_{PC}/(1-\theta_{PC})c]$ vs θ_{PC}. The adsorption isotherms for differently prepared Bi electrodes are presented in Fig. 16. According to the experimental data, the isotherms for PC electrodes are located between the partial isotherm for the less-active Bi(111) and more-active $Bi(01\bar{1})$ planes (except $(Bi_{PC})^{MP\,CE}$). The isotherm for cut $Bi(111)^{C}$ is linear in a very large region of θ_{PC}, and the values of attraction interaction ($a_0 = 1.8$) and adsorption equilibrium constant ($B_0 = 18\ dm^3\ mol^{-1}$) are very close to the parameters for EP Bi(111) [47–49]. The computer simulation shows that at the surface of $Bi(111)^{C}$ there exist regions (5–10% of surface), adsorption characteristics which differ from those for $Bi(111)^{EP}$.

The adsorption isotherm for $Bi(111)^{ECE}$ and $Bi(001)^{ECE}$ consists of two practically linear segments, separated by a very well exposed bend at $\theta_{PC} \sim 0.5$. The isotherm of this form is characteristic for PC electrodes, at the surface of which there are two large homogeneous surface regions with clearly different adsorption characteristics [4, 48, 49]. According to the data of computer simulation, the surface of $Bi(111)^{ECE}$ is mainly covered by large homogeneous regions with adsorption characteristics similar to Bi(111) ($X_{(111)} \sim 50$–60%) and Bi(001) ($X_{(001)} \sim 40$–30%). The nonlinearity of the isotherm at small θ_{PC} is more pronounced than for $Bi(111)^{C}$, and is caused by the adsorption of CH at small crystallites (surface defects) with share $X_{other} \sim 0.1$ having higher adsorption activity than Bi(001) and Bi(111) planes.

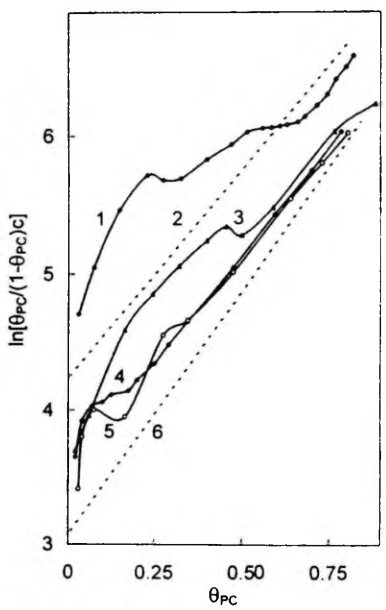

Fig. 16. Adsorption isotherms of cyclohexanole at $(Bi_{PC})^{MP\,CE}$, 1; $Bi(01\bar{1})^{EP}$, 2; $Bi(001)^{ECE}$, 3; $Bi(111)^{C}$, 4; $Bi(111)^{CE}$, 5 and $Bi(111)^{EP}$, 6.

The adsorption isotherm for $Bi(111)^{CE}$ has a more complicated shape. At $\theta_{PC} \leq 0.15$ the adsorption isotherm is nonlinear. At $0.15 \leq \theta_{PC} \leq 0.30$ the isotherm can be considered linear at the very rough approximation. At $0.30 < \theta_{PC} < 0.40$ a very well-pronounced bend can be found and only at high $\theta_{PC}(\theta_{PC} > 0.6)$ is the adsorption isotherm approximately linear. The computer simulation shows that the isotherm of this form can be described by the following collection of parameters: $a_{(111)} = 1.83$, $B_{(111)} = 17\ dm^3\ mol^{-1}$, $X_{(111)} \sim 0.4$–0.3; $a_{(001)} = 1.45$, $B_{(001)} = 34\ dm^3\ mol^{-1}$, $X_{(001)} \sim 0.2$–0.3; $a_{(01\bar{1})} = 1.45$, $B_{(01\bar{1})} = 70\ dm^3\ mol^{-1}$, $X_{(01\bar{1})} = 0.2$–0.3; $a_{other} = 1.95$; $B_{other} = 100\ dm^3\ mol^{-1}$; $X_{other} \sim 0.2$–0.1. Thus, the successful fitting of the experimental and calculated isotherms can be achieved only after taking into account the corrections which allow for the influence of small crystallites in addition to the three monocrystalline regions at the $Bi(111)^{CE}$ surface.

The adsorption isotherms for $Bi(111)^{MP}$ as well as for $(Bi_{PC})^{MP\,CE}$ have a very complicated shape, being nonlinear in the whole region of θ_{PC} investigated, and therefore it is impossible to obtain the share of various homogeneous regions at such a prepared PC surface. The nonlinear character of isotherms shows that there prevail very small ($r^* \leq 10$ nm) crystallites at the surface of $Bi(111)^{MP}$ and $(BiPC)^{MP}$, and the CDL model would be valid.

4. CONCLUSIONS

The systematic investigations at variously prepared (electrochemically polished single crystal Sb, Bi and Cd planes, cleaved at the temperature of liquid nitrogen, Bi(111), Sb(111) and Cd(0001), electrochemically etched at high anodic currents Bi single crystal electrodes, chemically etched Bi, Sb and Cd electrodes, mechanically polished with Al_2O_3 and therefore electrochemically polished or chemically etched electrodes, wedge-shape two plane model polycrystalline electrodes with known crystallographic heterogeneity, solid drop Bi and Sb electrodes with remelted and without additional remelting of surface) electrodes show that the electric double layer and adsorption characteristics systematically depend on the geometrical structure of the

electrode surface (roughness) and energetic inhomogeneity of the electrode surface. It was found that the value of differential capacity at the potential of diffuse minimum increases (c_{el} = const.) if the surface roughness increases in the order of electrodes $(Bi_{DE})^R$ < EP single crystal < cut single crystal < ECE single crystal < $(Bi_{DE})^{WR}$ < CE single crystal < MP single crystal < MP and CE PC. The deviation from linearity of Parsons–Zobel plots, as well as the values of Parsons–Zobel factor $f_{P\text{-}Z}$ increase in the same order. The formally found values of the inner layer capacity and roughness factor (fitting coefficient) increase in the same order of electrodes. In the case of ECE, CE and MP electrodes it is impossible to establish the "correct" values of the fitting coefficient $f_{P\text{-}Z}$, at which the $C_H(\sigma)$-curves would have a smooth shape. The computer simulation of the electric double layer and adsorption data of many electrodes shows that in the case of $(Bi_{DE})^R$, EP single crystal planes, ECE single crystal planes and CE single crystal planes, the independent diffuse layer (IDL) model is valid. The linear parameter of homogeneous surface regions which prevail at the surface of EP, ECE and $(Bi^{DE})^R$ electrodes $y^* \gg 10$ nm. Probably, the surface of MP CE polycrystalline electrodes and $(Bi_{DE})^{WR}$ consists mainly of many very small crystallites, which $y^* \leq 10$ nm, and therefore for these electrodes the common diffuse layer (CDL) model might be valid.

The so-called "Debye length dependent roughness function" has been calculated, and using the non-linear regression analysis the various surface roughness models (sinusoidal corrugation, random Gaussian roughness, periodical system of linear defects, rectangular grating, proposed in [30, 31]), have been simulated.

As found in the case of an EP single crystal, the surface roughness is very small and it is impossible to choose the "true" surface roughness model. The experimental data for MP and MP CE electrodes show that in the concentrated electrolyte solutions ($0.05\ M \leq c \leq 0.1\ M$) the model of random Gaussian roughness or the periodic system of linear defects [30] would be valid. It must be noted that the further experimental investigations of differently prepared PC electrodes in various electrolyte solutions and theoretical simulations of experimental results using various roughness models should be done for a more substantiated conclusion.

ACKNOWLEDGEMENTS

This work was supported in part by the Estonian Science Foundation under grant No. 612. The authors would like to thank Professors A. A. Kornyshev, M. A. Urbakh and L. I. Daikhin for the stimulative theoretical discussions and the referee for the very useful discussion.

REFERENCES

1. A. Hamelin, T. Vitanov, E. Sevastyanov and A. Popov, *J. Electroanal. Chem.* **145**, 225 (1983).
2. M. A. Vorotyntsev, in J. O'M. Bockris, B. E. Conway and R. E. White (eds), *Modern Aspects of Electrochemistry*, Vol. 17, p. 131, Plenum Press, New York (1986).
3. J. Lipkowski and L. Stolberg, in J. Lipkowski and P. N. Ross (eds), *Molecular Adsorption at Metal Electrodes*, VCH, New York (1992).
4. E. J. Lust, K. K. Lust and A. A.-J. Jänes, *Russ. J. Electrochem.* **31**, 807 (1995).
5. R. R. Adzic, in J. O'M Bockris, B. E. Conway and R. E. White (eds), *Modern Aspects of Electrochemistry*, Vol. 22, p. 163, Plenum Press, New York (1986).
6. G. Stoikov, E. Budevski, W. Obretenov and W. Lorenz, *J. Electroanal. Chem.* **349**, 355 (1993).
7. M. Hoptner, W. Obretenov, K. Jüttner, W. J. Lorenz, G. Stoikov, V. Bostanov and E. Budevski, *Surface Sci.* **248**, 225 (1991).
8. X. Gao, A. Hamelin and M. W. Weaver, *Phys. Rev. Lett.* **67**, 616 (1991).
9. A. Hamelin, *Nanoscale Probes of the Solid/Liquid Interface* (Edited by A. A. Gewirth and H. Siegenthaler), NATO ASI Series E: Applied Sciences, Kluwer Academic Publishers **288**, 285 (1995).
10. J. R. La Graff and A. A. Gewirth, *Nanoscale Probes of the Solid/Liquid Interface* (Edited by A. A. Gewirth and H. Siegenthaler), NATO ASI Series E: Applied Sciences, Kluwer Academic Publishers **288**, 83 (1995).
11. V. V. Batrakov and B. B. Damaskin, *J. Electroanal. Chem.* **65**, 361 (1975).
12. A. R. Alumaa, E. J. Lust, N. A. Paltusova and U. V. Palm, *Elektrokhimiya* **19**, 1582 (1983).
13. S. Trasatti and O. Petrii, *Elektrokhimiya* **29**, 557 (1993).
14. R. Parsons and F. R. G. Zobel, *J. Electroanal. Chem.* **9**, 333 (1965).
15. G. Valette and A. Hamelin, *J. Electroanal. Chem.* **45**, 301 (1973).
16. D. I. Leikis, K. V. Rybalka, E. S. Sevastyanov and A. N. Frumkin, *J. Electroanal. Chem.* **46**, 161 (1973).
17. A. J. Bard, *Anal. Chem.* **33**, 11 (1961).
18. V. E. Kazarinov, D. Horani, Yu. B. Vasilyev, V. N. Andreyev, *Itogi nauki i tekhniki. Elektrokhimiya* **22**, 97 (1985).
19. R. H. Burshtein, *Elektrokhimiya* **3**, 349 (1967).
20. N. B. Grigoryev, *Dokl. Akad. Nauk SSSR* **229**, 647 (1976).
21. U. V. Palm, M. P. Pärnoja and N. B. Grigoryev, *Elektrokhimiya* **13**, 1074 (1977).
22. I. A. Bagotskaya, M. D. Levi and B. B. Damaskin, *J. Electroanal. Chem.* **115**, 189 (1980).
23. M. A. Vorotyntsev, *J. Electroanal. Chem.* **123**, 379 (1981).
24. M. A. Vorotyntsev, *Elektrokhimiya* **17**, 1018 (1981).
25. M. A. Vorotyntsev, Proc. 6th Symp. on Double Layer and Adsorption at Solid Electrodes, Tartu, p. 59 (1981).
26. E. J. Lust and U. V. Palm, *Sov. Electrochem. Engl. tr.* **22**, 535 (1986).
27. E. Lust, M. Salve and U. Palm, *Sov. Electrochem. Engl. tr.* **23**, 520 (1987).
28. E. J. Lust and U. V. Palm, *Sov. Electrochem. Engl. tr.* **24**, 524 (1988).
29. U. V. Palm and B. B. Damaskin, *Itogi Nauki i Tekhniki. Electrokhimiya* **12**, 99 (1977).
30. L. I. Daikhin, A. A. Kornyshev and M. A. Urbakh, *Phys. Rev. E* **53**, 6192 (1996).
31. L. I. Daikhin, A. A. Kornyshev and M. A. Urbakh, Proc. of the Baltic Conf. on Interfacial Electrochemistry, Tartu, p. 57 (1996).

32. V. N. Vigdorovich, G. A. Ukhlimov, V. V. Marychev and V. P. Shumyalov, Sbornik Nauchnykh Trudov po Problemam Mikroelektroniki. Khimiko-Tekhnologicheskaya Seriya. Collection of Scientific Papers on Microelectronics, Ser. Chemical Technology. *Mosk. Inst. Elektronnoi Tekhniki* **8**, 24 (1972).
33. A. P. Korotkov, E. B. Bezlepkina, B. B. Damaskin and E. F. Golov, *Elektrokhimiya* **22**, 1298 (1985).
34. E. J. Lust, A. A.-J. Jänes, K. K. Lust and J. J. Ehrlich, *Russ. J. Electrochem.* **32**, 597 (1996).
35. D. D. Perrin and W. L. F. Armanego, *Purification of Laboratory Chemicals*, 3rd ed., Pergamon Press, Oxford, New York (1986).
36. V. Semevsky, P. Pärsimägi, M. Väärtnõu and A. Alumaa, Proc. 9th Symp. on Double Layer and Adsorption at Solid Electrodes, Tartu, p. 175 (1991).
37. J. Richer and J. Lipkowski, *J. Electroanal. Chem.* **251**, 217 (1988).
38. E. Lust, K. Lust and A. Jänes, *J. Electroanalyt. Chem.* **413**, 111 (1996).
39. E. J. Lust, K. K. Lust and A. A.-J. Jänes, *Russ. J. Electrochem.* **31**, 807 (1995).
40. M. Salve and U. Palm, *Trans. Tartu State Univ.* **332**, 71 (1974).
41. M. A. Vorotyntsev, *Itogi nauki i tekhniki. Elektrokhimiya*, **21**, 3 (1984).
42. L. Nyikos and T. Pajkossy, *Electrochim. Acta* **30**, 1533 (1985).
43. B. B. Mandelbrot, *The Fractal Geometry of Nature*, Freeman, San Francisco (1982).
44. A. Hamelin and L. Stoicoviciu, *J. Electroanal. Chem.* **236**, 267 (1987).
45. A. Hamelin and L. Stoicoviciu, *J. Electroanal. Chem.* **271**, 15 (1989).
46. A. Hamelin, *J. Electroanal. Chem.* **329**, 247 (1992).
47. D. Debye and W. Hückel, *Physik. Z.* **24**, 305 (1924).
48. E. J. Lust and U. V. Palm, *Sov. Electrochem.* **22**, 383 (1986).
49. E. Lust and U. Palm, *Trans. Tartu University* **757**, 105 (1986).
50. E. Lust, A. Jänes, P. Miidla and K. Lust, *J. Electroanalyt. Chem.* **425** (1997) 25.
51. E. J. Lust and U. V. Palm, *Sov. Electrochem.* **21**, 1304 (1985).
52. M. Salve, A. Alumaa and U. Palm, *Trans Tartu Univ.* **289**, 54 (1971).
53. B. B. Damaskin, O. A. Petrii and V. V. Batrakov, *Adsorption of Organic Compounds on Electrodes*, Plenum Press, New York (1971).
54. M. D. Levi, M. A. Vorotyntsev and V. E. Kazarinov, Proc. of the 7th Symp., Double Layer and Adsorption at Solid Electrodes. VII, Tartu, p. 186 (1985).
55. E. Lust and U. Palm, *Sov. Electrochemistry Engl Tr.* **24**, 227 (1988).
56. A. R. Alumaa and U. V. Palm, *Trans Tartu Univ.* **378**, 68 (1976).

IX

Reprinted from the *Journal of Electroanalytical Chemistry*, Vol. 431,
E. Lust, A. Jänes, K. Lust and R. Pullerits,
Adsorption of Organic Compounds and Hydrophilicity
of Bismuth, Cadmium and Antimony Electrodes, pages 183–201,

ELSEVIER

Journal of Electroanalytical Chemistry 431 (1997) 183–201

Adsorption of organic compounds and hydrophilicity of bismuth, cadmium and antimony electrodes

E. Lust *, A. Jänes, K. Lust, R. Pullerits

Institute of Physical Chemistry, University of Tartu, 2 Jakobi Str., EE-2400 Tartu, Estonia

Received 28 October 1996; revised 18 February 1997

Abstract

The adsorption behavior of various organic compounds at bismuth, antimony, cadmium, mercury and other "mercury-like" metals has been discussed. The systematic trends of the influence of the chemical nature of electrode metal and adsorbate to the molecular interaction parameter, a; limiting Gibbs adsorption, $\Gamma_{A,max}$; and Gibbs energy of adsorption, ΔG_A^0, have been analyzed. The ingredients of the total Gibbs energy of organic compound adsorption have been found. A new more general method for obtaining the metal–water interaction Gibbs energy has been worked out and used. It was found that the dependence of Gibbs energy of metal–water interaction on the chemical nature of metal and aliphatic organic compound studied is weak. Only in the case of chemically very different metals, for example for Sb and Zn, the difference of Gibbs energy of metal–water interaction values is somewhat higher than the exactness of the determination of the experimental values of Gibbs energy of organic compound adsorption. © 1997 Elsevier Science S.A.

Keywords: Organic adsorption; Hydrophilicity; Thermodynamics; Bismuth, cadmium, antimony, mercury, tin, lead and zinc electrodes

1. Introduction

For several decades the quantitative analysis of the electric double layer (edl), adsorption of ions and organic molecules at the polycrystalline (PC) bismuth and antimony electrodes have been studied in the Laboratory of Electrochemistry of the University of Tartu.

The adsorption parameters of various organic compounds (aliphatic alcohols, ketones, esters, carboxylic acids, amines, as well as pyridine, toluene, benzene and other aromatic compounds) have been established [1–7]. It was found that, to the first approximation, the adsorption process of various aliphatic compounds at the PC-Bi and PC-Sb electrodes can be described by the generalized Frumkin–Damaskin adsorption theory [8,9]. The systematic trends of the dependence of attractive constant, limiting surface concentration and the shift of zero charge potential, due to the displacement of the surface monolayer of H_2O by adsorbate molecules, on the chemical nature of metal and organic compound structures have been established and discussed [1–7]. Since 1978 the adsorption behavior of cyclohexanol (CH) [9–11], isomers of butanol (BA) [12,13], butyl acetate (BAC) [14], cyclohexanone (CHE) [15], cyclohexane carboxylic acid (CCA) [16] and pyridine (PY) [17] on the single crystal Bi, Sb and Cd electrodes has been studied. It is generally accepted [1–28] that all the compounds mentioned above (except PY) are physically adsorbed at Hg, Bi, Sb and Cd electrodes and the interaction between the hydrocarbon chains of adsorbate molecule and the metal surface must have mainly the character of dispersive forces. This interaction is weak and slightly depends on the nature of the metal and its crystallography, and at the first approximation it was assumed that Gibbs energy of metal–organic compound interaction $\Delta G^0_{Me-org} = \text{const.}$ [1–28]. Therefore the only plausible explanation for observed changes in Gibbs energy of adsorption of the same aliphatic organic compound ($\Delta G^0_{ads} = \text{const.}$; ΔG^0_{ads} Gibbs energy of adsorption of the organic compound at the air–solvent interface) from a certain electrolyte system ($\Delta G^0_{sol} = \text{const.}$; ΔG^0_{sol} increase of the Gibbs energy of adsorption of the organic compound at the air–solution interface induced by the addition of a strong, surface inactive, electrolyte to the solvent) at various metals is conditioned by the dependence of the hydrophilicity of the surface on the chemical nature of the metal ($\Delta G_{Me-H_2O} \neq \text{const.}$; $\Delta G^0_{Me-H_2O}$ is the Gibbs energy of adsorption of H_2O at the metal surface). As found in Ref.

* Corresponding author. E-mail: enn@chem.ut.ee

PII S0022-0728(97)00150-2

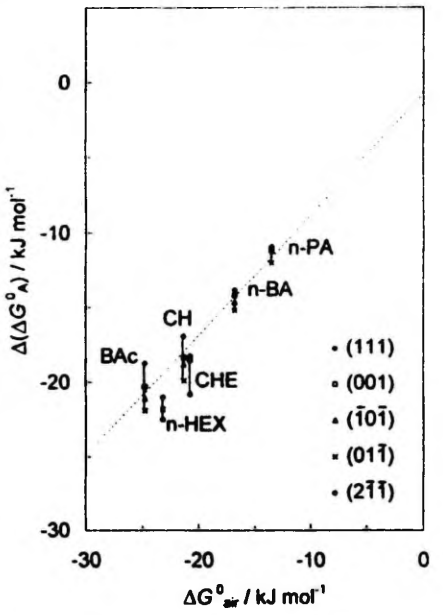

Fig. 1. Dependences of the difference between the Gibbs energy of adsorption of an organic compound at a metal–electrolyte interface (ΔG^0_A) and the increase of Gibbs energy of organic compound adsorption, caused by the addition of electrolyte into the solution ΔG^0_{sol} [$\Delta(\Delta G^0_A) = \Delta G^0_A - \Delta G^0_{sol}$] on the Gibbs adsorption energy of the organic compound at the air–solution interface (ΔG^0_{air}) for various compounds and single crystal planes of bismuth. (Notation of compounds and planes in the figure.)

[16], the value of the Gibbs energy of metal–H_2O interaction, $\Delta G^0_{Me-H_2O}$, obtained in Refs. [1–7,9–16] depends on the aliphatic compound studied, and with the increase of the adsorption activity of the adsorbate at the air–solution interface (ΔG^0_{air}) the difference between the adsorption activities for various metals, as well as for different single crystal planes of the same metal, increases (Fig. 1). In Fig. 1 the values of ΔG^0_A have been corrected by the term ΔG^0_{sol}, as chemically various surface inactive electrolytes with different concentrations have been used. The methods for obtaining ΔG^0_{sol} values will be discussed later. The results of Fig. 1 indicate that using the adsorption data only for one organic compound to establish the $\Delta G^0_{Me-H_2O}$ values for different metals or different single crystal planes is a very rough approximation. The main aim of this work is to establish some systematic trends of the influence of the chemical nature and crystallographic structure of electrode surface to the hydrophilicity of single crystal Bi and polycrystalline Bi, Sb and Cd electrodes, and to give a more generalized approach to find the $\Delta G^0_{Me-H_2O}$ values for various metals.

2. Results and discussion

2.1. Basic concepts of organic compound adsorption at the ideally polarizable electrode surface

According to the Andersen–Bockris model [22] the adsorption process of an adsorbate at the electrode surface can be described by the well-known equilibrium

$$A_b + nW_s \rightleftarrows A_s + nW_b \quad (1)$$

where A stands for the adsorbate; W for solvent (water); b for bulk and s for surface, and n is the size ratio parameter which shows the number of solvent (W) molecules displaced from the surface to solution by one adsorbate (A) molecule. Thus, the Gibbs energy of adsorption ΔG^0_A is given as the sum of the differences between the chemical potentials of the adsorbate (μ^0_A) and n solvent (water) molecules ($n\mu^0_w$) at the surface and in the bulk, respectively

$$\Delta G^0_A = \left(\mu^0_{A,s} - n\mu^0_{W,s}\right) + \left(n\mu^0_{W,b} - \mu^0_{A,b}\right) \quad (2)$$

where the second term is surface (metal) independent. The above presented scheme was introduced by Bockris et al. [22,29], Gileadi [30] and Everett [31,32] and it has been widely adopted by electrochemists, but there is no agreement over the size ratio parameter, since up to now its determination has presumed model assumptions.

The number of the desorbed solvent molecules n also depends on the orientation of the adsorbed molecule which is related with the molecular area (structure) of the adsorbate, as well as on the adsorbed H_2O monolayer structure (hydrophilicity) at the electrode surface studied. The number of desorbed solvent molecules can be calculated according to equation:

$$n = \Gamma_{A,max}/\Gamma_{sol,max} = A_A/A_{sol} \quad (3)$$

where $\Gamma_{A,max}$ and $\Gamma_{sol,max}$ are the maximum Gibbs adsorption values of adsorbate and solvent respectively; A_A and A_{sol} are the maximum molecular areas of adsorbate and solvent, accordingly. The estimation of n by this equation may involve very big errors (up to 40%) since the "absolute" value of surface coverage θ_A of adsorbate at $\Gamma_{A,max}$ is uncertain. Reasonable values of $\Gamma_{H_2O,max}$ are in the range between 1.2 and 1.6×10^{-9} mol cm^{-2}, corresponding to the molecular area A_{sol} from 0.14 to 0.10 nm^2 and the values of A_A for various monofunctional aliphatic compounds are in the range from 0.40 to 0.25 nm^2 [1,2,8,9,22,29–34]. Thus, the comparison of the area corresponding to a water molecule with the area corresponding to the maximum adsorption of many aliphatic compounds appears to contradict the assumption that the adsorbed particles of the solvent (H_2O) and the adsorbate occupy equal areas on the electrode surface. The probable explanation of this result is that a group of bonded H_2O molecules instead a single water molecules occupies one adsorption

site on the mercury and "mercury-like" metal surface. From the thermodynamic standpoint this may mean that the work of transfer of the associated molecules from the surface into the volume is less than the total work of transfer of all the solvent molecules individually [1–34]. This view is supported by the sigmoid shape of the isotherms of H_2O vapor adsorption from the gas phase on Hg [35] as well by the quantum chemical calculations of H_2O adsorption at metal clusters [36] indicating considerable attraction between the adsorbed H_2O molecules. Guidelli and co-workers [37,38] and Nikitas [39,40] have shown that the models which treat the solvent as distinct entities and with strong lateral hydrogen bond interactions predict an apparent Frumkin behavior. The concept of associated H_2O molecules adsorbed on Hg and "Hg-like" metal surfaces justifies, to the first approximation, the use of the Frumkin isotherm as the semiempirical basis for the examination of the adsorption of organic molecules at the electrolyte–electrode interface in the form

$$B_A^{0,F} c_A = \frac{\theta_A}{1-\theta_A} \exp(-2a\theta_A) \tag{4}$$

where $B_A^{0,F}$ is the adsorption equilibrium constant of the organic compound at zero charge potential $E = 0$; $\theta_A = \Gamma_A/\Gamma_{A,max}$ is the surface coverage of the organic compound at the electrode surface and a is a certain quantity characterizing the interaction between the adsorbed particles at $E = 0$. In this case the following equation of state is valid

$$\pi = \nu_{\theta_A=0} - \nu_{\theta_A} = -RT\Gamma_{A,max}\left[\ln\left(1-\frac{\Gamma_A}{\Gamma_{A,max}}\right) + a\left(\frac{\Gamma_A}{\Gamma_{A,max}}\right)^2\right] \tag{5}$$

where $\pi = \Delta\nu = \nu_{\theta_A=0} - \nu_{\theta_A}$ is the surface pressure of the film of adsorbed adsorbate molecules equal to the decrease of the surface tension $\Delta\gamma$ caused by the addition of adsorbate to solution.

To verify the applicability of the Frumkin adsorption isotherm and to obtain the values of $B_A^{0,F}$ and a usually the value of $\ln[\theta_A/(1-\theta_A)c_A]$ is plotted against θ_A and the slope of this linear dependence ($0.1 < \theta_A < 0.8$) gives the molecular interaction parameter ($-2a$) and the intercept provides the adsorption equilibrium constant ($\ln B_A^{0,F}$) at $E = 0$.

The Gibbs energy of adsorption of the organic compound corresponding to the standard state being the unit mole fraction of the organic species in the bulk ($X_A = 1$) and the monolayer coverage ($\theta_A = 1$) of the ideal noninteracting adsorbate [22–26] has been obtained by

$$\Delta G_A^0 = -RT\ln(B_A^{0,F} \times 55.5) \tag{6}$$

The preference of this choice of standard state is that the determined Gibbs energies can be easily compared with the literature data, because the adsorption behavior of many organic substances at the solution–electrode interface has been described by the classical Frumkin isotherm [1–21]. The disadvantage of this standard state is that the ΔG_A^0 values depend on the magnitude of the limiting Gibbs excess, $\Gamma_{A,max}$ (limiting surface concentration) [8,20,23–26]. Consequently, when the values of ΔG_A^0 for different organic compounds are compared, some of the observed differences are caused by the variation of the $\Gamma_{A,max}$ values. For the organic compounds discussed in this paper, the changes of $\Gamma_{A,max}$ values never exceed 30 to 40%, and the changes of the reported values caused by the variation of $\Gamma_{A,max}$ will never be greater than ± 0.8 kJ mol^{-1}, which is of the same order as the error in the determination of experimental ΔG_A^0 values and, to the first approximation, the influence of $\Gamma_{A,max}$ to ΔG_A^0 values can be ignored. A more detailed discussion about the influence of $\Gamma_{A,max}$ to the ΔG_A^0 values for organic compounds will be given in the following paper.

For a more profound solution of the problem connected with the experimental determination of the value of n, a generalized Frumkin isotherm must be used [41–43]

$$B_A^0 c_A = \frac{\theta_A}{n(1-\theta_A)^n} \exp(-2a\theta_A) \tag{7}$$

in which it is taken into account that n solvent molecules are displaced from the surface when one organic molecule is adsorbed. As shown in [37,38] this isotherm can be obtained from the random mixing approximation (RMA) taking into consideration the different sizes of solvent and solute molecules. To verify the generalized Frumkin adsorption isotherm, represented by Eq. (7), the value of $\ln[\theta_A/n(1-\theta_A)^n c_A]$ is plotted against θ_A at various values of n and the more linear isotherm at n = const. would be selected. An analysis of many experimental data of simple aliphatic compounds adsorption on Hg and "Hg-like" metals shows that the experimental values of n are very close to unity [1–8,14,44–46].

A more convenient method for establishing the deviation of the real experimental system from the Frumkin model would be to compare the experimental impedance data with a more general equation for the description of the adsorption behavior of organic compounds at the metal–electrolyte interface from which the various surface layer models (Frumkin [8,9], Hansen [47] and Parsons [41,42] models) could be obtained as particular cases. Such an equation can be written as follows:

$$\sigma = \frac{[C_0(1-\theta_A) + nC_1\theta_A]E - nC_1E_N[k(1-\theta_A)]\theta_A}{1 + n\theta_A - \theta_A} \tag{8}$$

where σ is the surface charge density; n and k are the parameters, characterizing the deviation of the real system from the various simplified theoretical models noted be-

fore [8,9,41,42,47]; C_0 and C_1 are the values of differential capacity at $\theta_A = 0$ and at $\theta_A = 1$, respectively, and E_N is the limiting adsorption potential equal to the change of the zero charge potential due to the displacement of a monolayer of water molecules by a monolayer of organic compound. It should be pointed out that the parameters n and k, in the case of adsorption of simple monofunctional aliphatic compounds at Hg and "Hg-like" metals investigated in this work does not differ very much from unity [8,9,44,45] and therefore the corrections to parameters, obtained by the classical Frumkin model, would be made according to Eqs. (9a), (9b) and (9c):

$$A_A = A_A^F\, 4n/(n+1)^2 \tag{9a}$$

$$E_N = E_N^F\, 4/[4-(n-1)(k-1)] \tag{9b}$$

$$B_A^0 = B_A^{0,F}/n \tag{9c}$$

where $A_A^F = RT\Gamma_{A,max}$ and the superscript F denotes the effective parameters of organic compound adsorption, obtained according to the classical Frumkin isotherm and the Frumkin–Damaskin adsorption theory [1–9,40–48]. In this work the corrected values of B_A^0 and a have been used to establish the values of Gibbs energy of adsorption ΔG_A^0 of some organic compounds at various polycrystalline and monocrystalline electrodes.

A somewhat different method for obtaining the value of n has been discussed in Refs. [39,40,49] where the adsorption isotherms have been expressed in the terms of the molar fraction of the organic compound in the adsorption state $X_{A,ads}$ and of the solvent in the adsorption state $X_{sol,ads}$ by the following equations:

$$X_{A,ads} = \frac{\theta_A}{n-(n-1)\theta_A} \text{ and } X_{sol,ads} = 1 - X_{A,ads} \tag{10}$$

As found in Refs. [39,40,49] the values of n for 2-butanol and for other simple organic compounds are very close to unity.

Thus, at the first approximation we assume that the adsorption of one organic molecule at the electrode surface causes the desorption not a single solvent molecule but their groups, and the Gibbs adsorption energy of the uncharged organic compound on the uncharged metal–electrolyte interface can be expressed as

$$\Delta G_A^0 = \Delta G_{air}^0 + \Delta G_{sol}^0 + \Delta G_{Me-A}^0 - \Delta G_{Me-H_2O}^0 \tag{11}$$

where the value of the Gibbs energy of the metal–water interaction $\Delta G_{Me-H_2O}^0$ (hydrophilicity) corresponds to the model that the value of $n \approx 1$.

The value of ΔG_{air}^0 depends on the molar volume of the adsorbate, its molecular structure and the presence of hydrophilic (polar) groups on it, because the solution of the organic compound in water (electrolyte solution) breaks the hydrogen bonds between the associated water molecules and therefore changes both the entropy and the internal energy of water. ΔG_{Me-A}^0 is determined by the geometrical and electronic structure of the adsorbate, as well as by the chemical and crystallographic structure of the electrode surface. $\Delta G_{Me-H_2O}^0$ depends on the hydrophilicity of the electrode, i.e. on the H_2O–metal interaction energy, and on the adsorbed layer structure of the monolayer of water molecules at the metal surface. Consequently, the Gibbs adsorption energy of the organic compound ΔG_A^0 is determined by the physical and chemical properties of the adsorbate, as well as by the chemical nature and crystallographic structure of the electrode surface. To establish the values of $\Delta G_{Me-H_2O}^0$ and ΔG_{Me-A}^0 it is necessary to obtain the ΔG_{air}^0 and ΔG_{sol}^0 values [1,2,8,18–20,27,28].

2.2. Gibbs energy of adsorption of organic compound at the air–solution interface

Usually the Gibbs energy of adsorption of organic molecules at the air–solution interface (without electrolyte) has been calculated from the initial part of the $\pi(\ln c_{org})$ curves, where the adsorption of organic compound is very small ($\theta_A \sim 0$) and the Henry isotherm is valid

$$\Gamma_A/\Gamma_{A,max} = B_A^H c_A \tag{12}$$

where B_A^H is the adsorption equilibrium constant of organic compound A at the air–solution interface. It must be noted that in the limit of zero coverage the Henry, Langmuir and Frumkin isotherms, describing the adsorption from solution, reduce to the Henry isotherm [23,46]. At these conditions the following equation of state is valid:

$$\pi = RT\Gamma_A \tag{13}$$

and the adsorption equilibrium constant is related to the standard Gibbs energy of adsorption through the equation

$$\Delta G_A^H = -RT \ln B_A^H \tag{14}$$

To obtain the values of Gibbs energy of organic compound adsorption at the air–solution interface ΔG_A^0 at the similar standard state as in the case of adsorption at the metal–solution interface (Frumkin isotherm, $X_A = 1$; $n = 1$ and $\theta = 1$ for ideal noninteracting adsorbate) the Eq. (13) should be rewritten in the following form [20,23,24]:

$$\pi = RT\Gamma_{A,max} B_A^H c_A/55.5 = RT\Gamma_{A,max} B_A^H X_A \tag{15}$$

where X_A is the mole fraction of the organic species in the bulk of solution.

In this work the values of π have been obtained by the maximum bubble pressure method for solutions without addition of surface inactive electrolyte and also by the drop weight method [50]. The coincidence of the π values obtained by these two methods was good. The statistically treated $\pi(X_A)$ curves at low mole fractions have been differentiated by the computer. Thereafter the values of ΔG_{air}^0 have been calculated according to Eqs. (14) and (15). The error analysis shows that at higher values of $\ln c$

the values of π can be obtained with an accuracy of ± 0.2 μJ cm^{-2}.

The values of $\Gamma_{A,max}$ have been obtained from the slope of the linear part of the $\pi(\ln c_A)$ dependence at the region of high $\ln c_A$ according to the Gibbs relation

$$\Gamma_A = \frac{1}{RT}\left(\frac{\partial \pi}{\partial \ln c}\right)_{T,P} \quad (16)$$

The $\pi(\ln c)$ dependences have a good linearity at higher $\ln c$ values and therefore the values of $\Gamma_{A,max}$ are quite precise [12,17,20]. The standard deviation for $\Gamma_{A,max}$ has been obtained from the linear regression analysis and it may be summarized that the maximum error of $\Gamma_{A,max}$ varies from $\pm 0.3 \times 10^{-10}$ to $\pm 0.5 \times 10^{-10}$ mol cm^{-2}. Therefore the maximum error for ΔG^0_{air} is not over ± 0.5 kJ mol^{-1}. The values of ΔG^0_{air} for aliphatic alcohols and carboxylic acids obtained in this work are in a good agreement with those presented in Refs. [4,6,27,28,30–33]. The errors are: $\Delta(\Delta G^0_{air})_{\text{aliphatic alcohols}} = \pm 0.5$ kJ mol^{-1}, $\Delta(\Delta G^0_{air})_{\text{carboxylic acids}} = \pm 0.6$ kJ mol^{-1}.

As shown in Refs. [27,28], in the case of linear aliphatic compounds —alcohols (AA), esters (AE), ketones (AK), amines (AAM) and carboxylic acids (ACA)— the values of ΔG^0_{air} at the first approximation can be obtained by the following generalized correlation equation

$$\Delta G^0_{air} = -0.8 R_A(1 - 2.5 \cdot 10^{-3} R_A) \quad (17)$$

where the molar refraction of the organic compound

$$R_A = M(n_D^2 - 1)/d(n_D^2 + 2) \quad (18)$$

In Eq. (18) n_D is the refractive index, M is the molar mass, and d is the density of the organic compound.

The values of ΔG^0_{air} obtained by Eqs. (15) and (17) coincide with one another with the accuracy of ± 0.5 kJ mol^{-1} [54].

The $\Delta G^0_{air}(R_A)$ dependences for the homologues series of various organic compounds are presented on Fig. 2. The values of ΔG^0_{air} have been calculated according to Eqs. (14) and (15) using the experimental $\pi(\ln c)$ dependences. The chemically different organic compounds give us different linear $\Delta G^0_{air}(R_A)$ plots with the values of correlation coefficient R^2 varying from 0.9308 for AA to 0.9889 for ACA. But the dependence of ΔG^0_{air} on the chemical nature of adsorbate is very weak and at the first approximation the collection of all experimental ΔG^0_{air} data can be described with the common $\Delta G^0_{air}(R_A)$ dependence with a correlation coefficient $R^2 = 0.9686$. The maximum standard deviation for ΔG^0_{air} obtained from the linear regression analysis is ± 0.5 kJ mol^{-1}, which is in the same order as the precision of determination of experimental values of ΔG^0_{air}.

2.3. Salting-out effect of adsorbate and the method for obtaining ΔG^0_{sol} values

The values of ΔG^0_{sol} have been calculated according to the equation

$$\Delta G^0_{sol} = -2.3 RTK_{sol} c_{sol} \quad (19)$$

where K_{sol} is the salting-out constant of adsorbate and c_{sol} the concentration of the surface inactive electrolyte. The correction of the experimental ΔG^0_A values by the ΔG_{sol} term is indispensable as the adsorption behavior of various organic compounds at different polycrystalline (PC) electrodes have been studied from various electrolyte solutions (in surface inactive electrolytes with different chemical composition and ionic strength I) and there are no systematic experimental adsorption data for one fixed electrolyte at I = const. Moreover the values of Gibbs energy of adsorption at the air–solution interface ΔG^0_{air} have been

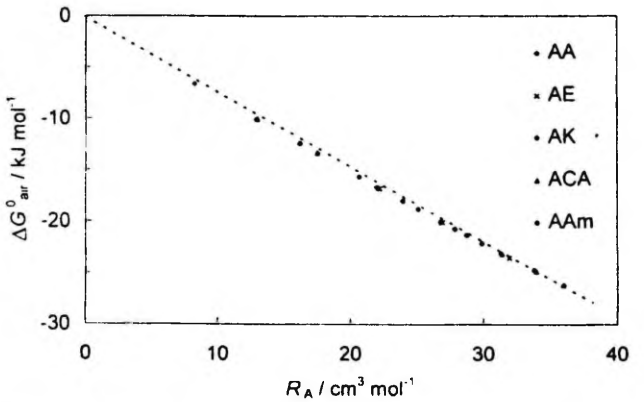

Fig. 2. Dependence of the Gibbs energy of organic compound adsorption at the air–solution interface ΔG^0_{air} (without addition of surface inactive electrolyte) on the molar refraction R_A of various aliphatic compounds.

mainly obtained at the condition $I = 0$. But as established in Refs. [1,8,9,51–64] the values of B_A^0 and therefore the values of ΔG_A^0 depend on the chemical nature and concentration of the surface inactive electrolyte.

Using the Setchenov's law ($\log S^0_{A,I=\text{const}} = \log S^0_{A,I=0} + K_{sol}c_{sol}$ where $\log S^0_{A,I=\text{const}}$ and $\log S^0_{A,I=0}$ are the solubilities of the organic compound in solution at $I = \text{const.}$ and at $I = 0$, respectively, the value of the adsorption constant at $I = \text{const.}$ can be expressed as

$$\log B^0_{A,I=\text{const}} = \log B^0_{A,I=0} + K_{sol}c_{sol} \quad (20)$$

where $B^0_{A,I=0}$ is the adsorption equilibrium constant at $I = 0$ [56,59]. The values of K_{sol} have been calculated from the dependence of the potential of adsorption–desorption maximum of the organic compound E^{max} on the concentration of the surface inactive electrolyte solution c_{sol}. At the minimum of the $E^{max}(\log c_{sol})$ dependence the value of term $(\partial E_{max}/\partial \log c_{sol})_{c_A} = 0$ and K_{sol} can be obtained according to the following equation [56,59]:

$$2.3K_{sol} = \frac{4A}{FT_{max}\sqrt{c_{sol}}}\sinh^2\left[\frac{1}{2}\operatorname{arcsinh}\left(\frac{\sigma_0}{2A\sqrt{c_{sol}}}\right)\right] \quad (21)$$

where $A = \sqrt{\epsilon RT/2\pi}$ and ϵ is the dielectric constant of the solvent, σ_0 is the charge density of the electrode in the surface inactive electrolyte solution. A more detailed discussion is given in Refs. [56,59].

According to the experimental data [27,28,55,56,59], at the first approximation it can be supposed that the dependence of K_{sol} on the chemical nature of the aliphatic compound studied is weak and so the following values of K_{sol} have been used [27,28,55,56,59]: $K_{sol}(Na_2SO_4) = 0.37$; $K_{sol}(H_2SO_4) = 0.1$; $K_{sol}(NaF) = 2.8$. Thus, the following corrections to ΔG_A^0 values have been made in kJ

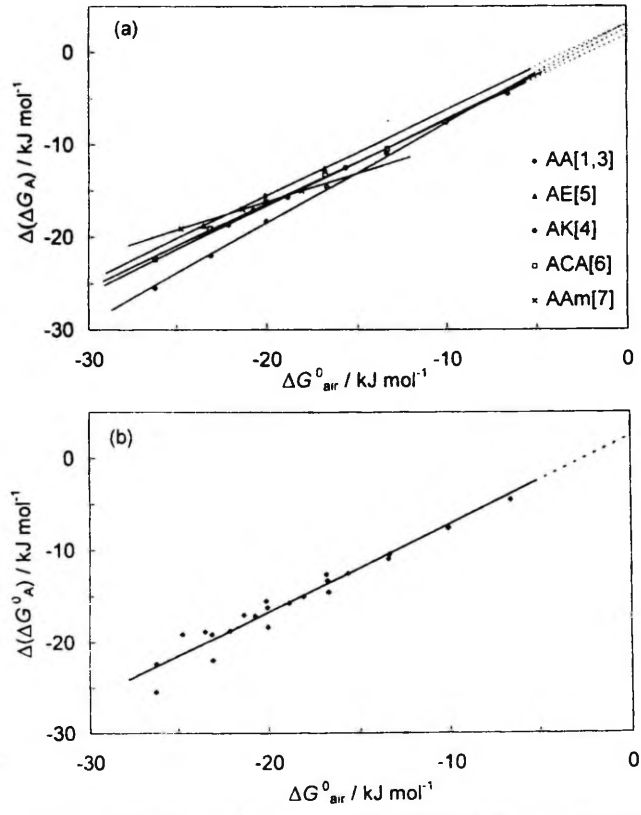

Fig. 3. $\Delta(\Delta G_A^0), \Delta G_{air}^0$ dependences of adsorption of various aliphatic compounds at a PC-Bi electrode (a) (notation of compounds and references in the figure). Common $\Delta(\Delta G_A^0), \Delta G_{air}^0$ dependence of organic compound adsorption at a PC-Bi electrode (b).

mol^{-1}; ΔG^0_{sol}(0.05M Na_2SO_4) = 0.21; ΔG^0_{sol}(0.04M Na_2SO_4 + 0.01M H_2SO_4) = 0.17; ΔG^0_{sol}(0.1M NaF) = 1.60; ΔG^0_{sol}(0.4M Na_2SO_4 + 0.1M H_2SO_4) = 1.70; ΔG^0_{sol}(0.5M Na_2SO_4) = 2.10; ΔG^0_{sol}(0.5M H_2SO_4) = 0.57.

Comparison of the adsorption data for AA, ACA and AE from the solutions with different concentration and chemical composition of various surface inactive electrolytes on Hg and PC-Bi electrodes [1,2,8,27,28,56–63] shows that the values of ($\Delta G^0_A - \Delta G^0_{sol}$) can be established with an accuracy of $\pm$0.3 kJ mol^{-1}.

2.4. ($\Delta G^0_A - \Delta G^0_{sol}$), ΔG^0_{air} plots for Hg and polycrystalline Bi electrode

Using the data of Refs. [1–7] the values of ($\Delta G^0_A - \Delta G^0_{sol}$) $\equiv \Delta(\Delta G^0_A)$ calculated by Eqs. (6), (7), (19) and (20) and Eq. (21) have been used for constructing of the $\Delta(\Delta G^0_A)$, ΔG^0_{air} dependences for polycrystalline Bi (PC-Bi) and Hg electrodes (Figs. 3 and 4). As it can be seen on Figs. 3 and 4, the different classes of aliphatic organic compounds give different linear dependences with the correlation coefficient varying from 0.938 for AA (PC-Bi) to 0.999 for AAM (PC-Bi). At higher absolute values of ΔG^0_{air} = const. $\Delta(\Delta G^0_A)$ depends on the chemical nature of the organic compound studied and the adsorption activity of organic molecules at the PC-Bi–solution interface increases in the order: AAM ≤ AE < ACA < AK < AA and at the Hg–solution interface in the order: AE < ACA < AK < AA. This effect is usually explained by the weak specific interaction between the functional group of the adsorbate and the surface atoms of the electrode. But in the case of adsorption of AAM, ACA, AK and AE on PC-Bi,

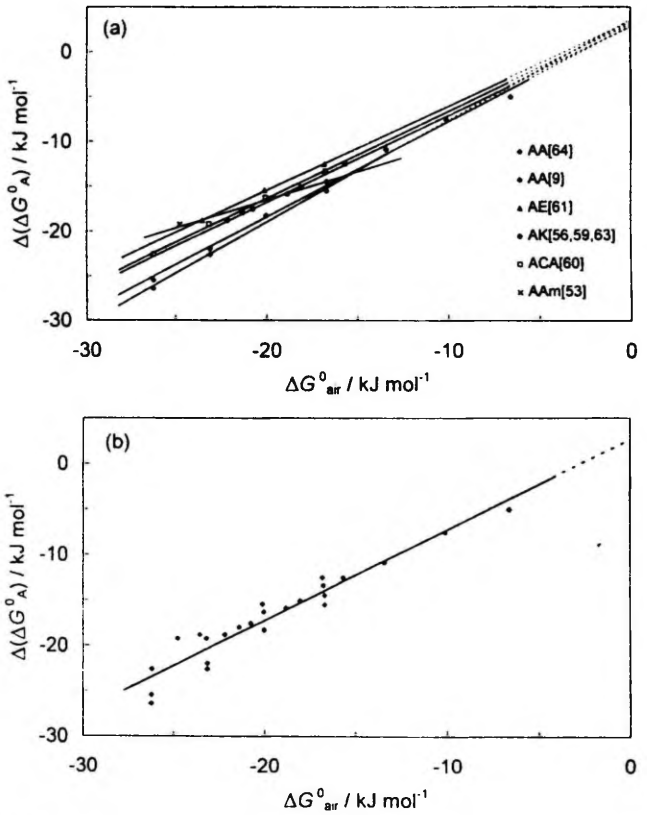

Fig. 4. $\Delta(\Delta G^0_A)$,ΔG^0_{air} dependences of adsorption of various aliphatic compounds at a Hg electrode (a) (notation of compounds and references in the figure). Common $\Delta(\Delta G^0_A)$,ΔG^0_{air} dependence of aliphatic compound adsorption at Hg (b).

Table 1
Electric double layer and adsorption parameters for various electrodes

Electrode	Compound	$\Delta G^0_{Me\cdot A} - \Delta G^0_{Me\cdot H_2O}$ (kJ mol^{-1}) ±0.6	$\Delta\bar{G}^0_{Me\cdot A} - \Delta\bar{G}^0_{Me\cdot H_2O}$ (kJ mol^{-1}) ±0.6	$-\Delta G^0_{Me\cdot H_2O}$ (kJ mol^{-1}) ±0.6	W_z (eV) ±0.25	ΔX (V)	$E_{\sigma=0}$ (V) ±0.01 (SHE)	W_e^* (eV) (Eq. (24))	W_e^* (eV) (Eq. (25))	ΔX^* (V) (Eq. (24))	ΔX^* (V) (Eq. (25))	$l_H = 1/4\pi C_H$ (nm)
PC-Bi	AA [1,3]	2.9	2.4	2.4	4.40	0.070	−0.38	4.38		0.075		0.034
	AK [4]	2.2										
	AE [5]	3.0										
	ACA [6]	1.8										
Hg	AA [8]	3.9	2.7	2.7	4.49	-	−0.193	-		-		0.029
	AA [9]	2.9										
	AK [36]	2.6										
	AE [34,37]	3.3										
	ACA [32,33]	3.1										
PC-Sb	AA [2]	2.3	-	2.3	4.55	0.020	−0.395	4.55		0.020		0.035
PC-Sn	AA [67]	2.9	-	2.9	4.42	0.125	−0.395	4.37		0.085		0.024
In(Ga)	AA [73]	2.8	-	2.8	4.12	0.095	−0.650	4.17		0.150		0.014
PC-Pb	AA [66]	3.4	-	3.4	4.21	0.130	−0.605	4.25		0.170		0.028
PC-Cd	AA [68–70]	3.7	-	3.7	4.22	0.260	−0.735	4.11		0.165		0.040
Zn(0001)	AA [71,72]	3.9	-	3.9	4.90	0.960	−0.775	4.08	4.24	0.180	0.320	0.007
PC-Zn	AA [79]	-	-	-	4.33	0.450	−0.795	4.07	4.21	0.180	0.325	0.005
Ga	AA [74]	-	-	-	4.20	0.210	−0.690		4.15		0.160	0.006

($\Delta G^0_{Me\cdot A} - \Delta G^0_{Me\cdot H_2O}$): difference between the Gibbs energy of organic compound interaction with metal ($\Delta G^0_{Me\cdot A}$) and the Gibbs energy of water adsorption at the electrode surface ($\Delta G^0_{Me\cdot H_2O}$).
$-\Delta G^0_{Me\cdot H_2O}$: Gibbs energy of water adsorption at metal, if $\Delta G^0_{Me\cdot A} = 0$.
W_z: work function into UHV.
ΔX: relative interfacial parameter [21,77–79].
$E_{\sigma=0}$: zero charge potential.
W_e^*: electrochemical work function, obtained according to Refs. [21,77–79].
ΔX^*: relative interfacial parameter, obtained from electrochemical data according to Refs. [21,72–75].
l_H: thickness of inner layer in surface inactive electrolyte at $E_{\sigma=0}$.

this interaction very weakly depends on the length of the hydrocarbon chain (except the methanoic and ethanoic acids [62]), as the values of the slope of the $\Delta(\Delta G_A^0)$, ΔG_{air}^0 dependence for these compounds are very close to unity (from 0.996 to 1.003). Therefore the increase of the adsorption activity of adsorbate at the PC-Bi | solution interface with increasing length of the hydrocarbon chain is caused mainly by the increase of the adsorption activity of the organic compound at the air | solution interface. In the case of AA adsorption, the slope of the $\Delta(\Delta G_A^0)$, ΔG_{air}^0 dependence is noticeably higher than unity (1.110), and so the adsorption activity at the metal–electrolyte interface increases faster than at the air | solution interface. Probably it is caused mainly by the weak specific interaction of the AA functional group with the surface atoms of PC-Bi, which increases when the vertical orientation of AA molecules decreases with the lengthening of the AA hydrocarbon chain. This conclusion is also valid in the case of AA and ACA adsorption at the Hg electrode [8,18,19,64] (Fig. 4). Adsorption behavior of AAM at PC-Bi and Hg electrodes is somewhat different from other aliphatic compounds studied as the slope of the $\Delta(\Delta G_A^0)$, ΔG_{air}^0 dependence is very slow in comparison with other compounds (for PC-Bi the slope is equal to 0.632 and for Hg 0.622). Accordingly the adsorption activity of AAM at the air–solution interface with increasing length of hydrocarbon radical increases faster than at the metal–electrolyte solution interface.

The values of $(\Delta G^0_{Me\ -\ A} - \Delta G^0_{Me-H_2O})$ have been obtained by the extrapolation of the linear $\Delta(\Delta G_A^0)$, ΔG_{air}^0 dependence to $\Delta G_{air}^0 \rightarrow 0$. According to the data of Figs. 3 and 4, at $\Delta G_{air}^0 = 0$ the dependence of $\Delta(\Delta G_A^0)$ on the chemical nature of the adsorbate is very weak and at the first approximation one can assume that $\Delta G^0_{Bi-A} \approx$ const. or the difference between ΔG^0_{Bi-A} values for various aliphatic compounds does not exceed ± 0.6 kJ mol^{-1}, which is comparable with the total error of obtaining $\Delta(\Delta G_A^0)$ values for the PC-Bi electrode (± 0.4 kJ mol^{-1} for the same metal). The values of $(\Delta G^0_{Me-A} - \Delta G^0_{Me-H_2O})$ obtained by the extrapolation of the $\Delta(\Delta G_A^0)$, ΔG_{air}^0 dependence to $\Delta G_{air}^0 \rightarrow 0$ are presented in Table 1. It must be noted that the experimental adsorption data for various organic compounds at PC-Bi can be described by a total $\Delta(\Delta G_A^0)$, ΔG_{aq}^0 dependence with a not very bad correlation coefficient $R^2 = 0.956$ (Fig. 3b). As it can be seen, the value of $(\Delta G^0_{Me\ -\ A} - \Delta G^0_{Me-H_2O})$ obtained from this total dependence very well corresponds with the values obtained from $\Delta(\Delta G_A^0)$, ΔG_{air}^0 dependences for different compounds (Table 1). The difference between the values of $(\Delta G^0_{Hg\ -\ A} - \Delta G^0_{Hg\ -\ H_2O})$ obtained by the extrapolation of the $\Delta(\Delta G_A^0)$, ΔG_{air}^0 dependence to $\Delta G_{air}^0 \rightarrow 0$ for various organic compounds adsorption on Hg does not exceed ± 0.6 kJ mol^{-1}, which is of the same order as the total experimental error of obtaining $\Delta(\Delta G_A^0)$ values. As in the case of PC-Bi, the experimental adsorption data of various aliphatic compounds at Hg can be described by a total $\Delta(\Delta G_A^0)$, ΔG_{air}^0 dependence with the correlation coefficient $R^2 = 0.966$ and the values of $(\Delta G^0_{Me\ -\ A} - \Delta G^0_{Me\ -\ H_2O})$ are presented in Table 1. According to the data of Fig. 4a, the harmony of $\Delta(\Delta G_A^0)$ values for AA adsorption on Hg established in Refs. [9,64] is good ($\Delta[\Delta(\Delta G_A^0)]$ does not exceed ± 0.7 kJ mol^{-1}).

2.5. $(\Delta G_A^0 - \Delta G_{vac}^0)$, ΔG_{air}^0 plots for adsorption of aliphatic alcohols at various electrodes

The adsorption data for aliphatic alcohols at various polycrystalline electrodes have been used to establish the $(\Delta G^0_{Me\ -\ A} - \Delta G^0_{Me-H_2O})$ values for other "mercury-like" metals, i.e. for PC-Pb [66]; for PC-Sn [67]; for PC-Cd [68–70]; for Zn(0001) [71,72]; for In(Ga) liquid alloy [73]; for Ga [74] and for Ag(111) [18,19,75]. According to the data of Table 1 and Fig. 5, the absolute value of $(\Delta G^0_{Me\ -\ A} - \Delta G^0_{Me-H_2O})$ (obtained by the extrapolation of the $\Delta(\Delta G_A^0)$, ΔG_{air}^0 dependence to $\Delta G_{air}^0 = 0$) seems to increase in the sequence of metals PC-Sb ≤ Hg < PC-Bi ≤ PC-Sn < In(Ga) < PC-Pb < Ga < PC-Cd ≤ Ag(111) < Zn(0001). It must be noted that the position of PC-Pb, Ga and Ag(111) would be seen as probable (but not conclusive) because in the literature there are only a few data for

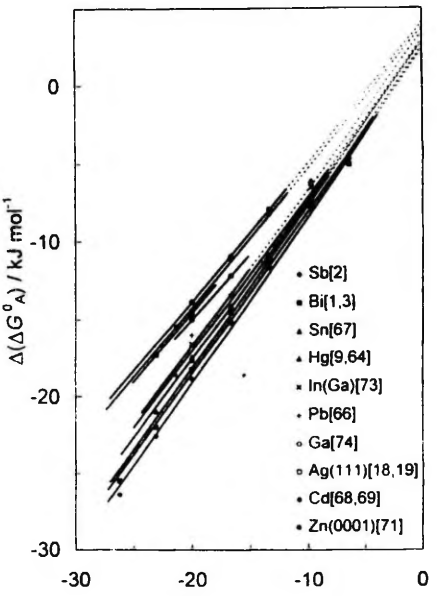

Fig. 5. $\Delta(\Delta G_A^0), \Delta G_{air}^0$ dependences of adsorption of aliphatic compounds at various liquid, polycrystalline and monocrystalline metals (notation of electrodes in the figure).

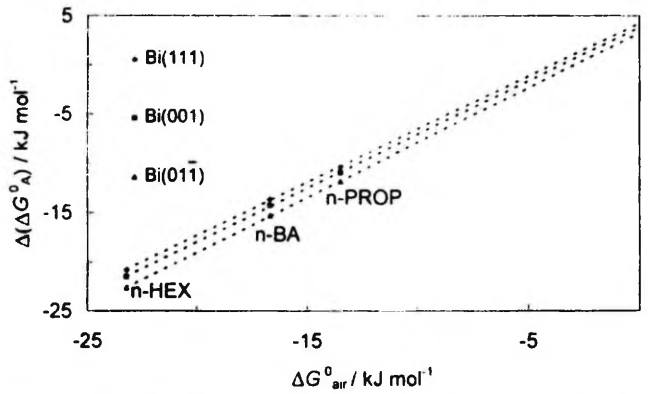

Fig. 6. $\Delta(\Delta G^0_A)$, ΔG^0_{air} dependences of aliphatic alcohol adsorption at bismuth single crystal planes (notation of planes in the figure).

aliphatic alcohol adsorption at these metals (for n-pentanol and n-hexanol at Ag(111) [18,19], for n-butanol and n-pentanol at Ga [74] and PC-Pb [66]) and for this reason the extrapolation of the $\Delta(\Delta G^0_A)$, ΔG^0_{air} dependence to $\Delta G^0_{air} = 0$ is impossible.

If we assume that, to the first (very rough) approximation, the metal–aliphatic alcohol specific interaction energy is metal independent and this interaction is very weak, i.e. $\Delta G_{Me-AA} \approx 0$, then the $\Delta(\Delta G^0_A)$ values at $\Delta G^0_{air} = 0$ would correspond to the Gibbs energy of water adsorption at various electrodes [1–49,51–74]. According to the data of Table 1, the dependence of $\Delta G^0_{Me-H_2O}$ on the chemical nature of the metal is very weak and only for chemically very different metals (for example, PC-Sb or PC-Bi and PC-Cd or Zn(0001)) the difference in $\Delta G^0_{Me-H_2O}$ values is noticeably higher than the total error in obtaining $\Delta(\Delta G^0_A)$. The same order of the hydrophilicity of metals has been established in Refs. [17–21,27,28,48–52]. At

Table 2
Electric double layer and adsorption parameters for various single crystal plane electrodes

Electrode	Ref.	$\Delta G^0_{Me-A} - \Delta G^0_{Me-H_2O}$ (kJ mol^{-1}) ±0.5	W_e (eV) ±0.25	ΔX (V)	$E_{\sigma=0}$ (V) ±0.01 (SHE)	W_e^* (eV) (Eq. (24))	W_e^*/e (V) (Eq. (25))	ΔX^* (V) (Eq. (24))	ΔX^* (V) (Eq. (25))	$l_H = 1/4\pi C_H$ (nm)
Bi(111)		3.6	4.5	0.205	−9.410	4.45		0.085		0.035
Bi(001)	[16.83]	3.4			−0.340	4.40		0.055		0.031
Bi(01$\bar{1}$)		3.0			−0.335	4.41		0.050		0.033
Bi(2$\bar{1}\bar{1}$)		3.1			−0.325	4.42		0.045		0.033
Sb(111)		-	-	-	−0.215	4.50		0.040		0.038
Sb(001)	[16.83]	-	4.7	0.140	−0.125	4.57		0.005		0.032
Sb(01$\bar{1}$)		-	-	-	−0.145	4.55		0.010		0.034
Sb(2$\bar{1}\bar{1}$)		-	-	-	−0.095	4.59		0.000		0.035
Sn(001)		-	-	-	−0.335	4.41		0.060		0.024
Sn(1$\bar{1}$0)	[85]	-	-	-	−0.375	4.38		0.075		0.024
Sn(110)		-	-	-	−0.385	4.37		0.078		0.024
Pb(111)		-	-	-	−0.625	4.19		0.135		0.023
Pb(100)	[86,87]	-	-	-	−0.595	4.21		0.125		0.029
Pb(110)		-	-	-	−0.585	4.22		0.120		0.029
Pb(112)		-	-	-	−0.585	4.22		0.120		0.029
Cd(0001)		-	-	-	−0.715	4.12		0.155		0.023
Cd(10$\bar{1}$0)	[16.83]	-	-	-	−0.765	4.09		0.170		0.019
Cd(11$\bar{2}$0)		-	-	-	−0.775	4.08		0.180		0.018
Zn(0001)		3.9	4.9	0.960	−0.775	4.08	4.24	0.175	0.320	0.007
Zn(10$\bar{1}$0)	[71]				−0.865	4.01	4.15	0.210	0.330	0.003
Zn(11$\bar{2}$0)					−0.875	4.00	4.13	0.215	0.335	0.002

higher negative values of ΔG^0_{ads} ($\Delta G^0_{ads} < -15$ kJ mol^{-1}), the dependence of $\Delta(\Delta G^0_A)$ on the chemical nature of the metal is noticeable and the difference between the values of $\Delta(\Delta G^0_A)$ for different electrodes increases when the adsorption activity (negative value of ΔG^0_{ads}) of organic compound increases. This effect is mainly caused by the fact that with decreasing of the molar volume of adsorbate transformations in the adsorption layer structure (caused by the adsorption of surfactant) are not so noticeable, if the adsorption of large adsorbate molecules occurs. Therefore the difference between adsorption properties of various metals is smaller in comparison with the situation, if the adsorption of large adsorbate molecules takes place.

At Fig. 6, the $\Delta(\Delta G^0_A)$, ΔG^0_{ads} dependences for single crystal bismuth electrodes are presented. According to the data of Table 2, the adsorption energy of H_2O increases in the order of planes Bi(01$\bar{1}$) < Bi(2$\bar{1}\bar{1}$) < Bi(001) < Bi(111), but the dependence of $\Delta(\Delta G^0_A)$ on the reticular density of planes is very weak. Only for planes having a different electron configuration [10–17,54,76] the difference in $\Delta G^0_{Me-H_2O}$ values is somewhat higher than the error in obtaining the $\Delta(\Delta G^0_A)$ values. Comparison of the aliphatic alcohol data for Bi(01$\bar{1}$), Bi(2$\bar{1}\bar{1}$), Bi($\bar{1}$0$\bar{1}$), Bi(001) and Bi(111) planes with the data for Ag(111), Ag(100), Ag(110) [18,19,75] and for Zn(0001), Zn(10$\bar{1}$0) and Zn(11$\bar{2}$0) [71] shows that the hydrophilicity of the electrodes increases in the presented order of planes.

2.6. $\Gamma^*_{A,max}(\Delta G^0_{ads})$ and $\alpha(\Delta G^0_{ads})$ plots

The slight dependence of $\Delta(\Delta G^0_A)$ on the nature of the organic compound studied at ΔG^0_{ads} = const. may be caused

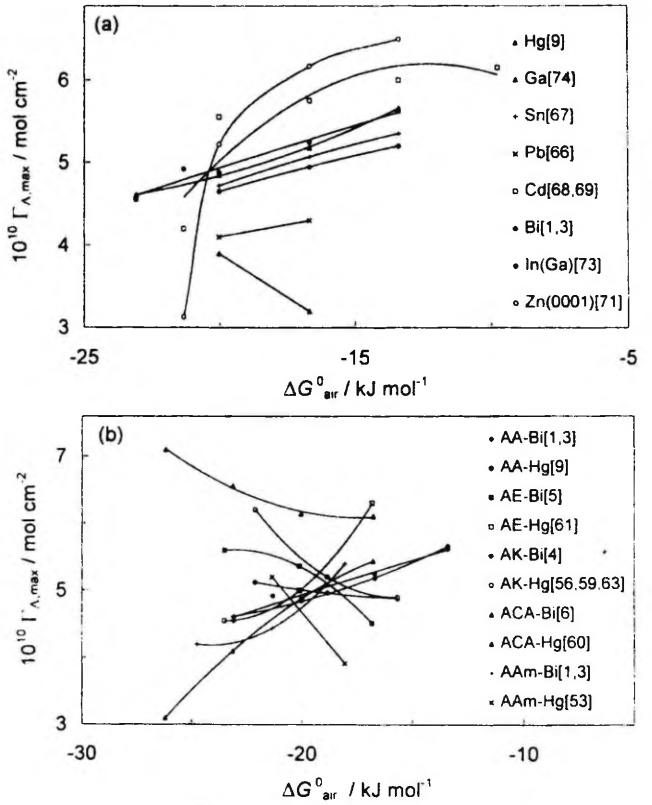

Fig. 7. Dependences of the limiting Gibbs adsorption (Γ^*_{max}) on the Gibbs energy of adsorption at the air–solution interface (ΔG^0_{ads}) for various organic compounds at Bi and Hg electrodes (a) (notation of compounds and electrodes in the figure). $\Gamma^*_{max}(\Delta G^0_{ads})$ dependences of aliphatic alcohol adsorption at various polycrystalline electrodes (b) (notation of metals in the figure).

by the dependence of the limiting surface concentration $\Gamma_{A,max}$ on the nature of the adsorbate [1–21,23–26]. According to the data of Fig. 7, the dependence of $\Gamma_{A,max}$ on the chemical nature and geometrical structure of the adsorbate (hydrocarbon chain structure), as well as on the chemical nature of the metal is very complicated. The value of $\Gamma_{A,max}$ seems to decrease (except ACA, AK and AAM on Hg; AE and ACA on Bi) if the negative value of ΔG^0_{ad} increases. The value of $\Gamma^*_{A,max}$ seems to increase if the hydrophilicity of the electrode metal increases. As noted before, the influence of $\Gamma_{A,max}$ values on ΔG^0_A values will be discussed in the next paper.

According to the data of Fig. 8 the molecular interaction parameter a nearly linearly depends on the ΔG^0_{ad} or $(\Delta G^0_A - \Delta G^0_{ad})$ values (except AK on Hg) and increases when the adsorption activity of the organic compound at the air–solution or at the metal–solution interface increases. The values of a depend on the chemical nature of the electrode metal, as well as on the energetic homogeneity of the surface [1,8,21,46], and at $\Delta G^0_{ad} \leq -20$ kJ mol^{-1} a increases in the order of polycrystalline metals: Sb < Bi < Cd ≤ Sn ≤ Pb < Zn(0001) < Hg, i.e. except Hg and Cd, as $\Delta G^0_{Me-H_2O}$ increases. The interaction parameter a depends on the chemical nature of the aliphatic compound studied [1–21,30–47] (on the structure of hydrocarbon chain and on the chemical nature and structure of the functional group), and in the case of Hg and Bi electrodes, a increases in the order of compounds AA < ACA ≤ AAM < AE < AK. But according to the data of Refs. [1–7,9–21,66–72] the value of a noticeably depends on

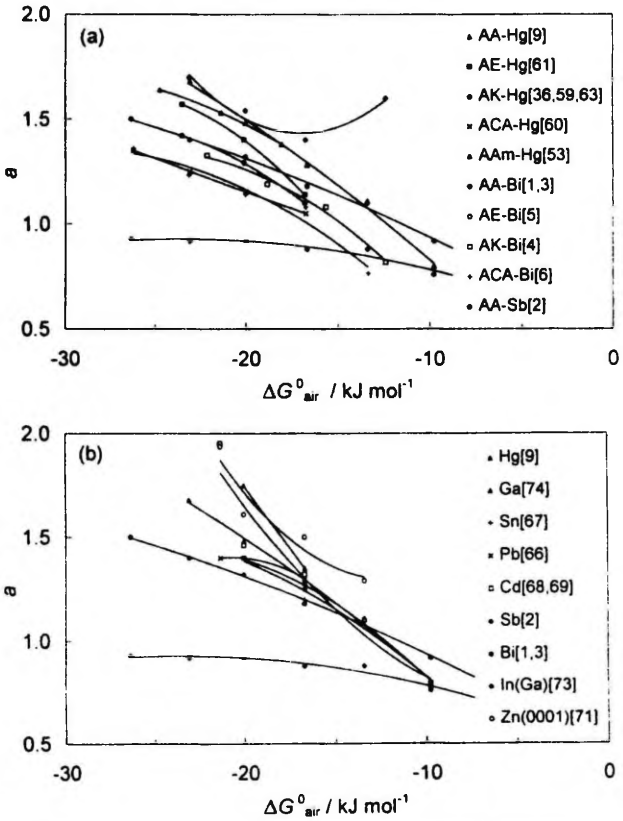

Fig. 8. Dependences of the molecular interaction parameter (a) on the Gibbs energy of organic compound adsorption at the air–solution interface (ΔG^0_{ad}) for various aliphatic compounds at Bi and Hg electrodes (a) (notation of compounds and metals in the figure). $a(\Delta G^0_{ad})$ dependences of adsorption of aliphatic alcohols at various polycrystalline electrodes (b) (notation of metals in the figure).

the crystallographic structure of the electrode surface studied and in the case of polycrystalline electrodes a more detailed discussion is somewhat speculative.

2.7. The interfacial parameter X and the adsorption activity of organic compounds at electrodes

If the potential of zero charge is measured against a given reference electrode, then the following dependence is valid [77–83]:

$$E_{\sigma=0} \text{ vs. ref} = W_e/e + \delta\chi_{Me} + \delta\chi_{sol} + \text{const.} \quad (22a)$$

where W_e is the electron work function in ultra high vacuum (UHV); $\delta\chi_{Me}$ expresses the perturbation of the electron distribution in the thin surface layer at the metal–electrolyte interface; χ_{Me} is the surface potential of the bare metal surface in UHV; $\delta\chi_{sol}$ expresses the change in orientation of the solvent at the metal–electrolyte phase boundary (χ_{sol} is the surface potential at the free surface) and the value of the constant depends on the reference electrode used. Since, the two perturbation terms ($\delta\chi_{Me}$ and $\delta\chi_{sol}$) are specific to the given interface and are experimentally inseparable, they can be grouped into a single quantity X, called the interfacial term [77–79]

$$E_{\sigma=0} \text{ vs. ref} = W_e + X + \text{const.} \quad (22b)$$

As the interfacial parameter X cannot be measured directly, usually the values of X have been obtained from the linear dependence of W_e versus $E_{\sigma=0}$ (SHE). If X were metal independent and equal to the value for Hg, all points should be on a straight line of the unit slope passing through the point of Hg. The $W_e(E_{\sigma=0})$ dependence presented on Fig. 9 has been constructed using the values of $E_{\sigma=0}$ published in Ref. [79] and the values of W_e, recommended in Ref. [84]. The horizontal distance between a given point for a metal M and the straight line of the unit slope measures the difference between $E_{\sigma=0}$ of the given metal corresponding to the point and $E_{\sigma=0}$ of the "hypothetical" metal (lying on the line), with the same work function as metal M, but with the same value of X as Hg [76–78]. Thus, from Eq. (22b) and Fig. 9 we can obtain the relative values of interfacial parameter ΔX

$$\Delta X = X_{Me} - X_{Hg} \quad (23)$$

which coincides with the relative change of W_e between M and Hg upon the different adsorption of water. The values of ΔX obtained are reported in Table 1. If, to a first approximation, we assume that $\delta\chi_{Me}$ is metal independent [77–83], then the hydrophilicity, i.e. the affinity of the metal surface atoms for water molecules increases in the order of the metals: Hg ≤ Sb ≤ Bi < In(Ga) < Sn ≤ Pb < Ga < Cd < Zn. It must be noted that the value of the electronic work function W_e noticeably depends on the crystallographic orientation of the plane as well as on the crystallographic surface structure of the electrode studied, and therefore the surface pretreatment method used has a very noticeable effect. In the case of polycrystalline electrodes from metals with low melting point the accuracy of obtaining W_e values is of the order of ±0.25 eV (sometimes ±0.5 eV). The reproducibility of the $E_{\sigma=0}$ values for solid "mercury-like" metals is noticeably better if mainly two (or three) surface pretreatment methods have been used. Electrochemically (sometimes chemically) polished polycrystalline Sn, Pb, Cd and Zn electrodes have been used [65–72,79] for edl and adsorption studies, the error in the $E_{\sigma=0}$ value is of the order of ±10 mV. Usually polycrystalline Sb and Bi solid drop electrodes

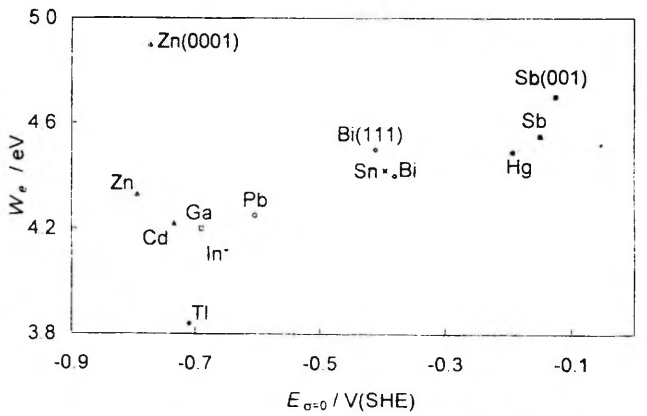

Fig. 9. Dependence of the electron work function (into UHV), W_e, on the potential of zero charge, $E_{\sigma=0}$ (SHE), for various polycrystalline and monocrystalline electrodes (notation of electrodes in the figure). (————) Straight line of the unit slope through the point for Hg.

with a remelted surface in an atmosphere of very pure molecular hydrogen have been used for edl and adsorption studies [1–7]. In this case the error of establishing $E_{\sigma=0}$ is of the order of ± 10 mV and for the value of ΔG_A^0 for organic compound adsorption of the order of ±0.5 kJ mol^{-1}. Sometimes electrochemically polished polycrystalline Sb and Bi electrodes have been investigated. Comparison of $E_{\sigma=0}$ values for polycrystalline Sb and Bi electrodes, prepared by different methods, shows that the error in $E_{\sigma=0}$ is usually ± 15 mV [1–7,82,83].

Fig. 10 shows $\Delta(\Delta G_A^0)$, ΔX plots for various aliphatic alcohol adsorption on various polycrystalline sp-metals. These plots can be considered linear and the adsorption energy of aliphatic alcohol decreases in the order of the metals: Sb ≥ Hg ≥ Bi > In(Ga) ≥ Sn > Pb ≥ Ag(111) > Ga > Cd > Zn, if the water adsorption energy increases. Similar trends have been reported for n-hexanol [19] and for n-pentanol [18,21,78]. But according to the data of Fig. 10, the dependence of $\Delta(\Delta G_A^0)$ on ΔX decreases as the adsorption activity of the aliphatic compound at the air–solution interface decreases. This result is in very good accordance with the data of Fig. 5.

In the literature there are no work function data on the "mercury-like" low melting point sp-metal (Zn, Cd, Sn, Pb) and sp-semimetal (Bi, Sb) single crystal plane electrodes (except Zn(0001), Bi(111) and Sb(001)). For that reason the so-called electrochemical work function W_e^* values for monocrystalline and polycrystalline electrodes have been calculated according to Trasatti's concept [21,77–79]. The electrochemical work function for Sb, Bi, Cd, Sn [85] and Pb [86,87] mono- and polycrystalline electrodes have been obtained according to the equation:

$$E_{\sigma=0} = 1.33W_e^* - 6.20 \quad (24)$$

and for Zn and Ga according to the equation:

$$E_{\sigma=0} = W_e^* - 5.01 \quad (25)$$

The established values of W_e^* for polycrystalline and monocrystalline electrodes are presented in Tables 1 and 2. Comparison of W_e and W_e^* values for polycrystalline Sb, Bi, Cd, Pb, Zn and liquid metal alloys In(Ga) and Ga shows that the accordance is not very bad and, to a first approximation, it was assumed that the values of $E_{\sigma=0}$ for single crystal planes and Eqs. (24) and (25) can be used for obtaining the W_e^* values for single crystal plane electrodes. The values of W_e^* as well as $E_{\sigma=0}$ for Sb, Bi, Cd and Zn planes (except Bi(111) and Sb(111)) increase with the surface atom density of the planes, and this result is in a good accordance with W_e data for Ag, Au and Cu electrodes [76–79]. As seen from Fig. 11, the values of W_e^* for single crystal Zn electrodes calculated according to Eq. (25) do not lie at the same straight line as for Sb, Bi, Pb, Sn and Cd electrodes, and therefore Eq. (24) has additionally been used for obtaining the W_e^* values for Zn single crystal plane electrodes. Values obtained by using Eq. (24) of W_e^* lie at the common for all "mercury-like" metals line and therefore these values have been used additionally for obtaining the ΔX^* values according to Eqs. (22b) and (23) and the method described before. The established values of ΔX^* for single crystal planes are presented in Table 2. As seen, the dependence of ΔX^* on the crystallographic orientation of the plane is weak, but ΔX^* seems to increase with the decrease of the reticular density of the planes. The obtained values of ΔX^* have been used for constructing the $(\Delta G_A^0 - \Delta G_{sol}^0)$, ΔX^* dependence for monocrystalline Sb, Cd, Zn [72], Pb [86,87] and Sn [85] electrodes. Fig. 12 shows that the $\Delta(\Delta G_A^0)$,

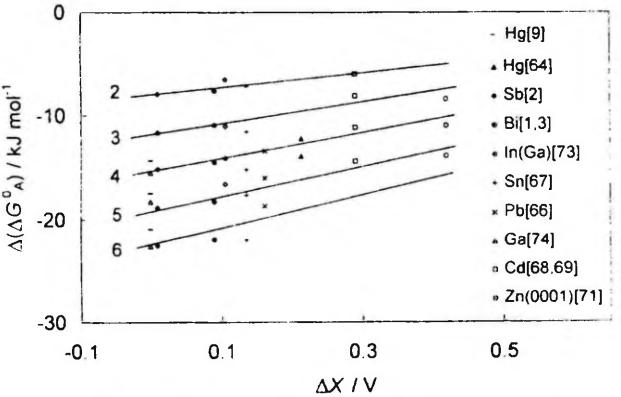

Fig. 10. Dependences of the difference $\Delta(\Delta G_A^0)$ for various alcohols on the relative value of the interfacial parameter ΔX of various metals. The number of each plot denotes the number of carbon atoms of the given aliphatic compound.

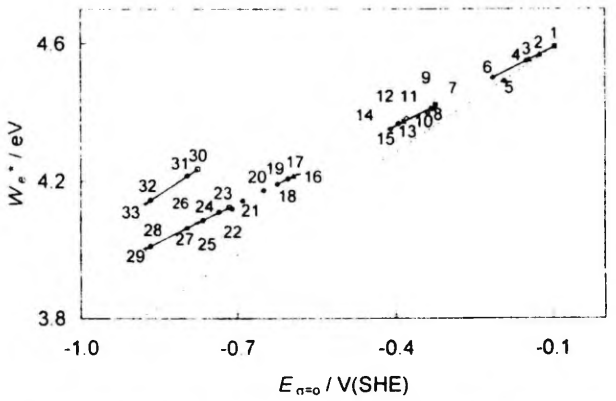

Fig. 11. Dependence of the electrochemical work function W_e^* on the potential of zero charge $E_{\sigma=0}$ for various single crystal and polycrystalline electrodes: 1, Sb(2$\bar{1}\bar{1}$); 2, Sb(001); 3, Sb(01$\bar{1}$); 4, PC-Sb (PC = polycrystalline); 5, Hg; 6, Sb(111); 7, Bi(2$\bar{1}\bar{1}$); 8, Bi($\bar{1}$01); 9, Bi(01$\bar{1}$); 10, Bi(001); 11, Sn(110); 12, PCBi; 13, Sn(1$\bar{1}$0); 14, PC-Sn; 15, Bi(111); 16, Pb(110); 17, Pb(100); 18, PC-Pb; 19, Pb(111); 20, In(Ga); 21, Ga; 22, Tl(Ga); 23, Cd(0001); 24, PC-Cd; 25, Cd(10$\bar{1}$0); 26', Cd(11$\bar{2}$0); 26", Zn(0001); 27, PC-Zn; 28, Zn(10$\bar{1}$0); 29, Zn(11$\bar{2}$0); 30, Zn(0001); 31, PC-Zn; 32, Zn(10$\bar{1}$0); 33, Zn(11$\bar{2}$0). The values of W_e^* 1–29 have been calculated according to Eq. (24) and 30–33 according to Eq. (25).

ΔX^* plots for cyclohexanole adsorption at various metals studied can be considered linear, and the adsorption energy of cyclohexanole decreases when ΔX^* increases. The same tendency is valid for the other compounds adsorption at Bi and Sb monocrystalline electrodes. Thus, the adsorption energy of water at single crystal plane electrodes increases in the order of the metals: Sb < Bi < Sn < Pb < Ag < Cd < Zn, but the difference between Sb, Bi, Sn [85] and Pb [86,87], as well as for Cd and Zn [71] is very small. This result is in a very good accordance with the adsorption data of aliphatic alcohols at polycrystalline Sb, Bi, Sn and Pb electrodes (Fig. 5 and Table 1). In the case of single crystal Sb, Bi, Cd and Zn electrodes the metal–water adsorption energy (except Bi(111) and Sb(111)) increases as the interfacial density of planes decreases, i.e. increases in the order of the electrodes: Sb(2$\bar{1}\bar{1}$) < Sb(001) < Sb(111) < Bi(01$\bar{1}$) < Bi(2$\bar{1}\bar{1}$) < Bi(001) < Bi(111) < Cd(0001) < Cd(10$\bar{1}$0) < Cd(11$\bar{2}$0) < Zn(0001) < Zn(10$\bar{1}$0) < Zn(11$\bar{2}$0). This result is in accordance with the conclusions of Refs. [19,20,77,78] for Ag and Au electrodes.

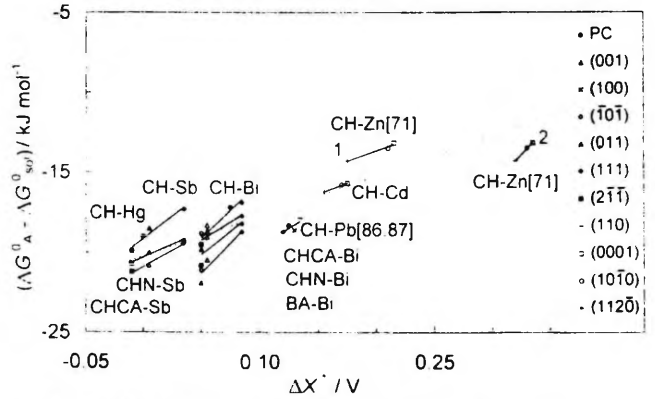

Fig. 12. Dependences of the difference $\Delta(\Delta G^0_A)$ for cyclohexanole (CH), cyclohexanone (CHN) and for cyclohexane carboxylic acid (CHCA) adsorption on the relative value of interfacial parameter ΔX^* for Sb, Bi, Pb, Cd and Zn single crystal plane electrodes. (Notation of planes and metals in the figure.) 1, values of W_e^* and ΔX^* obtained according to the Eq. (24) and 2, according to Eq. (25).

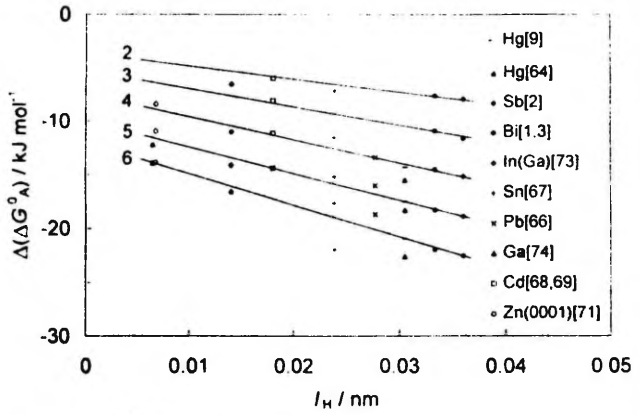

Fig. 13. Dependence of the difference $\Delta(\Delta G^0_A)$ for adsorption of various aliphatic alcohols on the thickness of the inner layer l_H (for the surface inactive electrolyte solution at $E_{\sigma=0}$) for various metals. The number in each plot denotes the number of carbon atoms of the given aliphatic alcohol.

The anomalous position of Sb(111) and Bi(111) planes is probably caused by the different semimetallic nature of various Bi and Sb planes and their work functions include a surface contribution from the space charges. As shown in Refs. [82,83], the value of $\delta\chi_{Me}$ depends noticeably on the crystallographic orientation of Sb and Bi planes, and so the simplification $\delta\chi_{Me}$ = const. is not a good approximation.

The established experimental order of hydrophilicity of Cd and Zn planes is in accordance with the results of quantum chemical calculations of H_2O adsorption at Zn(0001), Zn(10$\bar{1}$0), Cd(0001) and Cd(10$\bar{1}$0) clusters [36], but the experimental order of the metals is in contradiction with the theoretical predictions of these calculations. Comparison of aliphatic alcohol adsorption data for Bi and Zn and Ag data shows that the hydrophilicity of metals increases in the order Bi < Ag < Zn. The direction of the dependence of $E_{\sigma=0}$, ΔX and $\Delta G^0_{Me\ H_2O}$ on the reticular density of Pb planes is a bit surprising, because the Pb crystallizes in the same fcc (face centered cubic) system as

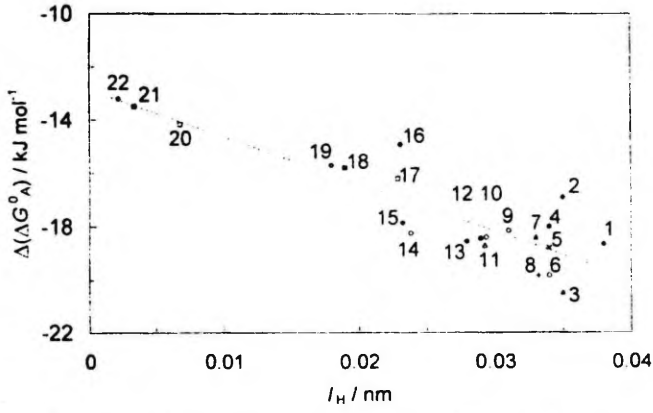

Fig. 14. Dependence of the difference $\Delta(\Delta G^0_A)$ of cyclohexanole adsorption on the thickness of inner layer l_H at $\sigma = 0$ in a solution of surface inactive electrolytes for various electrodes: 1, Sb(111); 2, Bi(111); 3, Sb(2$\bar{1}\bar{1}$); 4, PC-Bi (PC = polycrystalline); 5, Bi(10$\bar{1}$); 6, Sb(001); 7, Bi(2$\bar{1}\bar{1}$); 8, Bi(01$\bar{1}$); 9, Bi(001); 10, Pb(001); 11, Pb(110); 12, Hg; 13, PC-Pb; 14, Sn(001); 15, Pb(111); 16, PC-Cd; 17, Cd(0001); 18, Cd(10$\bar{1}$0); 19, Cd(11$\bar{2}$0); 20, Zn(0001); 21, Zn(10$\bar{1}$0); 22, Zn(11$\bar{2}$0).

Au, Ag and Cu, and for Ag and Au the water adsorption energy increases as the reticular density of planes decreases [18,19,76–78]. But the dependence of W_e^* and E_{M-O} values on the reticular density of the Pb and Sn surface is very weak and future experimental and theoretical simulation of edl and adsorption data are indispensable.

At Figs. 13 and 14 the dependences of $\Delta(\Delta G_A^0)$ on the inner layer thickness l_H ($l_H = 1/4\,\pi C_H^{\prime\prime\,0}$, where $C_H^{\prime\prime\,0}$ is the differential capacity of the inner layer at $E_{\sigma=0}$), i.e. $\Delta(\Delta G_A^0)$, l_H plots are presented. The values of $C_H^{\prime\prime\,0}$ presented in Refs. [16,79,81–83] have been used. According to the data of Figs. 13 and 14, at the first approximation, these plots can be considered linear and the adsorption activity of organic compounds at the electrode–solution interface decreases as the thickness of the double layer decreases, i.e. as the hydrophilicity of the electrode increases. But the slope of $\Delta(\Delta G_A^0)$, l_H plots decreases if the adsorption activity of the aliphatic alcohol at the air–solution interface decreases. This result is in a very good agreement with the data of Figs. 1, 5, 6 and 11. Data for Bi(111) and Sb(111) planes show a noticeable deviation from the general plot which is mainly caused by the more pronounced influence of the capacity of the metal phase of these electrodes in comparison with other Bi and Sb single crystal planes [16,83].

3. Conclusions

A systematic analysis of the influence of the chemical nature of the electrode metal as well as of the hydrocarbon chain structure and the functional group nature to the adsorption characteristics of organic compounds at various electrodes has been carried out. The ingredients of the standard Gibbs energy of adsorption, such as Gibbs energy of adsorption at the air–solution interface; the increase of Gibbs energy of adsorption at the metal–electrolyte interface caused by the addition of surface inactive electrolyte to the solution; the metal–organic compound interaction energy and the metal–water interaction energy have been calculated. It was found that the values of $\Delta(\Delta G_A^0) = \Delta G_A^0 - \Delta G_{ad}^0$ (where ΔG_A^0 was obtained by using the generalized Frumkin isotherm and corresponding to the standard state the unit mole fraction of the organic species in the bulk of solution and monolayer coverage $\theta_A = 1$ of an ideal noninteracting adsorbate) very weakly depend on the chemical nature of the adsorbate; on the chemical properties of the functional group and on the structure of the adsorbed layer. This effect was explained by the weak dependence of $\Delta(\Delta G_A^0)$ on the value of $\Gamma_{A,max}$. Systematic analysis shows that the interaction energy of functional groups >C=O, –COOH, and –COOR with Bi, Cd, Sb, Hg and other "Hg-like" metals is very weak and is practically independent of the length of the hydrocarbon chain (except for HCOOH and CH_3COOH). It was found that the standard Gibbs energy of adsorption of a neutral organic compound which interacts weakly with metals can also be used as a measure of their hydrophilicity. In the case of higher aliphatic alcohols adsorption the more pronounced interaction of the –OH group with the surface atoms is possible [18,19]. But this interaction is very weak in comparison with the interaction established in the case of aromatic compounds studied [1,8,20].

The hydrophilicity of electrodes increases in the sequence of metals PC-Sb ≤ PC-Bi ≤ Hg ≤ In(Ga) ≤ PC-Sn < PC-Pb ≤ Ag(111) < Ga ≤ PC-Cd ≤ Zn(0001). However, the dependence of $\Delta G_{Me-H_2O}^0$ on the chemical nature of the metal is very weak, and only for the chemically more different electrodes (for example PC-Sb and Zn(0001)) the difference in $\Delta G_{Me-H_2O}^0$ values is noticeably higher than the total error of obtaining the $\Delta(\Delta G_A^0)$ values. Approximately the same order of hydrophilicity of the metal has been established in Refs. [7–21,27,28,77–83]. According to the data of cyclohexanol adsorption the hydrophilicity of "mercury-like" and single crystal plane electrodes increases in the order of Sb(01$\bar{1}$) < Sb(001) < Sb(111) < Bi(01$\bar{1}$) < Bi(2$\bar{1}\bar{1}$) < Bi(001) < Bi(111) < Pb(111) < Pb(100) ≤ Pb(110) < Sn(110) < Cd(0001) < Cd(10$\bar{1}$0) < Cd(11$\bar{2}$0) < Zn(0001) < Zn(10$\bar{1}$0) < Zn(11$\bar{2}$0) i.e. with the decrease of the reticular density of planes, except all Pb planes, Bi(111) and Sb(111). The anomalous position of Bi(111) and Sb(111) is mainly caused by the different electronic structure of this plane [10–17,43]. According to the data of aliphatic alcohol adsorption the hydrophilicity of single crystal planes increases in the order of Bi(01$\bar{1}$) < Bi(001) < Bi(111) < Ag(111) < Ag(100) < Ag(110) < Zn(0001) < Zn(10$\bar{1}$0) < Zn(11$\bar{2}$0).

The hydrophilicity of electrodes has been tested using the work function values W_e in UHV as well as the electrochemical work function values W_e^*, obtained according to Trasatti's concept [77–80]. The established relative values of the so-called interfacial parameter ΔX ($\Delta X = (\delta\chi_v + \delta\chi_M)_{Hg} - (\delta\chi_v + \delta\chi_M)_M$) increase in the order of the electrodes Hg ≤ Sb < Bi < In(Ga) < Sn < Pb < Ga < Cd < Zn. Using the established ΔX values and $\Delta(\Delta G_A^0)$ values for various aliphatic compounds for different metals the $\Delta(\Delta G_A^0)$, ΔX dependences have been constructed. At the first approximation these dependences can be considered linear and $\Delta(\Delta G_A^0)$ decreases when the value of ΔX increases. But the slope of $\Delta(\Delta G_A^0)$, ΔX plots decreases if the adsorption activity of the organic compound at the air–solution interface decreases and for n-propanol the difference between $\Delta(\Delta G_A^0)$ values for chemically very different metals (for example, Sb and Zn(0001)) is only somewhat higher than the total error of obtaining the $\Delta(\Delta G_A^0)$ values. This result is in a very good agreement with the data obtained from $\Delta(\Delta G_A^0)$, ΔG_{ad}^0 dependences.

As in the literature there are no work function data for single crystal electrodes, prepared from "mercury-like" metals with low melting point, the electrochemical work function values W_e^* and corresponding ΔX^* values have been obtained according to Trasatti's concept [21,77–80].

As found the value of ΔX^* increases in the order of $Sb(2\bar{1}\bar{1}) < Sb(001) < Sb(111) < Bi(01\bar{1}) < Bi(2\bar{1}\bar{1}) < Bi(001) < Bi(111) < Sn(001) < Pb(112) \leq Pb(110) \leq Pb(100) < Pb(111) < Cd(0001) < Cd(10\bar{1}0) < Cd(11\bar{2}0) < Ag(111) < Ag(100) < Ag(110) < Zn(0001) < Zn(10\bar{1}0) < Zn(11\bar{2}0)$ as the interfacial density of planes decreases, except for single crystal Pb planes, Bi(111) and Sb(111). Using the obtained ΔX^* values and the data of cyclohexanole adsorption at different single crystal electrodes the $\Delta(\Delta G_A^0)$, ΔX^* dependence has been constructed. As found, at the first approximation the adsorption behavior of cyclohexanole at Sb, Bi, Pb, Cd and Zn single crystal plane electrodes can be described by a common linear $\Delta(\Delta G_A^0)$, ΔX^* dependence and accordingly the hydrophilicity of single crystal plane electrodes increases in the order of $Sb(2\bar{1}\bar{1}) < Sb(001) < Sb(111) < Bi(01\bar{1}) < Bi(2\bar{1}\bar{1}) < Bi(001) < Bi(111) < Pb(111) \leq Pb(100) \leq Pb(110) < Cd(0001) < Cd(10\bar{1}0) < Cd(11\bar{2}0) < Zn(0001) < Zn(10\bar{1}0) < Zn(11\bar{2}0)$. Thus, the two different approximations used in this work give practically the same order of the hydrophilicity of the electrodes.

It must be noted that further extensive theoretical and experimental investigations at the metal–UHV, metal–solution and air–solution interfaces are inevitable to obtain the correct quantitative $\Delta G^0_{Me-H_2O}$ values for single crystal Sb, Pb, Sn, Cd, Ag, $Zn(10\bar{1}0)$ and $Zn(11\bar{2}0)$ electrodes.

Acknowledgements

This work was supported in part by Estonian Science Foundation under Project No. 612. The authors wish to thank the referee for useful discussion.

References

[1] U.V. Palm, B.B. Damaskin, Itogi Nauki i Tekhniki, Elektrokhimiya 12 (1977) 99.
[2] V. Past, R. Pullerits, M. Moldau, Trans. Tartu State Univ. 757 (1986) 140.
[3] R.J. Pullerits, M.E. Moldau, U.V. Palm, Elektrokhimiya 11 (1975) 487.
[4] J.J. Ehrlich, U.V. Palm, Elektrokhimiya 10 (1974) 1866.
[5] J.J. Ehrlich, T.E. Ehrlich, U.V. Palm, Elektrokhimiya 11 (1975) 1009.
[6] U.V. Palm, V.E. Past, J.J. Ehrlich, T.E. Ehrlich, Elektrokhimiya 9 (1973) 1399.
[7] J.J. Ehrlich, T.E. Ehrlich, U.V. Palm, Trans. Tartu Univ. 441 (1978) 87.
[8] B. Damaskin, A. Frumkin, A. Chizov, J. Electroanal. Chem. 28 (1970) 93.
[9] B.B. Damaskin, O.A. Petrii, V.V. Batrakov, Adsorption of Organic Compounds on Electrodes, Plenum, New York, 1971, pp. 35–253.
[10] E.J. Lust, A.A.J. Jänes, Russ. J. Electrochem. 30 (1994) 357.
[11] E.J. Lust, U.V. Palm, Sov. Electrochem. 21 (1985) 1304.
[12] E.J. Lust, U.V. Palm, Sov. Electrochem. 22 (1986) 378.
[13] E. Lust, A. Jänes, K. Lust, P. Miidla, J. Electroanal. Chem. 413 (1996) 175.
[14] E.J. Lust, J.J. Ehrlich, U.V. Palm, Sov. Electrochem. 22 (1986) 695.
[15] A.A.J. Jänes, E.J. Lust, Russ. J. Electrochem. 31 (1995) 566.
[16] E. Lust, K. Lust, A. Jänes, Russ. J. Electrochem. 31 (1995) 876.
[17] E. Lust, A. Jänes, P. Miidla, K. Lust, J. Electroanal. Chem. J. Electroanal. Chem. 425 (1997) 25–37.
[18] L.M. Doubova, S. Valcher, S. Trasatti, J. Electroanal. Chem. 376 (1994) 73.
[19] M.L. Foresti, M. Innocenti, R. Guidelli, J. Electroanal. Chem. 376 (1994) 85.
[20] J. Lipkowski, I. Stolberg, in: J. Lipkowski, P.N. Ross (Eds.), Molecular Adsorption at Metal Electrodes, VCH, New York, 1992, p. 174.
[21] S. Trasatti, L.M. Doubova, J. Chem. Faraday Trans. 91 (1995) 3311.
[22] T.N. Andersen, J.O'M. Bockris, Electrochim. Acta 9 (1964) 343.
[23] R. Parsons, Proc. R. Soc. London A 261 (1961) 79.
[24] J. Jastrzebska, M. Jurkiewicz-Herbich, S. Trasatti, J. Electroanal. Chem. 216 (1987) 21.
[25] J. Torrent, F. Sanz, J. Electroanal. Chem. 286 (1990) 207.
[26] U.E. Past, A.A. Alumaa, U.V. Palm, Elektrokhimiya 23 (1987) 568.
[27] B.N. Afanasjev, Yu.P. Akulova, Elektrokhimiya 30 (1994) 1357.
[28] B.N. Afanasjev, Yu.P. Akulova, Elektrokhimiya 30 (1994) 1397.
[29] J.O'M. Bockris, M.V. Devanathan, K. Müller, Proc. R. Soc. London A 274 (1963) 55.
[30] E. Gileadi, J. Electroanal. Chem. 11 (1966) 137.
[31] D.H. Everett, Trans. Faraday Soc. 60 (1964) 1803.
[32] D.H. Everett, Trans. Faraday Soc. 61 (1965) 2478.
[33] S. Trasatti, J. Electroanal. Chem. 53 (1974) 335.
[34] D. Rolle, J.W. Schultze, J. Electroanal. Chem. 229 (1987) 141.
[35] M.E. Nicholas, P.A. Joyner, B.M. Tessem, M.D. Olson, J. Phys. Chem. 65 (1961) 1373.
[36] A.M. Kuznetsov, R.R. Nazmutdinov, M.S. Shapnik, Electrochim. Acta 34 (1989) 1821.
[37] R. Guidelli, J. Electroanal. Chem. 110 (1980) 205.
[38] R. Guidelli, in: J. Lipkowski, P.N. Ross (Eds.), VCH, New York, 1992, p. 1.
[39] P. Nikitas, Electrochim. Acta 32 (1987) 205.
[40] P. Nikitas, J. Electroanal. Chem. 263 (1988) 147.
[41] R. Parsons, J. Electroanal. Chem. 7 (1964) 136.
[42] R. Parsons, J. Electroanal. Chem. 8 (1964) 93.
[43] B.B. Damaskin, Elektrokhimiya 1 (1965) 63.
[44] B.N. Afanasyev, B.B. Damaskin, Elektrokhimiya 12 (1976) 307.
[45] B.B. Damaskin, Yu.N. Kuryakov, Elektrokhimiya 13 (1977) 98.
[46] A. Daghetti, C. Gatti, S. Trasatti, J. Electroanal. Chem. 196 (1985) 179.
[47] R.S. Hansen, D.J. Kelsh, D.H. Grantham, J. Phys. Chem. 67 (1963) 2316.
[48] B.B. Damaskin, A.V. Chizov, Elektrokhimiya 6 (1970) 1741.
[49] P. Nikitas, A. Pappa-Louisi, Electrochim. Acta 34 (1989) 1869.
[50] A.W. Adamson, Physical Chemistry of Surfaces, Wiley–Interscience, New York, 1990, p. 18.
[51] V.M. Gerovich, B.B. Damaskin, Elektrokhimiya 15 (1979) 707.
[52] R.I. Gaganovich, Yu.M. Gerovich, T.G. Osotova, Dokl. Akad. Nauk SSSR 155 (1964) 893.
[53] A.N. Frumkin, B.B. Damaskin, Yu.M. Gerovich, Dokl. Akad. Nauk SSSR 158 (1964) 706.
[54] E. Lust, J. Ehrlich, T. Ehrlich, K. Lust, M. Moldau, R. Pullerits, Proc. of Baltic Conference on Interfacial Electrochemistry, Tartu, 1996, p. 156.
[55] B.N. Afanasjev, DSc Thesis, Technological University of Leningrad, 1975.
[56] O.A. Gusakova, B.B. Damaskin, N.V. Fedorovich, S.D. Pirozkov, Elektrokhimiya 10 (1974) 1112.
[57] A.V. Chizov, B.B. Damaskin, in: A.N. Frumkin, B.B. Damaskin (Eds.), Adsorption and Electrical Double Layer in Electrochemistry, Nauka, Moscow, 1972, p. 55.

[58] N.A. Borovaya, B.B. Damaskin, Elektrokhimiya 8 (1972) 1529.
[59] B.B. Damaskin, E.V. Stenina, V.A. Yusupova, N.V. Fedorovich, Elektrokhimiya 8 (1972) 1409.
[60] A.V. Chizov, C.D. Pirozkov, B.B. Damaskin, in: A.N. Frumkin, B.B. Damaskin (Eds.), Adsorption and Electrical Double Layer in Electrochemistry, Nauka, Moscow, 1972, p. 59.
[61] A.V. Vosekalnš, PhD Thesis, University of Moscow, 1975.
[62] J. Ehrlich, PhD Thesis, University of Tartu, 1975.
[63] O.A. Gusakova, B.B. Damaskin, N.V. Fedorovich, Elektrokhimiya 9 (1973) 1134.
[64] M.R. Moncelli, M.L. Foresti, R. Guidelli, J. Electroanal. Chem. 295 (1990) 225.
[65] J. Setchenow, Z. Physik. Chem. 4 (1889) 117.
[66] N.B. Grigoryev, D.N. Machavariani, Elektrokhimiya 5 (1969) 87.
[67] N.B. Grigoryev, V.P. Kuprin, Yu.M. Loshkaryev, Elektrokhimiya 9 (1973) 1812.
[68] L.E. Rybalka, B.B. Damaskin, D.I. Leikis, Elektrokhimiya 11 (1975) 9.
[69] L.E. Rybalka, B.B. Damaskin, Elektrokhimiya 9 (1973) 1562.
[70] N.B. Obrastsov, Yu.A. Parfenev, F.I. Danilov, Elektrokhimiya 29 (1993) 699.
[71] Yu.P. Ipatov, V.V. Batrakov, V.V. Shalagimov, Elektrokhimiya 12 (1976) 286.
[72] Yu.P. Ipatov, V.V. Batrakov, Elektrokhimiya 11 (1975) 1282.
[73] N.V. Grigoryev, A.M. Kalyuzhnaya, Elektrokhimiya 10 (1974) 1287.
[74] G. Pezzatini, M.R. Moncelli, M. Innocenti, R. Guidelli, J. Electroanal. Chem. 295 (1990) 275.
[75] T. Vitanov, A. Popov, Elektrokhimiya 12 (1976) 319.
[76] W.B. Pearson, The Crystal Chemistry and Physics of Metals and Alloys, Wiley–Interscience, New York, 1972, p. 280.
[77] S. Trasatti, J. Electroanal. Chem. 33 (1971) 351.
[78] S. Trasatti, Electrochim. Acta 37 (1992) 2137.
[79] A.N. Frumkin, Potentsialy Nulevogo Zaryada (Potentials of Zero Charge), Nauka, Moscow, 1979.
[80] A. Frumkin, B. Damaskin, N. Grigor'ev, I. Bagotskaya, Electrochim. Acta 19 (1974) 69.
[81] I.A. Bagotskaya, Itogi Nauki i Tekh. Elektrokhimiya 23 (1986) 60.
[82] E.J. Lust, Sov. Electrochem. Engl. Tr. 27 (1991) 94.
[83] E. Lust, K. Lust, A. Jänes, J.J. Ehrlich, Russ. J. Electrochem. 32 (1996) 597.
[84] CRC Handbook of Chemistry and Physics, 76th edition, D.R. Lide (Ed), CRC Press, Boca Raton, 1995, pp. 12–123.
[85] L.P. Khmelevaya, B.B. Damaskin, Elektrokhimiya 17 (1981) 1721.
[86] L.P. Khmelevaya, A.V. Chizov, B.B. Damaskin, Elektrokhimiya 14 (1978) 1304.
[87] L.P. Khmelevaya, A.V. Chizov, B.B. Damaskin, Elektrokhimiya 16 (1980) 257.

Reprinted from the *Journal of Electroanalytical Chemistry*, Vol. 436,
E. Lust, A. Jänes, K. Lust and P. Miidla,
Adsorption of Propanol on Bismuth Single Crystal Plane Electrodes, pages 141–153,

ELSEVIER

Journal of Electroanalytical Chemistry 436 (1997) 141–153

Adsorption of propanol on bismuth single-crystal-plane electrodes

E. Lust *, A. Jänes, K. Lust

Institute of Physical Chemistry, University of Tartu, 2 Jakobi Street, EE-2400 Tartu, Estonia

Received 11 March 1997; received in revised form 3 June 1997

Abstract

Cyclic voltammetry, impedance and chronocoulometry have been employed for quantitative study of *n*-propanol (*n*-PA) adsorption at the bismuth single-crystal plane|aqueous Na_2SO_4 solution interface. The adsorption characteristics of *n*-PA, obtained from the impedance and chronocoulometric measurements, are in good agreement within the limits of surface charge densities $-16 < \sigma < 10\ \mu C\ cm^{-2}$. The adsorption characteristics (Gibbs energy of adsorption $-\Delta G_A^0$; limiting Gibbs adsorption Γ_{max}; limiting potential shift of zero charge E_N; molecular interaction parameter *a*, etc.) of *n*-PA depend on the crystallographic structure of the electrode surface. Comparison of the adsorption parameters for *n*-PA, *n*-butanol (*n*-BA), isobutanol (iso-BA), *sec*-butanol (*sec*-BA), *tert*-butanol (*tert*-BA), butylacetate (BAC) and cyclohexanol (CH) shows that the adsorption activity and other parameters depend on the length and structure of hydrocarbon radical of the organic compound studied. The adsorption activity of *n*-PA rises in the order of Bi planes (111) < (001) < (01$\bar{1}$). The difference between the adsorption activities of various Bi planes decreases as the adsorption activity of the organic compound at the metal|solution interface decreases in the order of adsorbates BAC > CH > *n*-BA > *n*-PA. The molecular interaction parameter *a* decreases in order of planes (001) ≥ (111) > (01$\bar{1}$) as the reticular density of planes increases, and in order of adsorbates *n*-PA < *n*-BA < CH as the molar volume of adsorbate rises. The limiting Gibbs adsorption Γ_{max} increases in order of planes (01$\bar{1}$) < (111) < (001) as the superficial density of planes decreases. Very low Γ_{max} and E_N values for Bi(01$\bar{1}$) plane indicate that *n*-PA molecules probably have a flat orientation on the chemically most active Bi(01$\bar{1}$) single-crystal plane in the region of maximum adsorption. © 1997 Elsevier Science S.A.

Keywords: *n*-propanol adsorption; Impedance; Chronocoulometry

1. Introduction

This work is part of a project devoted to the study of the influence of the crystallographic structure of electrode surfaces on the adsorption characteristics of neutral organic molecules at the Bi|solution interface [1–6]. Adsorption of various organic compounds at the polycrystalline bismuth and antimony solid drop electrode has been described previously [7–9]. The adsorption behaviour of various aliphatic compounds with different geometrical structures of the hydrocarbon radical, but with the same functional group (*n*-propanol (*n*-PA), *n*-butanol (*n*-BA), isobutanol (iso-BA), *tert*-butanol (*tert*-BA), *sec*-butanol (*sec*-BA) and cyclohexanol (CH) [1,2,5]) at electrodes with the same crystallographic structure of the surface under other identical conditions would provide further useful information on the role of the hydrocarbon chain structure of the adsorbate to the formation process of the adsorbed layer and their molecular structure, i.e., on the orientation of adsorbed molecules and to the process of the formation of the hydrogen bonds between adsorbate–adsorbate, H_2O–adsorbate and H_2O–H_2O molecules in the inner layer region of the electric double layer (edl). In fact, the chemical nature of the metal and the crystallographic structure of the single-crystal-plane electrode is known to affect the structuring of interfacial water molecules [1–28], which has been studied extensively from both experimental and theoretical points of view. This is therefore used to exert an indirect influence upon the adsorption behaviour of the same aliphatic compound on different metals. Systematic adsorption measurements of *n*-aliphatic alcohols and their isomers from aqueous electrolyte solutions have been carried out on various sp-metals, such as Hg, Pb, Bi, Cd, Sn, Sb, Zn, Ag, In–Ga and Ga [1–20,22,24–28]. In

* Corresponding author. Tel.: +372-7-465-165; fax: +372-7-465-160; e-mail: enn@chem.ut.ee.

PII S0022-0728(97)00317-3

general, these measurements indicate that the adsorption of aliphatic compounds is weaker when the metal is more hydrophilic. However, as found in Refs. [27,28] the difference between the adsorption activities of the same compound at various metals depend on the adsorption activity of adsorbate at the electrode|solution interface, as well as on the adsorption activity of the compound at the air|solution interface [28]. The difference between various metals diminishes if the adsorption activity at the metal|solution, as well as at the air|solution interface, decreases.

A further difficulty in comparing results from different laboratories lies in the fact that different experimental techniques are often used. In the specific case of organic adsorption on single-crystal planes of various metals, there are three main approaches: (a) static capacitance measurements by means of a manually operated bridge; (b) dynamic capacitance measurements by means of a lock-in amplifier; (c) charge measurements by potential steps (chronocoulometry). Dynamic measurements are not usually considered an equilibrium approach in view of the continuous potential scan, while full confidence is placed on chronocoulometric experiments [5,6,12–15].

Therefore we have carried out systematic simultaneous impedance (capacity bridge) and chronocoulometric investigations of the adsorption of various organic substances on Bi single-crystal planes [5,6]. For a more profound understanding of the importance of the crystallographic structure of the electrode surface and the geometrical structure of the hydrocarbon chain of the adsorbate in adsorption phenomena, in the present work we have studied the adsorption of propanol (*n*-PA) on singular Bi faces (111), (001) and (01$\bar{1}$). The results obtained have been compared with the data for butanol isomers (*n*-BA, iso-BA, *sec*-BA and *tert*-BA), butylacetate (BAC) and CH adsorption at various electrodes.

2. Experimental

The experimental procedure used in this work has been described in Refs. [1–6]. The crystallographic orientation was determined by X-ray analysis, using a special crystal holder and a goniometric head. The electrode was cut along the chosen crystallographic orientation with the precision $\pm 0.3^{\circ}$. The isolation of the faces was carried out by a thin polystyrene film (dissolved in toluene) covering the part of no interest, and then the sample was placed in a Teflon holder. The surface was polished to a mirror finish by using standard metallographic procedures. The final surface preparation was obtained by electrochemical polishing in an aqueous KI + KCl solution. Thereafter the second X-ray diagram was used to determine the precise angle, and only the samples whose precision on the orientation was better than $\pm 0.10^{\circ}$ were used for electrochemical investigations. After the last stage of surface preparation (electrochemical polishing), the electrodes were very well rinsed with ultrapurified water and were polarised at -1.2 V vs. the saturated calomel electrode (SCE) in the surface inactive electrolyte solutions.

For an additional characterisation of the working surface of electrodes, electron microscopic analysis by JEOL-JSM-35CF at the SEI regime was made (40 000 × maximum). According to these measurements, the electrochemically polished surfaces of bismuth electrodes were smooth (understandably, within the range of the sensitivity of electron microscopy) [27].

2.1. Solutions

The water for preparing the solutions was purified by triple distillation (a quartz system was used for the last) and purified additionally by using the special method described in Refs. [1–6,27]. Solutions were prepared volumetrically using Na_2SO_4 purified by triple recrystallization from water, followed by vacuum heating to dryness. Na_2SO_4 was calcined at 700°C immediately prior to the measurements. The change of the Na_2SO_4 solution pH in the range 4.0 to 6.0 was effected by the addition of a calculated amount of H_2SO_4 solution prepared from triply distilled concentrated sulphuric acid. The solution pH was determined with a pH-meter. Electrolytic hydrogen was bubbled for 1 to 2 h through the electrolyte before the submersion of the electrode in the solution. The temperature was kept at 298 K and an aqueous SCE was used as the reference electrode. The *n*-propanol was purified according to Ref. [29].

3. Results and discussion

3.1. Cyclic voltammograms (CV's)

The CV's were recorded in order to determine the quality of the surfaces investigated and the potential range in which the adsorption of *n*-PA occurred. The shape of the CV recorded for the supporting electrolyte was characteristic of the bismuth single-crystal planes in accord with our previous studies [1–6]. The cyclic voltammetry curves also indicated that the bismuth single-crystal planes investigated are ideally polarizable in the potential range of -1.8 to -0.35 V (SCE) in aqueous 0.05 M Na_2SO_4 solution. In aqueous 0.0499 M $Na_2SO_4 + 1 \times 10^{-2}$ M H_2SO_4 solution, bismuth electrodes are ideally polarizable in the range of -1.3 to -0.1 V (SCE).

3.2. Differential capacity vs. potential curves (C(E) curves)

The edl differential admittance was measured from 60 to 21 000 Hz. The capacity dispersion with frequency ν is very small in the proximity of the differential capacity minimum (in the region of maximum adsorption), whereas it increases somewhat in the region of the adsorption–de-

sorption peaks, but this dependence is noticeably smaller than for *n*-BA, CH or for pyridine [5,6,30]. As shown in Refs. [5,6,10,30–32], if the rate of the adsorption of the organic compound is limited by diffusion, the equilibrium values of the differential capacity at $\nu = 0$ can usually be found of a sufficient degree of accuracy by extrapolation of the $C_{add}(\omega^{1/2})$ curve ($\omega = 2\pi\nu$) to $\omega^{1/2} = 0$. In the region of 60 Hz < ν < 610 Hz, the $C_{add}(\omega^{1/2})$ curves have a good linearity and, accordingly, we can obtain the equilibrium values of the differential capacity. According to the method [5,6,10,27,30–33], the equilibrium values of the differential capacity can be calculated by Eq. (1):

$$C_{add}(\omega = 0) = C_{add}^2(\omega) R_p^2(\omega) \omega^2 + 1 \Big/ \left\{ \left[C_{add}(\omega) R_p(\omega) \omega - 1 \right] R_p(\omega) \omega \right\} \quad (1)$$

where $C_{add}(\omega)$ and $R_p(\omega)$ are the values of differential capacity and solution resistance at ω = constant.

The components of the adsorption impedance were calculated from the impedance data of the cell used for the measurements (series circuit), i.e., $C_S(\omega)$ and $R_S(\omega)$, following the procedure described in Refs. [5,6,10,30–34]. By extrapolating the $R_S(\omega)$-values to $\omega \rightarrow \infty$ we determined the solution resistance $R_S(\omega) = R_{sol}$. Since the amount of organic compounds added is small and does not affect the solution resistance, one can assume R_{sol} to be equal to the ohmic component R_S of the impedance in the pure base electrolyte solution. Then the series equivalents $R_S(\omega) - R_{sol}$ and $C_S(\omega)$ of the impedance were converted into the parallel equivalents $C_P + C_{true}$ and R_P via the relations given in Refs. [5,6,10,30–33]. The equilibrium values of $C_{add}(\omega = 0)$, calculated according to Eq. (1) (for example for 1.0 M *n*-PA solution the values of $C_{add}(\omega = 0)$ are 28 ± 3; 33 ± 3 and 35 ± 4 μF cm^{-2} for Bi(01$\bar{1}$), Bi(111) and Bi(001) planes, respectively) are in good agreement with the values obtained from $C_{add}(\omega^{1/2})$ curves (26 ± 3; 35 ± 3 and 38 ± 4 μF cm^{-2}, respectively).

For accurate determination of the precision of the experimental data, a statistical analysis was carried out at ν = 210 Hz [5,27]. The statistical analysis showed that in the case of electrochemically polished single-crystal Bi electrodes, the values of C, surface charge density σ and the decrease of the specific surface work (surface tension) ($\gamma - \gamma_0$) can be determined sufficiently accurately by the measuring procedure used, and the error of these parameters is not greater than 5%. The values of the potential of maximum adsorption E_{max} and of the potential of the adsorption–desorption maximum, E^{max}, can be established with accuracies of ±25 mV and ±5 mV, accordingly.

All the $C(E)$ curves (ν = 210 Hz) determined in the presence of *n*-PA in the solutions investigated merge with the curve for the supporting electrolyte at −1.8 V (SCE), indicating that *n*-PA molecules are completely desorbed from the bismuth surface at these negative potentials (Fig. 1). At less negative potentials, the $C(E)$ curves display characteristic adsorption–desorption peaks. The height of the peak at $E < E_{\sigma=0}$ increases and its potential shifts in the negative direction with increasing *n*-PA concentration. The shape (the height and width) of the adsorption–desorption maximum at c_{org} = constant depends on the crystallographic structure of the electrode surface. The width decreases and the height of the peaks (at c_{org} = constant) increases in the sequence of planes (01$\bar{1}$) < (111) ≤ (001) as the reticular density of the planes decreases. Accordingly, the attractive interaction between the adsorbed *n*-PA molecules increases in the sequence of planes (01$\bar{1}$) < (111) ≤ (001).

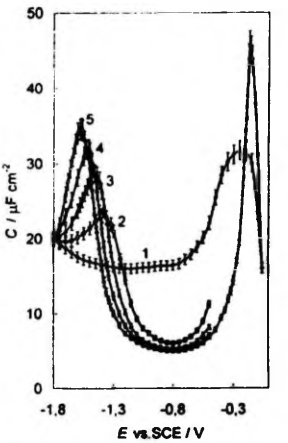

Fig. 1. Differential capacity vs. potential curves (ν = 210 Hz) for (1) Bi(111) in 0.05 M Na_2SO_4 and with addition of *n*-propanol: (2) 0.6 M; (3) 1.0 M; (4) 1.5 M; (5) 2.0 M.

The height of peaks at c_{org} = constant increases and the width decreases in the sequence *n*-PA > *tert*-BA > *sec*-BA > iso-BA > *n*-BA > BAC > CH (Fig. 2), which means that at $E < E_{\sigma=0}$ the attractive interaction between the adsorbed aliphatic compound molecules increases in the sequence of adsorbates *n*-PA < *tert*-BA < *sec*-BA ≤ iso-BA < *n*-BA < CH as the molar volume of adsorbate increases (except BAC). The adsorption–desorption maximum potential in the relative scale $E^{max} - E_{\sigma=0}$ at $E < E_{\sigma=0}$ (c_{org} = constant) depends on the geometrical structure of the adsorbate, and the adsorption activity of aliphatic alcohols increases in the sequence *n*-PA < *n*-BA < CH. The value of $E^{max} - E_{\sigma=0}$ depends on the crystallographic structure of the electrode surface (Fig. 3); and the adsorption activity of the surface increases in the order of planes (111) < (001) < (01$\bar{1}$).

Going further in the positive direction, the differential capacity decreases to a value much smaller than that observed for the pure base electrolyte, indicating that *n*-PA

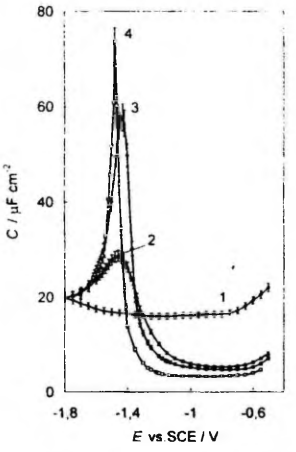

Fig. 2. Differential capacity vs. potential curves ($\nu = 210$ Hz) for (1) Bi(111), Bi(001) and Bi(01$\bar{1}$) planes in 0.05 M Na_2SO_4 and with addition of various alcohols (0.1 M): (2) *n*-PA; (3) *n*-BA; (4) CH.

molecules are replacing water at the interface. The limiting capacity C_1 at E_{max} decreases in the sequence of planes (01$\bar{1}$) < (111) ≤ (001). According to the Helmholtz equation for a parallel plate condenser $C = \varepsilon/4\pi d$ (ε is the macroscopic permittivity (dielectric constant) and d is the thickness of adsorbed layer), there are two possibilities: (i) the value of C_1 decreases if the amount of H_2O molecules at surface coverage $\theta = 1$ in the adsorbed layer decreases (ε decreases); and (ii) C_1 decreases as the vertical orientation of molecules increases (d increases) in the order of planes (01$\bar{1}$), (111) < (001). A more detailed discussion will be given later.

The adsorption–desorption maxima at $E > E_{\sigma=0}$ for *n*-PA were found at $E > -0.3$ V (SCE) for all planes investigated. Thus, the desorption of adsorbed *n*-PA molecules occurs at positively charged surfaces. At $E > E_{\sigma=0}$, the height of peaks in the $C(E)$ curves decreases and the width increases in the same order of planes as at $E < E_{\sigma=0}$. Thus, at $E > E_{\sigma=0}$ a increases in the sequence (01$\bar{1}$) < (111) ≤ (001) as the reticular density of planes decreases.

3.3. Charge density–potential curves

The $\sigma_0(E)$ curve for base electrolyte solution was obtained by integration of the $C(E)$ curve, extrapolated to the condition $\nu = 0$, starting from the potential of zero charge (pzc) $E_{\sigma=0}$. The values of $E_{\sigma=0}$ for different Bi singe-crystal planes were obtained from the position of the diffuse layer minimum on independently measured differential capacity curves for dilute solutions of the base electrolyte [5,6,27,34]. The $\sigma(E)$ curves for solutions with different additions of adsorbate were obtained by back integration of the $C(E)$ curves (extrapolated to $\nu = 0$), starting from $E = -1.8$ V (SCE) and assigning the value of σ ($E = -1.8$ V) equal to σ_0 ($E = -1.8$ V), because there is no adsorption at $E = -1.8$ V (SCE).

The $\sigma(E)$ curves for different concentrations of *n*-PA investigated intersect the σ_0, E curve obtained for the base electrolyte, which is nearly linear in the region of $E \leq E_{\sigma=0}$. The potential at which the curves intersect is the potential of maximum adsorption E_{max}. As we can see from Fig. 4, E_{max} is practically independent of c_{ads} and the values of E_{max} are equal to -0.90, -0.85 and -0.80 V for the Bi(111), Bi(001) and Bi(01$\bar{1}$) planes, respectively. The charge density σ_{max} at which the maximum adsorption takes place depends slightly on the plane, and σ_{max} decreases in the order (01$\bar{1}$) > (001) > (111) (-4.0 ± 0.5; -5.0 ± 0.5 and -5.5 ± 0.5 μC cm^{-2}). The nearly linear segments are observed on the $\sigma(E)$ curves around E_{max}. By linear extrapolation of these fragments of the curve to $\sigma = 0$, one can determine the potential of zero charge corresponding to the surface covered by adsorbate molecules. The difference between these experimental values and the value of $E_{\sigma=0}$ for the pure base electrolyte solution is equal to the change in the surface potential due to the displacement of a monolayer of water molecules by a monolayer of adsorbate (E_N). The established values of E_N are presented in Table 1, and we can see that the values of E_N increase in the sequence of Bi planes (01$\bar{1}$) < (001) < (111). The same order of planes is valid for *tert*-BA, pyridine (PY), *n*-BA, BAC and CH adsorption at Bi planes [1,2,5,6,27,34]. With the help of the unrationalized Helmholtz formula, E_N can be expressed as

$$E_N = 4\pi\Gamma_{max}(\mu^{org} - n\mu^{w})/\varepsilon \qquad (2)$$

where Γ_{max} is the limiting surface excess of *n*-PA; μ^{org} and μ^{w} are the components of the dipole moment normal to the surface of the electrode for the organic compound and H_2O molecules, respectively; n is the number of H_2O

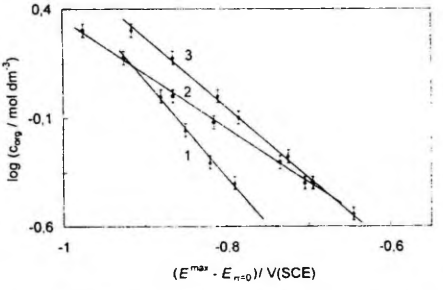

Fig. 3. Dependence of the difference between the potential of the adsorption–desorption maximum and the zero charge potential $E^{max} - E_{\sigma=0}$ on log c_{org} of *n*-PA for various Bi single-crystal planes: (1) (01$\bar{1}$); (2) (001); (3) (111).

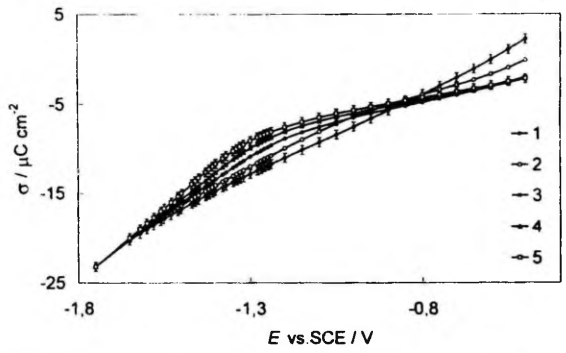

Fig. 4. Charge density vs. potential curves (obtained from chronocoulometry) for (1) Bi(01$\bar{1}$) in 0.05 M Na_2SO_4 and with addition of *n*-PA: (2) 0.2 M; (3) 0.5 M; (4) 1.0 M; (5) 2.0 M.

molecules, displaced by one adsorbed *n*-PA molecule; and ε is the permittivity of the inner layer. The positive sign of E_N indicates that either (1) $|\mu^{org}| > |n\mu^{w}|$ and $\mu^{org} > 0$ ($\mu^{w} \gtrless 0$) or (2) $|\mu^{org}| < |n\mu^{w}|$ and $\mu^{org} < 0$ ($\mu^{org} \gtrless 0$). In the first case μ^{org} is positive which means that the molecules of *n*-PA are oriented with the hydrocarbon chain facing the Bi surface at E_{max}. In the second case *n*-PA molecules may be oriented with the hydrocarbon tail towards the electrode surface ($\mu^{org} > 0$), as well as the –OH group facing the electrode surface ($\mu^{org} < 0$). In these two latter cases, the very large positive values of E_N would suggest a strong preferential orientation of H_2O with oxygen atoms towards the electrode surface at E_{max} (not far from $E_{\sigma=0}$) with $\mu^{w} < 0$, which for Bi planes is in contradiction with the data of our previous work [1–6,27,28,34]. As the maximum adsorption of *n*-PA takes place at the negatively charged surfaces (from $\sigma_0 \approx -4.0 \pm 0.5$ to -5.5 ± 0.5 μC cm^{-2}), it seems that the first possibility for Bi(111), Bi(001) and Bi(01$\bar{1}$) planes is more plausible. Thus, the effective dipole moment of the organic molecules must be positive and in the region of E_{max}, the *n*-PA molecules on bismuth single-crystal planes are oriented with the hydrocarbon radical facing the bismuth surface and the functional –OH group facing the solution side of the interface. The same conclusions are valid if the adsorption of aliphatic alcohols (C_2H_5OH, *n*-PA) takes place at Hg and Zn single-crystal planes [8,10–12,20,35]. The noticeably lower value of E_N for the Bi(01$\bar{1}$) plane probably indicates that a more pronounced horizontal orientation of *n*-PrOH at this chemically most active plane is plausible. Accordingly, the increase of C_1 for (01$\bar{1}$) compared with (001) and (111) is mainly caused by the decrease of adsorption layer thickness for the (01$\bar{1}$) plane. According to the data of Table 1 and Refs. [1,2,5], E_N depends on the geometrical structure of the hydrocarbon chains of adsorbate, and the effective dipole moment increases in the order BAC < iso-BA ≤ *sec*-BA < *n*-BA < *tert*-BA < *n*-PA. Thus, at Bi(001) and Bi(111) planes the

Table 1
Adsorption parameters of *n*-propanol at the various electrodes

Electrode	$a_m \pm 0.1$	$C_1 \pm 0.15$ (μF cm^{-2})	$E_N \pm 0.05$ (V (SCE))	$(10^{10} \times \Gamma_{max}) \pm 0.4$ (mol cm^{-2})	S_{max} (nm^2)	$B_0 \pm 0.20$ (dm^3 mol^{-1})	$-\Delta G_A^0 \pm 0.2$ (kJ mol^{-1})
Bi(111)	1.03	5.05	0.54	5.1	0.32	1.65	11.2
Bi(001)	0.86	5.00	0.44	6.4	0.26	1.84	11.5
Bi(01$\bar{1}$)	0.65	5.40	0.37	3.1	0.54	2.83	12.3
Hg [10,11]	1.11	4.85	0.33	5.7	0.30	3.00	12.7

a_m is the attraction interaction constant at E_{max} (impedance data).
C_1 is the limiting capacity ($\theta = 1$) at E_{max} (impedance data).
E_N is the limiting potential shift of $E_{\sigma=0}$ due to the displacement of the monolayer of H_2O by the monolayer of adsorbate molecules (chronocoulometry data).
Γ_{max} is the limiting Gibbs adsorption (chronocoulometry data).
S_{max} is the limiting projected surface area at $E_{\sigma=0}$ (chronocoulometry data).
B_0 is the adsorption equilibrium constant at $E_{\sigma=0}$ (Frumkin isotherm; impedance data).
$-\Delta G_A^0$ is the Gibbs adsorption energy at $E_{\sigma=0}$ and at the standard state being the unit mole fraction of the organic species in the bulk of solution and monolayer coverage $\theta = 1$ of the ideal noninteracting adsorbate (Frumkin isotherm; impedance data).

n-PA molecules would have more vertical orientation compared with the *n*-BA, BAC, CH or iso-BA molecules adsorbed.

3.4. Potential step measurements

The values of the initial and final potentials for the potential step experiments were chosen with the help of the $C(E)$ and cyclic voltammetric $j(E)$ curves. The initial potential E_i was varied from −0.40 to −1.80 V (SCE). The final potential E_f was equal to −1.60 V (SCE) for $c_{org} \leq 0.01$ M and −1.80 V (SCE) for $c_{org} > 0.01$ M. Its value was chosen carefully in order to: (1) achieve the complete desorption of *n*-PA; (2) keep the current of hydrogen evolution small enough so that the faradaic reaction would not interfere with the determination of the electrode charge density (σ) [5,6,12–15,34].

The chronoamperometric curves were integrated digitally to obtain the charge transients [5,6,12–15,34]. The chronocoulometric curves display an initial fast-rising section, corresponding to the charging of the edl followed by a quasi-plateau in which the charge varies slowly and linearly with time. The slope of this segment is small (owing to a very slight hydrogen evolution reaction). In this way, the faradaic contribution from hydrogen evolution was minimized. The relative charge densities $\Delta\sigma$ were determined from these step measurements:

$$\Delta\sigma(E) = \sigma(E_i) - \sigma(E_f) \quad (3a)$$

In Eq. (3a), $\sigma(E_i)$ and $\sigma(E_f)$ are the charge densities at the metal side of the interface at potentials E_i and E_f, respectively. Knowing the value of $E_{\sigma=0}$, determined by impedance measurements [5,6,27,34], the absolute charge densities were calculated for each value of E by using the formula

$$\sigma(E) = \Delta\sigma(E) - \Delta\sigma(E_{\sigma=0}) \quad (3b)$$

The precision of charge measurements is about 2 to 3%. The shape of these curves is typical and all the curves merge at −1.8 V (SCE). Accordingly, a complete desorption of *n*-PA takes place at $E = -1.8$ V (SCE).

Starting from $E = -1.8$ V (SCE) and going in the positive direction, a sharp rise in the charge density is observed if *n*-PA is present in the bulk of the solution. The increase in σ slows quickly, and the charge becomes nearly linearly dependent on the potential. The $\sigma(E)$ curves for different concentrations of *n*-PA intersect the $\sigma_0(E)$ curve at the potential of maximum adsorption E_{max}. At E = constant, the values of σ are practically independent of the direction of potential step measurements, which means that the adsorption of *n*-PA is practically reversible. The comparison of the σ, E plots from the impedance and chronocoulometry measurements shows that the difference between the values of σ, obtained by these methods, does not exceed ± 0.5 μC cm^{-2}. A particularly good agreement has been established at surface charge densities from −16 to 10 μC cm^{-2}, where the analysis of the experimental data of *n*-PA was carried out. Comparison of σ, E curves, obtained from impedance and chronocoulometric measurements for *n*-PA, *tert*-BA, *n*-BA, CH and PY [5,6,27,34], shows that the difference between σ values in the region $-16 < \sigma < 10$ μC cm^{-2} increases as the adsorption activity of the organic compound at the electrode rises.

3.5. Specific surface work and film pressure curves

The capacitance curves were twice back-integrated to obtain a specific surface work decrease $(\gamma - \gamma_0)$ as a function of E and adsorbate concentration [5,6,12–15,27,34]. The second integration was performed from the same negative charge at first, assigning the value of zero to the specific surface work at the pzc in the base solution. Our data show a progressive decrease of the specific surface work when c_{org} increases. The shape of the $(\gamma - \gamma_0), E$ curve is typical for the adsorption of the organic compound. A good accordance between $(\gamma - \gamma_0), E$ curves, obtained from impedance and chronocoulometry measurements, can be seen between −12 and 6 μJ cm^{-2}, where the thermodynamic analysis takes place. The adsorption activity of bismuth electrodes increases in the sequence of planes (111) < (001) < (01$\bar{1}$). According to Refs. [12–15,22,35–39], the adsorption activity of aliphatic organic compounds at Zn, Ag and Au planes rises as the superficial density of the plane increases. The superficial density of Bi planes increases in the order (001) < (111) < (01$\bar{1}$). The anomalous position of the Bi(111) plane is evidently determined by the competitive adsorption of water and the organic substance, as well as by the crystallographic and electronic structure of Bi electrodes. Just as in the case of cyclohexanol [1,27,34], butanol isomers [5], PY [6] and BAC [4] adsorption, the basal plane (111), where the surface atoms are chemically saturated (electron configuration sp^3d^2) [1–6,40], has the lowest adsorption activity. The most active one is the singular Bi(01$\bar{1}$), where unsaturated covalent bonds are distributed uniformly over the whole surface (s^2p^3).

The comparison of the $\pi(E)$ curves obtained from impedance and chronocoulometry measurements shows that the departure from the equilibrium is probably very small under the peak at negative rational potentials. Thus, thermodynamic analysis is still possible in the potential range studied; however, the capacitance at the minimum of the curves should be substantially reliable, since no noticeable frequency effects are expected in that potential range. The pressure of the film of adsorbate π can be determined as

$$\pi(E) = \gamma_{c=0} - \gamma_c = \int_{E_{pzc}}^{E} \sigma_c \, dE - \int_{E_{pzc}}^{E} \sigma_{c=0} \, dE \quad (4)$$

where subscripts c and c = 0 indicate the presence or absence of the adsorbate in the bulk of the electrolyte

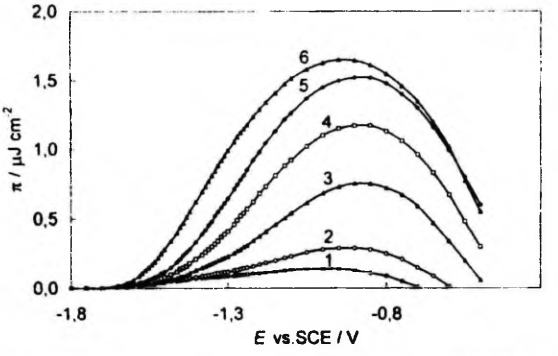

Fig. 5. Surface pressure vs. potential curves for Bi(111) (chronocoulometry) in 0.05 M Na_2SO_4 aqueous solution with addition of *n*-PA: (1) 0.1 M; (2) 0.2 M; (3) 0.5 M; (4) 0.7 M; (5) 1.0 M; (6) 2.0 M.

respectively [10,15]. The calculated $\pi(E)$ curves are plotted in Fig. 5. For more concentrated solutions of *n*-PA ($c \geq 0.01$ M), the curve displays a maximum, the potential of which is practically independent of c_{org} and this value is in good agreement with the value of E_{max} for $C(E)$-curves. The film pressure of the adsorbate increases in the sequence of compounds *n*-PA < *tert*-BA < *sec*-BA < iso-BA < *n*-BA < BAC and in the sequence of planes (111) ≤ (001) < (01$\bar{1}$) (Fig. 6). Accordingly, the adsorption activity of compounds and electrodes increases in the sequence of adsorbates and planes presented.

3.6. Gibbs excess–potential and Gibbs excess–log c_{org} curves

The film pressure data were used to calculate the relative Gibbs surface excess. First the film pressure was plotted against log c_{org} at E = constant (Fig. 7). The curves display a long linear section at higher c_{org} and its slope gives the limiting value of Γ_{max} [10,15,36–39,41,42]:

$$\Gamma = \frac{1}{RT}\left(\frac{\partial \pi}{\partial \ln c}\right)_{E,T,p} \quad (5)$$

The mole fraction on *n*-PA never exceeds 2.5%, hence at the first approximation it was assumed that the activity of *n*-PA depends linearly on its concentration according to Henry's law [8–15,38,41–44]. The values of Γ_{max} obtained are presented in Table 1. Calculated according to the values of Γ_{max}, the values of molecular surface area S_{max}, corresponding to the area of one adsorbed molecule at the maximum adsorption potential E_{max}, increase in order of Bi planes (01$\bar{1}$) < (111) < (001). If the adsorbed molecules of *n*-PA and *n*-BA were oriented perpendicu-

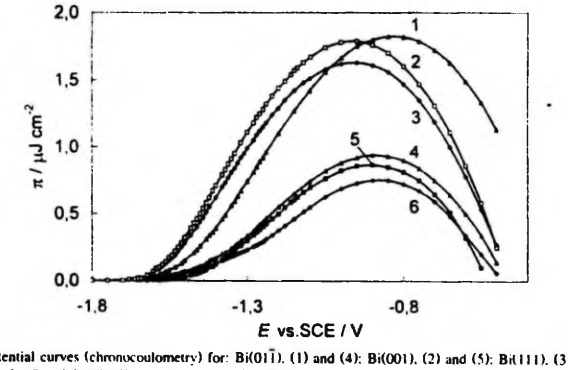

Fig. 6. Surface pressure vs. potential curves (chronocoulometry) for: Bi(01$\bar{1}$), (1) and (4); Bi(001), (2) and (5); Bi(111), (3) and (6) in 0.05 M Na_2SO_4 aqueous solution with addition of *n*-PA: (1), (2), (3) 2.0 M and (4), (5), (6) 0.5 M.

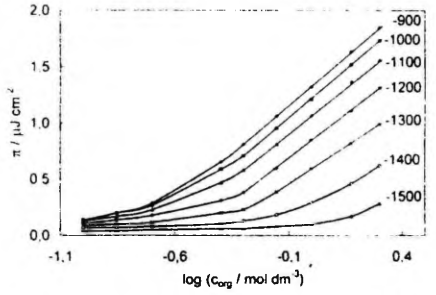

Fig. 7. Surface pressure vs. log c curves (chronocoulometry) for the Bi(001) plane at different electrode potentials (mV), noted by numbers.

larly at the Bi|electrolyte interface, the values of S_{max} should be the same for n-PA and n-BA and would be equal to $S_{max}^{theory} \sim 0.21$ nm^2 [8–15,24]. The same conclusion would be valid, if the orientation of adsorbed molecules is independent of the crystallographic structure of the electrode surface. The lower experimental values of Γ_{max} and the increase of the projected area S_{max} can be explained by more tilted orientation of adsorbate molecules going from n-PA to n-BA, as well as from Bi(001) to Bi(01$\bar{1}$). This conclusion is in good accordance with the noticeable decrease of E_N and a values in the sequence of planes Bi(001) ≥ Bi(111) > Bi(01$\bar{1}$).

In the bent region of the π(ln c) curves, the slope changes noticeably and the error of differentiation of π(ln

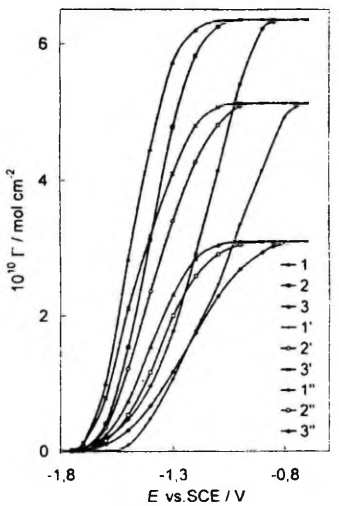

Fig. 8. Gibbs excess vs. potential curves (chronocoulometry) for: Bi(001) (1–3); Bi(111) (1'–3') and Bi(01$\bar{1}$) (1"–3") with different additions of n-PA (M): 0.5 (1, 1', 1"); 1.0 (2, 2', 2"); 2.0 (3, 3', 3").

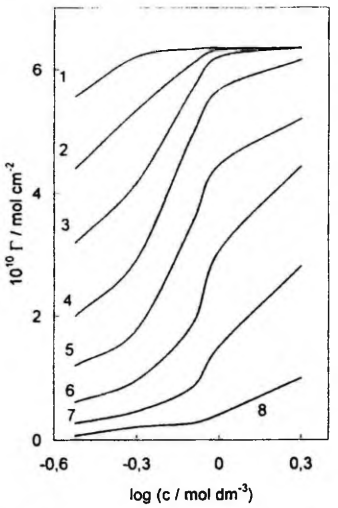

Fig. 9. The Gibbs excess vs. log c curves (chronocoulometry) for Bi(001) at different electrode potentials (mV), noted by numbers.

c) curves is large [15] and the related Gibbs excess values for the intermediate coverages were determined from the σ, E curves using the well-known formula [10]

$$\Gamma = \frac{\sigma_\Gamma - \sigma_{\Gamma=0}}{\sigma_{\Gamma_{max}} - \sigma_{\Gamma=0}} \Gamma_{max} \qquad (6)$$

The values of $(\sigma_{\Gamma_{max}} - \sigma_{\Gamma=0})$ were obtained by the extrapolation of the linear sections of the $\sigma(E)$ curves. The shape of the $\Gamma(E)$ curves for different c_{org} (Fig. 8) and of the Γ(log c) curves (Fig. 9) suggest that the relative maximum of the adsorption of n-PA on all the planes investigated is reached at -0.9 V $< E < -1.2$ V (SCE) and it depends on the crystallographic structure of the Bi surface. The values of Γ_{max} increase in the order of electrodes (01$\bar{1}$) < (111) < Hg < (001). These values are in good accordance with Γ_{max}, obtained from π(ln c) curves using Eq. (5), and this indicates the absence of big systematic errors in the data analysis. The slope of the $\Gamma(E)$ curves at the region of intermediate values of Γ (c_{org} = constant) increases in the order of planes (01$\bar{1}$) < (111) < (001) and in the order of adsorbates n-PA < *tert*-BA ≤ n-BA < *sec*-BA ≤ iso-BA < CH as the attraction between the adsorbed molecules rises.

3.7. Adsorption isotherms

The differential capacity C_1 at the coverage $\theta = 1$ was obtained by extrapolating the $1/C$ vs. $1/c_{org}$ plots to $(1/c_{org}) \rightarrow 0$. The data taken at the maximum adsorption potential E_{max} lie satisfactorily on a straight line and values of C_1 are presented in Table 1.

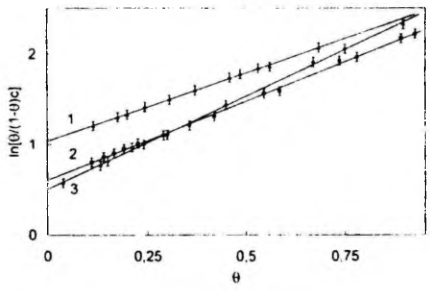

Fig. 10. Frumkin adsorption isotherm (ν = 210 Hz) for *n*-PA adsorption on Bi single-crystal planes: (1) (01$\bar{1}$); (2) (001); (3) (111).

The surface coverage at $E = E_{max}$ was first estimated from Eq. (7) based on Frumkin's two parallel condensers model [8,10,11].

$$\theta = (C_0 - C_\theta)/(C_0 - C_1). \quad (7)$$

Thereafter, at the first approximation, the applicability of the Frumkin adsorption isotherm

$$B_m c = \frac{\theta}{1-\theta} \exp(-2a_m\theta) \quad (8)$$

for the interpretation of *n*-PA|Bi data was assumed. In Eq. (8) B_m and a_m are the adsorption equilibrium constant and molecular interaction parameter respectively, at E_{max}. The applicability of Eq. (8) was tested using the log[$\theta/(1-\theta)c$],θ plots. Fig. 10 shows that these plots have a good linearity in the region of $0.1 < \theta < 0.9$ for all the faces investigated. Thus, the slope gives the molecular interaction parameter ($-2a_m$) and the intercept provides the adsorption equilibrium constant log B_m at E_{max} accordingly.

The adsorption isotherms at various σ = constant were calculated by the methods described in Refs. [10,12,15,38–44]. The adsorption isotherms at σ = constant show larger deviations from the Frumkin isotherm behaviour than those at E = constant, where the deviations in the region -0.6 V $< E < -1.2$ V (SCE) are small. A more detailed discussion will be given in a future paper.

3.8. Gibbs adsorption energy–potential and lateral interaction– potential curves

The energetics of *n*-PA adsorption are characterised by the magnitude of the Gibbs energy of adsorption. Fig. 11 shows the $\Delta G_A^0(E)$ curves determined from the initial slope of $\pi(\ln X_A)$ curves at E = constant, according to Eqs. (9) and (10), following Henry's law isotherm [8,10,15,36–39,41–44]

$$\pi = RT\Gamma_{max} B_A c_A/55.5 = RT\Gamma_{max} B_A X_A \quad (9)$$

$$\Delta G_A^0 = -RT \ln B_A \quad (10)$$

where X_A is the mole fraction of organic compound in solution and ΔG_A^0 is the Gibbs adsorption energy. As is shown in [15,36,37,41–44], the values of ΔG_A^0 obtained according to Eqs. (9) and (10) correspond to a similar standard state as the Gibbs adsorption energy of the organic compound, obtained according to the Frumkin isotherm (Eq. (8)), being the unit mole fraction of the organic species X_A in the bulk of solution and a monolayer coverage of the ideal noninteracting adsorbate at the electrode surface. According to the data of Fig. 11, the $\Delta G_A^0(E)$ curves display a parabolic behaviour. It must be noted that the precision of ΔG_A^0 values obtained by this method is improved by avoiding the differentiation of $\pi(\ln X_A)$ plots as the values of Γ_{max}, obtained from the linear part of the $\pi(\ln c)$ plots are quite precise [15]. Thus, the precision of the film pressure data must be very high in order to obtain the precise values of ΔG_A^0. Therefore, in addition to the previously described method, the ΔG_A^0 values at zero coverage as a function of E were obtained by fitting the experimental isotherms at E = constant to the Frumkin isotherm [13,15]:

$$X_A \exp\left(\frac{-\Delta G_A^0}{RT}\right) = \frac{\theta}{1-\theta} \exp(-2a\theta) \quad (11)$$

where a is the Frumkin interaction parameter at E = constant. The values of ΔG_A^0 and a were obtained from the intercepts and slopes of the least-squares fittings to a straight line of ln[$\theta/(1-\theta)c$] vs. θ plots at E = constant over the range of θ from 0.1 to 0.9. A good fit to Eq. (11)

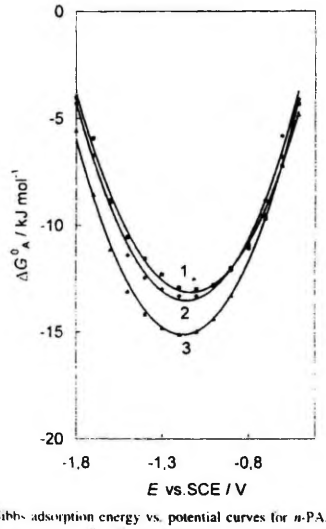

Fig. 11. Gibbs adsorption energy vs. potential curves for *n*-PA, obtained from chronocoulometry, for Bi single-crystal planes: (1) (111); (2) (001); (3) (01$\bar{1}$).

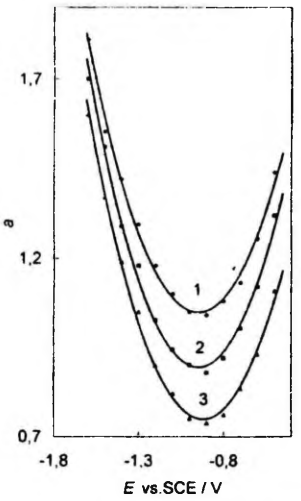

Fig. 12. Attraction interaction constant vs. potential curves for (1) Bi(111); (2) Bi(001); (3) Bi(01$\bar{1}$).

was achieved with the parameter a noticeably depending on the electrode potential (Fig. 12). The accordance of the ΔG_A^0 values of n-PA adsorption, obtained from $\pi(\ln c)$ plots and the Frumkin isotherm, is good (the error of ΔG_A^0 is ± 1.0 kJ mol^{-1}), which indicates the absence of big systematic errors in the data established. The values of ΔG_A^0, obtained from $\pi(\ln c)$ plots, are always somewhat higher than those, obtained from the Frumkin isotherm.

The adsorption data of n-PA on the Bi single-crystal planes are collated in Table 1, which shows that the adsorption activity of n-PA increases in the sequence of planes (111) < (001) < (01$\bar{1}$). The surface activity of adsorbates increases in the sequence n-PA < *tert*-BA < *sec*-BA ≤ iso-BA < n-BA < BAC as the adsorption at the air|solution interface increases.

The lateral interaction constants a are positive (Fig. 12 and Table 1) and the dependence of E is approximately parabolic. This result shows that the value of the projected area of the organic compound at the electrode surface decreases linearly as θ increases. According to Fig. 12, the attractive interaction at $E_{\sigma=0}$ and at E_{max} increases in the sequence of planes Bi(01$\bar{1}$) < Bi(001) < Bi(111). The same order of planes at E_{max} was found in the case of adsorption of n-BA, *sec*-BA, *tert*-BA, iso-BA, CH, BAC and PY adsorption at Bi single-crystal electrodes [1–6,34]. In the case of adsorption of organic compounds at the metal surfaces from solution, the value of a can be expressed in terms of different particle–particle interactions at the interface [6,10,12–15,24,36–39]

$$2a = (2Z_{W\ A} - Z_{A\ A} - Z_{W\ W})/RT \qquad (12)$$

where $Z_{i\ j}$ is the particle–particle interaction energy, W stands for H_2O and A for adsorbate. The positive values of a mean that $2Z_{W\ A} > Z_{A\ A} + Z_{W\ W}$, i.e., the adsorbate–adsorbate and water–water interactions are much more attractive than the adsorbate–water interaction ($Z_{W\ A}$). The same conclusions are valid in the case of adsorption of aliphatic alcohols at Hg, Ag(111), Ag(110), Ag(100), Au(100), Au(110), Au(111), Zn(0001), Zn(10$\bar{1}$0) and Zn(21$\bar{1}$0) electrodes [8,10–15,20,35–39]. If we assume to the first approximation that the water–water interaction energy at the same Bi single-crystal plane is independent of the aliphatic compound studied ($Z_{W\ W}$ = constant) then the positive values of a indicate that the A–A interactions are stronger than the W–A interactions. The shorter alcohols are presumably better and more strongly solvated by H_2O molecules compared with longer alcohols. Thus, the increase of a values in the order n-PA < *tert*-BA ≤ n-BA < *sec*-BA ≤ iso-BA < CH can be explained by the increase of A–A interaction energy in the order of compounds presented, as well as by the decrease of W–A interaction energy in the same order of adsorbates. However, the later effect seems to be small for the organic compounds studied in this work.

3.9. Analysis of the adsorption–desorption peaks

If the Frumkin–Damaskin model [1–6,8,10,11] is accepted, further information on adsorption parameters can be obtained from an analysis of the adsorption–desorption peaks. The following analysis is not unquestionable per se. First, frequency effects are included and the established $C_{add}^{max}(\omega = 0)$ values have been used; secondly, the validity of the formulae entails in particular a congruence of isotherms with respect to the potential and constants C_0 and C_1. However, the analysis is carried out in order to compare the adsorption of the same compound at the various planes of the same metal, using the same experimental variable. Therefore, the relevance of the conclu-

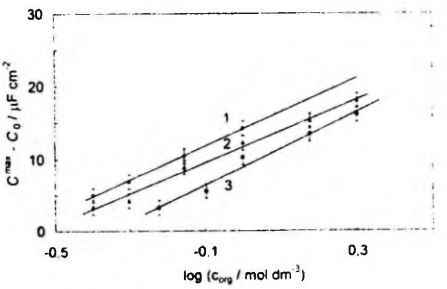

Fig. 13. ($C^{max} - C_0$) vs. log c plots ($\nu = 0$) at negative potentials of n-PA adsorption–desorption peaks for Bi single-crystal planes: (1) (001); (2) (111); (3) (01$\bar{1}$).

sions reached with the aid of the present analysis is believed to be incontestable. Fig. 13 shows that the variation of $(C^{max} - C_0)$ at $\omega = 0$ with log c_{org} (at $c_{org} \geq 0.1$ M) is linear for all the systems studied. The slope of the plot in Fig. 13 is given by Eq. (13) [5,6,10,14,30]

$$d(C^{max} - C_0)/d\log c_{org} = 2.3(C_0 - C_1)/(2 - a^{max}). \quad (13)$$

Since C_0 and C_1 are known independently, a value of attraction interaction a^{max} at $E = E^{max}$ can be obtained from Eq. (13). The established values of a^{max} for the Bi (001), (111) and (01$\bar{1}$) planes are equal to 1.43, 1.45 and 1.40, respectively, and are in good agreement with the values of a^{max} obtained from the width of the adsorption–desorption peaks according to the analysis of refs. [10,11,14]. The intercept of the plots in Fig. 13 is given by

$$\text{intercept} = \text{slope}(\log B_m + a^{max}/2.3) + (C_0 + C_1)/2. \quad (14)$$

Using the values of a^{max} obtained from Eq. (13), the adsorption equilibrium constant B_m at E_{max} can be obtained from Eq. (14). From the experimental data analogous to Fig. 13, we obtained log B_m values for the single-crystal Bi electrodes which are in agreement with the values of log B_m obtained directly from adsorption isotherms.

According to Frumkin's model, $(E^{max} - E_{max})^2$ should be linearly related to log c with a slope given by Eq. (15) [10,11,14]:

$$d(E^{max} - E_{max})^2/d\log c = 4.6\,RT\Gamma_{max}/(C_0 - C_1). \quad (15)$$

Since C_0 and C_1 are known; Γ_{max} can be estimated from Eq. (15). Fig. 14 shows that the plots are satisfactorily linear; the values of Γ_{max} obtained for *n*-PA adsorption at Bi(001), Bi(111) and Bi(01$\bar{1}$) are equal to 6.35×10^{-10}, 5.13×10^{-10} and 3.08×10^{-10} mol cm^{-2}, respectively. Thus, the values of Γ_{max}, obtained on the basis of Eq. (14), are in satisfactory agreement with the values obtained from Figs. 9 and 10.

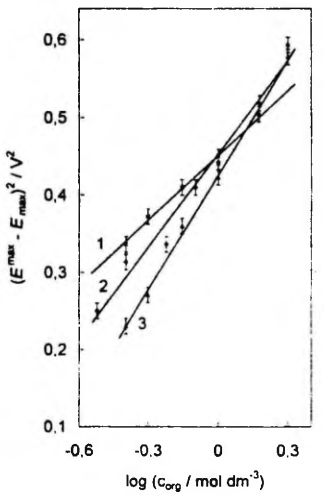

Fig. 14. $(E^{max} - E_{max})^2$ vs. log c plots at negative potentials of *n*-PA adsorption–desorption peaks for Bi single-crystal planes: (1) (01$\bar{1}$); (2) (111); (3) (001).

4. Conclusions

The adsorption behaviour of *n*-propanol at singular Bi(111), Bi(001) and Bi(01$\bar{1}$) has been studied by cyclic voltammetry, impedance and chronocoulometry methods. The results presented indicate that the adsorption parameters of *n*-PA depend on the crystallographic structure of Bi planes. The adsorption parameters for *n*-PA derived from the capacitance data (at $-16 < \sigma < 10$ μC cm^{-2}) are in good accordance with the data from the chronocoulometric measurements. However, the comparison of the impedance and chronocoulometry data for *n*-PA, *tert*-BA, CH and PY shows [5,6,27,34] that the difference between σ values, obtained by these two methods, increases when the adsorption activity of adsorbate at the Bi surface rises. It was found that the difference between the adsorption activities of various Bi planes increases in order of adsorbates *n*-PA < *tert*-BA ≤ *sec*-BA ≤ iso-BA < *n*-BA < BAC as the adsorption activity of the organic compound at the air|solution interface, as well as at the Bi|solution interface rises.

The values of the Gibbs energy of adsorption have been obtained from the initial part of the $\pi(\ln X_A)$ curves, as well as from the Frumkin isotherm. The difference between ΔG_A^0 values is not greater than ± 1.0 kJ mol^{-1}. The adsorption activity of *n*-PA increases in the order of planes Bi(111) < Bi(001) < Bi(01$\bar{1}$). The same order of Bi single-crystal plane electrodes (Bi(111) < Bi(001) < Bi(2$\bar{1}\bar{1}$) < Bi(01$\bar{1}$)) has been established if the adsorption of *n*-BA, iso-BA, *sec*-BA, *tert*-BA, CH, PY and BAC occurs [1–6,34]. Thus, except Bi(111), the adsorption activity of the Bi planes rises as the superficial density of planes increases in the order of planes Bi(001) < Bi(111) < Bi(2$\bar{1}\bar{1}$) < Bi(01$\bar{1}$). The same tendency is valid for Ag [13,15,22], Au [15,22,36–39] and Zn [20,35] electrodes if the adsorption of various aliphatic compounds occurs. The anomalous position of Bi(111) is probably caused mainly by the less active surface state of this chemically saturated (electron configuration sp^3d^2 [40]) basal plane. The most active one is the singular face Bi(01$\bar{1}$), where unsaturated covalent bonds are distributed uniformly over the whole surface. The adsorption activity of *n*-PA at Bi(001) is very

close to that for a polycrystalline bismuth solid drop electrode [7], and this result is in very good accordance with the conclusions of Refs. [1–6,27,28,30,34], where it was found that the surface of the polycrystalline Bi electrode mainly consists (from 50 to 70%) of comparatively large homogeneous surface areas (grains), the adsorption characteristics of which are very close to the Bi(001) plane characteristics. The comparison of the $-\Delta G_A^0$ values of *n*-PA and cyclohexanol adsorption at Bi, Hg and Zn electrodes [1–6,10,11,20,35] shows that the hydrophilicity of electrodes increases in the sequence Bi(01$\bar{1}$) < Hg < Bi(2$\bar{1}\bar{1}$) < Bi(001) < Bi(111) < Zn(0001) < Zn(10$\bar{1}$0) < Zn(11$\bar{2}$0).

The positive values of the lateral interaction constant a means that the surfactant–surfactant and water–water interactions are much more attractive than the surfactant–water interaction. At negative surface charge densities, the molecular interaction parameter a decreases in the sequence of planes (001) ≥ (111) > (01$\bar{1}$) as the superficial density of planes increases and the limiting Gibbs adsorption decreases. The dependence of a on E is approximately parabolic and this result shows that the value of the projected area of the organic compound at the electrode surface linearly decreases as the surface coverage increases. The value of a increases in the order Bi(01$\bar{1}$) < Bi(111) < Hg < Bi(001) < Zn(0001) [10,11,20] as the value of Γ_{max} and the hydrophilicity of electrodes increases. The stronger water adsorption causes a more vertical orientation of adsorbate molecules, and the increase of E_N values. The value of a increases in the order of adsorbates *n*-PA < *tert*-BA < *n*-BA ≤ *sec*-BA ≤ iso-BA < CH as the molar volume of the adsorbate increases (except BAC). The lower value of a for *n*-BA than for *sec*-BA and iso-BA probably indicates that the hydrocarbon tail in the adsorption layer is not linear or the *n*-BA molecules would have the more tilted orientation.

The limiting Gibbs adsorption Γ_{max} increases in the order of electrodes Bi(01$\bar{1}$) < Bi(111) < Bi(001) as the superficial density of planes decreases. The projected area S_{max} decreases and Γ_{max} increases in the order *n*-BA < *n*-PA. The decreases of Γ_{max} and of the limiting potential shift E_N values and the increase of S_{max} as the number of carbon atoms in the aliphatic alcohol molecule increases, can be explained by an increasingly tilted orientation of *n*-BA molecules compared with *n*-PA at the single-crystal Bi(001) and Bi(111) planes, as well as at Hg [10–12] electrodes. Very low values of Γ_{max} and the E_N values for Bi(01$\bar{1}$) indicate that the *n*-PA molecules probably have a flat orientation on the chemically most active Bi(01$\bar{1}$) plane.

Acknowledgements

This work was supported in part by the Estonian Science Foundation under Project No. 612.

References

[1] E.J. Lust, U.V. Palm, Soviet Electrochem. 21 (1985) 1304, Engl. tr.
[2] E.J. Lust, U.V. Palm, Soviet Electrochem. 22 (1986) 378, Engl. tr.
[3] E.J. Lust, U.V. Palm, Soviet Electrochem. 22 (1986) 383, Engl. tr.
[4] E.J. Lust, J.J. Ehrlich, U.V. Palm, Soviet Electrochem. 22 (1986) 695, Engl. tr.
[5] E. Lust, A. Jänes, K. Lust, P. Mindla, J. Electroanal. Chem. 413 (1996) 175.
[6] E. Lust, A. Jänes, P. Mindla, K. Lust, J. Electroanal. Chem. 425 (1997) 25.
[7] R.J. Pullerits, M.E. Moldau, U.V. Palm, Elektrokhim. 11 (1975) 487.
[8] B.B. Damaskin, U.V. Palm, Itogi Nauki Tekh.: Elektrokhim. 14 (1977) 99.
[9] V.E. Past, R.J. Pullerits, M.E. Moladau, Trans. Tartu Univ. 757 (1986) 140.
[10] B.B. Damaskin, O.A. Petrii, V.V. Batrakov, Adsorption of Organic Compounds on Electrodes, Plenum, New York, 1971, p. 35.
[11] B.B. Damaskin, A.A. Survila, L.E. Rybalka, Elektrokhim. 3 (1967) 146.
[12] M.R. Moncelli, M.L. Foresti, R. Guidelli, J. Electroanal. Chem. 295 (1990) 225.
[13] M.L. Foresti, M. Innocenti, R. Guidelli, J. Electroanal. Chem. 376 (1994) 85.
[14] L.M. Doubova, S. Valcher, S. Trasatti, J. Electroanal. Chem. 376 (1994) 73.
[15] J. Lipkowski, L. Stolberg, in: J. Lipkowski, P.N. Ross (Eds.), Molecular Adsorption at Metal Electrodes, VCH, New York, 1992, p. 171.
[16] N.B. Grigoryev, D.N. Machavariani, Elektrokhim. 5 (1969) 87.
[17] N.B. Grigoryev, V.P. Kuprin, Y.M. Loshkaryev, Elektrokhim. 9 (1973) 1812.
[18] N.B. Grigoryev, A.M. Kalyuzhnaya, Elektrokhim. 10 (1974) 1287.
[19] L.E. Rybalka, B.B. Damaskin, D.I. Leikis, Elektrokhim. 11 (1975) 9.
[20] Y.P. Ipatov, V.V. Batrakov, V.V. Shalaginov, Elektrokhim. 12 (1976) 286.
[21] S. Trasatti, Electrochim. Acta 37 (1992) 2137.
[22] L.M. Doubova, S. Trasatti, J. Chem. Soc., Faraday Trans. 91 (1995) 3311.
[23] S. Amokrane, J.P. Badiali, in: J.O.M. Bockris, B.E. Conway, R.E. White (Eds.), Modern Aspects of Electrochemistry 22, 1992, p. 1.
[24] D. Rolle, J.W. Schultze, J. Electroanal. Chem. 229 (1987) 141.
[25] A.N. Frumkin, Potentsialy Nulevogo Zaryada, Nauka, Moskva, 1979, p. 276.
[26] I.A. Bagotskaya, Itogi Nauki Tekh.: Elektrokhim. 22 (1986) 60.
[27] E. Lust, K. Lust, A. Jänes, Russ. J. Electrochem. 31 (1995) 876.
[28] E. Lust, A. Jänes, K. Lust, R. Pullerits, J. Electroanal. Chem. 1997, submitted.
[29] D.D. Perrin, W.L.F. Armanego, Purification of Laboratory Chemicals, 3rd edn., Pergamon, Oxford, 1986.
[30] E.J. Lust, U.V. Palm, Soviet Electrochem. 24 (1988) 227, Engl. tr.
[31] G.A. Tedoradze, R.A. Arakelyan, Dokl. Akad. Nauk SSSR 156 (1964) 1170.
[32] R.P. Armstrong, W.P. Race, H.R. Thirsk, J. Electroanal. Chem. 16 (1968) 517.
[33] K. Takashasi, Electrochim. Acta 13 (1968) 1609.
[34] E. Lust, A. Jänes, K. Lust, M. Väärtnõu, Electrochim. Acta 42 (1997) 771.
[35] Y.P. Ipatov, V.V. Batrakov, Elektrokhim. 11 (1975) 1282.
[36] J. Richer, J. Lipkowski, J. Electroanal. Chem. 251 (1988) 217.
[37] J. Lipkowski, C.N. Van Huong, C. Hinnen, R. Parsons, J. Chevalet, J. Electroanal. Chem. 143 (1983) 375.
[38] J. Richer, J. Lipkowski, Langmuir 2 (1986) 630.

[39] A. Ianelli, J. Richer, L. Stolberg, J. Lipkowski, Plating Surf. Finish 77 (1990) 47.
[40] W.B. Pearson, The Crystal Chemistry and Physics of Metals and Alloys, Wiley-Interscience, New York, 1972, p. 280.
[41] A. Daghetti, S. Trasatti, I. Zagorska, Z. Koczorowski, J. Electroanal. Chem. 204 (1986) 298.
[42] L. Stolberg, D.E. Irish, J. Lipkowski, J. Electroanal. Chem. 238 (1987) 333.
[43] R. Parsons, J. Electroanal. Chem. 7 (1964) 136.
[44] R. Parsons, J. Electroanal. Chem. 8 (1964) 93.

XI

Journal of Electroanalytical Chemistry, accepted JEC 07041,
E. Lust, A. Jänes, K. Lust and P. Miidla,
Adsorption of Normal Hexanol
on Bismuth Single Crystal Plane Electrodes, pages 1–27,

ADSORPTION OF NORMAL HEXANOL ON BISMUTH SINGLE CRYSTAL PLANE ELECTRODES

E. Lust, A. Jänes, K. Lust and P. Miidla*

Institute of Physical Chemistry, University of Tartu,
2 Jakobi Street, EE-2400 Tartu, Estonia
*Institute of Applied Mathematics, University of Tartu,
2 Liivi Street, EE-2400 Tartu, Estonia.

Abstract

Cyclic voltammetry, impedance and chronocoulometry have been employed for quantitative study of 1-hexanol (*n*-HA) adsorption at the bismuth single crystal plane | aqueous Na_2SO_4 solution interface. The adsorption characteristics obtained from the impedance and chronocoulometric measurements are in reasonable agreement within the limits of surface charge densities $-18 < \sigma < 5$ μC cm^{-2}. The adsorption isotherms, Gibbs energies of adsorption ΔG_A^0, the limiting surface excess Γ_{max} and other adsorption parameters, dependent on the crystallographic structure of electrodes, have been determined. The adsorption of *n*-HA on Bi single crystal planes is mainly physical and is limited by the rate of diffusion of organic molecules to the electrode surface. Comparison of the adsorption data for *n*-HA with normal propanol (*n*-PA), normal butanol (*n*-BA), butyl acetate (BAC), cyclohexanone (CHN), cyclohexane carboxylic acid (CHCA) and cyclohexanol (CH) shows that the adsorption characteristics depend on the structure of hydrocarbon radical, as well as on the chemical nature of functional group of adsorbate. The adsorption activity of adsorbates at bismuth | solution interface increases in the sequence *n*-PA < *n*-BA < CH < CHCA < CHN < BAC < *n*-HA as the adsorption at the air | solution interface increases, except CHCA. In the case of all compounds studied, the adsorption activity increases in the sequence of planes (111) < (001) < ($01\bar{1}$). According to the values of the standard Gibbs energy of adsorption it was established that the hydrophilicity of electrodes increases in the sequence Sb($2\bar{1}\bar{1}$) <Sb(001) < Sb(111) < Bi($01\bar{1}$) < Bi($2\bar{1}\bar{1}$) < Bi($\bar{1}0\bar{1}$) ≤ Hg ≤ Bi(001) < Bi(111) < Cd(0001) < Cd($10\bar{1}0$) < Cd($11\bar{2}0$) < Ag(111) < Ag(100) < Ga < Ag(110) < Zn(0001) < Zn($10\bar{1}0$) < Zn($11\bar{2}0$).

1. Introduction

This work is a part of the project devoted to the study of the influence of the crystallographic structure of bismuth on the adsorption of neutral organic molecules at the Bi | solution interface [1–8]. Adsorption of various organic compounds at the polycrystalline bismuth solid drop electrode (BDE) has been described previously

[9–14]. The statistical treatment of the electron diffraction studies and capacity data shows that the surface of the BDE consists mainly (*ca* 60%) of homogeneous segments whose crystallographic, double layer and adsorption characteristics are similar to those for the (001) plane of bismuth [9, 15].

The electrosorption behaviour of the same aliphatic compounds from electrolyte solutions on different metals under the other identical conditions may provide further useful information on the role played by metal–water and water–water interactions upon electrosorption [1–24]. In fact, the chemical nature and crystallographic structure of the single crystal plane electrode is known to affect the structuring of interfacial water molecules; which has been studied extensively from both experimental and theoretical points of view [1–8, 16–28]. Systematic adsorption measurements of *n*-aliphatic alcohols and their isomers from aqueous electrolyte solutions have been carried out on various sp-metals, such as Hg, Pb, Bi, Cd, Sn, Sb, Zn, In-Ga and Ga [9–14, 18–24, 29–39]. In general, these measurements indicate that the adsorption of aliphatic compounds is weaker the more hydrophilic is the metal. Comparison of the adsorption data of *n*-PA, *n*-BA, CH, CHN, CHCA and BAC shows that the difference of the adsorption parameters for various planes increases as the adsorption activity of adsorbate at the air | solution, as well as at the electrode | electrolyte solution interface rises [6, 35, 36, 40–42]. This is mainly caused by the fact that with decreasing the molar volume of adsorbate the transformations in the adsorption layer structure, caused by the adsorption of one surfactant molecule, decrease in comparison with the situation when the adsorption of very large particles takes place. The adsorption investigation of various butanol isomers [5] shows that the adsorption parameters depend on the geometrical structure of hydrocarbon tail of adsorbate, and thus the comparison of adsorption behaviour of *n*-HA with CH would provide more information on the influence of the hydrocarbon chain structure on the adsorption process and about the attractive interactions in the adsorbed layer. However, a further difficulty in comparison the results from different laboratories lies in the fact that different experimental techniques are often used [18–21].

Therefore we have carried out systematic simultaneous impedance (capacity bridge) and chronocoulometric investigations of the adsorption of various organic substances on Bi single crystal planes. For a more profound understanding of the importance of the crystallographic structure of the electrode surface and the geometrical structure of the hydrocarbon chains of adsorbate in adsorption phenomena, in the present work we investigated the adsorption of normal hexanol (*n*-HA) on singular (111), (001) and $(01\bar{1})$ faces of bismuth and compared the established results with the adsorption data of various organic compounds on Bi planes [1–8].

2. Experimental

The experimental procedure used in this work has been described in Refs. [1–8]. The final surface preparation was obtained by electrochemical polishing in the aqueous KI + HCl solution. Thereafter, the second X-ray diagram was used to de-

termine the precise angle, and only the samples whose precision on the orientation was better than $\pm 0.10°$ were used for electrochemical investigations. After the electrochemical polishing, the electrodes were very well rinsed with ultra purified water and were polarised at –1.0 V vs. a saturated calomel electrode (SCE) in the working surface-inactive solution.

For an additional characterisation of the working surface of electrodes, electron microscopic analysis by JEOL-JSM-35CF at the SEI regime was made (40000 × max.). According to these measurements, the electrochemically polished surfaces of bismuth electrodes were smooth (naturally within the range of the sensitivity of electron microscopy) [7].

Water for preparing the solutions was treated with the Milli Q+ purification system. Solutions were prepared volumetrically using Na_2SO_4 purified by triple recrystallization from water, and treated in vacuum to dryness. Na_2SO_4 was calcined at 700°C immediately prior to the measurements. The change of the Na_2SO_4 solution pH in the range 4.0 to 6.0 was effected by the addition of a calculated amount of H_2SO_4 solution prepared from triply distilled concentrated sulphuric acid. Electrolytic hydrogen was bubbled for 1–2 hours through the electrolyte before the submersion of the electrode into the solution and the temperature was kept at 298 K. (normal hexanol) was purified according to Ref. [43].

3. Results and discussion

3.1. Cyclic voltammograms (CVs)

The CVs were recorded in order to determine the quality of the surfaces investigated and the potential range in which the adsorption of *n*-HA occurred. The shape of the CV recorded for the supporting electrolyte was characteristic of the bismuth single crystal planes in accordance with our previous studies [1–8]. The cyclic voltammetry curves also indicate that the bismuth single crystal planes investigated are ideally polarizable in the potential range of –1.8 to –0.35 V (SCE) in aqueous 0.05 M Na_2SO_4 solution. In aqueous 4.99×10^{-2} M Na_2SO_4 + 1×10^{-4} M H_2SO_4 solution, bismuth electrodes are ideally polarizable in the range of –1.3 to –0.1 V (SCE).

3.2. Differential capacity vs. potential curves (C(E)-curves)

The edl differential admittance was measured at *ac* frequency ν from 60 to 21000 Hz. The capacity dispersion with ν is small in the proximity of the differential capacity minimum (in the region of maximum adsorption), whereas it increases noticeably in the region of the adsorption–desorption peaks. Comparison of the $(C^{max} - C_0)$ vs. $\omega^{1/2}$ curves (C^{max} — differential capacity at the potential of adsorption-desorption maximum E^m; C_0 — differential capacity at E^m in the base electrolyte; — $\omega = 2\pi\nu$) for *n*-PA, *n*-BA, CH, *n*-HA, BAC and pyridine (PY) shows that this dependence increases in the presented order of compounds as the adsorption

activity at the air | solution or at the metal | solution interface rises, thus as the molecular weight and the molar volume of the adsorbate increases, except PY. The anomalous position of PY is probably caused by the weak chemical interaction of this compound with the Bi electrode surface [8]. The same conclusion is valid if the adsorption of PY at Ag and Au single crystal planes occurs [20, 45, 46]. As shown in Refs. [23, 47], if the rate of the adsorption of organic compounds is limited by diffusion, the equilibrium values of differential capacity at $\nu = 0$ can usually be found with a sufficient degree of accuracy by extrapolation of the $C_{add}(\omega^{1/2})$-curve to $\omega^{1/2} = 0$. According to the experimental results, in the region of $60 < \nu < 410$ Hz, the $C_{add}(\omega^{1/2})$-curves have a good linearity and, accordingly, we can obtain the equilibrium values of differential capacity.

According to the method described in Refs. [23, 47–49], the equilibrium values of differential capacity can be calculated by Eq. (1)

$$C_{add}(\omega = 0) = C_{add}^2(\omega) R_p^2(\omega)\omega^2 + 1 / \{[C_{add}(\omega) R_p(\omega)\omega - 1] R_p(\omega)\omega\}, \quad (1)$$

where $C_{add}(\omega)$ and $R_p(\omega)$ are the values of differential (additional) capacity and parallel resistance at $\omega = \text{const}$. The components of the adsorption impedance were calculated from the impedance data of the cell used for the measurements (series circuit), i.e. $C_S(\omega)$ and $R_S(\omega)$, following the procedure described in Refs. [23, 47–49]. By extrapolating the $R_S(\omega)$- values to $\omega \to \infty$ the solution resistance $R_S(\omega) = R_{sol}$ was determined. Since the amount of organic compounds added is small and does not affect the solution resistance, one can assume R_{sol} to be equal to the ohmic component R_S of the impedance in the pure base electrolyte solution. The values of R_{sol} and R_S obtained in this work are in good agreement with the data of Refs. [5, 50]. Then the series equivalents $R_S(\omega) - R_{sol}$ and $C_S(\omega)$ of impedance were converted into the parallel equivalents $C_P + C_{true}$ and R_P using the relations given in Refs. [23, 47–49].

The equilibrium values of $C_{add}(\omega = 0)$ for 0.04 M *n*-HA + 0.05 M Na_2SO_4 system, calculated by Eq. (1), at E^m are 77–82 μF cm^{-2}, 74–79 μF cm^{-2} and 71–77 μF cm^{-2} for Bi(001); Bi(111) and Bi(01$\bar{1}$) respectively. These values are in good agreement with the values obtained from $C_{add}(\omega^{1/2})$-curves at the condition $\omega^{1/2} = 0$ (76 ± 5.0 μF cm^{-2} for Bi(111); 76 ± 5.0 μF cm^{-2} for Bi(001) and 73 ± 6.0 μF cm^{-2} for Bi(01$\bar{1}$)).

All the $C(E)$-curves ($\omega = 0$) determined in the presence of *n*-HA in the solutions investigated merge with the curve for the supporting electrolyte at –1.8 V (SCE) (Fig. 1), indicating that *n*-HA molecules are completely desorbed from the bismuth surface at these negative potentials. At less negative potentials the $C(E)$-curves display the characteristic adsorption–desorption peaks. The height of the peak increases and its potential shifts to the negative direction with increasing *n*-HA concentration. As we can see from Fig. 1 and Fig. 2, the shape (the height and width) of the adsorption–desorption maximum at $c_{org} = \text{const}$. depends on the geometrical structure of the adsorbate hydrocarbon chains and at $E < E_{\sigma=0}$ the attractive interaction between the adsorbed molecules increases in the sequence *n*-PA < *n*-BA < *n*-HA < BAC < CH. The potential of the adsorption–desorption maximum E^m at

$E < E_{\sigma=0}$ (c_{org} = const.) depends on the geometrical structure of the adsorbate, and the adsorption activity of adsorbates increases in the sequence of *n*-PA to *n*-HA (Fig. 3). The height and potential of the adsorption–desorption peaks depend on the geometrical structure of the electrode surface and this dependence is more pronounced for CH in comparison with *n*-PA adsorption at Bi planes (Fig. 4). According to the experimental data these maxima increase in height in the sequence of faces $(01\bar{1}) < (111) \leq (001)$. Accordingly, the attractive interaction constant a^m at peak potentials E^m increases as the superficial density of atoms decreases. The same tendency is valid for *n*-PA, *n*-BA, CH, CHE, CHCA and PY adsorption at the Bi single crystal plane electrodes [1–8].

At $E \sim E_{\sigma=0}$ the differential capacity decreases to a value much smaller than that observed for the pure base electrolyte. The potentials of capacity minimum of the $C(E)$-curves E_{max} are independent of the concentration of adsorbate indicating that the orientation of adsorbed *n*-HA molecules is practically independent of the surface coverage θ in the region of maximum adsorption. The values of the limiting capacity C_1 at the surface coverage $\theta = 1$ at $E = E_{max}$, obtained by the extrapolation of the linear dependence of $1/C$ on $1/c_{org}$ to $1/c_{org} = 0$ (c_{org} — concentration of organic compound in solution), increase in order of planes $(001) < (111) < (01\bar{1})$ (Table 1). According to the Helmoltz equation for the plate condenser $C = \varepsilon / 4\pi d$ (where ε is the dielectric permittivity of the adsorbed layer, and d is the thickness of the adsorbed layer) the decrease of C_1 can be explained by the decrease of ε caused by the increase of the amount of organic compound in the adsorbed layer, as well as by the increase of the adsorbed layer thickness, which may be caused by the more vertical orientation of the adsorbed molecules. The same order of the dependence of C_1 on the crystallographic structure of the electrode surface is valid for *n*-PA, *n*-BA, CH and BAC adsorption at Bi electrodes. A more detailed discussion will be given late.

The adsorption–desorption maxima at $E^m > E_{\sigma=0}$ for *n*-HA were found at $-0.3 < E < -0.05$ V (SCE). For more concentrated solutions of *n*-HA ($c_{org} > 0.035$ M), the peaks lie at very positive potentials ($E > -0.15$ V (SCE)) and are probably distorted by a slight specific adsorption of anions [2–6]; therefore, they were not used for the calculation of adsorption parameters. As in the region of potentials $E^m < E_{\sigma=0}$, the height of peaks at $E^m > E_{\sigma=0}$ increase in the order of planes $(01\bar{1}) < (111) \leq (001)$, but the maxima at $E^m > E_{\sigma=0}$ are noticeably narrower than those at $E < E_{\sigma=0}$. Thus, the attractive interaction at $E > E_{\sigma=0}$ is somewhat higher than that for negatively charged surface.

3.3. Charge density–potential curves

The charge density–potential $\sigma_0(E)$-curve for base electrolyte solution was obtained by the integration of the $C(E)$-curve ($\omega = 0$), starting from the potential of zero charge $E_{\sigma=0}$. The values of $E_{\sigma=0}$ for different Bi singe crystal planes were obtained from the position of the diffuse layer minimum on independently measured differential capacity curves for a dilute solutions of the base electrolyte. The established

values of $E_{\sigma=0}$ were in good agreement with our previous data [5–7, 28, 50]. The charge density–potential curves for solutions with different additions of adsorbate were obtained by back integration of the $C(E)$-curves ($\omega = 0$), starting from $E = -1.8$ V (SCE) and assigning the value of σ ($E = -1.8$ V) equal to σ_0 ($E = -1.8$ V), because there is no adsorption at $E = -1.8$ V (SCE). The shape of $\sigma(E)$-curves is typical observed for the adsorption of neutral organic molecules at ideally polarizable electrodes [2–8] (Fig. 5) and will be discussed later.

The values of the initial and final potentials for the potential step experiments were chosen with the help of the $C(E)$- and cyclic voltammetric $i(E)$-curves. The initial potential E_i was varied from –0.40 to –1.80 V (SCE). The final potential E_f was equal to –1.60 V (SCE) for $c_{org} \leq 0.005$ M and –1.80 V (SCE) for $c_{org} > 0.005$ M. This value was chosen carefully in order to: (1) achieve the complete desorption of *n*-HA, (2) keep the current of hydrogen evolution small enough so that the faradaic reaction would not interfere with the determination of the electrode charge density (σ) [5, 8, 18–21, 29, 45, 46]. Five series of step experiments were made for *n*-HA concentrations from 2×10^{-4} to 4×10^{-2} M.

The chronoamperometric curves were integrated digitally to obtain the charge transients [8, 18–21, 29, 45, 46]. The chronocoulometric curves display an initial fast-rising section, corresponding to the charging of the edl followed by a quasi-plateau in which the charge varies slowly and linearly with time. The slope of this segment is small (owing to a very slight hydrogen evolution reaction), but it is smaller than this for *n*-PA or *n*-BA, and thus, the adsorption of *n*-HA causes the rise of the hydrogen evolution overpotential. These linear segments of the transients were extrapolated to zero time to obtain the relative charge densities $\Delta\sigma$. In this way, the faradaic contribution from hydrogen evolution was minimised. The relative charge densities $\Delta\sigma$ were determined from these step measurements:

$$\Delta\sigma(E) = \sigma(E_i) - \sigma(E_f) \tag{2a}$$

In Eq. (2a) $\sigma(E_i)$ and $\sigma(E_f)$ are the charge densities at the metal side of the interface at potentials E_i and E_f respectively. Knowing the value of $E_{\sigma=0}$, determined by impedance measurements in the dilute solutions of base electrolyte [5, 50], the absolute charge densities for surface inactive electrolyte solution were calculated for each value of E by using the formula

$$\sigma(E) = \Delta\sigma(E) - \Delta\sigma(E_{\sigma=0}) \tag{2b}$$

The absolute charge densities for solutions with addition of *n*-HA were calculated according to the Eq. 2c

$$\sigma(E) = \sigma_0(E = -1.8 \text{ V (SCE)}) - \Delta\sigma(E) \tag{2c}$$

were $\sigma_0(E = -1.8$ V (SCE)) is the surface charge density obtained for the base electrolyte solution at $E = -1.8$ V (SCE), as there is no adsorption of *n*-HA at this potential. The precision of charge measurements is about 2–3%.

The $\sigma(E)$-curves for different concentrations of *n*-HA investigated intersect the curve obtained for the base electrolyte (Fig. 5). The comparison of the charge–potential data for the capacitance and potential step measurements shows that the

difference between the values of σ, obtained by these different methods, does not exceed ± 0.75 μC cm^{-2} which is only slightly higher than the experimental error of the obtaining of σ values. The small deviation of σ,E-curves, obtained from impedance, from the chronocoulometric σ,E-curves indicate that in spite of the extrapolation of C,E-curves to $\omega = 0$ these curves are non-equilibrial. Comparison of the charge — potential data for *n*-PA, *n*-BA, *tert*-BA, CH, *n*-HA and PY [6–8, 50] shows that the difference between σ values obtained by these methods increases in the sequence of adsorbates *n*-PA < *n*-BA < *tert*-BA < CH < *n*-HA < PY as the adsorption activity of organic compound at the electrode rises. Therefore, the quantitative data, presented in this work, are mainly obtained from the chronocoulometric measurements. The potential at which the curves intersect is the potential of maximum adsorption E_{max}. As we can see from Fig. 5, E_{max} is practically independent of C_{ads} and the values of E_{max} are equal to –0.85; –0.75 and –0.70 V for Bi(111), Bi(001) and Bi($01\bar{1}$) planes respectively. These values of E_{max} are in good agreement with the potential of capacity minimum at $C(E)$-curves. The charge density $-\sigma_{max}$, at which the maximum adsorption takes place, slightly depends on the plane, and the absolute value of σ_{max} decreases in order $(01\bar{1}) < (001) < (111)$ ($-\sigma_{max}$ is equal to 3.5; 4.0 5.0 μC cm^{-2} respectively). The nearly linear segments are observed on the $\sigma(E)$-curves close to E_{max}. By linear extrapolation of these fragments of the curve to $\sigma = 0$, one can determine the potential of zero charge corresponding to the surface covered by adsorbate molecules. The difference between these experimental values and the value of $E_{\sigma=0}$ for the pure base electrolyte solution is equal to the change in the surface potential due to the displacement of a monolayer of water molecules by a monolayer of adsorbate (E_N). Thus, the variation of the charge and the potential of maximum adsorption reflects changes in the shift of the potential of zero charge. The established values of E_N are presented in Table 1. These quantities are related by the following equation derived from the model of two parallel capacitors [23]

$$E_{max} - E_{\sigma=0} = -E_N C_1/(C_0 - C_1); \qquad \sigma_{max} = -E_N C_1 C_0/(C_0 - C_1) \tag{3}$$

The calculations show that the values of E_N increase in the sequence of Bi planes $(01\bar{1}) < (001) \leq (111)$, and this is in good agreement with the decrease of absolute values of σ_{max} in the sequence of the planes $(111) > (001) > (01\bar{1})$. The same order of planes is valid for *n*-PA, *n*-BA, CH, BAC, PY, CHE and CHCA adsorption at Bi planes [1–8, 50]. With the help of the unrationalized Helmholtz formula, E_N can be expressed as

$$E_N = 4\pi\Gamma_{max}(\mu^{org} - n\mu^w)/\varepsilon \tag{4}$$

where Γ_{max} is the limiting surface excess of *n*-HA; μ^{org} and μ^w are the components of the dipole moment normal to the surface of the electrode for organic compound and H_2O molecules respectively; $\mu^{org} - n\mu^w = \bar{\mu}_{eff}$ where $\bar{\mu}_{eff}$ is the effective dipole moment; n is the number of H_2O molecules, displaced by the one adsorbed *n*-HA molecule; and ε is the permittivity of the inner layer. The positive sign of E_N indicates that either (1) $|\mu^{org}| > |n\mu^w|$ and $\mu^{org} > 0$ ($\mu^w \lessgtr 0$) or (2) $|\mu^{org}| < |n\mu^w|$ and

$\mu^{org} < 0$ ($\mu^{org} <_{>} 0$). In the first case μ^{org} is positive what means that the molecules of *n*-HA are oriented with the hydrocarbon chain facing the Bi surface at E_{max}. In the second case *n*-HA molecules may be oriented with the hydrocarbon tail towards the electrode surface ($\mu^{org} > 0$), as well as the –OH group facing the electrode surface ($\mu^{org} < 0$). In these two latter cases, the positive values of E_N would suggest a strong preferential orientation of H_2O with oxygen atoms towards the electrode surface at E_{max} (not far from $E_{\sigma=0}$) with $\mu^{w} < 0$, which is in contradiction with the data of very weak H_2O adsorption at Bi planes [1–8, 28, 42]. As the maximum adsorption of *n*-HA takes place at the slightly negatively charged surfaces it seems that the first possibility for Bi(111), Bi(001) and Bi($01\bar{1}$) planes is more plausible. Thus, the effective dipole moment of the organic molecules must be positive and in the region of potentials of maximum adsorption *n*-HA molecules on bismuth single crystal planes are oriented with the hydrocarbon radical facing the bismuth surface and the functional –OH group facing the solution side of interface. The same conclusions are valid if the adsorption of aliphatic alcohols *n*-PA ($E_N = 0.33$V); *n*-BA ($E_N = 0.24$V); and *n*-HA ($E_N = 0.20$V) takes place at Hg electrode from 0.1 M NaF aqueous solution [21, 22, 23, 29]. The noticeably lower value of E_N for Bi($01\bar{1}$) plane probably indicate that a more pronounced horizontal orientation of *n*-HA at this chemically most active plane is plausible. The value of E_N depends on the geometrical structure of the hydrocarbon chain of adsorbate, and the effective dipole moment $\overline{\mu}_{eff}$ increases in the sequence of adsorbates *n*-HA < BAC < *n*-BA < CH ≤ CHCA < CHE < *n*-PA < PY [1–8]. Thus, at Bi planes investigated the *n*-HA molecules would have the more horizontal orientation compared with *n*-PA or *n*-BA molecules adsorbed [3, 5–7]. The same conclusion is valid for Hg electrode [22, 23, 29]. The effective dipole moment of compounds, containing six carbon atoms, increases in the sequence *n*-HA < BAC < CH < CHE [1–7] as the effective dipole moment of organic compound in gas phase rises [43, 51].

3.4. Specific surface work and film pressure curves

The capacitance curves were twice back–integrated, and the chronocoulometric $\sigma(E)$-curves were once back-integrated to obtain a specific surface work decrease ($\gamma - \gamma_0$) as a function of the electrode potential and adsorbate concentration [6–8, 18–21, 50]. The second integration was performed from the same negative charge at first, assigning the value of zero to the specific surface work at the pzc in the base solution. A good accordance between ($\gamma - \gamma_0$)(E)-curves, obtained from capacity–potential and potential step measurements ($\Delta(\gamma - \gamma_0) = \pm 0.50$ μJ cm^{-2}), can be seen between –13 and 4 μJ cm^{-2}, where the thermodynamic analysis takes place.

The pressure of the film of adsorbate π can be determined as

$$\pi(E) = \gamma_{c=0} - \gamma_c = \int_{E_0}^{E} \sigma_c \, \mathrm{d}E - \int_{E_0}^{E} \sigma_{c=0} \, \mathrm{d}E \qquad (5)$$

where subscripts c and $c = 0$ indicate the presence or absence of the adsorbate in the bulk of the electrolyte respectively. The calculated $\pi(E)$-curves are plotted in Fig. 6.

For more concentrated solutions of *n*-HA ($c \geq 0.005$ M) the curve displays a maximum, the potential of which is practically independent of c_{org} and this value is in good agreement with the value of E_{max} for $C(E)$-curves. The comparison of the $\pi(E)$-curves, obtained from capacity–potential ($\omega = 0$) and potential step measurements, shows that the departure of Bi | *n*-HA system from the equilibrium is small under the peak at negative rational potentials. The film pressure of the adsorbate at c_{org} = const. increases in the sequence of compounds n-PA < *n*-BA < CH < CHCA < CHE < BAC < *n*-HA (Fig. 7). Accordingly, the adsorption activity of compounds increases in the presented sequence of adsorbates.

The adsorption activity of bismuth electrodes increases in the sequence of planes (111) < (001) < $(01\bar{1})$ as the surface density of atoms increases (except Bi(111)). This deviation is evidently determined by the competitive adsorption of water and the organic substance, as well as by the crystallographic and electronic structure of electrodes. Just as in the case of CH, BAC, CHE, CHCA [1–7, 50], butanol isomers [5] and PY [8] adsorption, the basal plane (111), where the surface atoms are chemically saturated (electron configuration sp^3d^2) [52], has the lowest adsorption activity. The most active one is the singular face Bi$(01\bar{1})$, where unsaturated covalent bonds are distributed uniformly over the whole surface (s^2p^3).

3.5. Gibbs excess — potential and Gibbs excess — log c_{org} curves

The film pressure data were used to calculate the relative Gibbs surface excess. First the film pressure was plotted against ln c_{org} at E = const. (Fig. 8). The curves display a long linear section, its slope giving the limiting value of Γ_{max}

$$\Gamma = \frac{1}{RT}\left(\frac{\partial \pi}{\partial \ln c}\right)_{E,T,p} \tag{6}$$

As the mole fraction of *n*-HA never exceed 1.5%, at the first approximation, it was assumed that the activity of *n*-HA depends linearly on its concentration according to Henry's law [6, 16–27, 53–55]. The values of Γ_{max} obtained for *n*-HA are presented in Table 1 and the comparison of these data with data of Refs. [2–7, 50] shows that Γ_{max} decreases in the sequence of adsorbates: *n*-PA >*n*-BA > CH > *n*-HA as the molar volume of organic compounds increases. Calculated according to the values of Γ_{max} the values of the molecular surface area S_{max} (Table 1), corresponding to the area of one adsorbed molecule on the electrode surface at the maximum adsorption potential E_{max}, decrease in order of Bi planes $(01\bar{1})$ > (111) ≥ (001). If the adsorbed molecules of *n*-PA, *n*-BA and *n*-HA were oriented perpendicularly at the Bi | electrolyte interface, the values of S_{max} should be the same for *n*-PA, *n*-BA and *n*-HA and would be equal to $S_{max}^{theor} \sim 0.21$ nm^2 [23, 24]. The same conclusion would be valid, if the orientation of adsorbed molecules is independent of the crystallographic structure of the electrode surface. The theoretical value of S_{max}, corresponding to the horizontal orientation of *n*-HA, is equal to 0.42 nm^2 (Γ_{max} 3.95×10^{-10} mol cm^{-2}). The increase of the projected area S_{max} as the number of carbon atoms n_C in the hydrocarbon radical increases can be explained by more tilted ori-

entation of adsorbate molecules going from *n*-PA to *n*-HA [5, 6], as well as from Bi(001) to Bi($01\bar{1}$). This conclusion is in good accordance with the noticeable decrease of E_N and $\bar{\mu}_{eff}$ values for *n*-HA compared with *n*-BA and *n*-PA, and with the noticeable decrease of attractive interaction constant a in the sequence of planes Bi(001) ≥ Bi(111) > Bi($01\bar{1}$). The same tendency is valid for Ag, Hg and Zn(0001) electrodes if the adsorption of aliphatic alcohols occurs [23, 29, 35, 36].

As in the bent region of the π(ln$c$)-curves the slope changes noticeably and the error of differentiation of π(ln$c$)-curves is large [20], the related Gibbs excess values for the intermediate coverages were determined from the electrode charge densities using the well-known formula [20, 23]

$$\Gamma = \frac{\sigma_\Gamma - \sigma_{\Gamma=0}}{\sigma_{\Gamma_{max}} - \sigma_{\Gamma=0}} \Gamma_{max} \tag{7}$$

The values of $(\sigma_{\Gamma_{max}} - \sigma_{\Gamma=0})$ were obtained by the extrapolation of the linear sections of the $\sigma(E)$-curves. The shape of the $\Gamma(E)$-curves for different c_{org} and of the Γ(log$c$)-curves (Fig. 9 and Fig. 10) suggest that the relative maximum of the adsorption of *n*-HA on all the planes investigated reaches at $-0.6 < E < -1.4$ V (SCE) and Γ_{max} depends on the crystallographic structure of the surface. The values of Γ_{max} increase in the order of electrodes ($01\bar{1}$) < (111) < (001) and these values are in good accordance with Γ_{max}, obtained from π(ln$c$)-curves. The slope of $\Gamma(E)$-curves at the region of intermediate values of Γ (c_{org} = const.) increases in the order of planes ($01\bar{1}$) < (111) < (001) and in the order of adsorbates *n*-PA < *n*-BA < *n*-HA < CH as the attraction between the adsorbed molecules rises.

The decrease of Γ_{max} values causes the decrease of the thickness and the effective dielectric constant of the adsorbed layer, and according to the Helmholtz equation, it causes the increase of C_1 values in the order of planes Bi(111) < Bi(001) < Bi($01\bar{1}$). The value of Γ_{max} rises in the sequence of electrodes Ag(100) < Ag(111) < Bi($01\bar{1}$) < Bi(111) < Bi(001) < Hg [19, 29].

3.6. Adsorption isotherms

The surface coverage at $E = E_{max}$ was first estimated from Eq. (8) based on Frumkin's two parallel condensers model [18, 23, 29].

$$\theta = (C_0 - C_\theta)/(C_0 - C_1), \tag{8}$$

Thereafter, at the first approximation, the applicability of the Frumkin isotherm

$$B_m c = \frac{\theta}{1-\theta} \exp(-2a_m\theta) \tag{9}$$

for the interpretation of *n*-HA | Bi data was assumed. In Eq. (9) B_m and a_m are the adsorption equilibrium constant and the molecular interaction parameter at E_{max} respectively. The next step is the test of the Frumkin isotherm (log[θ/(1−θ)c] vs. θ plot) to derive the adsorption parameters. Fig. 11 shows that the plots have a good

linearity in the region of $0.1 < \theta < 0.8$ for all the faces investigated. Thus, the slope gives the molecular interaction parameter ($-2a_m$) and the intercept provides the adsorption equilibrium constant $\log B_m$ at E_{max} accordingly.

The adsorption isotherms at various E = const. and at various σ = const. were calculated by the methods described in Refs. [6–9, 16–24, 53–55]. The adsorption isotherms at σ = const. show larger deviations from the Frumkin isotherm behaviour than those at E = const. where the deviations in the region $-0.6 < E < -1.2$ V (SCE) are small. A more detailed discussion will be published in our next paper.

3.7. Gibbs adsorption energy — potential and lateral interaction — potential curves

The energetics of *n*-HA adsorption are characterised by the magnitude of the Gibbs energy of adsorption (Fig. 12). In the limit of zero coverage the adsorption of *n*-HA must be described by the Henry's law isotherm and the film pressure should then linearly depend on the concentration of *n*-HA as described by the following equation [8, 9, 16–23, 52–55]:

$$\pi = RT\Gamma_{max}B_A c_A/55.5 = RT\Gamma_{max}B_A X_A \tag{10}$$

where X_A is the mole fraction of *n*-HA in the solution, and the adsorption equilibrium coefficient B_A (Henry isotherm) is related to the Gibbs energy of adsorption through the equation

$$\Delta G_A^0 = -RT \ln B_A \tag{11}$$

As shown in [52–55], the values of ΔG_A^0 obtained according to the relations (10) and (11) correspond to the similar standard state as the Gibbs adsorption energy of organic compound, obtained according to the Frumkin isotherm, being the unit mole fraction of the organic species in the bulk of solution and a monolayer coverage of the ideal non-interacting adsorbate at the electrode surface. According to the data of Fig. 12, the $\Delta G_A^0(E)$-curves have a parabolic shape. It must be noted that the precision of ΔG_A^0 values obtained by this method is improved by avoiding the differentiation of $\pi(\ln X_A)$-plots as the values of Γ_{max}, obtained from the linear part of the $\pi(\ln c)$-plots are quite precise [5–8, 18–21]. Thus, the precision of the film pressure data must be very high in order to obtain the precise values of ΔG_A^0. Therefore, in addition to the previously described method, the standard Gibbs energy of adsorption ΔG_A^0 at zero coverage as a function of the applied potential E was obtained by fitting the experimental isotherms at constant potential to the Frumkin isotherm

$$X_A \exp\left(\frac{-\Delta G_A^0}{RT}\right) = \frac{\theta}{1-\theta}\exp(-2a\theta) \tag{12}$$

where a is the Frumkin interaction parameter. The values of ΔG_A^0 and a were obtained from the intercepts and slopes of the least-square fittings to a straight line

of $\ln[\theta/(1-\theta)c]$ vs. θ plots at E = const. in the range of θ from 0.1 to 0.8. A good fit to Eq. (12) was achieved with the parameter a depending parabolically on the electrode potential (Fig. 13). The accordance of the Gibbs energies of *n*-HA adsorption, obtained from $\pi(\ln c)$-plots and from Frumkin isotherm, is good (maximum error does not exceed ±1.2 kJ mol^{-1}), what indicates the absence of big systematic errors in the data established. The values of ΔG_A^0, obtained from $\pi(\ln c)$-plots, are always somewhat higher than those, obtained from the Frumkin isotherm. This difference increases if the adsorption activity of organic compound rises [5, 6], thus as its molecular weight and molar volume increases.

The adsorption data of *n*-HA on the Bi single crystal planes are collated in Table 1, which shows that the adsorption activity of *n*-HA increases in the sequence of planes (111) < (001) < $(01\bar{1})$. The surface activity of adsorbates increases in the sequence *n*-PA < *n*-BA < CH < CHCA < CHE < BAC *n*-HA < PY as the adsorption at the air | solution interface increases, except PY [1–8]. The anomalous position of PY is mainly caused by the noticeably stronger specific interaction of PY molecules with Bi surface atoms compared with other organic compounds investigated. Comparison of the adsorption data of various aliphatic organic compounds shows that the value of ΔG_A^0 increases in the order of electrodes Zn$(2\bar{1}\bar{1}0)$ < Zn$(10\bar{1}0)$ < Zn(0001) < Ag(110) < Ga < Ag(100) < Ag(111) < Cd$(11\bar{2}0)$ < Cd$(10\bar{1}0)$ < Cd(0001) < Bi(111) < Bi(001) < Hg < Bi$(2\bar{1}\bar{1})$ < Bi$(01\bar{1})$ < Sb(111) < Sb(001) < Sb$(2\bar{1}\bar{1})$ as the hydrophilicity of electrode surface decreases [2–8, 18–23, 29, 35, 36, 50].

According to Fig. 13 the lateral interaction constants a are positive and their values decrease when the surface charge density decreases. According to Fig. 13, the attractive interaction at $E_{\sigma=0}$ and at E_{max} increases in the sequence of planes Bi$(01\bar{1})$ < Bi(001) < Bi(111). The same order of planes at E_{max} was found in the case of adsorption of *n*-PA, *n*-BA, BAC, CH, CHE, CHCA and PY adsorption at Bi single crystal electrodes [1–8, 50]. In the case of adsorption of organic compounds at the metal surfaces from solution the attractive interaction constant a can be expressed in terms of different particle–particle interactions at the interface [1–8, 16, 18–24, 50, 56]

$$2a = (2Z_{W\text{-}A} - Z_{A\text{-}A} - Z_{W\text{-}W})/RT \qquad (13)$$

where $Z_{i\text{-}j}$ is the particle–particle interaction energy, W stands for H_2O and A for adsorbate. The positive values of a mean that $2Z_{W\text{-}A} > Z_{A\text{-}A} + Z_{W\text{-}W}$, i.e. the adsorbate–adsorbate and water–water interactions are much more attractive than the adsorbate–water interaction. The value of a increases in the sequence of adsorbates *n*-PA < *n*-BA < *n*-HA < BAC < CH as the length of hydrocarbon radical and the molar volume of adsorbates increases, except *n*-HA. The lower values of a for *n*-HA than those for CH probably indicate a less vertical orientation of *n*-HA molecules or the non-linear character of the hydrocarbon radical of *n*-HA in the adsorbed state. The same order of adsorbates is valid in the case of adsorption of aliphatic alcohols at Hg, Zn(0001), Zn$(11\bar{2}0)$, Zn$(10\bar{1}0)$, Ag(111), Ag(110) and Ag(100) electrodes [18–23, 29, 35, 36]. In the case of compounds containing six

carbon atoms the value of a increases in the order CHE < *n*-HA < BAC < CH. The value of a for *n*-HA adsorption increases in the order of electrodes Bi($01\bar{1}$) < Bi(001) < Bi(111) < Hg < Ag(100) < Ag(111) [18–20, 23, 25, 42, 50].

4. Conclusions

The adsorption behaviour of *n*-hexanol at singular Bi(111), Bi(001) and Bi($01\bar{1}$) has been studied by cyclic voltammetry, impedance and chronocoulometry methods. The presented results indicate that the adsorption parameters of *n*-HA depend on the crystallographic structure of Bi planes. The adsorption parameters derived from the capacitance data at $\omega = 0$ (at $-16 < \sigma < 5\ \mu C\ cm^{-2}$) are in reasonable accordance with the data from the chronocoulometric measurements, but the difference between impedance and chronocoulometric data diminishes when the adsorption activity of compound decreases. Accordingly, the impedance data are on some degree non-equilibrial in spite of extrapolation to $\omega \equiv 0$.

The comparison of the Gibbs energies of adsorption for various organic compounds shows that the adsorption activity of organic compounds at the Bi | solution interface increases in order *n*-PA < *n*-BA < CH < CHE < CHCA < BAC < PY as the adsorption of organic compound at the air | solution interface rises, except PY. The anomalous position of PY is mainly caused by the weak chemisorption of this compound at Bi planes [8], as well as on Ag and Au planes [20, 45, 46]. It was found that the difference between the adsorption activities of various Bi planes increases in the sequence of adsorbates *n*-PA < *n*-BA < CHE < CHCA < CH < BAC < *n*-HA if the adsorption activity of organic compound at the air | solution interface, as well as at the Bi | solution interface rises. This is mainly caused by the result that with the decreasing of the molar volume of adsorbate the changes in the adsorbed layer structure, caused by the adsorption of one molecule, decreases in comparison with the adsorption of more large surfactants. Comparison of the adsorption data of various aliphatic organic compounds shows that the value of ΔG_A^0 increases in the order of electrodes Zn($2\bar{1}\bar{1}0$) < Zn($10\bar{1}0$) < Zn(0001) < Ag(110) < Ga < Ag(100) < Ag(111) < Cd($11\bar{2}0$) < Cd($10\bar{1}0$) < Cd(0001) < Bi(111) < Bi(001) < Hg < Bi($2\bar{1}\bar{1}$) < Bi($01\bar{1}$) < Sb(111) < Sb(001) < Sb($2\bar{1}\bar{1}$) as the hydrophilicity of electrode surface decreases [18–23, 29, 35, 36].

The values of Gibbs energy of adsorption have been obtained from the initial part of $\pi(\ln X_A)$-curves, as well as from the Frumkin isotherm. The difference between the ΔG_A^0-values is not greater than ± 1.2 kJ mol^{-1}, but the absolute values of ΔG_A^0, obtained from chronocoulometric measurements, are always higher than those obtained from impedance data. Accordingly, the impedance data are on some degree non-equilibrial (in spite of extrapolation to $\omega \equiv 0$). The adsorption activity of *n*-HA at Bi(001) is very close to that for polycrystalline bismuth solid drop electrode [1–15], and this result is in very good accordance with the conclusions of Refs. [1–15, 28, 42, 44], where it was found that the surface of polycrystalline Bi

electrode mainly consists (from 50 to 70%) of the comparatively large homogeneous surface areas (grains), adsorption characteristics of which are very close to those for Bi(001) plane. The lower adsorption activity of Bi(111) is caused mainly, in addition to the more pronounced hydrophilicity, by a less active surface state of Bi(111), where the surface atoms are chemically saturated. The most active one is the singular Bi($01\bar{1}$) plane, where unsaturated covalent bonds are distributed uniformly over the whole surface.

The positive values of the lateral interaction constant a for *n*-HA means that the surfactant–surfactant and water–water interactions are much more attractive than the surfactant–water interaction. At the potentials of the adsorption-desorption maxima, the molecular interaction parameter a^m decreases in the sequence of planes (001) ≥ (111) > ($01\bar{1}$) as the superficial density of planes increases and the limiting Gibbs adsorption decreases. The dependence of the attractive interaction constant a on E is approximately parabolic and the value of a increases in the sequence of electrodes Bi < Hg < Zn.

The value of a increases in the order of adsorbates *n*-PA < *n*-BA ≤ *n*-HA < BAC < CH as the molar volume of the adsorbate molecule increases, except *n*-HA. The lower value of a for *n*-BA and *n*-HA molecules than that for CH and BAC probably indicates that the hydrocarbon tail of these compounds in the adsorption layer is not linear or these molecules will have the more tilted orientation. If we assume at the first approximation that the water–water and the organic compound–water interactions are independent of the aliphatic compound studied then the attraction between the adsorbed aliphatic alcohol molecules rises in the presented order of adsorbates.

The limiting Gibbs adsorption Γ_{max} increases in the order of electrodes Bi($01\bar{1}$) < Bi(111) < Bi(001) as the superficial density of planes decreases. The projected area S_{max} decreases and Γ_{max} increases in the order *n*-HA < *n*-BA ≤ CH < *n*-PA. The decrease of Γ_{max} and of the limiting potential shift E_N values and the increase of S_{max} as the number of carbon atoms in the aliphatic alcohol molecule increases, can be explained by an increasingly tilted orientation of *n*-HA molecules compared with *n*-PA at the single crystal Bi(001) and Bi(111) planes, as well as at Hg [8, 22, 23, 29] electrodes. Very low values of Γ_{max} and the E_N values for *n*-PA and *n*-HA at Bi($01\bar{1}$) plane will indicate that the *n*-PA and *n*-HA molecules probably have a practically flat orientation on the most active Bi plane investigated.

Acknowledgements — This work was partially supported by Estonian Science Foundation under Project No. 612.

Table 1.

Adsorption parameters of normal hexanol on Bi single crystals (chronocoulometry data, except C_1, a_m and B_m obtained by impedance method at $\omega = 0$)

Plane	a_m ±0.1	$C_1/\mu F\ cm^{-2}$ ±0.15	E_N/ V ±0.04	$10^{10}\ \Gamma_{max}$/ mol cm^{-2} ±0.4	S_{max} / nm^2 ±0.02	B_m/ $dm^3\ mol^{-1}$ ±20	$-\Delta G_A^0$ /kJ mol^{-1} ±0.3
(111)	1.37	2.50	0.18	5.9	0.28	92.8	–21.2
(001)	1.10	3.60	0.16	6.1	0.27	140.0	–22.2
$(01\bar{1})$	0.99	3.13	0.10	4.6	0.36	221.0	–23.3

Legends for Figures

Fig. 1. $C(E)$-curves ($\omega = 0$) for Bi(111) in 0.05 M Na_2SO_4 (1) and with addition of *normal*-hexanol (M): 0.005 (2); 0.01 (3); 0.02 (4); and 0.04 (5).

Fig. 2. $C(E)$-curves ($\nu = 210$ Hz) for Bi(001) in 0.05 M Na_2SO_4 (1) and with addition of various alcohols: *n*-BA (2,3); *n*-PA (4,5); CH (6,7); *n*-HA (8,9) (M): 0.06 (2); 0.15 (3); 0.6 (4) 1.5 (5); 0.02 (6,8) and 0.04 (7,9).

Fig. 3. Dependence of the difference between the potential of adsorption-desorption maximum and the zero charge potential ($E^{max} - E_{\sigma=0}$) on $\log c_{org}$ at Bi(111) for various organic compounds: *n*-HA (1); CH (2); PY (3); *n*-BA (4); *n*-PA (5).

Fig. 4. $C(E)$-curves ($\nu = 210$ Hz) for Bi(111) (1,3,5) and for Bi($01\bar{1}$) (2,4,6) with addition of 0.1 M *n*-PA (3,4) and 0.1 M CH (5,6), and 0.01 M *n*-HA (1,2).

Fig. 5. σ,E-curves obtained from impedance ($\omega = 0$) for Bi(001) (a) in 0.05 M Na_2SO_4 (1) and with addition of *n*-HA (M): 0.005 (2); 0.01 (3); 0.02 (4); 0.04 (5).

σ,E-curves for Bi(111) (b) obtained from impedance ($\omega = 0$) (1,3,5) and from chronocoulometry (2,4,6) in 0.05 M Na_2SO_4 (1,2) and with addition of *n*-HA (M): 0.02 (3,4); 0.04 (5,6).

Fig. 6. Surface pressure — potential (π,E) curves for Bi(111) (chronocoulometry) in 0.05 M Na_2SO_4 aqueous solution with addition of *n*-HA (M): 0.04 (1); 0.02 (2); 0.01 (3); 0.005 (4).

Fig. 7. π,E-curves for Bi(001) ($\omega = 0$) in 0.05 M Na_2SO_4 with addition of various alcohols *n*-BA (1,3); *n*-PA (2,5), *n*-HA (4,6) (M): 1.5 (1,2); 0.6 (3,5); 0.04 (4); 0.02 (6).

Fig. 8. $\pi,\ln c$-curves for Bi(001) at different electrode potentials, as noted at figure.

Fig. 9. Gibbs excess — potential (Γ,E) curves for Bi(001) (1,2); Bi(111) (3,4) and Bi($01\bar{1}$) (5,6) with different addition of *n*-HA (M): 0.04 (1,3,5); 0.01 (2,4,6).

Fig. 10. $\Gamma,\log c$ curves for Bi(111) at different electrode potentials (in V (SCE)) as noted at figure.

Fig. 11. Frumkin adsorption isotherm ($\omega = 0$) for *n*-HA adsorption on Bi single crystal planes: ($01\bar{1}$) (1); (001) (2); (111) (3).

Fig. 12. Gibbs adsorption energy vs. potential curves for *n*-HA, obtained from chronocoulometry for Bi single crystal planes: (111) (1); (001) (2); ($01\bar{1}$) (3).

Fig. 13. Attraction interaction constant vs. potential curves for Bi(111) (1); Bi(001) (2); Bi($01\bar{1}$) (3).

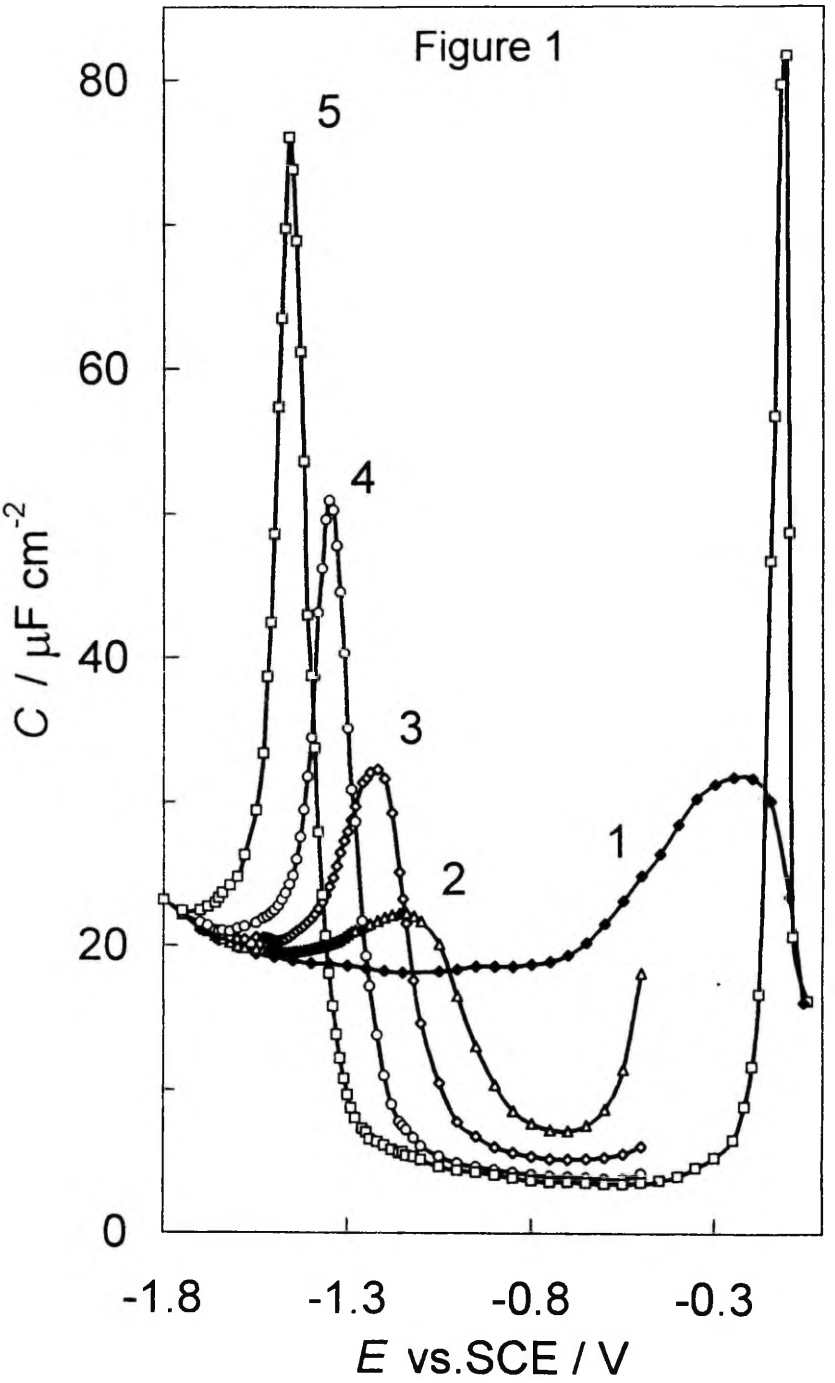
Figure 1
80
60
40
20
0
C / μF cm-2
5
4
3
2
1
-1.8
-1.3
-0.8
-0.3
E vs.SCE / V

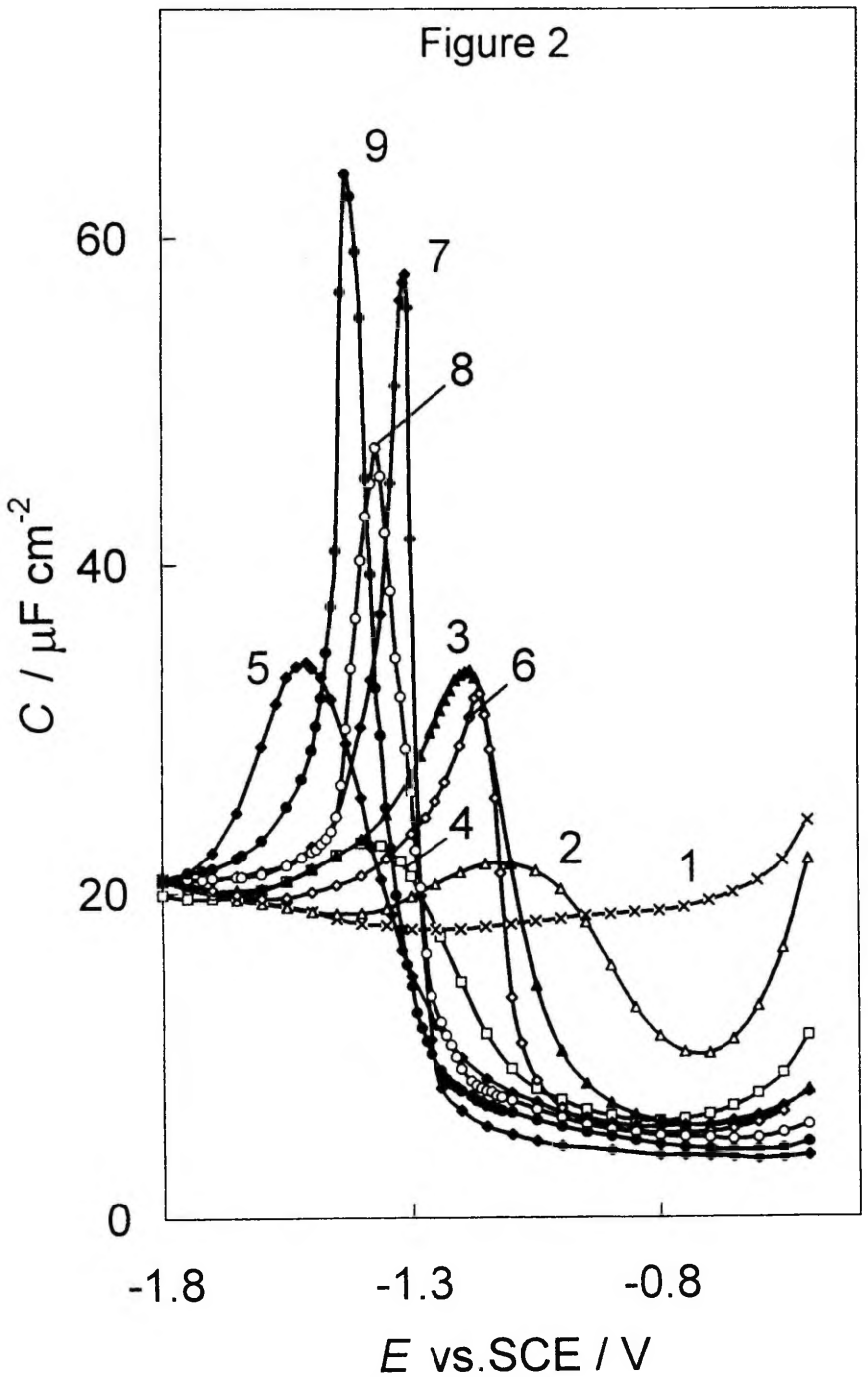
Figure 2
9
7
8
5
3
6
4
2
1
60
40
20
0
C / μF cm-2
-1.8
-1.3
-0.8
E vs.SCE / V

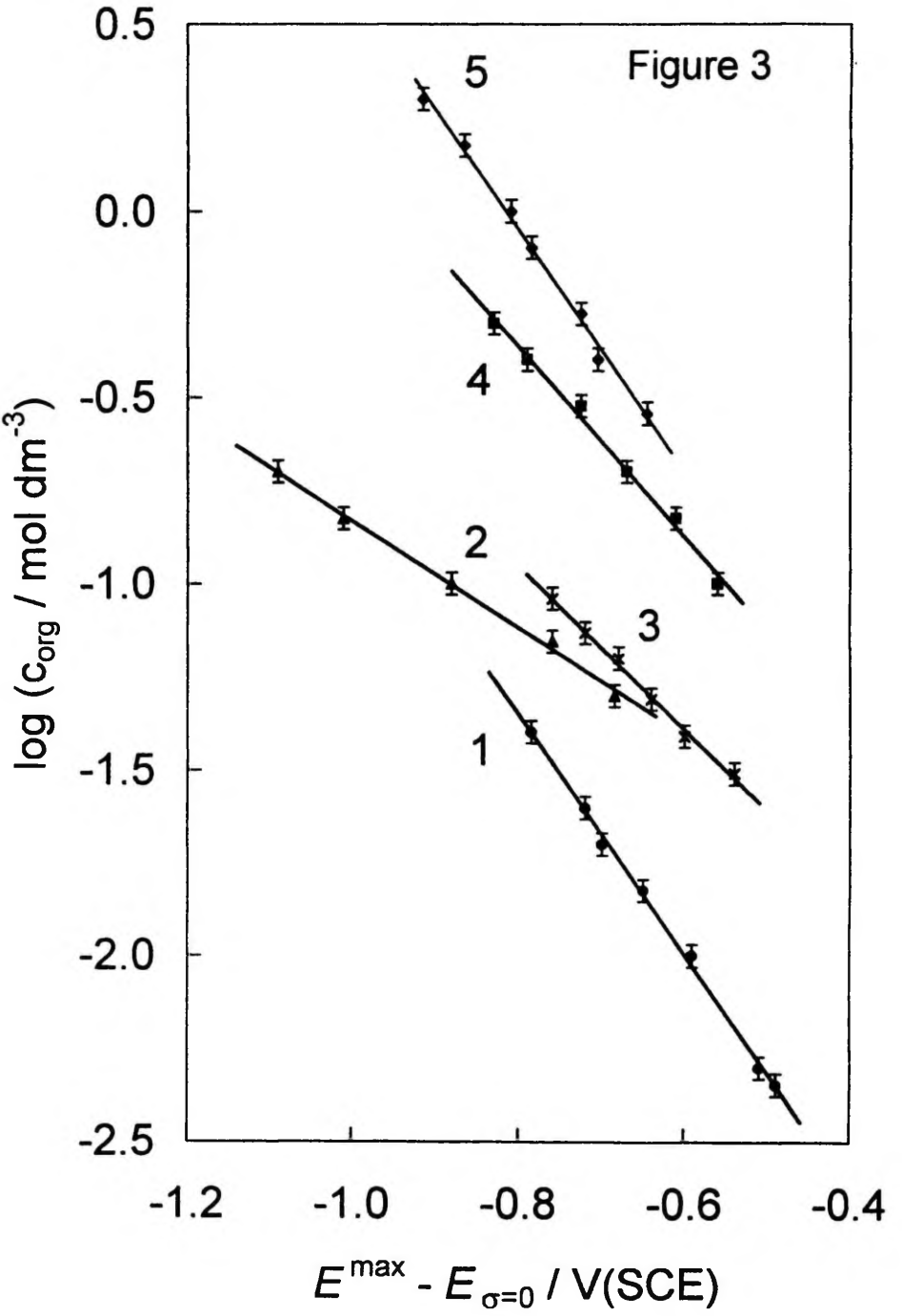
Figure 3
0.5
0.0
-0.5
-1.0
-1.5
-2.0
-2.5
log (c_{org} / mol dm^{-3})
-1.2
-1.0
-0.8
-0.6
-0.4
E^{max} - $E_{\sigma=0}$ / V(SCE)
1
2
3
4
5

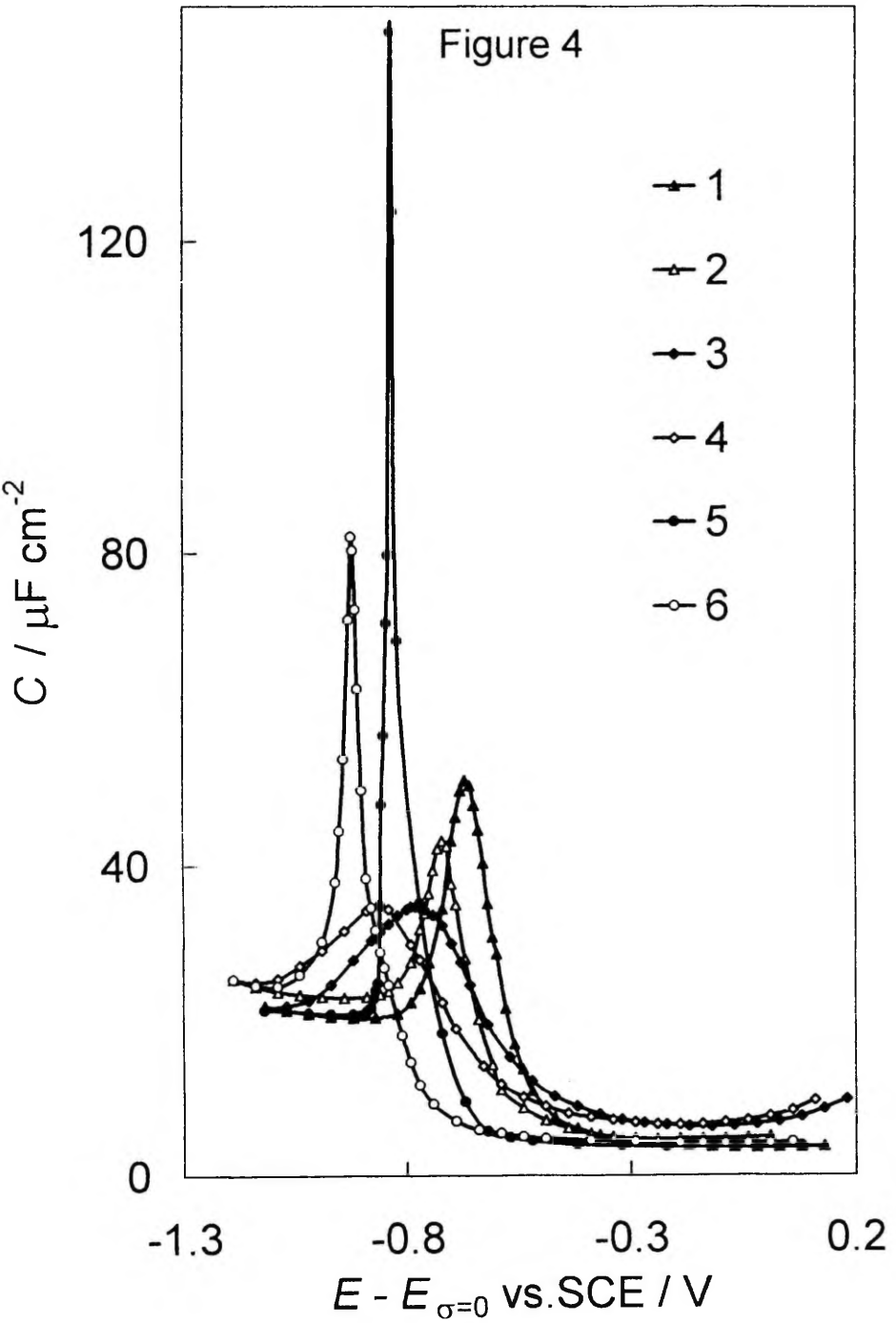
Figure 4
1
2
3
4
5
6
120
80
40
0
C / μF cm-2
-1.3
-0.8
-0.3
0.2
E - Eσ=0 vs.SCE / V

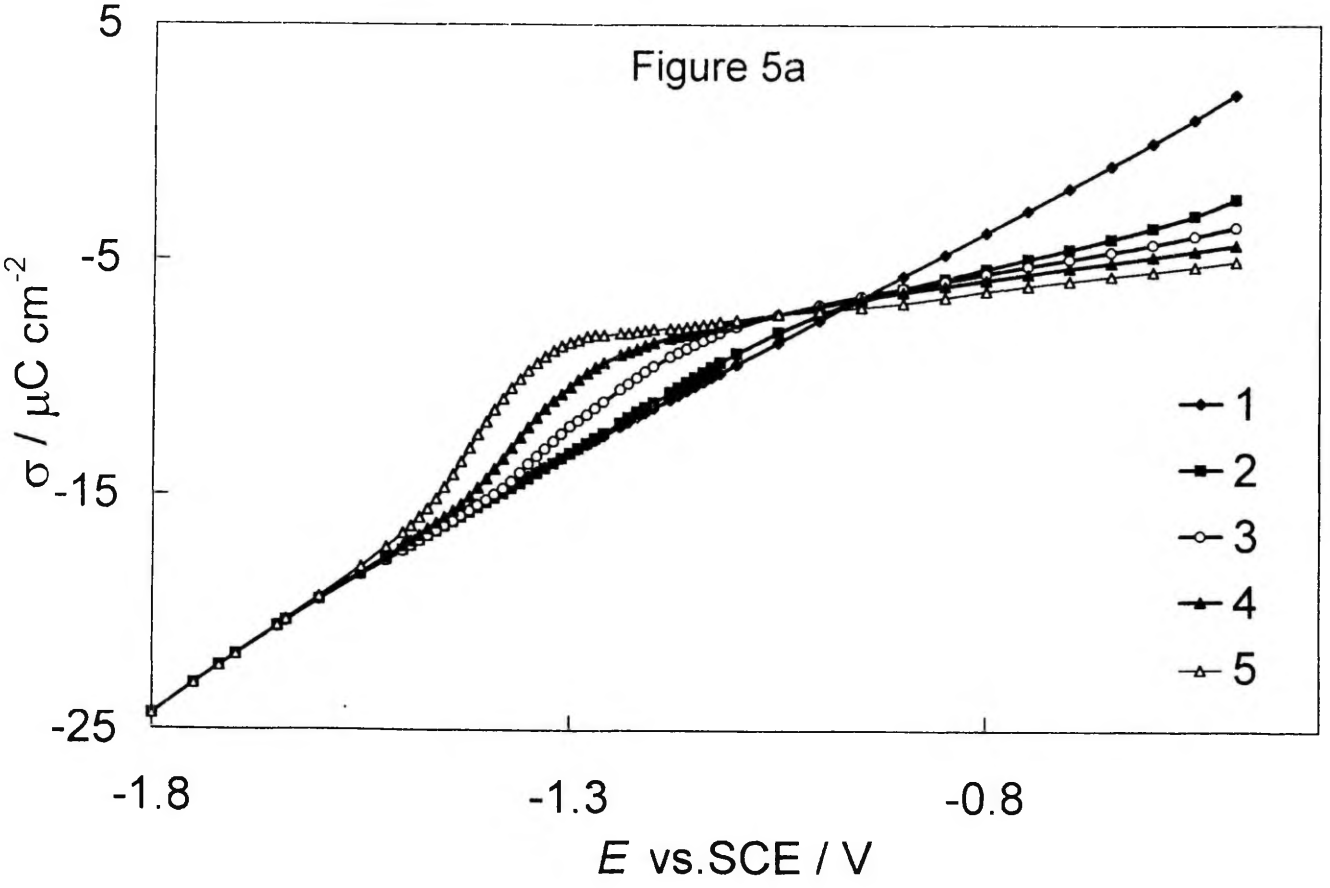
Figure 5a
5
-5
-15
-25
σ / μC cm-2
-1.8
-1.3
-0.8
E vs.SCE / V
1
2
3
4
5

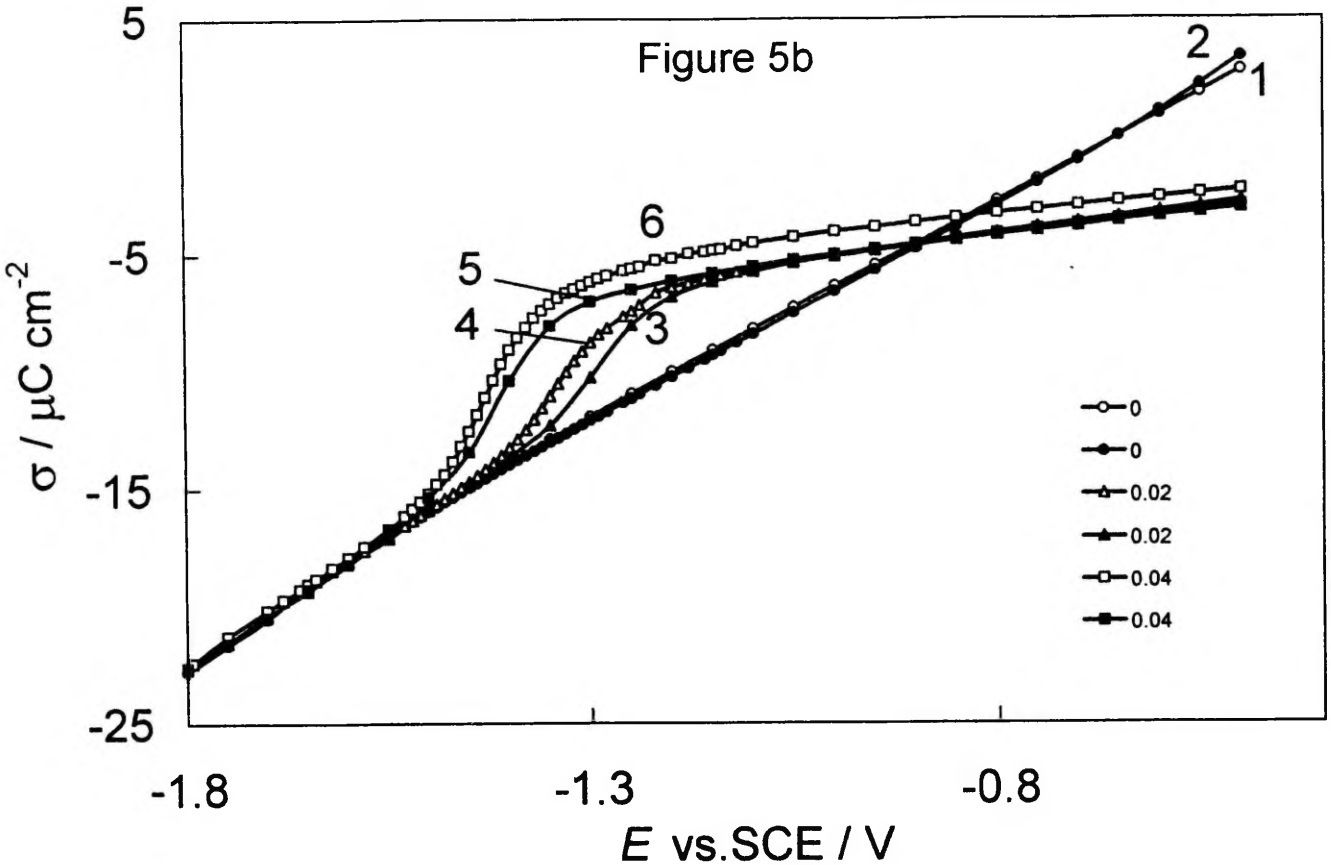
Figure 5b
5
-5
-15
-25
σ / μC cm-2
-1.8
-1.3
-0.8
E vs.SCE / V
1
2
3
4
5
6
0
0
0.02
0.02
0.04
0.04

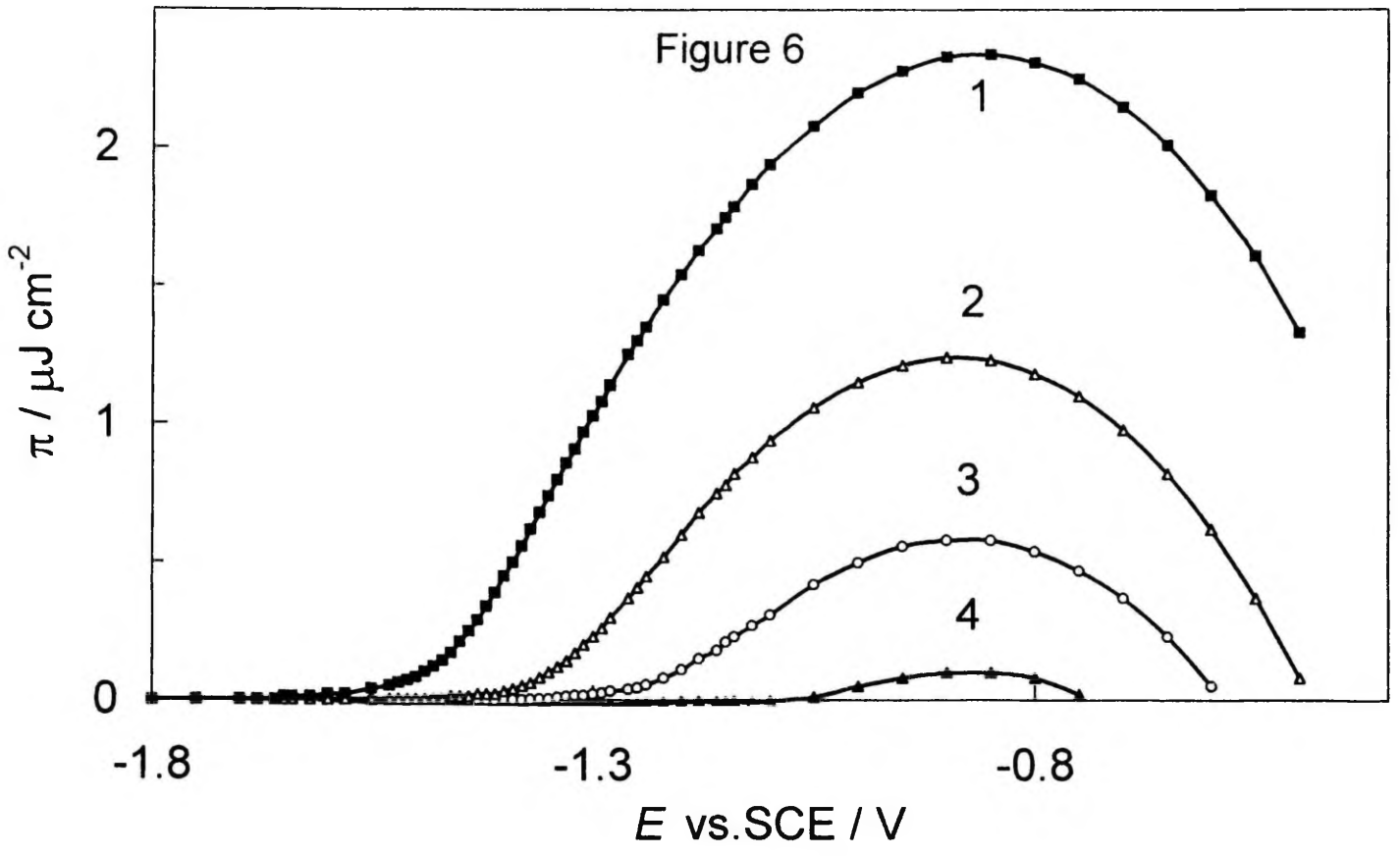
Figure 6
1
2
3
4
2
1
0
π / μJ cm-2
-1.8
-1.3
-0.8
E vs.SCE / V

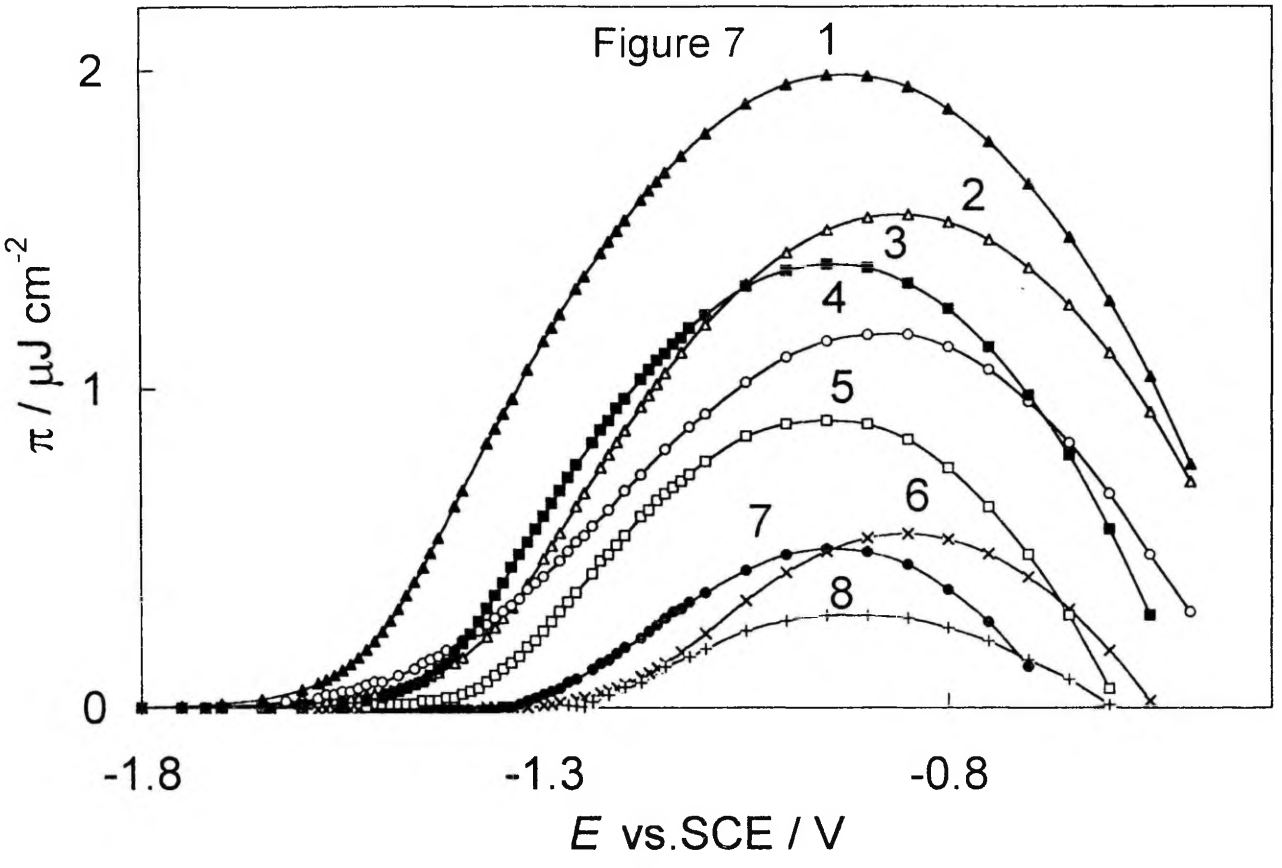
Figure 7
1
2
3
4
5
6
7
8
2
1
0
π / μJ cm-2
-1.8
-1.3
-0.8
E vs.SCE / V

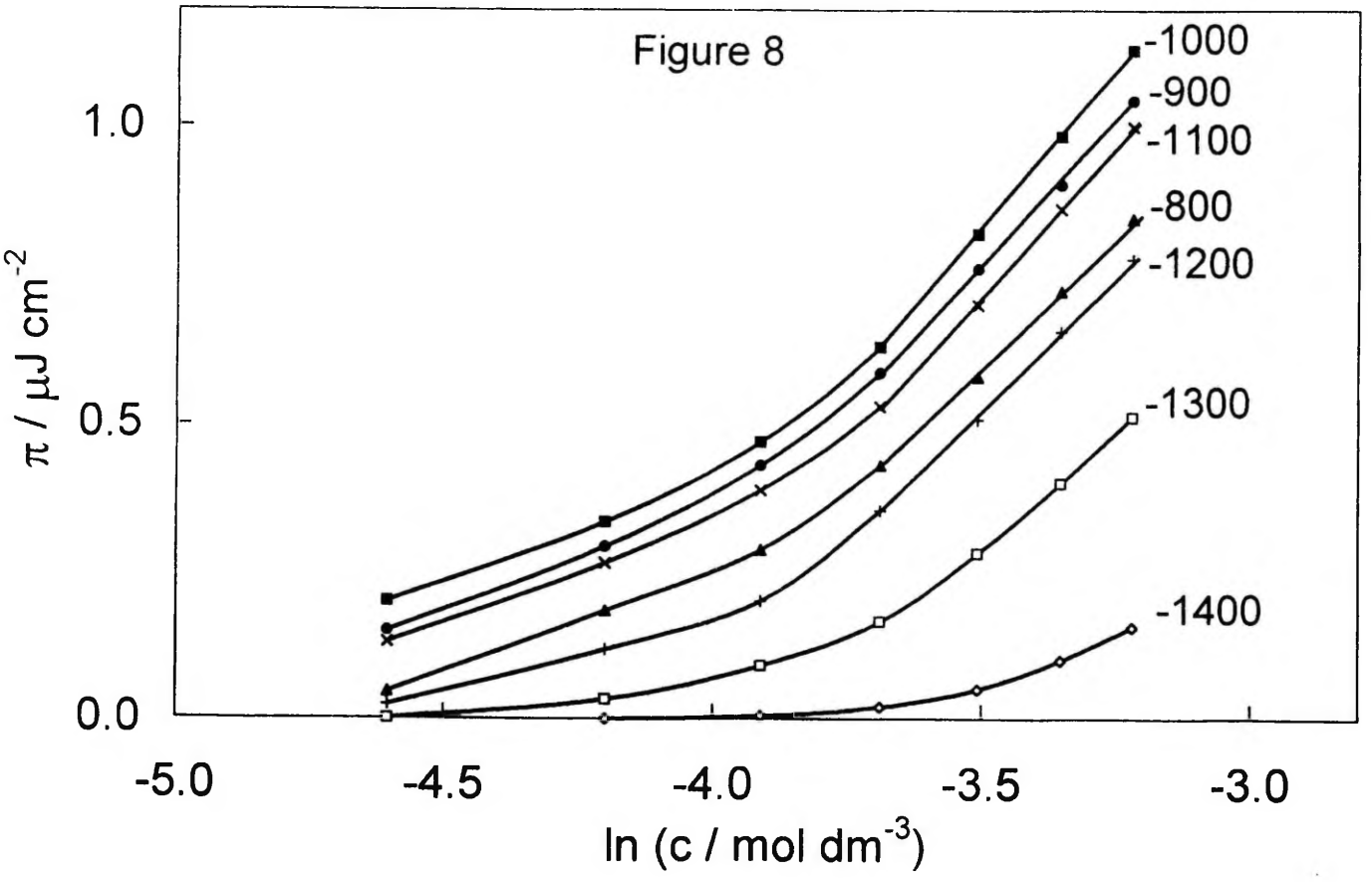
Figure 8
-1000
-900
-1100
-800
-1200
-1300
-1400
1.0
0.5
0.0
π / μJ cm-2
-5.0
-4.5
-4.0
-3.5
-3.0
ln (c / mol dm-3)

Figure 9

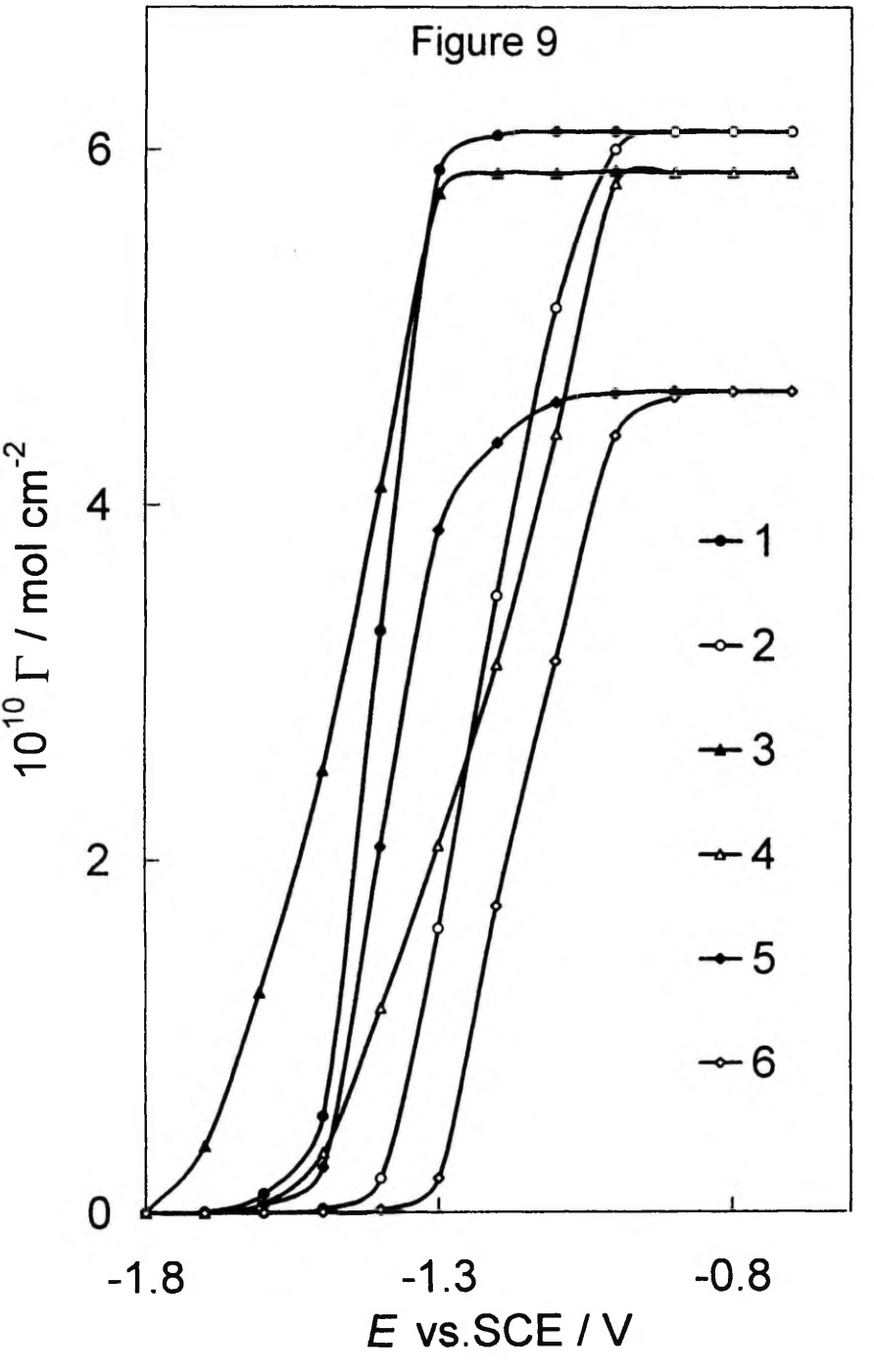

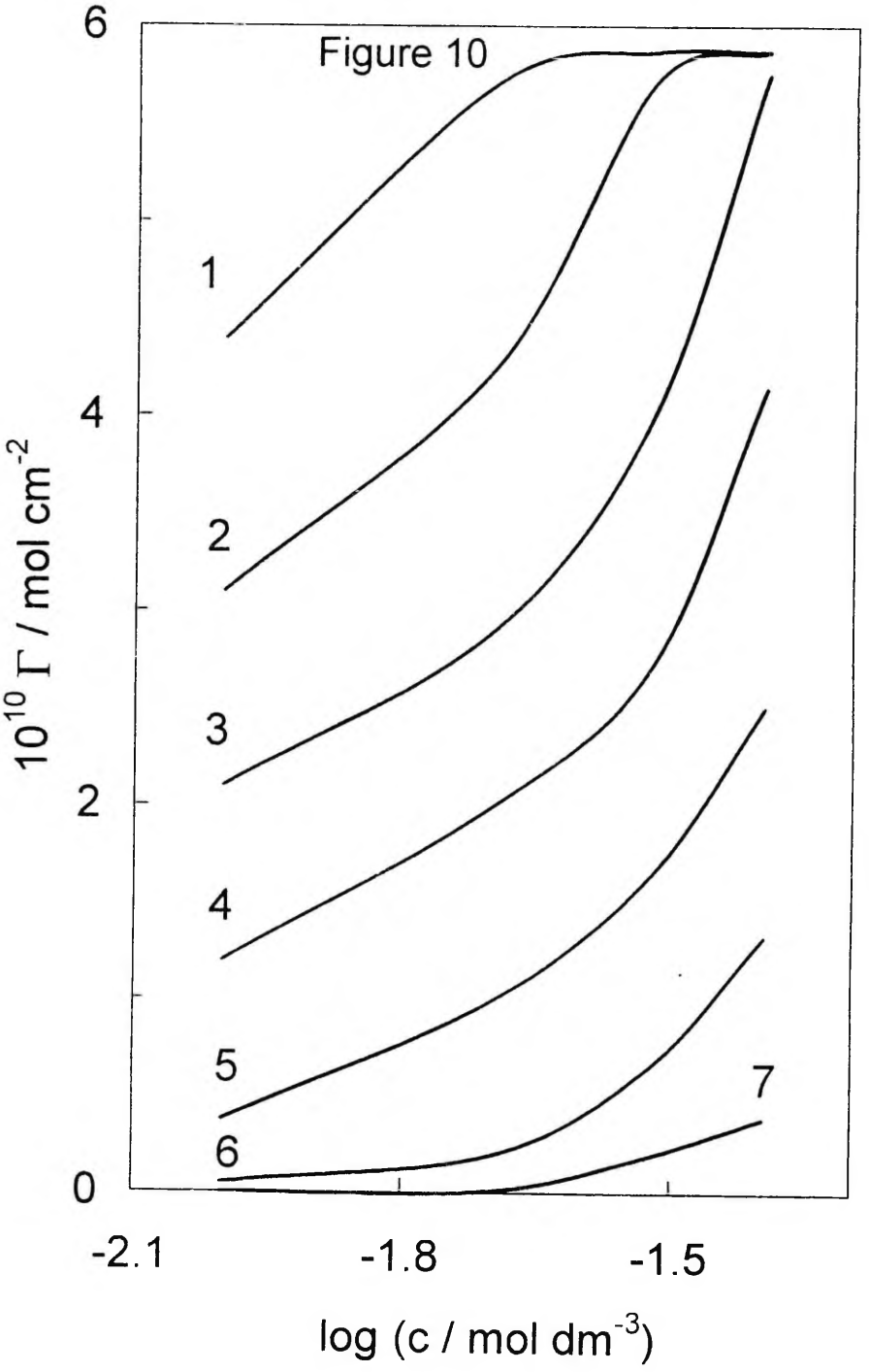
Figure 10
6
4
2
0
$10^{10}\Gamma$ / mol cm^{-2}
1
2
3
4
5
6
7
-2.1
-1.8
-1.5
log (c / mol dm^{-3})

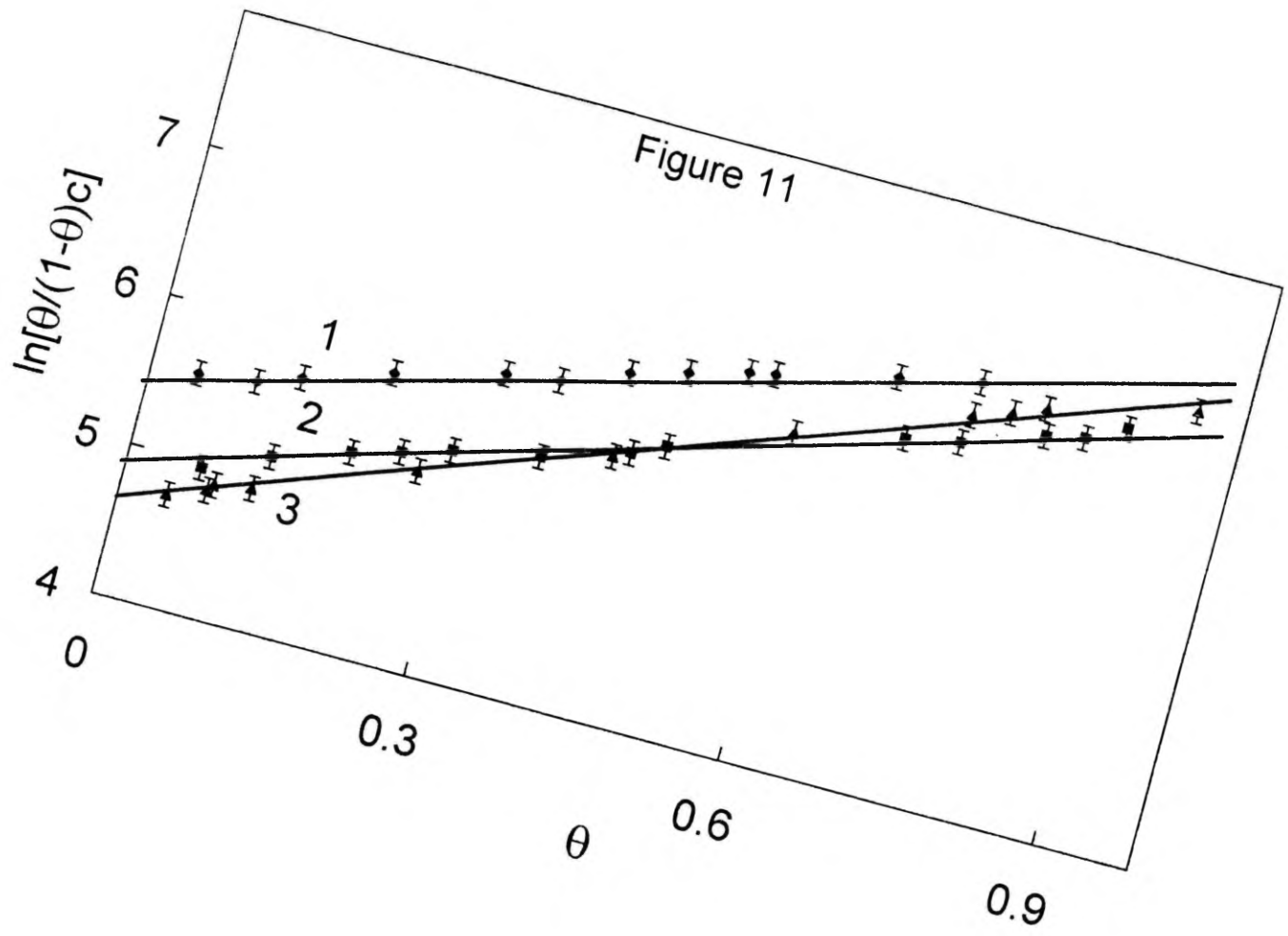
Figure 11
ln[θ/(1-θ)c]
7
6
5
4
1
2
3
0
0.3
0.6
0.9
θ

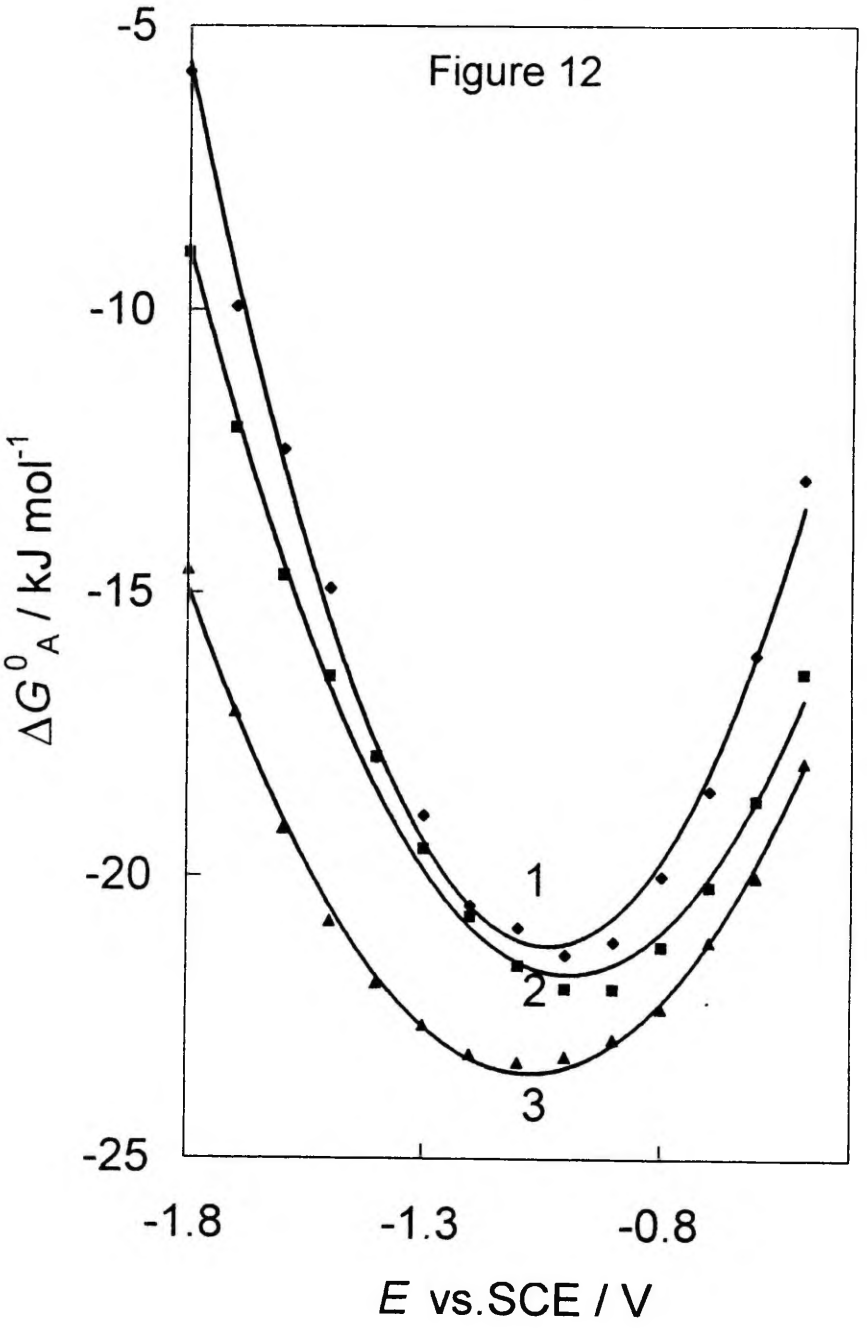
Figure 12
-5
-10
-15
-20
-25
-1.8
-1.3
-0.8
ΔG^0_A / kJ mol^{-1}
E vs.SCE / V
1
2
3

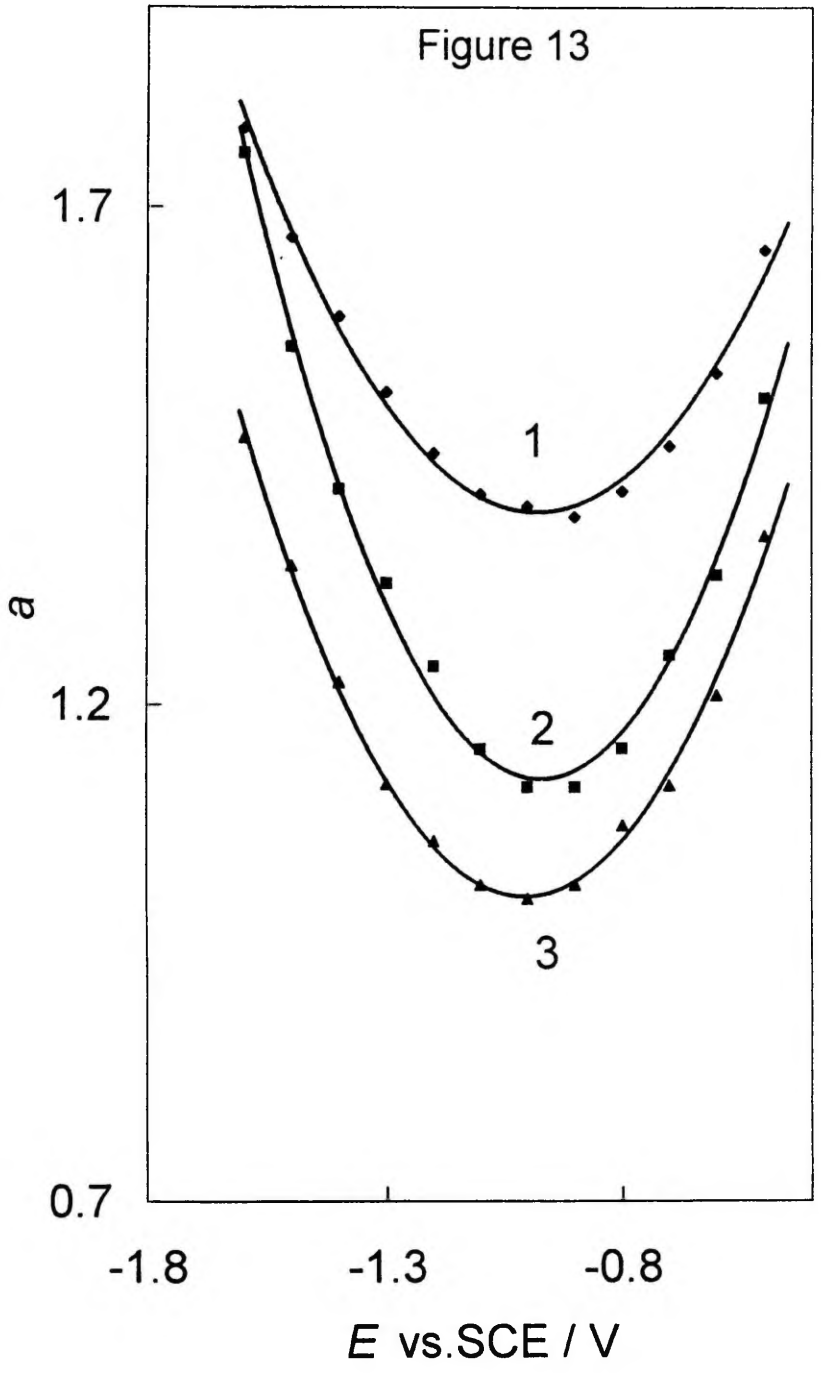
Figure 13
1.7
1.2
0.7
a
1
2
3
-1.8
-1.3
-0.8
E vs.SCE / V

CURRICULUM VITAE

ALAR JÄNES

Born:	Mai 20, 1964 in Elva, Estonia		
Citizenship:	Estonian		
Marital Status:	Single		
Address:	Institute of Physical Chemistry,	Tel.:	+372 7 465165
	University of Tartu,	Fax:	+372 7 465160
	2 Jakobi Str,	E-mail:	alar@chem.ut.ee
	Tartu, EE2400, Estonia		

EDUCATION

1982–1989	Student, Department of Chemistry, University of Tartu, (chemistry)
1989–1991	Research student, Department of Chemistry, University of Tartu
1991–1996	Ph.D. Student, Department of Chemistry, University of Tartu, doctoral advisor Prof. Enn Lust

MAIN SCIENTIFIC PUBLICATIONS

1. E. Lust, K. Lust, A. Jänes, Analysis of Electric Double-Layer Structure at Bismuth Single Crystal Faces in Aqueous Solutions of Surface-Inactive Electrolytes, Sov. Electrochem. Engl. Tr., 26, No. 12 (1990) 1448–1552.
2. E. Lust, A. Jänes, Electric Double-Layer Structure and Potentials of Zero Charge for the Antimony (111) and (001) Single-Crystal Faces, Sov. Electrochem. Engl. Tr., 28, No. 5 (1992) 650–653.
3. E. Lust, A. Jänes, Structure of the Electrical Double Layer and Adsorption of Cyclohexanol on the Faces of an Antimonium Single Crystal, Russ. J. Electrochem., 30, No. 3 (1994) 321–328.
4. A. A.-J. Jänes, E. J. Lust, Adsorption of Cyclohexanon on the Single Crystal Bismuth and Antimony Electrodes, Russ. J. Electrochem., 31, No. 6 (1995) 566–570.
5. E. J. Lust, K. K. Lust, A. A.-J. Jänes, Influence of the Crystallographic Structure of Electrode Surface on the Structure of the Electrical Double Layer and Adsorption of Organic Molecules, Russ. J. Electrochem., 31, No. 8 (1995) 876–890.
6. E. J. Lust, A. A.-J. Jänes, K. K. Lust, J. J. Ehrlich, Electric Double–Layer Structure at Bismuth, Antimony and Cadmium Single–Crystal Faces in

Surface–Inactive Electrolyte Solutions, Russian J. of Electrochemistry, 32, No. 5 (1996) 597–609.
7. A. A.-J. Jänes and E. J. Lust, Adsorption of Cyclohexancarboxylic Acid on Faces of the Bismuth and Antimony Single Crystals, Russian J. of Electrochemistry, 32, No 8 (1996) 943–945.
8. E. Lust, K. Lust and A. Jänes, Influence of the Surface Structure of Cadmium Electrodes on the Electric Double Layer Parameters in the Aqueous Surface–Inactive Electrolyte Solutions, J. Electroanalyt. Chem., 413 (1996) 111–121.
9. E. Lust, A. Jänes, K. Lust and P. Miidla, Adsorption of Isomers of Butanol on Bismuth Single Crystal Plane Electrodes, J. Electroanalyt. Chem., 413 (1996) 175–185.
10. E. Lust, A. Jänes, K. Lust and M. Väärtnõu, Electric Double Layer Structure and Adsorption of Cyclohexanol on Single Crystal Cadmium, Antimony and Bismuth Electrodes, Electrochimica Acta, 42 (1997) 771–783.
11. E. Lust, A. Jänes, P. Miidla and K. Lust, Adsorption of Pyridine on the (111), (001) and ($01\bar{1}$) Faces of Bismuth, J. Electroanalyt. Chem., 425 (1997) 25–37.
12. E. Lust, A. Jänes, K. Lust and R. Pullerits, Adsorption of Organic Compounds and Hydrophilicity of Bismuth, Cadmium and Antimony Electrodes, J. Electroanalyt. Chem., 431 (1997) 183–201.
13. E. Lust, A. Jänes, K. Lust, V. Sammelselg and P. Miidla, Influence of Surface Pretreatment of Bismuth and Cadmium Electrodes to the Electric Double Layer and Adsorption Characteristics of Organic Compounds, Electrochimica Acta, Vol. 42, No. 19 (1997) 2861–2879.
14. E. Lust, A. Jänes, K. Lust and P. Miidla, Adsorption of Propanol on Bismuth Single Crystal Plane Electrodes, J. Electroanal. Chem. . Electroanalyt. Chem., 436 (1997) 141–153.
15. E. Lust, A. Jänes, K. Lust and P. Miidla, Adsorption of Normal Hexanol on Bismuth Single Crystal Plane Electrodes, J. Electroanal. Chem. (accepted JEC 07041).
16. E. Lust, A. Jänes, V. Sammelselg, P. Miidla and K. Lust, Surface Roughness of Bismuth, Antimony and Cadmium Electrodes, Electrochimica Acta, (in press RA 2525).
17. E. Lust, A. Jänes and K. Lust, Adsorption of Adenosine on Bismuth Single Crystal Plane Electrodes, J. Electroanal. Chem., (accepted RPS 5580).

PARTICIPATION ON CONFERENCES

1. 6-th International Frumkin Symposium "Fundamental Aspects of Electrochemistry", Moscow, August 21–25, 1995: A. Jänes, K. Lust and E. Lust, Adsorption of Organic Compounds on Single Crystal Antimony, Bismuth and Cadmium Electrodes; E. Lust, A. Jänes, K. Lust and M. Väärtnõu, Electric Double Layer on the Single Crystal Bismuth, Antimony and Cadmium Electrodes in Surface Inactive Electrolyte Solutions.
2. "Baltic Conference on Interfacial Electrochemistry", Tartu, June 14–18, 1996: A. Jänes, E. Lust, K. Lust, Electrochemical Behaviour Na_2H_2EDTA and $Na_2CdEDTA$ on Single Crystal Bismuth and Cadmium Electrodes; A. Jänes, K. Lust, E. Lust, Adsorption of Pyridine on the Single Crystal Bismuth Electrodes, E. Lust, K. Lust, A. Jänes, M. Väärtnõu, Influence of the Chemical Composition and Crystallographic Structure of Single Crystal Bismuth, Cadmium and Antimony Electrodes on the Characteristics of metal|solution Interface.
3. "47th ISE Meeting", Veszprem & Balatonfüred, September 1–6, 1996: E. Lust, K. Lust, A. Jänes, Phase Boundary Structure on the Single Crystal Bismuth, Antimony and Cadmium Electrodes in Surface Inactive Electrolyte Solutions; A. Jänes, M. Väärtnõu, E. Lust, Influence of the Surface Pretreatment of Bi(111) to the Adsorption Characteristics of Pyridine.
4. "The 1997 Joint International Meeting", Paris, August 31 – September 5, 1997: A. Jänes, E. Lust, K. Lust and V. Sammelselg, Surface Roughness, Electric Double Layer and Adsorption Characteristics of Antimony, Bismuth and Cadmium Electrodes; E. Lust, A. Jänes and K. Lust, Adsorption of Organic Compounds on Bismuth Single Crystal Plane Electrodes.

CURRICULUM VITAE

ALAR JÄNES

Sündinud:	20. mail 1964 Elvas		
Kodakondsus:	Eesti		
Perekonnaseis:	vallaline		
Aadress:	füüsikalise keemia instituut	tel.:	(27) 465 165
	Tartu Ülikool, Jakobi 2,	faks:	(27) 465 160
	Tartu, EE2400, Eesti	E-mail:	alar@chem.ut.ee

HARIDUS

1982–1989	Tartu Ülikooli keemiaosakonna üliõpilane
1989–1991	Tartu Ülikooli keemiaosakonna stažöör-uurija
1991–1996	Tartu Ülikooli keemiaosakonna doktorant, juhendaja prof. Enn Lust

TÄHTSAMAD TEADUSPUBLIKATSIOONID

1. E. Lust, K. Lust, A. Jänes, Analysis of Electric Double-Layer Structure at Bismuth Single Crystal Faces in Aqueous Solutions of Surface-Inactive Electrolytes, Sov. Electrochem. Engl. Tr., 26, No. 12 (1990) 1448–1552.
2. E. Lust, A. Jänes, Electric Double-Layer Structure and Potentials of Zero Charge for the Antimony (111) and (001) Single-Crystal Faces, Sov. Electrochem. Engl. Tr., 28, No. 5 (1992) 650–653.
3. E. Lust, A. Jänes, Structure of the Electrical Double Layer and Adsorption of Cyclohexanol on the Faces of an Antimonium Single Crystal, Russ. J. Electrochem., 30, No. 3 (1994) 321–328.
4. A. A.-J. Jänes, E. J. Lust, Adsorption of Cyclohexanon on the Single Crystal Bismuth and Antimony Electrodes, Russ. J. Electrochem., 31, No. 6 (1995) 648–651 (in Russian).
5. E. J. Lust, K. K. Lust, A. A.-J. Jänes, Influence of the Crystallographic Structure of Electrode Surface on the Structure of the Electrical Double Layer and Adsorption of Organic Molecules, Russ. J. Electrochem., 31, No. 8 (1995) 876–890 (in Russian).
6. E. J. Lust, A. A.-J. Jänes, K. K. Lust, J. J. Ehrlich, Electric Double-Layer Structure at Bismuth, Antimony and Cadmium Single–Crystal Faces in Sur-

face-Inactive Electrolyte Solutions, Russian J. of Electrochemistry, 32, No. 5 (1996) 597–609.
7. A. A.-J. Jänes and E. J. Lust, Adsorption of Cyclohexancarboxylic Acid on Faces of the Bismuth and Antimony Single Crystals, Russian J. of Electrochemistry, 32, No 8 (1996) 1020–1022 (in Russian).
8. E. Lust, K. Lust and A. Jänes, Influence of the Surface Structure of Cadmium Electrodes on the Electric Double Layer Parameters in the Aqueous Surface–Inactive Electrolyte Solutions, J. Electroanalyt. Chem., 413 (1996) 111–121.
9. E. Lust, A. Jänes, K. Lust and P. Miidla, Adsorption of Isomers of Butanol on Bismuth Single Crystal Plane Electrodes, J. Electroanalyt. Chem., 413 (1996) 175–185.
10. E. Lust, A. Jänes, K. Lust and M. Väärtnõu, Electric Double Layer Structure and Adsorption of Cyclohexanol on Single Crystal Cadmium, Antimony and Bismuth Electrodes, Electrochimica Acta, 42 (1997) 771–783.
11. E. Lust, A. Jänes, P. Miidla and K. Lust, Adsorption of Pyridine on the (111), (001) and ($01\bar{1}$) Faces of Bismuth, J. Electroanalyt. Chem., 425 (1997) 25–37.
12. E. Lust, A. Jänes, K. Lust and R. Pullerits, Adsorption of Organic Compounds and Hydrophilicity of Bismuth, Cadmium and Antimony Electrodes, J. Electroanalyt. Chem., 431 (1997) 183–201.
13. E. Lust, A. Jänes, K. Lust, V. Sammelselg and P. Miidla, Influence of Surface Pretreatment of Bismuth and Cadmium Electrodes to the Electric Double Layer and Adsorption Characteristics of Organic Compounds, Electrochimica Acta, Vol. 42, No. 19 (1997) 2861–2879.
14. E. Lust, A. Jänes, K. Lust and P. Miidla, Adsorption of Propanol on Bismuth Single Crystal Plane Electrodes, J. Electroanal. Chem. J. Electroanalyt. Chem., 436 (1997) 141–153.
15. E. Lust, A. Jänes, K. Lust and P. Miidla, Adsorption of Normal Hexanol on Bismuth Single Crystal Plane Electrodes, J. Electroanal. Chem. (accepted JEC 07041).
16. E. Lust, A. Jänes, V. Sammelselg, P. Miidla and K. Lust, Surface Roughness of Bismuth, Antimony and Cadmium Electrodes, Electrochimica Acta, (in press RA 2525).
17. E. Lust, A. Jänes and K. Lust, Adsorption of Adenosine on Bismuth Single Crystal Plane Electrodes, J. Electroanal. Chem., (accepted RPS 5580).

OSALEMINE KONVERENTSIDEL

1. 6-th International Frumkin Symposium "Fundamental Aspects of Electrochemistry", Moscow, August 21–25, 1995: A. Jänes, K. Lust and E. Lust, Adsorption of Organic Compounds on Single Crystal Antimony, Bismuth and Cadmium Electrodes; E. Lust, A. Jänes, K. Lust and M. Väärtnõu, Electric Double Layer on the Single Crystal Bismuth, Antimony and Cadmium Electrodes in Surface Inactive Electrolyte Solutions.
2. "Baltic Conference on Interfacial Electrochemistry", Tartu, June 14–18, 1996: A. Jänes, E. Lust, K. Lust, Electrochemical Behaviour Na_2H_2EDTA and $Na_2CdEDTA$ on Single Crystal Bismuth and Cadmium Electrodes; A. Jänes, K. Lust, E. Lust, Adsorption of Pyridine on the Single Crystal Bismuth Electrodes, E. Lust, K. Lust, A. Jänes, M. Väärtnõu, Influence of the Chemical Composition and Crystallographic Structure of Single Crystal Bismuth, Cadmium and Antimony Electrodes on the Characteristics of metal|solution Interface.
3. "47th ISE Meeting", Veszprem & Balatonfüred, September 1–6, 1996: E. Lust, K. Lust, A. Jänes, Phase Boundary Structure on the Single Crystal Bismuth, Antimony and Cadmium Electrodes in Surface Inactive Electrolyte Solutions; A. Jänes, M. Väärtnõu, E. Lust, Influence of the Surface Pretreatment of Bi(111) to the Adsorption Characteristics of Pyridine.
4. "The 1997 Joint International Meeting", Paris, August 31 – September 5, 1997: A. Jänes, E. Lust, K. Lust and V. Sammelselg, Surface Roughness, Electric Double Layer and Adsorption Characteristics of Antimony, Bismuth and Cadmium Electrodes; E. Lust, A. Jänes and K. Lust, Adsorption of Organic Compounds on Bismuth Single Crystal Plane Electrodes.

DISSERTATIONES CHIMICAE UNIVERSITATIS TARTUENSIS

1. Toomas Tamm. Quantum-chemical simulation of solvent effects. Tartu 1993 110 p.
2. Peeter Burk. Theoretical Study of gas-phase acid-base equilibria. Tartu 1994, 96 p.
3. Victor Lobanov. Quantitative structure-property relationships in large descriptor spaces. Tartu 1995, 145 p.
4. Vahur Mäemets. The ^{17}O and ^{1}H nuclear magnetic resonance study of H_2O in individual solvents and its charged clusters in aqueous solutions of electrolytes. Tartu 1997, 140 p.
5. Andrus Metsala. Microcanonical rate constant in nonequilibrium distribution of vibrational energy redistribution on the basis of Slater's theory of unimolecular reactions. Tartu 1997, 150 p.
6. Uko Maran. Quantum-mechanical study of potential energy surfaces in different environments. Tartu 1997, 137 p.

ISSN 1406–0299
ISBN 9985–56–311–5